University of Hawai‘i at Mānoa

Application of Recycled Materials in Highway Projects

F I N A L R E P O R T

PRINCIPAL INVESTIGATOR:

Phillip S.K. Ooi, Ph.D., P.E.
Associate Professor

PREPARED IN COOPERATION WITH:

State of Hawaii, Department of Transportation, Materials and Testing Branch and
U.S. Department of Transportation, Federal Highway Administration

Honolulu, Hawaii
December 17, 2010

Technical Report Documentation Page

1. Report No.	2. Government Accession No.	3. Recipient's Catalog No.
HWY-L-2005-04		

4. Title and Subtitle	5. Report Date
Application of Recycled Materials in Highway Projects	December 17, 2010
	6. Performing Organization Code
7. Author(s) P.S.K. Ooi, A.R. Archilla, Y. Song & M.L.Q. Sagario	8. Performing Organization Report No.
9. Performing Organization Name and Address Department of Civil & Environmental Engineering University of Hawaii at Manoa 2540 Dole St., Holmes Hall 383 Honolulu, HI 96822	10. Work Unit No. (TRAIS)
	11. Contract or Grant No.
12. Sponsoring Agency Name and Address Hawaii Department of Transportation Highways Division 869 Punchbowl St., Honolulu, HI 96813	13. Type of Report and Period Covered FINAL 2/1/06 to 8/31/10
	14. Sponsoring Agency Code

15. Supplementary Notes

Prepared in cooperation with the U.S. Department of Transportation and Federal Highway Administration

16. Abstract

The impetus and pressure for pavement and geotechnical engineers to incorporate sustainability in engineering projects has led to a rise in the reuse of materials such as recycled concrete aggregate (RCA), reclaimed asphalt pavement (RAP) and recycled glass (RG) as fill and in pavement sub-layers. Consequently, an understanding of their behavior and characteristics are necessary prior to use in practice.

Tests to characterize the materials, to assess their compactability and to address the vulnerability of RCA to tufa formation and aluminum corrosion were performed. It was found that RCA from a mechanical viewpoint has superior strength and stiffness. However, when exposed to water, it has a tendency to hydrate. Initially, the hydration leads to a gain in strength and stiffness. Subsequently, the material is prone to shrinkage cracking. Nevertheless, the RCA stiffness and strength are still quite appreciable compared to the pre-cracked value. RCA made with Hawaiian basaltic aggregate was found to not produce tufa in significant quantities as compared to dolomitic-based RCA when subjected to an accelerated leaching experiment. However, corrosion of aluminum in the presence of RCA was found to cause significant swell pressures and as such, RCA should not be used in close proximity with any aluminum infrastructure or should not be contaminated with aluminum. RAP on the other hand is more inert. However, the mechanical properties are less desirable than those of virgin aggregate and RCA. While the resilient modulus of RAP is quite appreciable, it suffered significant permanent deformation or rutting and its use should be contained by limiting its percent content. The RG obtained in this study was crushed to a very fine gradation. The large quantities of fines make working with RG hazardous as it can cause skin irritation.

Finally, changes to the State of Hawaii Standard Specifications are proposed to incorporate the use of these three recycled materials as a fill or as an unbound layer in pavements. Two new sections (for RAP and RCA) are also proposed as additions to the current standard specifications.

17. Key Words	18. Distribution Statement
Reclaimed Asphalt Pavement, Recycled Concrete Aggregate, Recycled Glass, Tufa, Corrosion of Aluminum, Resilient Modulus, Permanent Deformation	Document is available to the U.S. public through the National Technical Information Service, Springfield, VA 22161

19. Security Classif. (of this report)	20. Security Classif. (of this page)	21. No. of Pages	22. Price
Unclassified	Unclassified	390	

Form DOT F 1700.7 (8-72) Reproduction of completed page authorized

This form was electronically produced by Elite Federal Forms, Inc.

ACKNOWLEDGEMENTS AND DISCLAIMER

The authors are grateful for the funding and support provided by the **Hawaii Department of Transportation** (HDOT) and the **Federal Highway Administration** (FHWA).

The authors greatly appreciate the many insightful contributions provided by:

Herbert Chu (HDOT)
Brandon Hee (HDOT)
Eric Hellebrand (University of Hawaii, Department of Geology and Geophysics)
David Muenow (University of Hawaii, Department of Chemistry)
Farshad Rajabipour (Pennsylvania State University, Department of Civil and Environmental Engineering)

The authors are also grateful to the following individuals and organizations for providing assistance gratis to the project:

- Richard Levins of Grace Pacific Corp. for providing the recycled materials and virgin aggregate for testing
- Jane Schoonmaker of the Department of Oceanography at the University of Hawaii for performing X-ray diffraction
- Karl Seff of the Department of Chemistry for providing input on the X-ray diffraction results
- Shiv Sharma of Hawaii Institute of Geophysics and Planetology at the University of Hawaii for performing Raman spectroscopy

The contributions of former graduate research assistants Dr. Yonghui Song, Michelle Sagario, Partheeban Selvarajah and Michael Skowronek, whose dissertation and theses form a great part of this research report. The authors also acknowledge Seungdon Joo for performing the swell pressure tests and numerical analysis in Chapter 5 and former undergraduate research assistant Melanie Li for performing tests on recycled glass.

TABLE OF CONTENTS

LIST OF TABLES

LIST OF FIGURES

CHAPTER 1 INTRODUCTION

The desire for improved sustainability has steered engineers towards greener design and construction practices. With about two billion tons of aggregate being consumed each year in the United States, there is concern about rising quantity of aggregate consumption, depletion of sources of virgin aggregate and destruction of natural landscapes (Gonzalez and Moo-Young, 2004). Consequently, local governments, including the State of Hawaii Department of Transportation (HDOT), have been encouraged to incorporate the use of recycled materials in their respective standard specifications. However, because recycled materials are not used universally and their properties can be widely divergent, engineers are unfamiliar with their short and long term behavior. Therefore, research on the behavior of these materials will help alleviate doubts on their use in engineering applications.

Although many types of recycled materials exist, the scope of work is limited to recycled glass (RG), recycled concrete aggregate (RCA) and reclaimed asphalt pavement (RAP).

1.1 RG

Glass recycling escalated with the introduction of the bottle bill in Hawaii, the eleventh state to adopt the bill. In November 2004, Hawaii consumers started paying a nickel deposit for beverage containers and a penny to run the collection and redemption program. In 2006, approximately 25,000 tons of glass was recycled on the island of Oahu alone, making recovery and reuse

of post-consumer glass a high priority. The fate of recycled glass is usually governed by economics.

1.1.1 Uses of RG

Excluding landfill disposal, the two options for glass reuse are in the container and aggregate markets. For reuse in the glass container market, the recycled bottles are typically first color-sorted and then melted, both of which can be costly. The bottles may or may not be crushed. If left uncrushed, storage volume and transportation costs increase. Ultimately, an economic analysis involving labor, transportation, storage, energy costs and other relevant factors have to be considered to determine the appropriate option. These costs and factors vary from region to region but the focus herein will be on glass reused as aggregate.

Many potential uses of RG aggregate in structural (e.g., base course, subbase, fills, etc.) and drainage (e.g., drains, filters, wells, leachate collection media, etc.) applications have been summarized by Wartman et al. (2004).

1.1.2 Challenges of Using RG

Working with RG may be hazardous (e.g., fine RG can cause skin irritation) and appropriate safety procedures should be adopted. The need for such safety procedures when working with RG along with its brittle nature and crushability have stymied the use of more RG in the engineering profession. However, under the right conditions, RG could have acceptable engineering characteristics for use as fill or as aggregates (e.g., lightly loaded trench backfill).

1.1.3 Properties

A literature review revealed that the shear strength of RG was previously measured in at least four states in the country:

1. Pennsylvania – project sponsored by the Department of Transportation (Wartman et al, 2004; Grubb et al., 2006; Pennsylvania Department of Transportation, 2007a and 2007b)
2. Washington – project sponsored by Clean Washington Center (Dames & Moore, Inc., 1994; Shinn and Sonntag, 1994; Soil and Environmental Engineers, Inc. and Re-Sourcing Associates, Inc., 1998)
3. Florida – project sponsored by the Department of Transportation (Cosentino et al., 1995)
4. Missouri – by the University of Missouri–Rolla (Browning, 1970).

Published friction angles of RG ranged from 34° to 62° for RG classified as SP, SW and GP based on the Unified Soil Classification System (USCS). When these friction angles are plotted versus dry unit weight, the results do not show definitive trends. Amidst the scatter, there is somewhat of a trend that friction angle increased with increasing dry unit weight and relative density. The friction angle of RG classified as gravel is not clearly higher than that classified as sand. One possible explanation may be particle crushing of the larger fraction during shear (Ooi et al, 2008).

Other noteworthy observations on RG from the literature include:

1. The specific gravity of RG ranges between 2.45 and 2.52.
2. Optimum water contents range from 5.2 to 11.2 % and maximum dry unit weights range from 17.0 to 18.7 kNm^{-3} based on ASTM D1557.
3. Minimum index dry densities range from 9.43 to 13.6 kNm^{-3} and maximum values from 15.5 to 17.6 kNm^{-3}.
4. Studies performed for the Clean Washington Center revealed that the passing 19 mm fraction RG underwent some particle crushing during modified Proctor compaction while particle crushing was minimal with the passing 6.35 mm fraction (Dames and Moore, Inc., 1993).
5. Cosentino et al. (1995) encountered difficulty in obtaining a Proctor moisture-density curve for RG that was mostly poorly graded. They observed that "glass particles spilled from the mold as the compaction hammer contacted the" RG.

1.2 RAP

RAP is derived either through milling or full-depth removal. Milling involves removal of only the top portion of the pavement. Typically this material does not have to be processed and can be used instantaneously. Upon removal, the gradation of milled RAP is typically finer than the original mix gradation (RMRC, 2008). If full-depth removal is used, the entire pavement layer is excavated and taken to a plant where it is crushed and blended to certain gradations and specifications. The characteristics of RAP mixtures vary significantly from site to site. Nearly 73 million tons of RAP are processed every year with approximately 80% being reused (Rathje et al., 2001).

1.2.1 Uses of RAP

RAP can be used to manufacture hot or cold mixed asphalt, as granular base and subbase course, and as embankment fill. According to the RMRC (2008), if RAP is used as an embankment fill, the aggregate sizes that are less than two inches can be mixed with soil or other fine aggregates and the larger aggregate sizes can be used in a base course.

1.2.2 Challenges of Using RAP

One challenge with RAP is its potential to creep under constant load as described by Cosentino et al. (2003) in their research to prepare RAP specifications for base, sub-base, and fill. They also determined that when standard Proctor tests are performed on RAP, a classical bell-shaped compaction curve is not observed. Also, a sample of 100% RAP typically has a low CBR (20% to 25%), while a blend of virgin aggregate with RAP has a higher CBR (RMRC, 2008).

1.2.3 Properties

There has been many research endeavors on the engineering characteristics of RAP. The compacted unit weight of RAP is in the range of 100 to 125 lb/ft^3 (FHWA, 2008). The drained shear strength of RAP was investigated by Rathje et al. (2002) using consolidated-drained triaxial compression tests and the friction angle was determined to be 39 degrees.

1.3 RCA

About 95 million tons of RCA are processed each year (Rathje at al., 2001). RCA is typically removed using a backhoe or payloader. RCA is processed

through crushers with magnets to remove rebar, and crushed to an appropriate gradation. The characteristics of RCA vary significantly from each site, as the concrete mixture is different for each job.

1.3.1 Uses of RCA

A study by the New Jersey Department of Transportation (Bennert and Maher, 2008) revealed that some states have used RCA as a base course, subbase course, pipe bedding, surface course aggregate and subgrade soil stabilizer. The RMRC (2008) added bulk fill material, flowable fill aggregate, shoreline protection and gabions as other possible uses.

1.3.2 Challenges of Using RCA

According to Chesner Engineering (2001), a potential problem with the use of RCA is tufa formation. Tufa, which is calcium carbonate, has a tendency to clog geotextiles or drains leading to premature failure of infrastructure. They also suggest that the RCA may cement the aggregates together thereby making the RCA less permeable, which could be problematic if RCA is used as a base or subbase. RCA has a high water absorbance, which may yield unusually high optimum moisture contents. Also, the use of RCA in the field may cause increased corrosion because of its high pH (Chesner Engineering, 2001). Other concerns when using RCA include: (a) alkali silica reaction; (b) sulfate attack; (c) alkali carbonate reaction; and (d) reaction with aluminum. These reactions occur when RCA is exposed to the various reagents such as silica, sulfates, a certain type of carbonate aggregate and aluminum, respectively.

1.3.3 Properties

According to the RMRC Guidelines (2008), processed RCA is typically more angular, rougher, has a lower specific gravity and a higher absorption than the virgin aggregate that it is derived from. RCA has high alkalinity due to the cement paste. In the RMRC Guidelines (2008), RCA is said to have an LA Abrasion of 20 to 45% and a CBR of 94 to 148%. Also, because RCA has a higher absorption, the optimum moisture content is significantly larger than the virgin aggregate that it is derived from (Chesner Engineering, 2001). Using consolidated-drained triaxial compression tests, the drained friction angle of RCA was determined to be 54º by Rathje et al. (2002).

RCA also has the ability to strengthen over time through hydration and pozzolanic reaction. This is especially true in RCA with finer gradations. There is usually some cement that has not been hydrated in concrete because of the production of calcium-silicate-hydrate, which forms around the cement and prevents water from reaching the unhydrated cement (Blankenagel, 2005). Therefore, the finer the RCA is crushed, the more unhydrated portions are revealed and available for additional reaction.

1.4 OBJECTIVES

As part of this project, the current HDOT specifications on the use of RG, RCA and RAP in the unbound granular layers (base course, sub-base course and backfill) were reviewed. Revisions are proposed to realize the benefits of using recycled materials. Prior to revising the specifications, major issues

relating to use of these recycled materials were identified. The following research objectives are intended to address some of these issues:

1. Review the current HDOT specifications (Sections 203 Excavation and Embankment, 204, Excavation and Backfill for Miscellaneous Facilities, 205 Excavation and Backfill for Bridge and Retaining Structures, 301 Plant Mix Asphalt Concrete Base Course, 304 Aggregate Base Course, 305 Aggregate Subbase Course, 306 Untreated Permeable Base Course, 624 Water System, 625 Sewer System, 703 Aggregates, 717 Cullet and Cullet-Made Materials) and suggest edits to incorporate the use of recycled materials.
2. Material characterization of the RG, RCA and RAP for use as a base/subbase and fill. These include shear strength, California Bearing Ratio (CBR), resilient modulus and permanent deformation.
3. Assess the compactability of RAP and RCA using a variety of devices such as the nuclear densometer, time domain reflectometry, portable falling weight deflectometer and Geogauge.
4. Investigate the potential for tufa formation with local RCA.
5. Perform forensic investigation on the heave of a pavement supported on a base course containing recycled materials.

1.5 ORGANIZATION OF REPORT

Chapter 2 presents a study to characterize the three types of recycled materials. In Chapter 3, the compactability of RAP and RCA are discussed.

Chapter 4 presents the potential of the local RCA for tufa formation. A forensic investigation of the heave of a pavement supported on a base course containing recycled materials is presented in Chapter 5. The major lessons learnt from this research and its implications on the specifications are discussed in Chapter 6. Revisions to HDOT's specifications are contained in the Appendix.

CHAPTER 2 MATERIAL CHARACTERIZATION

This chapter discusses the index properties, resilient modulus and permanent deformation characteristics of the recycled materials tested in this study.

2.1 MATERIAL SOURCE

Virgin aggregate (VA) and the three types of recycled materials were acquired from Grace Pacific Corporation's Makakilo quarry, on the island of Oahu, Hawaii. In Hawaii, it is customary for the quarries to distinguish between Type A and Type B basalt. Used mostly in the manufacture of concrete and hot mix asphalt, Type A basalt meets the requirements of American Society for Testing and Materials (ASTM) C33 for concrete aggregate and ASTM D448 for road and bridge construction while the inferior Type B basalt does not. Generally, the latter is vesiculated and is used in the layers below pavements (base, subbase and fill). Thus, RAP and RCA contain the superior Type A basalt while the VA is the inferior Type B variety that purportedly meets HDOT's base course requirements. .

While RAP and RCA were crushed by Grace Pacific, the RG was provided to Grace Pacific by the City and County of Honolulu pre-crushed. RCA from different sources were not stockpiled separately, as records on the sources of RCA were not readily available. RAP was crushed into 2 sizes: passing 3/4 inch (19 mm) and passing 3/8 inch (9.5 mm).

2.2 GRAIN SIZE DISTRIBUTION

Prior to sieving, the VA, RCA and RG were oven dried at 110°C. RAP was air dried in the sun for five days. Then a representative sample of each material was dry-sieved (AASHTO T27) and wet-sieved (AASHTO T11). Gradation curves using the wet sieve method generally showed slightly more fines. However, only the dry sieve gradation curves are presented.

The gradation of each recycled material was compared with the HDOT requirements for base, subbase and fill (Figures 2-1 through 2-6). VA gradation was also compared with HDOT requirements for base course (Figure 2-7). In summary, none of the recycled materials fit the HDOT gradation requirements for base, subbase or fill, suggesting that they have to be blended to meet HDOT gradation requirements prior to use. The VA did meet HDOT's requirements of 1.5-inch nominal untreated base course.

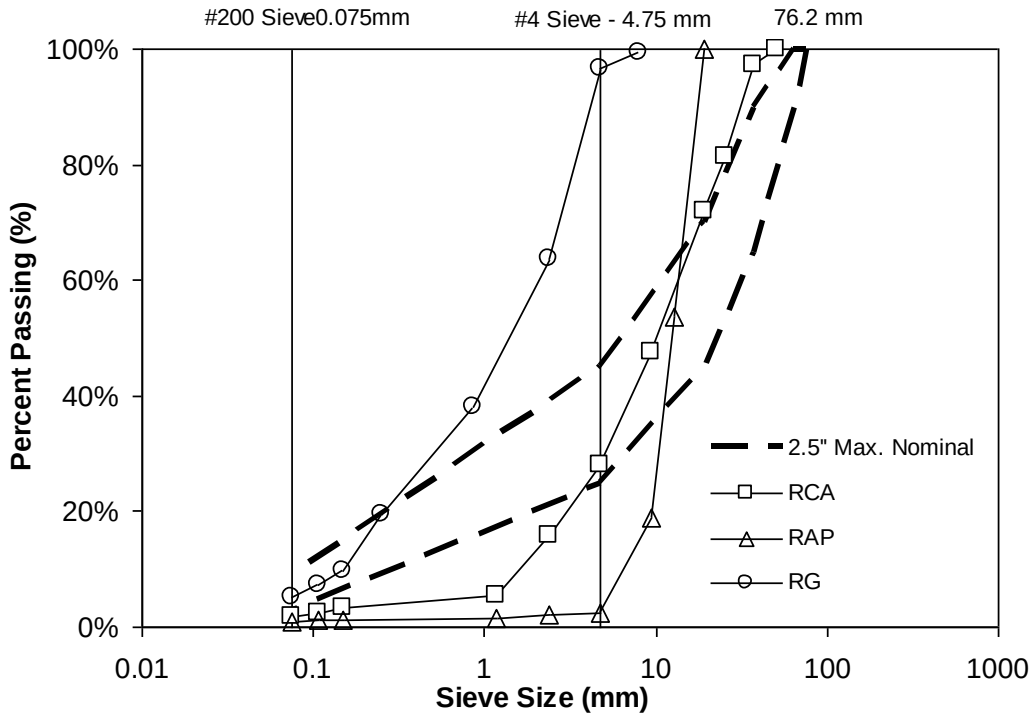

Figure 2-1 Comparison of grain size distribution of recycled materials with HDOT's 2.5-inch maximum nominal untreated base course requirements

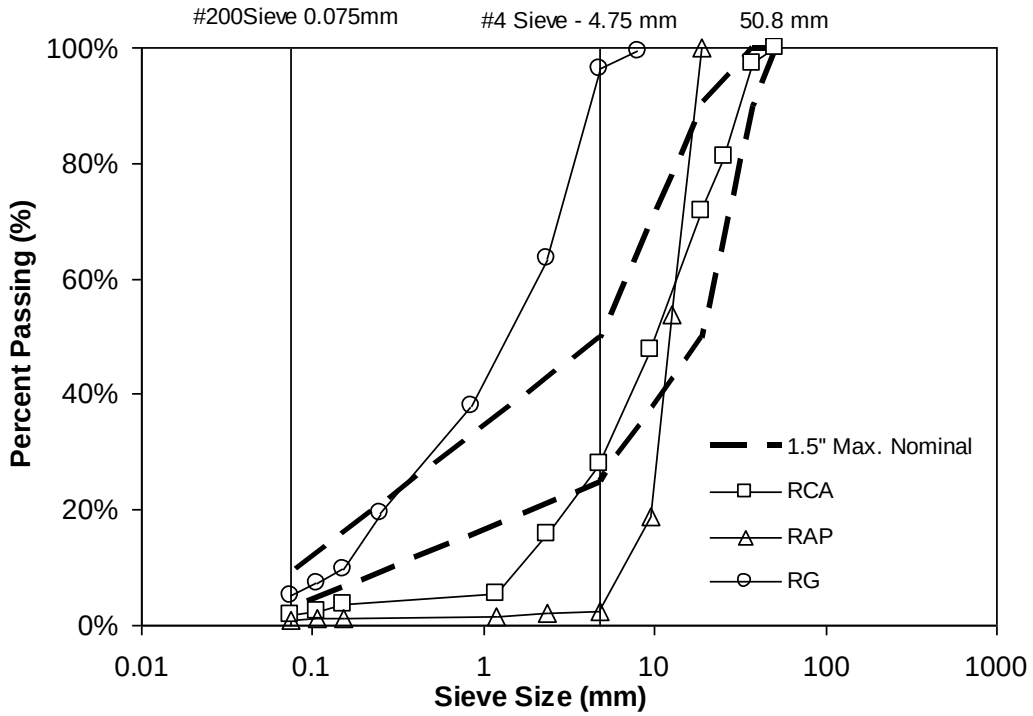

Figure 2-2 Comparison of grain size distribution of recycled materials with HDOT's 1.5-inch maximum nominal untreated base course requirements

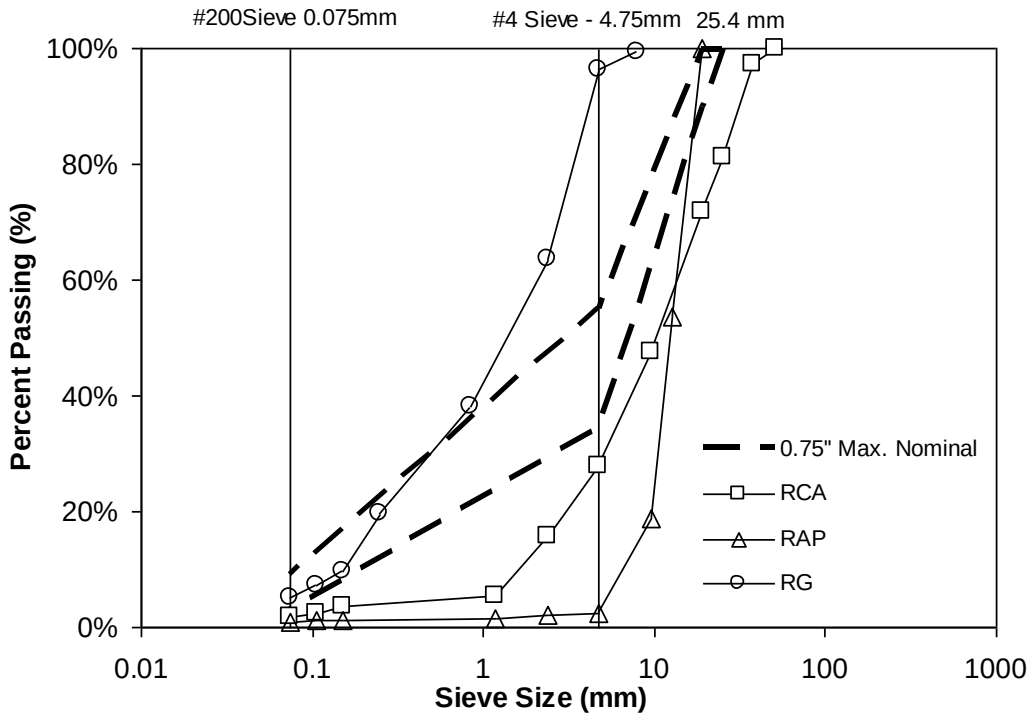

Figure 2-3 Comparison of grain size distribution of recycled materials with HDOT's 0.75-inch maximum nominal untreated base course requirements

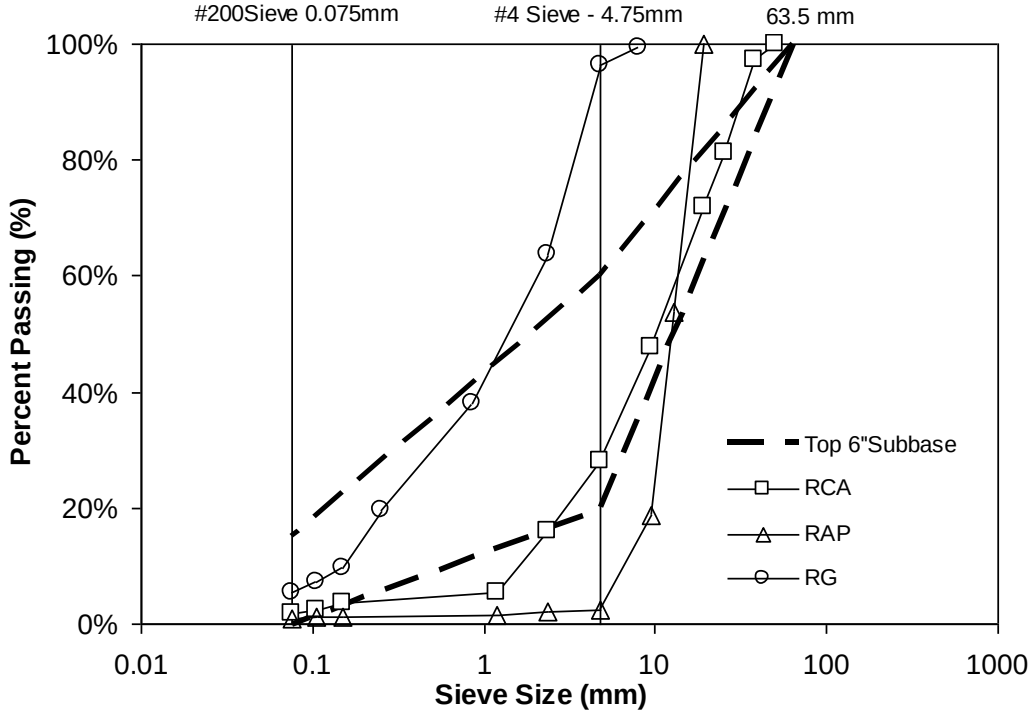

Figure 2-4 Comparison of grain size distribution of recycled materials with HDOT's top 6-inch subbase requirements

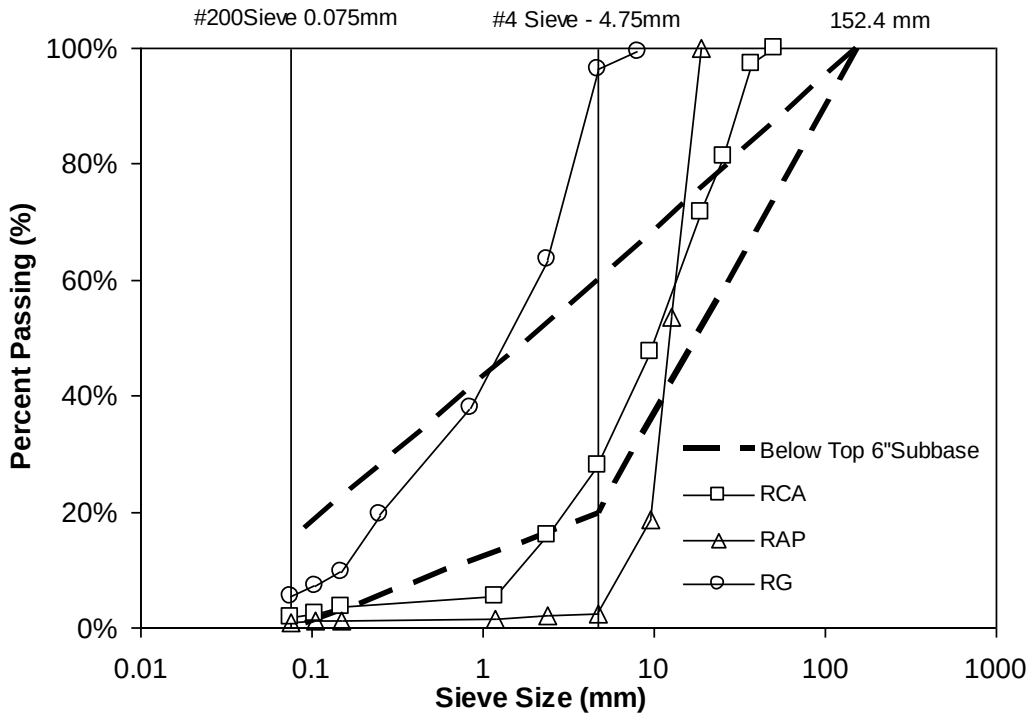

Figure 2-5 Comparison of grain size distribution of recycled materials with HDOT's requirements for subbase below top 6 inches

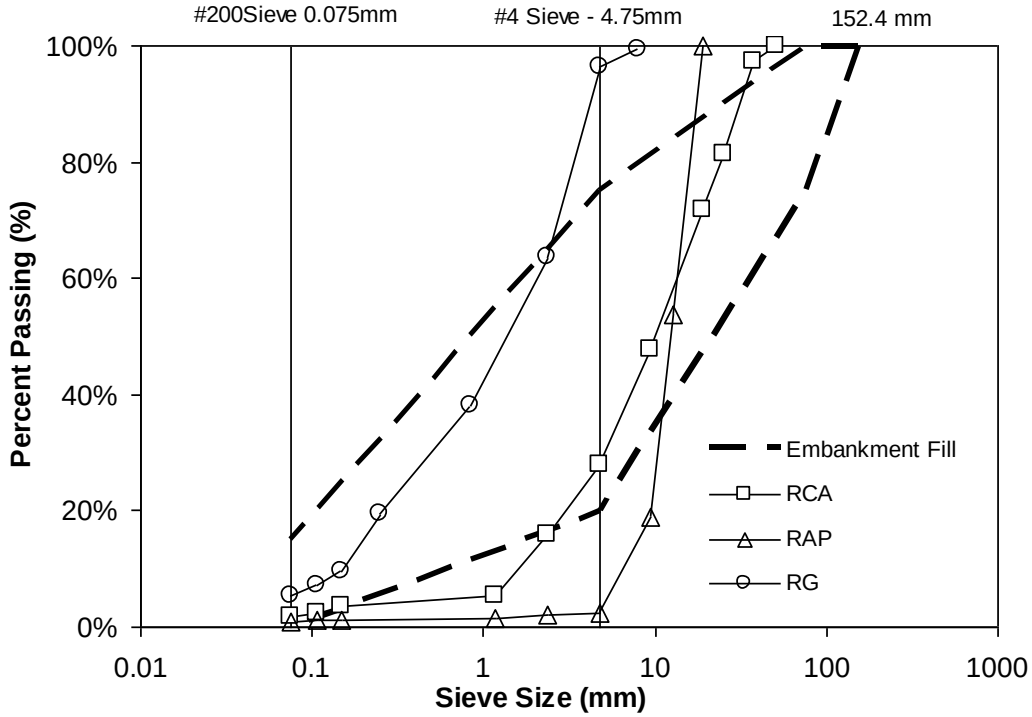

Figure 2-6 Comparison of grain size distribution of recycled materials with HDOT's embankment fill requirements

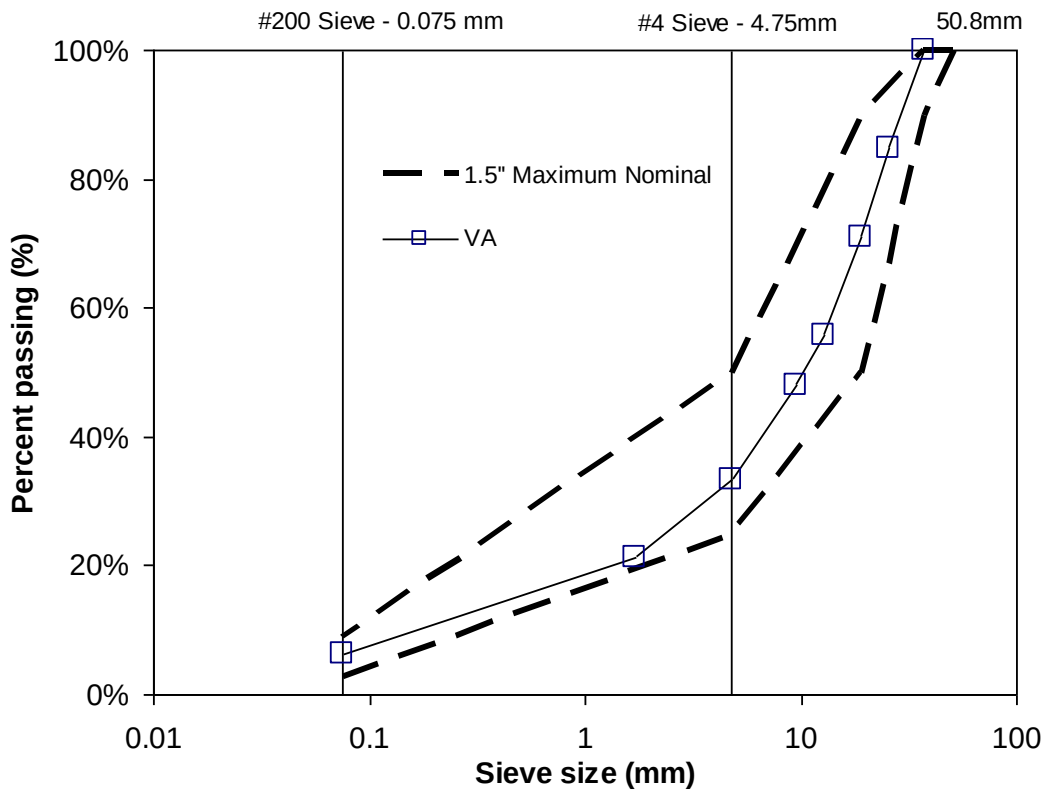

Figure 2-7 Comparison curves of VA with HDOT's 1.5-inch maximum nominal untreated base course requirements

2.3 SPECIFIC GRAVITY AND ABSORPTION

Specific gravity and absorption were measured in accordance with AASHTO T84 and AASHTO T85 for fine and coarse aggregates, respectively. Samples were tested using materials in their as-received gradation. The test results are summarized in Table 2-1. From this table, the finer recycled aggregates have consistently lower specific gravities and higher absorptions than the coarser ones. Among the recycled aggregates, the absorption of RCA is highest (11.8%) and that of RG the lowest (0.9%). For the VA, the apparent specific gravity for the fine aggregate is larger than that of the coarse

aggregate, probably because the larger Type B basalt aggregates contain more vesicles, making them difficult to be completely de-aired.

Table 2-1 Specific gravity and absorption

	VA[1]		**VA[2]**		**RG**		**RCA**		**RAP**	
	Fine	Coarse	Fine	Coarse	Fine	Coarse	Fine	Coarse	Fine	Coarse
Bulk specific gravity	2.26	2.33	2.25	2.37	2.46	2.50	2.13	2.45	2.17	2.54
Bulk specific gravity (SSD)[3]	2.49	2.48	2.49	2.52	2.48	2.51	2.38	2.59	2.31	2.61
Apparent specific gravity	2.95	2.77	2.95	2.80	2.51	2.52	2.84	2.85	2.52	2.72
Absorption	10.5%	6.8%	10.5%	6.5%	0.9%	0.2%	11.8%	5.7%	6.3%	2.5%

Notes
1, 2 Duplicate tests were conducted for VA.
3 SSD = saturated surface dry

2.4 LA ABRASION

LA Abrasion tests were conducted in accordance with AASHTO T96 to provide a measure of the aggregate's durability to impact loading. LA abrasion was measured for different gradings because the as-received recycled materials and VA all have different gradations. The test results are shown in Table 2-2. LA abrasion values for RCA and VA are comparable and are higher than those for RAP. This is reasonable since RCA contains cement paste which is brittle and easily degradable while the VA consists of the lower grade Type B basalt. The asphalt coating protects the already durable Type A basalt in RAP from degradation.

Table 2-2 LA abrasion test results of four materials

Material	Grading[1]	Weight after test (g)	Weight before test (g)	Percent of weight loss (%)
VA	A	3572	5000	29%
	B	3669	5000	27%
	D	3494	5000	30%
RCA	A	3626	5000	27%
	D	3472	5000	31%
RAP	B	4106	5000	18%
	C	4122	5000	18%
RG	C	3334	5000	33%
	D	3647	5000	27%

Currently, HDOT's maximum allowable LA abrasion for untreated base course is 40%, which is larger than any of the values obtained. HDOT does not have a minimum LA abrasion requirement for subbase and fill. So from an LA abrasion viewpoint for base course, all materials meet the HDOT requirement.

2.5 COARSE AGGREGATE VOID CONTENT

Coarse aggregate void content test was conducted in accordance with AASHTO TP56-99 Method A. The void content depends on the particle shape and texture. Using the uncompacted void content, aggregate angularity of different materials with the same grading can be compared. A decrease in the void content is associated with more rounded, spherical, smooth surfaced coarse aggregate or a combination of these factors. The coarse aggregate void content of each material is shown in Table 2-3. The VA

has the highest coarse aggregate void content (56.7%). RCA, RAP and RG have similar values.

Table 2-3 Void content of coarse aggregate of each material

Material	Void Content	Bulk Specific Gravity Used
VA	56.7%	2.77
RAP	50.0%	2.54
RCA	48.2%	2.45
RG	46.3%	2.50

2.6 SAND EQUIVALENT TEST

Sand equivalent (SE) tests were conducted in accordance with AASHTO T176. The test results are summarized in Table 2-4. SE is used to determine the characteristics of the finer grained portion of cohesionless soils. It is determined by performing a sedimentation test. The fraction of sand that passes through a 5 mm sieve is placed into a cylinder of water containing a flocculent, shaken and allowed to stand for twenty minutes. A deposit of sand of height, h, forms in the flocculated material of height, H, above which lies clear water. The sand equivalent, SE = h/H. If SE > 30%, the material is not plastic. The higher the SE, the higher is the percentage of sand and silt size particles. Typically, clays have sand equivalent between 0 and 5%, silty clays between 6 and 10%, clayey silts between 11 and 30%, clayey fine sands between 30 and 40%, and silty fine sands above 40%.

Table 2-4 Sand equivalent (SE) test results

Material	Sand Equivalent
VA	49%
RCA	68%
RAP	73%
RG	92%

HDOT's minimum allowable SE value for untreated base and subbase are 30% and 25%, respectively. The largest SE value obtained was 92% for RG, and the smallest was 49% for VA. Therefore, from a SE perspective, all materials meet HDOT requirements for base and subbase. HDOT has no minimum SE requirement for fill.

2.7 ATTERBERG LIMITS

Atterberg limit tests conducted include the plastic and liquid limit tests. The shrinkage limit test was not performed. Plastic limit test was conducted in accordance with AASHTO T90, and the liquid limit test was conducted in accordance with AASHTO T89. Test results showed that the finer fractions of all four materials are classified as non-plastic (NP).

2.8 ASPHALT CONTENT OF RAP

The RAP asphalt content was measured in accordance with AASHTO T 308 using a NCAT asphalt content tester (ignition oven). Asphalt binder in the RAP is burnt in the oven and the asphalt content is calculated as the difference between the initial RAP aggregate mass and the residual mass after burning. The moisture-free asphalt content is 5.8%.

2.9 CALIFORNIA BEARING RATIO

The California Bearing Ratio (CBR) test is used to evaluate the strength characteristics of the material for pavement support. This section presents the CBR test results for VA, RCA, RAP and RG. All CBR samples were first prepared to meet the State of Hawaii Department of Transportation's (HDOT) embankment fill gradation. This gradation was chosen because it was anticipated that it would yield the lowest CBR as compared to the base or subbase. CBR tests were also performed on blends of VA with each of the three recycled materials to evaluate the effect of blending ratio on CBR. Then, the effects of gradation on CBR were also evaluated for RCA and RAP using two types of HDOT gradations: embankment fill (finer) and base course (coarser).

2.9.1 OVERVIEW OF THE CBR TEST

The equipment and procedure for the CBR test are detailed in AASHTO T 193 and ASTM D1883. There are three stages in a CBR test. First, the specimen is dynamically compacted in a 6-inch (152 mm) diameter mold. Second, the specimen is soaked for 4 days with a surcharge load applied. Soaking the sample simulates the worst case moisture scenario in the field and the surcharge simulates the overburden due to the pavement. Third, with the same surcharge in place, a standardized piston having an area of 5806 mm^2 (3 $inch^2$) is used to penetrate the soil in the mold at a rate of 1.27 mm (0.05 inch) per minute (Figure 2-8). Generally, the load at 2.54 mm (0.1-inch) penetration is used to compute the CBR. The CBR is defined as the ratio of

the stress at 2.54 mm (0.1-inch) penetration to that of a standard. Standard values corresponding to a high quality crushed stone are summarized in Table 2-5. If the CBR at 5.08 mm (0.2-inch) penetration is higher than that at 2.54 mm (0.1-inch) penetration, the value at 5.08 mm (0.2 inch) penetration is used.

Table 2-5 Standard load for high quality crushed stone material

Penetration (inch)[1]	Standard load for crushed stone (psi)[2]
0.1	1000
0.2	1500
0.3	1900
0.4	2300
0.5	2600

Notes
1 1 inch = 25.4 mm
2 1 psi = 6.895 kPa

2.9.1.1 Compaction

The moisture-density relationships were established in accordance with AASHTO T180 Procedure D or ASTM D1557 Procedure C. The material was compacted in a 152.4-mm-diameter mold in 5 lifts with each lift receiving 56 blows. The compaction was facilitated using a Boart Longyear mechanical compactor that is bolted to the concrete floor. The compactor has a pie-shaped rammer. Before use, the mechanical compactor was calibrated in accordance with ASTM D 2168. The weight of the rammer was adjusted until

the deformation of lead cylinders from the mechanical compactor and a 10-lb manual modified Proctor hammer are equal.

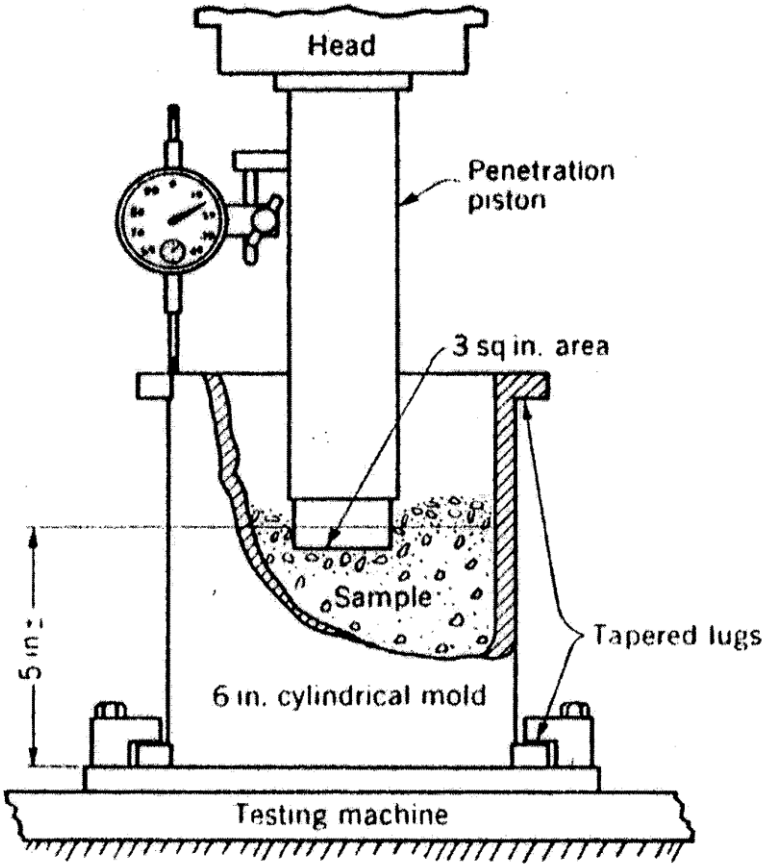

Figure 2-8 Penetration portion of CBR test (Porter 1949)

2.9.1.2 Soaking

After compaction, the samples were soaked for 4 days in a tub of water. A surcharge of 6.8 kilograms was applied to the sample during soaking and CBR testing to simulate the pavement overburden. The soaking was necessary to simulate the worst case scenario in the field. Very little swell was detected in all the materials during the soaking period.

2.9.1.3 CBR Testing

The CBR testing equipment consists of a loading frame supporting a plunger which penetrates the sample in the mold (Figure 2-9).

Figure 2-9 CBR test set up

A data acquisition system consisting of the following was used to record the load and penetration during the test:

- 10,000-lb rated load cell (Sensortronics 6000 1A-10K)
- Two Linear Variable Differential Transducers (LVDT) with a range of 25.4 mm (Schaevitz 1000MHR)
- Signal conditioner (PMG Precision Instruments SC-5B AC Transducer)
- Computer with analog to digital (A/D) board (Metrabyte)
- ATS software (Version 3.1)

During the test, the voltage output from the load cell and LVDTs were sent to the signal conditioner, which converts the voltage to an analog output. This in turn was translated by the A/D board to load and displacement. The LVDTs were placed diametrically opposite, with the average displacements used for determination of CBR.

After the test, a stress-displacement plot was made to interpret the CBR value. In some cases, the initial stress-penetration curve is not linear, but concave upward. For such cases, the CBR values were corrected using the method as specified in AASHTO T 193.

2.9.2 CBR TEST SAMPLE GRADATION AND RESULTS

2.9.2.1 Sample Gradation

The target gradation for CBR samples of VA, RCA and RAP is identical to the finer end of the range for embankment fill per HDOT specification (Figure 2-10). The only exception is that the maximum aggregate size was limited to ¾ inch (19 mm) as required by AASHTO T193. For RG [maximum nominal aggregate size = ⅜ inch (9.5 mm)] and its blends with VA, a finer gradation (Figure 2-11) was adopted due to the unavailability of the larger aggregates.

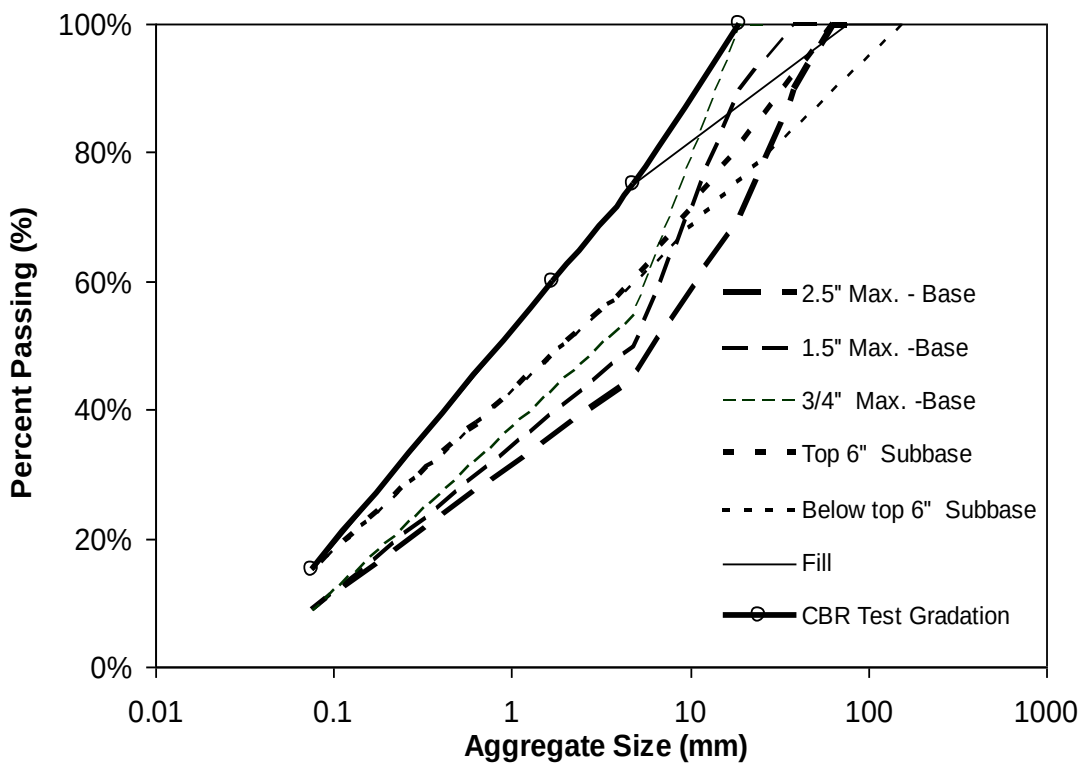

Figure 2-10 CBR test gradation for VA, RCA, RAP and their blends with respect to HDOT gradations (upper bound) for fill, subbase and base course

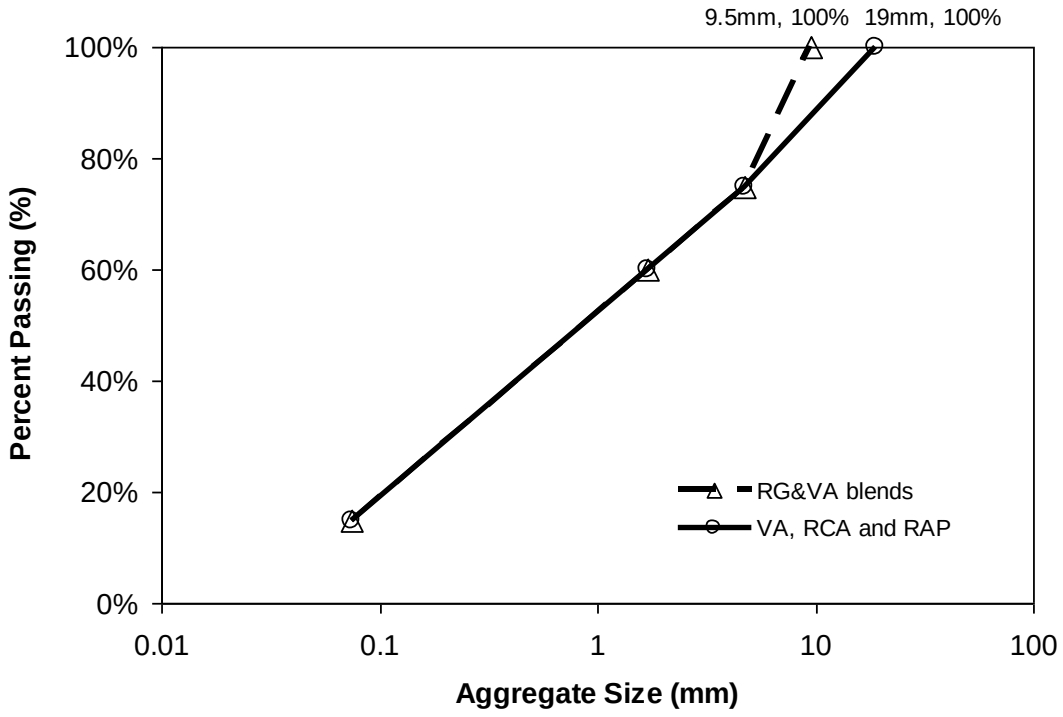

Figure 2-11 CBR test gradation for RG & VA blends

2.9.2.2 CBR

At least six CBR tests were conducted for each material. The results are presented as water content versus dry unit weight in Figure 2-12a and water content versus CBR in Figure 2-12b.

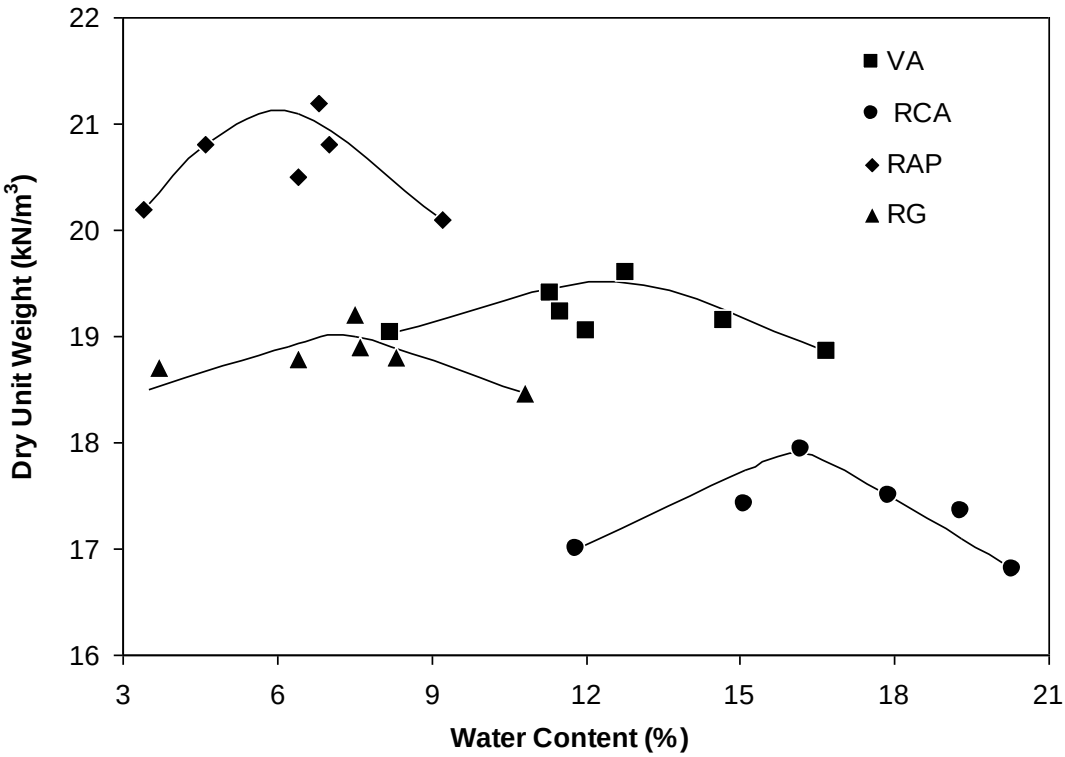

(a)

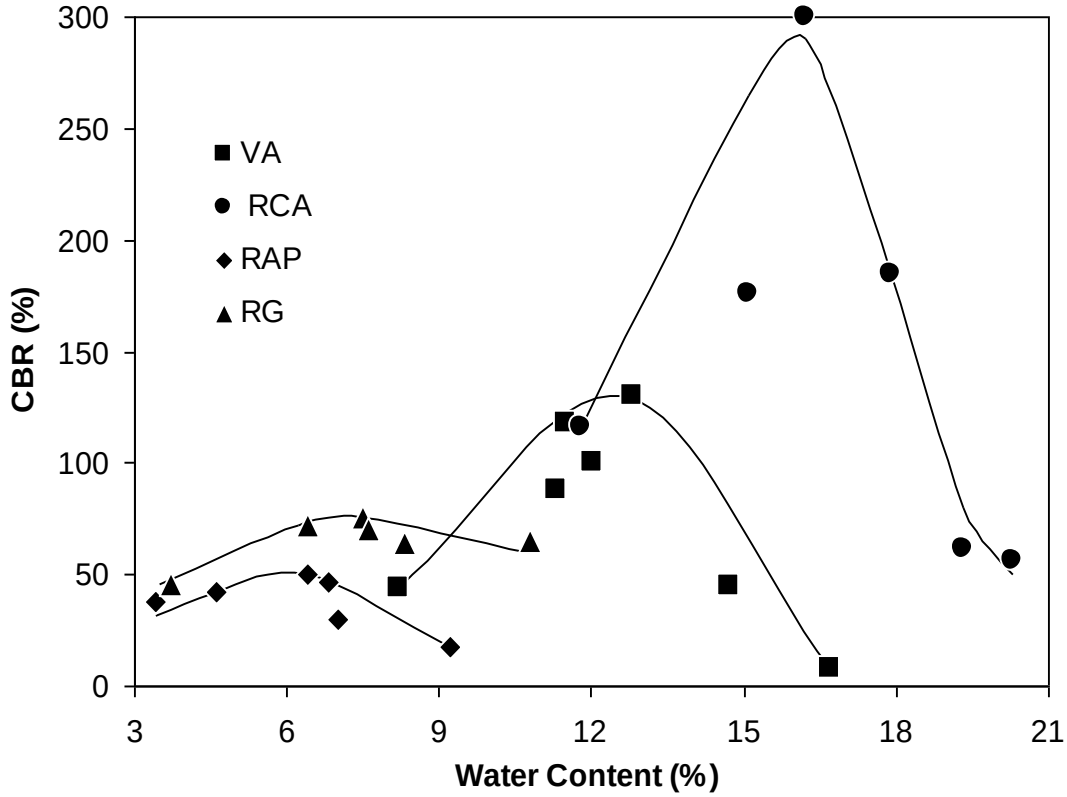

(b)

Figure 2-12 CBR test results (a) Dry unit weight versus water content and (b) CBR versus water content

Figure 2-12a shows that RAP has the lowest optimum water content and the highest maximum dry density, while RCA has just the opposite. The largest densities were observed in RAP probably because of the ability of the asphalt-coated particles to slip into a denser configuration. VA and RG have comparable dry unit weights but different optimum water contents. The optimum water contents of RAP and RG are similar.

Figure 2-12b shows that the maximum CBR occurred at the optimum water content and maximum dry unit weight for all four materials. At optimum, RCA is strongest (CBR = 300%) possibly due to hydration of the previously unhydrated cement particles and RAP weakest (CBR = 50%). RAP is weakest probably because the asphalt coating allows the particles to slip within themselves more readily during penetration leading to higher deformations. VA is weaker than RCA but stronger than RG.

The effect of water content on CBR is small for RAP and RG, but is significant for VA and RCA.

2.9.2.3 Changes in Gradation after Compaction and CBR testing

To evaluate whether the gradation changed due to compaction and CBR testing, sieve analyses were conducted after CBR testing for comparison. Both dry and wet sieve methods were used. The results (Figure 2-13) show that:

1) There was very little change in the gradation for RG despite the fact that glass is known to be brittle;

2) The VA appears finer after testing suggesting that some particle crushing occurred with the more vesiculated and weaker Type B basalt aggregate;

3) There was scatter on both sides of the target test gradation for RCA and RAP. It is not surprising for the gradations to be finer after testing. Reasons why some of the gradations become coarser after testing can be explained as follows. With RCA, some of the particles may have re-cemented together after soaking and testing. As for RAP, this may be due to the fact that the asphalt caused the particles to stick together after compaction and CBR testing.

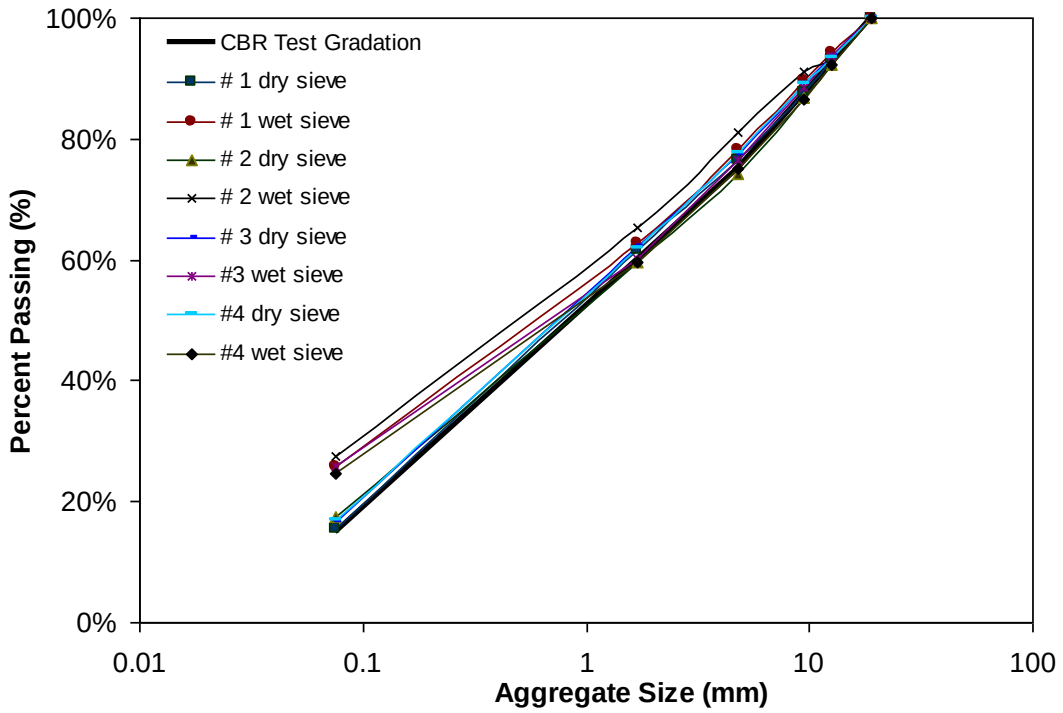

Figure 2-13a Variation of gradation before and after compaction and CBR test - VA

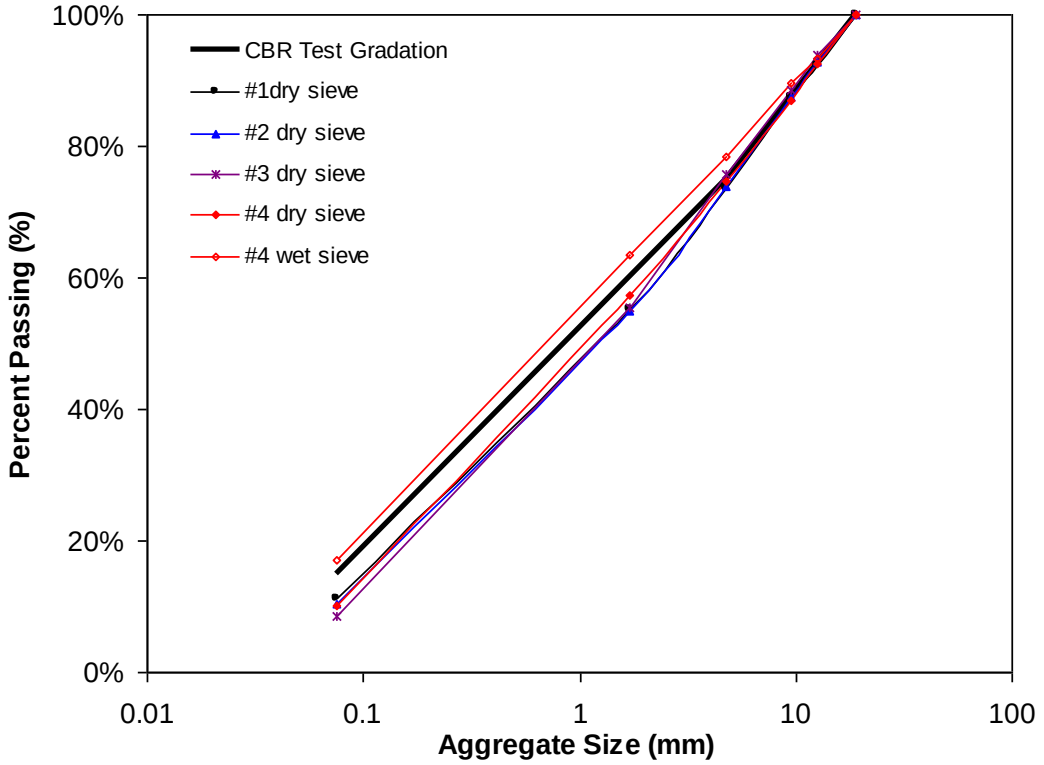

Figure 2-13b Variation of gradation before and after compaction and CBR test - RCA

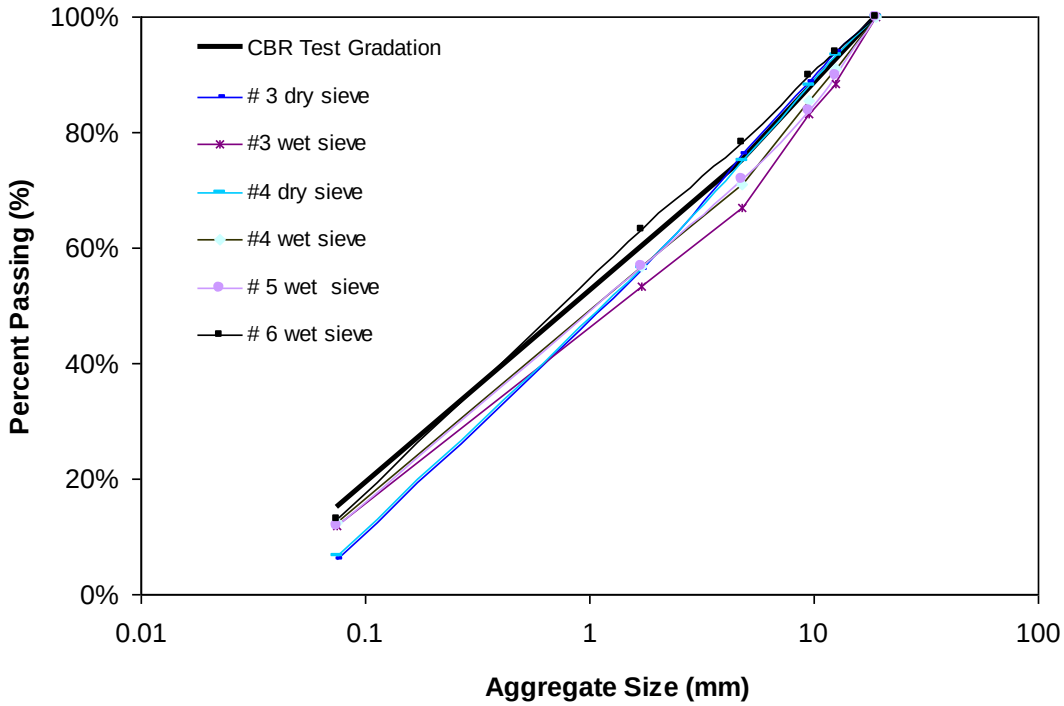

Figure 2-13c Variation of gradation before and after compaction and CBR test - RAP

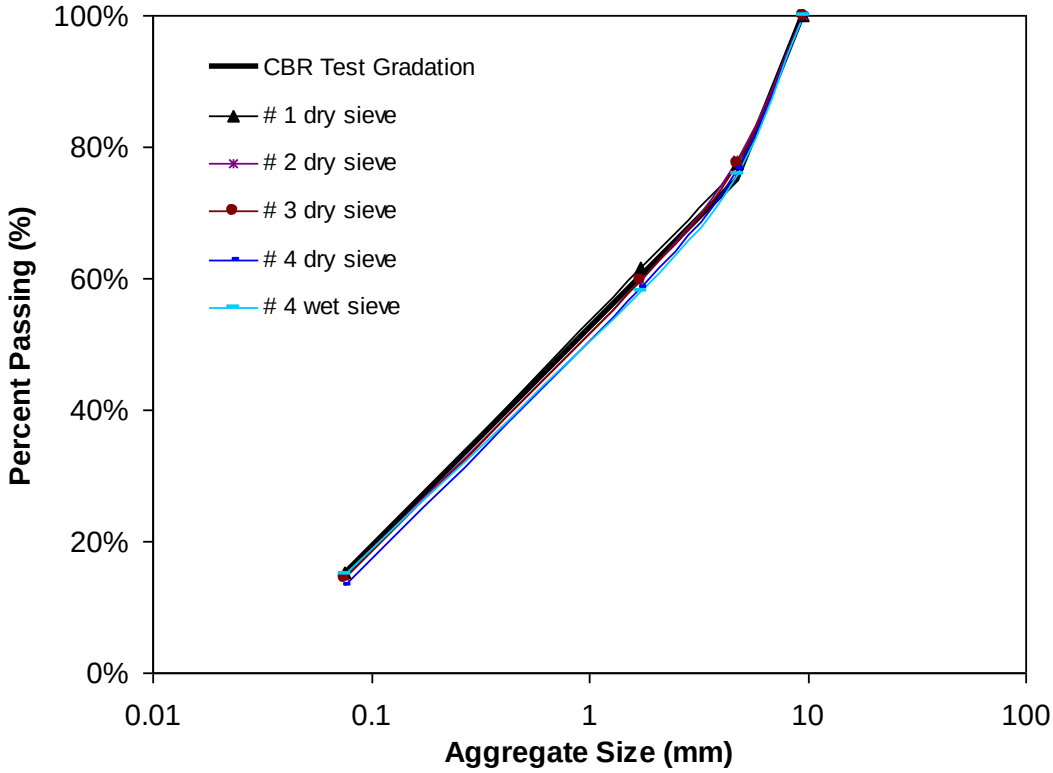

Figure 2-13d Variation of gradation before and after compaction and CBR test - RG

2.9.3 CBR OF BLENDS

As shown in Figs 2-1 through 2-6, the as-received RCA, RAP and RG did not meet any of HDOT's gradation requirements for base, subbase course or fill. Consequently, they would need to be blended prior to use. RCA, RAP and RG were blended with VA to investigate the effects of varying blend ratios on CBR. Two blend ratios were adopted for each material, i.e., 50% recycled material:50% VA and 25% recycled material:75% VA. The test results are summarized in Figures 2-14 through 2-16.

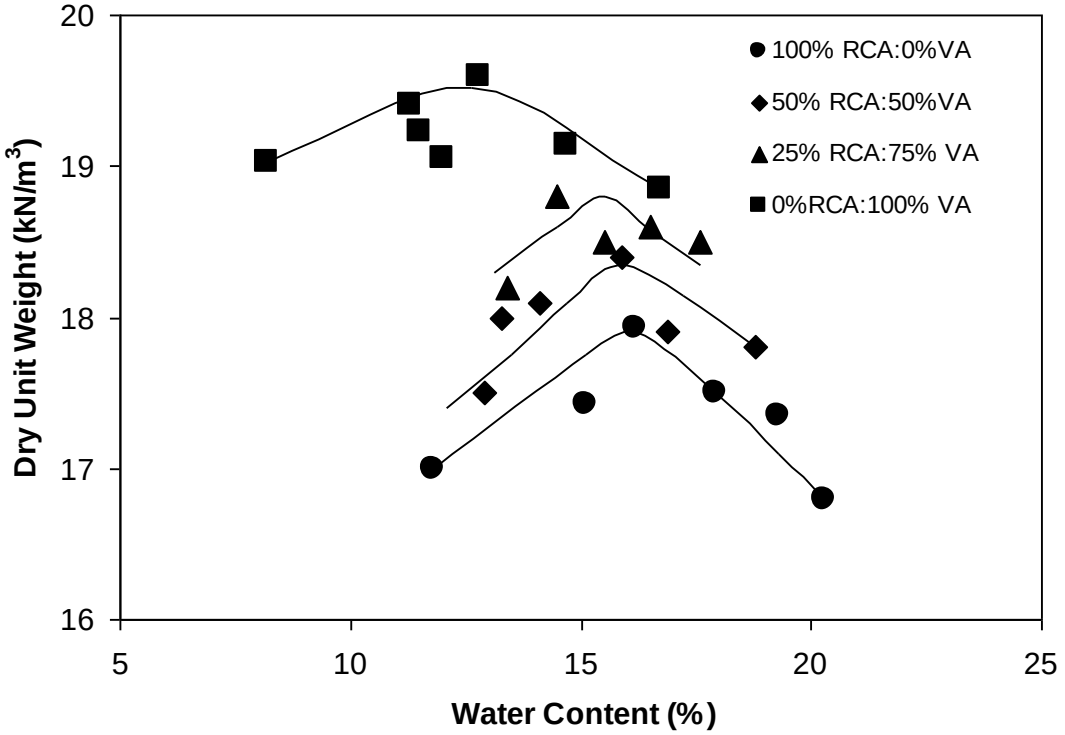

Figure 2-14a Dry unit weight versus water content for RCA blends

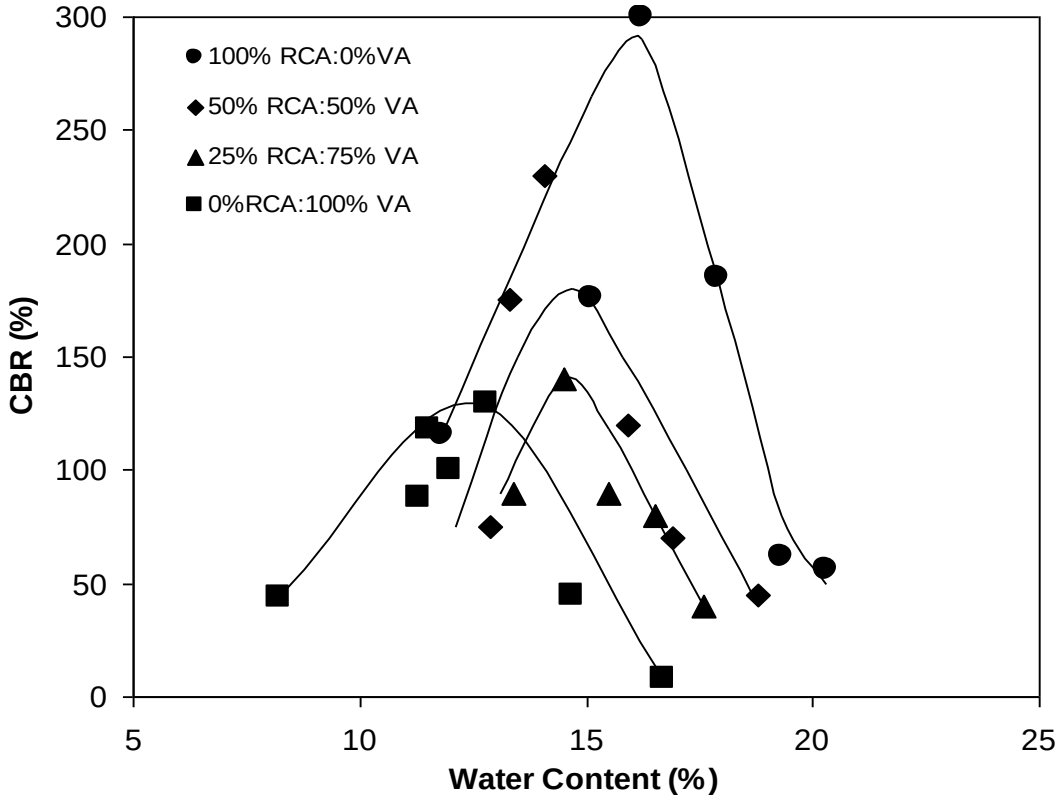

Figure 2-14b CBR versus water content for RCA blends

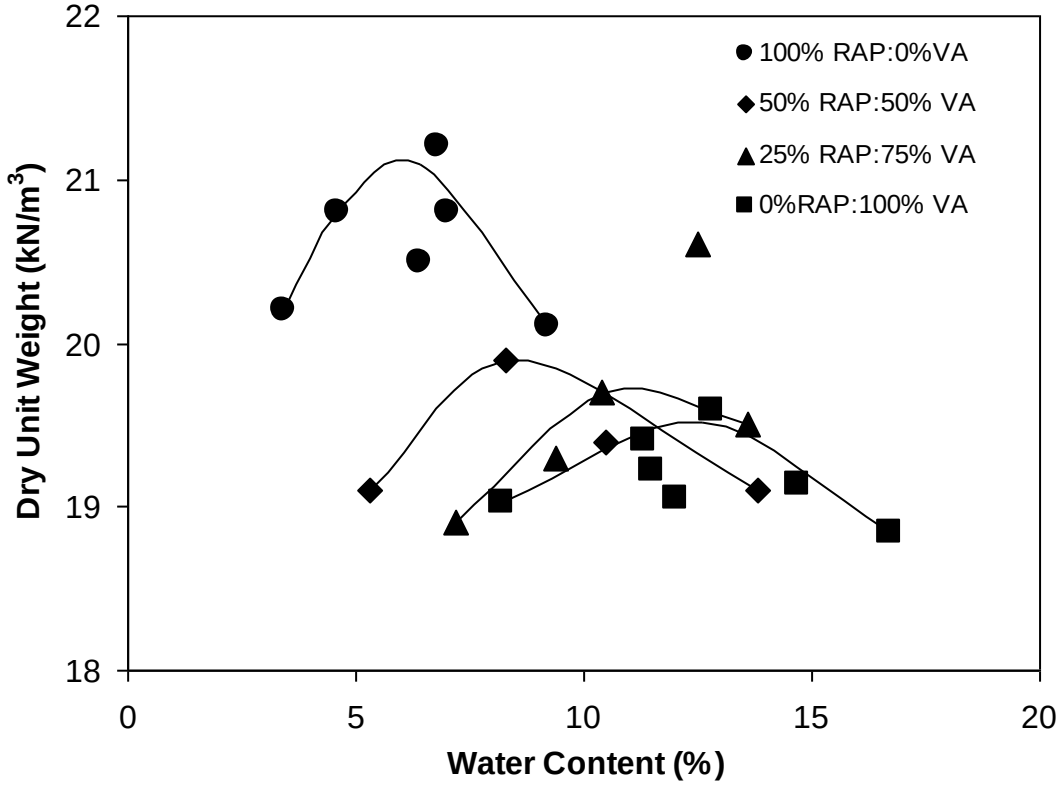

Figure 2-15a Dry unit weight versus water content for RAP blends

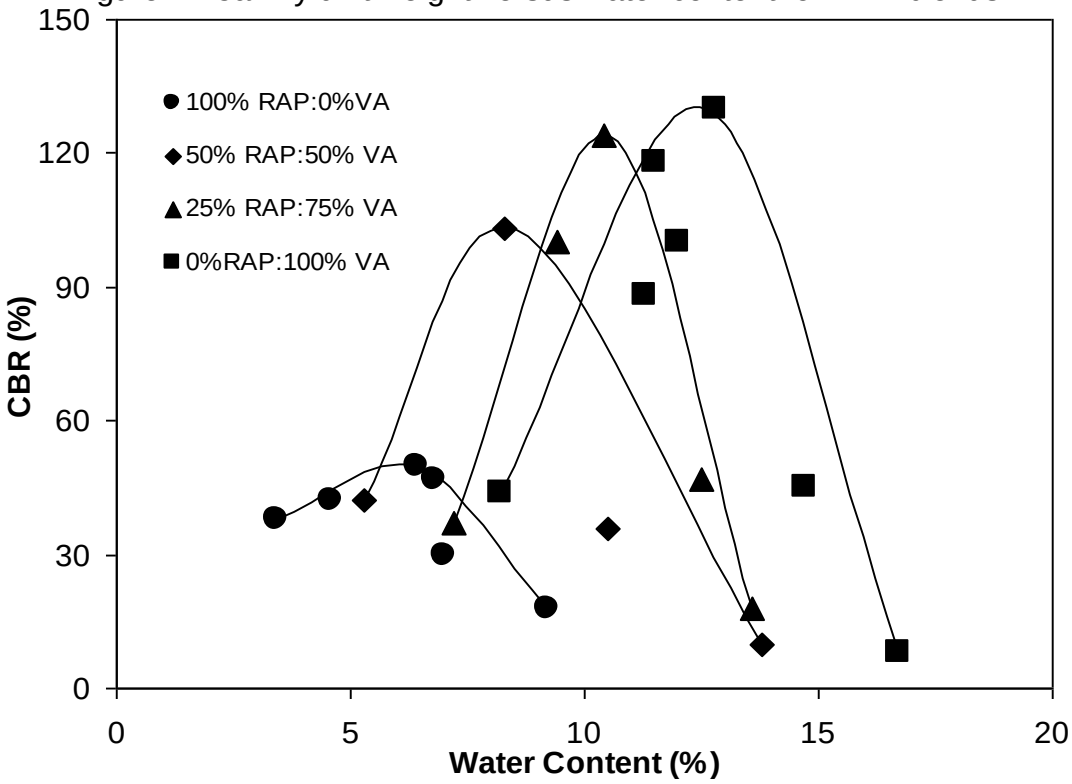

Figure 2-15b CBR versus water content for RAP blends

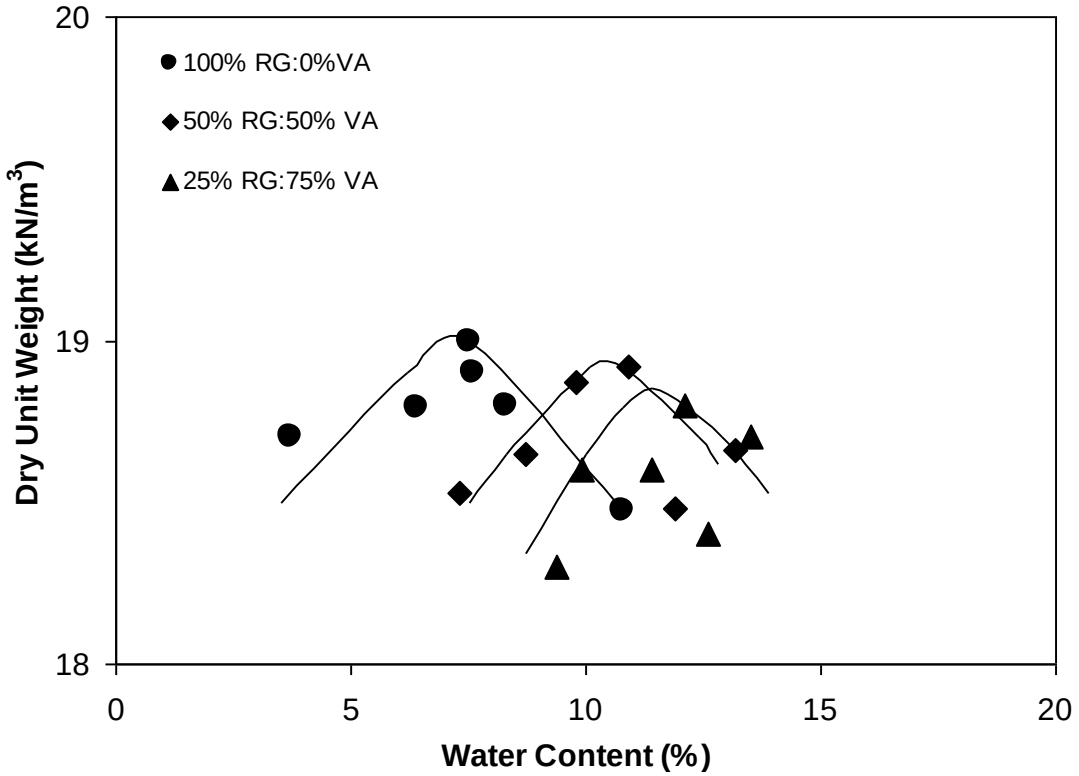

Figure 2-16a Dry unit weight versus water content for RG blends

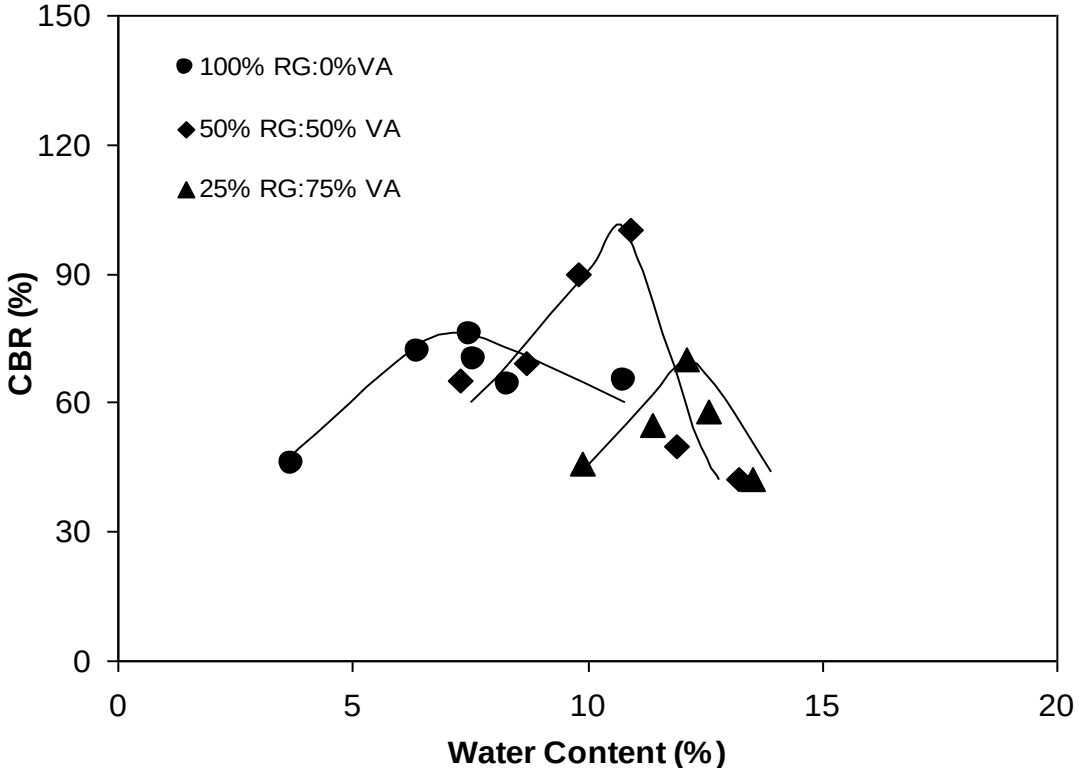

Figure 2-16b CBR versus water content for RG blends

The following observations are offered:

1) With increasing %RCA, the compaction curves of the RCA/VA blends shifted from top left to bottom right. This indicates an increase in the optimum water content and a decrease in the maximum dry unit weight with increasing %RCA.

2) With increasing %RAP, however, the compaction curves of the RAP/VA blends shifted from bottom right to top left. This indicates a decrease in the optimum water content and an increase in the maximum dry density with increasing %RAP.

3) For RG/VA blends, the trend in the variation of maximum dry unit weight and optimum water content with percent RG was not definitive with changes in %RG.

4) With increasing %RCA, the CBR curves of the RCA/VA blends shifted from bottom left to top right. This implies that the higher the RCA content, the higher the CBR probably due to (a) increasing Type A basalt with increasing %RCA and (b) more re-cementation upon soaking.

5) With increasing %RAP, however, the CBR curves of the RAP/VA blends shifted from top right to bottom left, which is opposite to RCA/VA. This implies that the higher the RAP content, the weaker is the material probably due to the fact that the asphalt caused the particles to deform within themselves more readily.

6) For RG/VA blends, there was also no clear trend in the variation of CBR with %RG.

2.9.4 EFFECTS OF GRADATION ON CBR OF RCA AND RAP

The effects of varying gradation on the CBR of RCA and RAP were studied. RG was not studied because there was insufficient coarse RG aggregate (9.5 mm minus) to constitute a base course gradation. A comparison of the CBRs was made using HDOT's embankment fill and base course gradations (Figure 2-17).

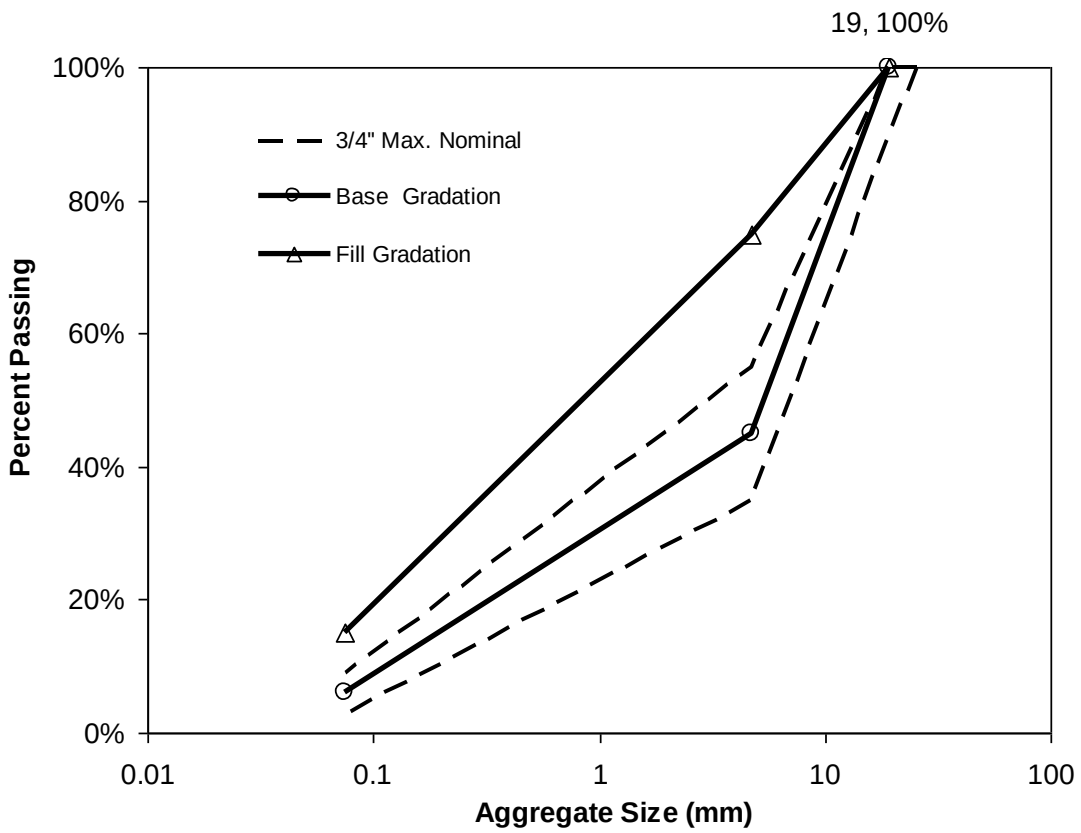

Figure 2-17 Gradations for CBR Test

The coefficients of uniformity of the base course and fill are 35 and 33, respectively, while the coefficients of curvature are 1.9 and 0.49, respectively. The percent fines for the base course and fill are 6% and 15%, respectively.

Thus, the Unified Soil Classification System (USCS) symbols are GW – GM (well graded gravel with silt and sand) for the base course and SM (silty sand with gravel) for the fill. Based on the AASHTO classification system, the base course and fill both fall into the A-1-a category.

The compaction and CBR curves for RCA and RAP are shown in Figures 2-18 and 2-19, respectively. For RCA, the base course compaction curve lies above and to the left of that for the fill, while that for RAP lies below and to the left. For both RCA and RAP, the embankment fill gradation have higher CBRs than the base course gradation. These results are somewhat surprising but may be explained as follows:

1) For RCA, the base course gradation is denser than the fill gradation. This seems logical. However, it can only be theorized that (a) the finer, fill-gradation CBRs are higher due to increased fines, and hence, increased cementation after 4 days of soaking; and (b) the base course CBRs are lower because of crushing of the brittle cement paste, especially if the paste is thick.

2) The compaction curve for RAP having a base course gradation lying below that of the fill is somewhat surprising but may be explained as follows: the asphalt-coated particles slip into a denser configuration quite readily with smaller particles being able to do this more so than coarser ones. Since the base course contains more coarse particles, this slippage cannot occur so readily leading to lower dry unit weights and lower CBRs in the base course gradation relative to the fill gradation.

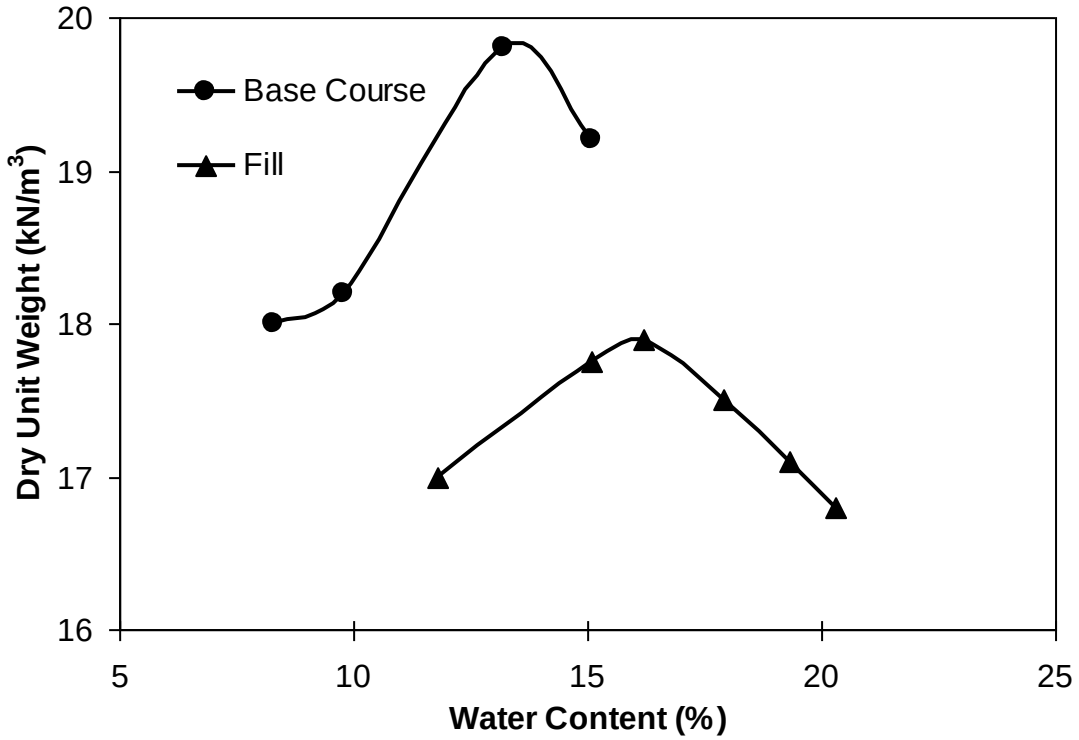

Figure 2-18a Effect of gradation on RCA compaction curve

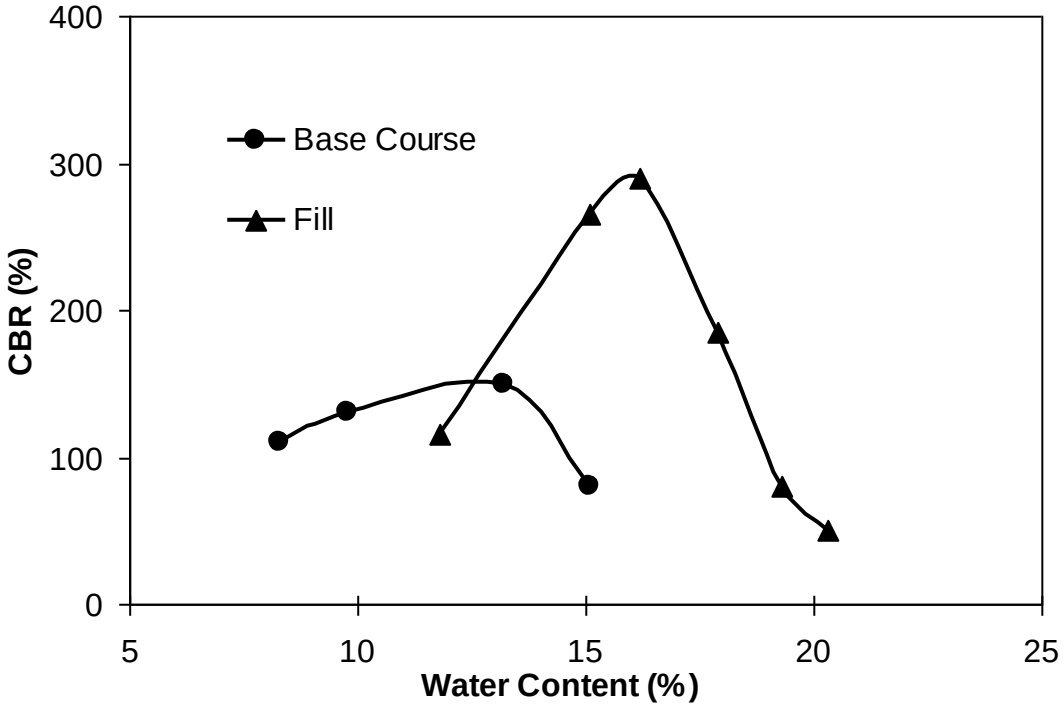

Figure 2-18b Effect of gradation on RCA CBR strength

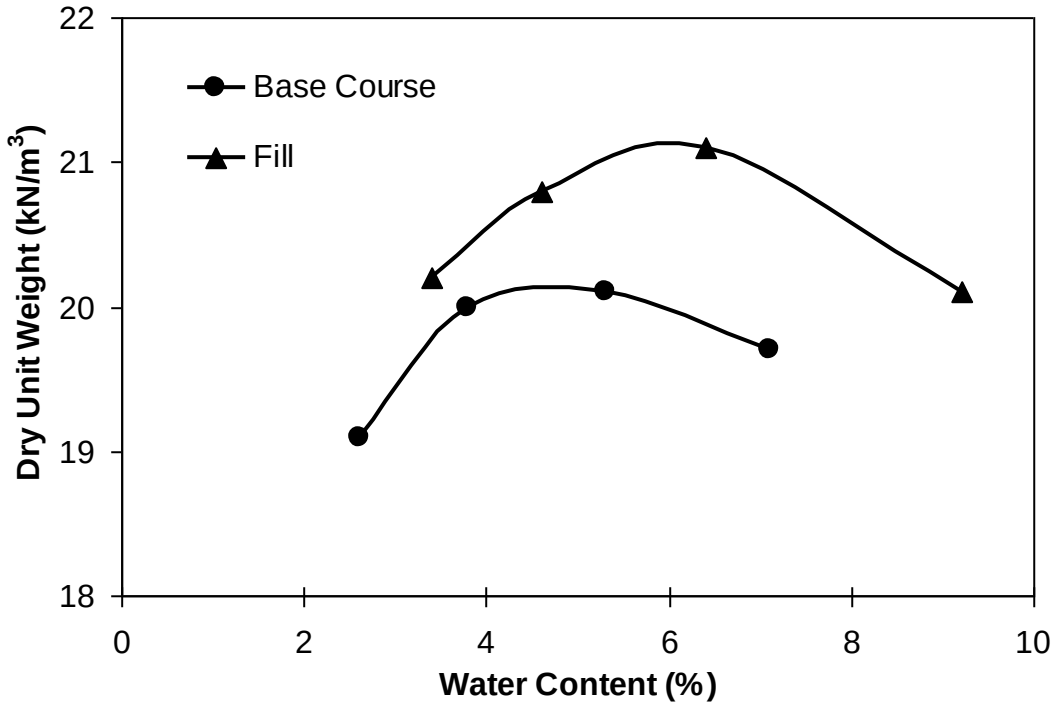

Figure 2-19a Effect of gradation on RAP compaction curve

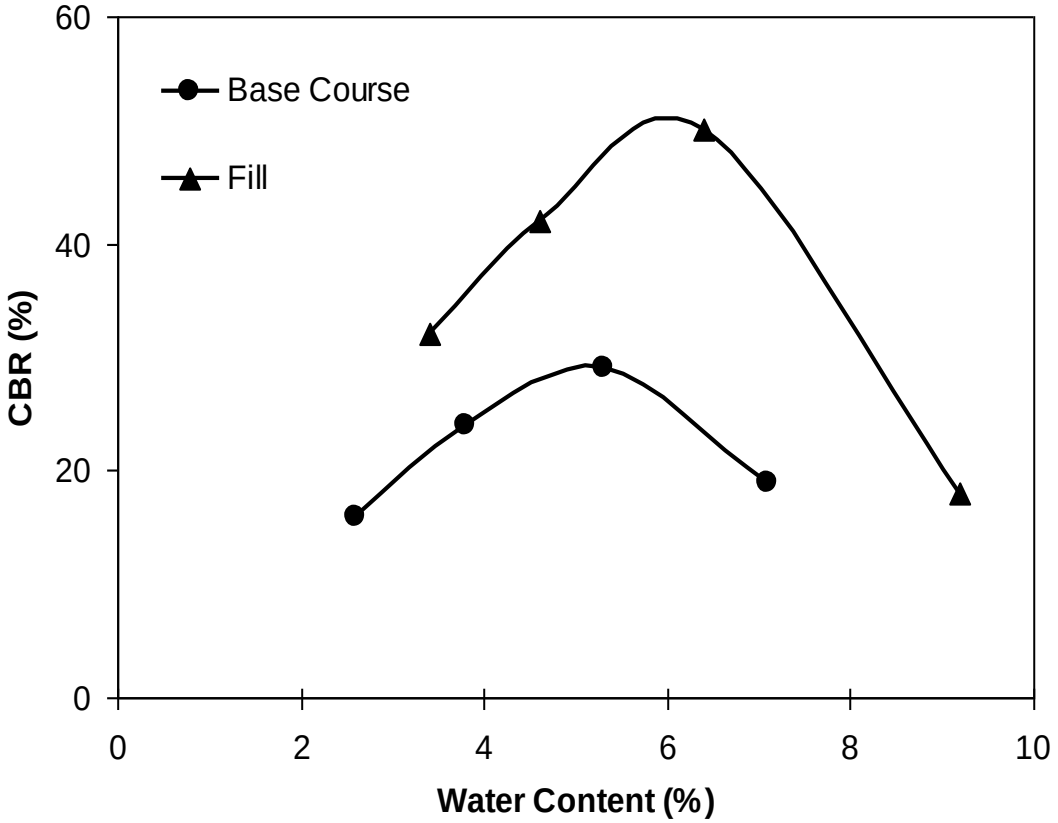

Figure 2-19b Effect of gradation on RAP CBR strength

2.9.5 CBR SUMMARY AND CONCLUSIONS

CBR tests were performed on three recycled materials, a basaltic VA, and their blends having gradations that meet HDOT's embankment fill gradations. The effects of varying gradations on CBRs were also studied for RCA and RAP, wherein the CBRs of the fill and base course gradations were compared. The following conclusions are offered:

- With all materials having the embankment fill gradation, RAP had the lowest optimum water content and the highest maximum dry unit weight, while RCA had just the opposite. VA and RG have comparable dry unit weights but different optimum water contents. The optimum water contents of RAP and RG, materials with very low absorptions, are similar but lower than those for VA and RCA.

- With all materials having the embankment fill gradation, the maximum CBR occurred at the optimum water content and maximum dry unit weight. At optimum, RCA had the highest CBR and RAP the lowest. VA is weaker than RCA but stronger than RG.

- With all materials having the embankment fill gradation, varying the water content had a small effect on the CBR for RAP and RG, but the effect was significant for VA and RCA.

- With all materials having the embankment fill gradation, there was very little change in the gradation for RG after CBR testing; the VA was finer after testing suggesting that some particle crushing occurred; there

was scatter on both sides of the target test gradation for RCA and RAP. It is not surprising for the gradations to be finer after testing. Reasons why some of the gradations became coarser after testing can be explained as follows. With RCA, some of the particles may have re-cemented together after soaking and testing. As for RAP, this may be due to the fact that the asphalt caused the particles to stick together during compaction and CBR testing.

- With increasing %RCA, the RCA/VA blends showed an increase in the optimum water content and a decrease in the maximum dry unit weight. RAP/VA blends showed the opposite trend. For RG/VA blends, the trend was not clear.

- The higher the RCA content, the stronger the material (higher CBR) probably due to more Type A basalt present and more re-cementation upon soaking; the higher the RAP content, the weaker the material probably due to the fact that the asphalt caused the particles to deform within themselves more readily; for RG/VA blends, there was no clear trend in the variation of CBR with %RG.

- The CBR of RCA is lower for the base course gradation than for the embankment fill gradation. This is not intuitive. It can only be theorized that (a) the finer, fill-gradation CBRs are higher due to an increase in fines, and hence, increased re-cementation after 4 days of

soaking; (b) the base course CBRs are lower because of crushing of the brittle cement paste, especially if the paste is thick..

- The CBR of RAP is lower for the base course gradation than for the embankment fill gradation. This can be explained as follows: the embankment fill gradation samples have very high densities due to the ability of the asphalt-coated particles to slip into a denser configuration. This deformation is more pronounced in the fill gradation because smaller particles are more able to slip into a denser configuration than coarser ones. Since the base course contains more coarse particles, this slippage cannot occur so readily leading to lower dry unit weights and lower CBRs in the base course gradation relative to the fill gradation.

2.10 RESILIENT MODULUS

This section presents the results of resilient modulus (M_r) testing on VA, RAP, RCA, 50% RAP:50% VA and 50% RCA:50% VA, all having gradations that mostly conform to the State of Hawaii Department of Transportation's (HDOT) base course gradation. In addition, one blend of VA with RG was tested (30% RG:70% VA). Because the RG was crushed very fine (9.5 mm minus), this ratio had to be utilized so that the blend could still meet HDOT's base course gradation requirements.

2.10.1 LITERATURE REVIEW

2.10.1.1 Use of M_r in Pavement Design

The concept of M_r was originally introduced by Seed et al. (1962). M_r provides a measure of the stiffness of the soil under confinement and repeated loading. It is defined as the deviator stress (σ_d) divided by the recoverable axial strain (ε_r) and is usually obtained from repeated load cyclic triaxial tests. It is a necessary and important input parameter required in the Mechanistic-Empirical Pavement Design Guide or MEPDG (ARA Inc. 2004). The MEPDG's philosophy is that the level of engineering effort to obtain M_r should be consistent with the relative importance, size and cost of the design project. In light of this, the material stiffness characterization may fall into one of the following three input levels. Level 1 represents the highest reliability where the M_r is measured directly through testing. In Level 2, the M_r is estimated from correlations with common soil parameters. In Level 3, the M_r

is estimated based on just the material classification. Clearly, increasing levels have successively lower reliabilities.

In National Cooperative Highway Research Program (NCHRP) Synthesis 382, Puppala (2008) summarized two nationwide surveys with input from DOT engineers in the materials/geotechnical division and in pavement design. The surveys revealed the state of practice for determining M_r of bases and subgrades. It was reported that overall satisfaction in the use of M_r for pavement design is low mainly attributable to the following: 1) constant modification of test procedures (in chronological order AASHTO T274-82, AASHTO T292-91, AASHTO T294-92, Long Term Pavement Performance (LTPP) Protocol P46-96, NCHRP 1-28 1997, AASHTO T307-99, AASHTO T307-03, and NCHRP 1-28A, 2003), 2) complicated laboratory or field test procedures and correlations required to determine M_r, and 3) design-related issues. Other pertinent survey findings are cited below.

Of the 41 respondents from the 50 state DOTs, 22 use M_r testing in routine pavement design. 12 of the 41 respondents use laboratory methods to determine M_r, with 9 using Repeated Load Triaxial (RLT) tests. With respect to RLT tests, four follow the AASHTO T-307 procedure, two the NCHRP 1-28A harmonized procedure, and the remainder the AASHTO T-294, LTTP TP-46 or a modified M_r test method. Problems relating to laboratory M_r testing, according to the respondents, are summarized in Figure 2-20.

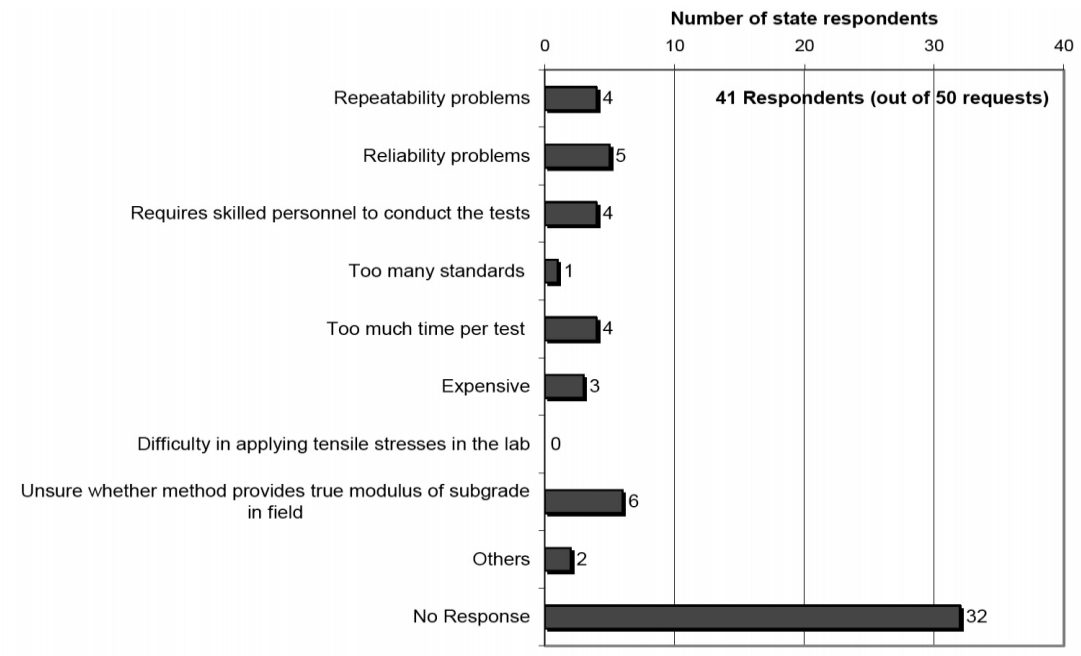

Figure 2-20 Problems related to laboratory M_r test (Puppala 2008)

Direct correlations between M_r and other soil properties (e.g., CBR or R-value) were used by 6 respondents for unbound bases (Figure 2-21). None utilize correlations between M_r and stress levels in the unbound bases where the model (k_i) parameters are regressed with common soil properties.

As for the reliability of correlations between M_r and common material properties, 8 agencies characterized the level of reliability of the correlations for unbound bases as *fair*, and only 3 noted as *very good* to *good*. "Most DOTs did not reply to this question, implying that they do not use correlations for moduli predictions" (Puppala 2008).

Puppala (2008) observed that reported M_r values of unbound granular base and subbase ranged from 10 to 45 ksi (about 70 to 310 MPa).

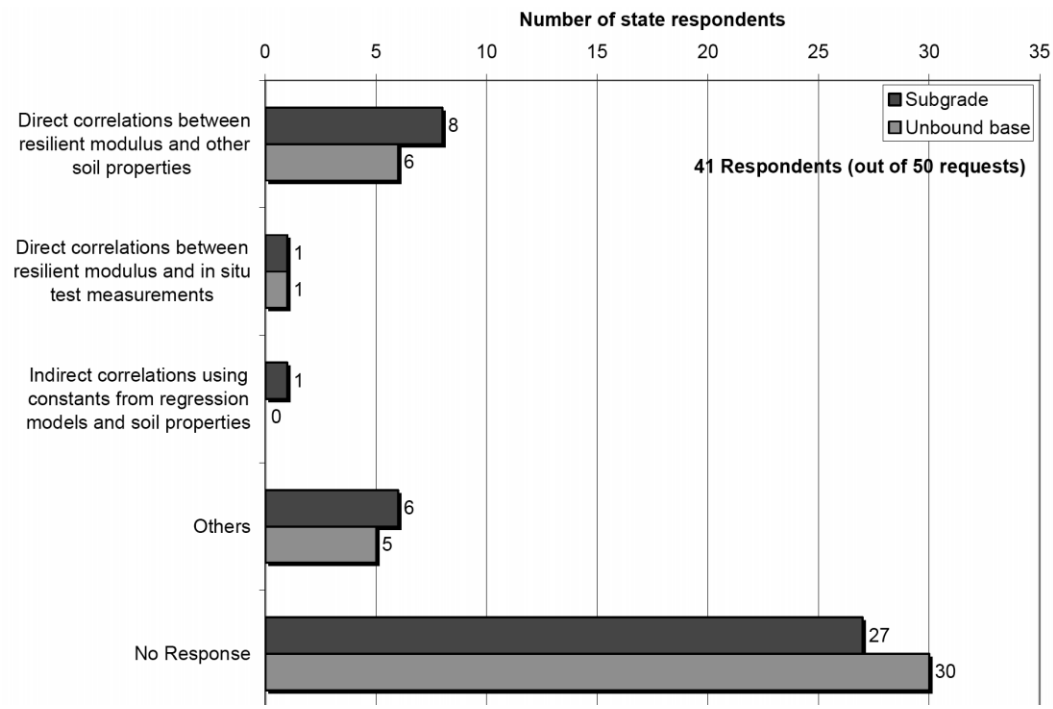

Figure 2-21 Types of correlations used for predicting M_r by the various state DOTs (Puppala 2008)

In the State of Hawaii, pavement design is mainly based on R-value. Although M_r is not currently used in pavement design, it may be in the foreseeable future.

2.10.1.2 Factors Influencing M_r of Unbound Granular Material

Li and Selig (1994) identified three factors that influence M_r: stress state, soil type/characteristics, and soil physical state. Hicks (1970) and Hicks and Monismith (1971) showed that M_r increases with increasing confining stress or bulk stress. For granular materials, it is common for M_r to increase with increasing deviator stress, implying a strain hardening response, whereas cohesive soils typically exhibit a strain softening behavior. Uthus (2007)

concluded that in granular materials, the effect of confining stress overwhelms that of the deviator stress.

M_r of geomaterials decreases as the moisture content increases. Moisture has two separate effects (Christopher et al., 2006). First, it affects the matric suction which in turn affects the effective stress and stiffness. Second, it can affect the cementation between soil particles. M_r also decreases with decreasing dry density or relative compaction.

2.10.1.3 M_r Test Procedures

Many M_r test protocols exist. In Europe, the European Committee for Standardization (CEN) EN 13286-7 (2004) is prevalent. In the USA, the most recent M_r test procedures are AASHTO T307 and NCHRP 1-28A (CTC & Associates LLC, 2008). Some of the major differences between T 307 and NCHRP 1-28A are highlighted below:

1) AASHTO T 307 divides the materials into two categories depending on function. Subgrade soils share the same test load sequence irrespective of whether the material is cohesive or cohesionless. Base/subbase materials have a separate test load sequence. NCHRP 1-28A specifies three separate materials by gradation. Different test load sequences exist for each of the three material categories.

2) Test load sequences - In AASHTO T 307, the large deviator stresses are applied to the sample early on in the test. In NCHRP 1-28A, the sample

experiences the largest deviator stress towards the end of the test and so it has the advantage of not prematurely failing weaker samples.

3) Placement of load cells and LVDTs - AASHTO T 307 specifies external load cell and LVDTs, while NCHRP 1-28A specifies internal load cell and LVDTs.

4) Conditioning - AASHTO T307 requires between 500 and 1000 repetitions of the conditioning deviator stress. If the sample height is still decreasing after 500 cycles, the number of cycles should be increased to 1000. In NCHRP 1-28A, 1000 load repetitions are required.

2.10.1.4 M_r Models

Models for estimating M_r are usually expressed as a function of the stress state. The most general form of a M_r model is the three-parameter model, which can be written as follows (Ooi et al., 2004):

$$M_r = k_1 p_a [f(c)]^{k2} [g(s)]^{k3} \qquad (2.1)$$

where $f(c)$ is a function for confinement, $g(s)$ is a function for shear and k_1, k_2 and k_3 are model constants. In this equation, the function for confinement can be expressed in terms of the minor principal stress (σ_3), bulk stress ($\theta = \sigma_1 + \sigma_2 + \sigma_3$), or octahedral normal stress (also known as mean confining stress, $\sigma_{oct} = p = \theta/3$), where σ_1, σ_2 and σ_3 are the major, intermediate and minor principal stresses, respectively. The function for shear can be expressed in terms of the deviator stress, σ_d or q, or octahedral shear stress

($\tau_{oct} = \sqrt{2}q/3$). This three-parameter model is versatile in that it applies to all soils and aggregates. Several variations of the M_r models exist, some of which are summarized in Table 2-6.

The K-θ model proposed by Seed et al. (1967) has been widely used in the past for modeling M_r of granular materials. Two limitations of this model include: (1) it is not dimensionally correct. The M_r and bulk stress can be normalized by the atmospheric pressure prior to raising the latter to a power; (2) multiple stress conditions can give the same modulus. For example, combinations of low confining stress and high deviator stress can result in the same bulk stress and hence, the same M_r, as high confining stress and low deviator stress.

A total of 6 M_r models may arise based on the three types of confinement and two types of shear stress combinations in Equation 2.1. When using these 6 models for a soil in an isotropic stress state, $M_r = 0$ when $k_3 > 0$ and $M_r \rightarrow \infty$ when $k_3 < 0$. By adding *1* to the normalized octahedral shear stress in the function for shear yields the MEPDG model.

Table 2-6 Summary of available Mr models

Author	Equation	Remarks
Biarez (1961)	$E = K(\sigma_m)^n$	E = Secant modulus K, n are empirical constants
Dunlap (1963)	$M_r = k_1 p_a \left(\frac{\sigma_3}{p_a}\right)^{k_2}$	
Seed et al. (1967)	$M_r = k_1(\theta)^{k_2}$	K-θ model
Seed et al. (1967)	$M_r = k_1 p_a \left(\frac{\theta}{p_a}\right)^{k_2}$	Primarily for granular soils.
Shackel (1973)	$M_r = k_1 \sigma_{oct}^{k_2} \tau_{oct}^{k_3}$	
Uzan (1985)	$M_r = k_1 p_a \left(\frac{\theta}{p_a}\right)^{k_2} \left(\frac{\sigma_d}{p_a}\right)^{k_3}$	Normalized Shackel (1973) model
Witczak and Uzan (1988)	$M_r = k_1 p_a \left(\frac{\theta}{p_a}\right)^{k_2} \left(\frac{\tau_{oct}}{p_a}\right)^{k_3}$	Adopted in the 1993 AASHTO design guide
Pezo (1993)	$M_r = k_1 p_a \left(\frac{\sigma_3}{p_a}\right)^{k_2} \left(\frac{\sigma_d}{p_a}\right)^{k_3}$	
Kolisoja (1997)	$M_r = A(n_{\max} - n) p_a \left(\frac{\theta}{p_a}\right)^{0.5}$	Effect of density included n = porosity of the aggregate
Ni et al. (2002)	$M_r = k_1 p_a \left(1+\frac{\sigma_3}{p_a}\right)^{k_2} \left(1+\frac{\sigma_d}{p_a}\right)^{k_3}$	
Ooi et al. (2004)	$M_r = k_1 p_a \left(1+\frac{\theta}{p_a}\right)^{k_2} \left(1+\frac{\sigma_d}{p_a}\right)^{k_3}$	
Ooi et al. (2004)	$M_r = k_1 p_a \left(1+\frac{\theta}{p_a}\right)^{k_2} \left(1+\frac{\tau_{oct}}{p_a}\right)^{k_3}$	
ARA, Inc. (2004)	$M_r = k_1 p_a \left(\frac{\theta}{p_a}\right)^{k_2} \left(1+\frac{\tau_{oct}}{p_a}\right)^{k_3}$	Adopted in the MEPDG (ARA Inc., 2004) and the NCHRP 1-28A procedure
Gupta et al. (2007)	$M_r = k_1 p_a \left(\frac{\sigma_b - 3k_6}{p_a}\right)^{k_2} \left(k_7 + \frac{\tau_{oct}}{p_a}\right)^{k_3} + \alpha_1 (u_a - u_w)^{\beta_1}$	$\mu_a - \mu_w$:matric suction α_1, β_1: regression constants

Notes: k_1, k_2, k_3, k_6 and k_7 are model constants
p_a = atmospheric pressure =14.7 psi = 101.3 kPa
σ_1, σ_2 and σ_3 are the major, intermediate and minor principal stresses, respectively
θ = bulk stress = $\sigma_1 + \sigma_2 + \sigma_3$
σ_m = mean normal stress = $\theta/3 = \sigma_{oct} = p$
σ_d = deviatoric stress = $\sigma_1 - \sigma_3 = q$
τ_{oct} = octahedral shear stress = $\frac{1}{3}[(\sigma_1 - \sigma_2)^2 + (\sigma_2 - \sigma_3)^2 + (\sigma_3 - \sigma_1)^2]^{1/2} = \sqrt{2}\sigma_d/3$.

Another generation of models can arise with *1* added to both the normalized confining and shear terms. This is reasonable because without adding unity to the normalized confining stress, a soil with no confinement will have a zero M_r. This is obviously not true. In addition, Ooi et al. (2004) showed that these models provide a superior fit to test data.

The M_r models can be extended by correlating the model constants k_i with basic soil parameters to take into account the effects of moisture, density, gradation and other factors on M_r. These correlations typically work well for the local soils that the models were developed for. Problems can arise when the correlations are applied to the same type of soils elsewhere (Wolfe and Butalia, 2004 and Malla and Joshi, 2006). This method of correlating the model constants k_i with basic soil parameters is mostly available for fine-grained soils and is rarely applied to coarse aggregates. This is probably because the M_r of bases and subbases are less sensitive to variations in water content and dry density than fine-grained soils.

2.10.1.5 Recent Studies on M_r of RCA and RAP

Based on a literature review, M_r of RCA and RAP have been studied by several researchers, some of which are summarized in Table 2-7. No study on M_r or permanent deformation of RG was found.

Table 2-7 M_r studies on RCA and RAP

Reference	Country	Recycled Material	Highlights from Study
Bennert et al. (2000)	USA	RCA and RAP	RAP and RCA all showed higher M_r than the dense-graded aggregate base course (DGABC) in New Jersey.
Nataatmadja and Tan (2001)	Australia	RCA	The original concrete compressive strength, the amount of soft material in the RCA, and the flakiness index of the RCA can significantly affect the M_r.
Molenaar and van Niekerk (2002)	Netherlands	RCA	Degree of compaction is the most important factor affecting M_r.
Blankenagel and Guthrie (2006)	USA	RCA	Both demolition and haul-back recycled concrete material had marked stiffening after a 7-day curing period.
Aurstad et al. (2006)	Norway	RCA	M_r of RCA is higher compared to gravel or crushed rock; M_r = 350 - 650 MPa with highest values for open-graded material.
Guthrie et al. (2007)	USA	RAP	M_r decreased when RAP content increased from 0 to 25 %. M_r then steadily increased as the RAP content increased from 25% to 100%.
Kim and Labuz (2007)	USA	RAP	M_r increased with an increase in confining pressure. There was little change in M_r with increasing deviator stress. Specimens with water contents at ~ 65% the value at optimum were stiffer than those at optimum regardless of confining pressure. Base materials with various RAP percentages performed similar to 100% virgin aggregate in terms of stiffness and strength.
Saeed (2008)	USA	RCA and RAP	The blends of RCA and VA, RAP and VA had lower stiffness due to the good performance of the VA selected; RAP and VA blends showed less water content susceptibility while the RCA and VA blends showed the opposite.

2.10.2 CHARACTERISTICS OF MATERIALS, TEST EQUIPMENT AND PROCEDURES

In this section, the gradation and compaction curves of the materials subjected to M_r testing are first described. This is followed by the test equipment and procedure.

2.10.2.1 Gradation and Compaction Curves

The gradations for the M_r test samples are shown in Figure 2-22. This gradation differs from the base course gradation used in the CBR tests (Figure 2-17) because of a lack of fines at this stage of the research. For the RG blend, because RG was crushed to 3/8'' minus, there was insufficient coarse RG aggregate to achieve the target gradation. Hence a finer gradation as shown in Figure 2-22 was used for the RG blend. According to Croney and Croney (1997), "the grading …… of crushed rock and crushed gravel have only a small influence on the modulus."

The moisture-density relationship for each material (Figures 2-23a to 2-23f) was determined using a 152-mm-diameter Proctor mold in accordance with AASHTO T180 Method D, wherein each sample was compacted using 5 lifts, and each lift received 56 blows from a 4.5-kg-hammer dropping 46 cm. It was difficult to obtain the dry unit weight (γ_d) and water content (w) wet of optimum for 4 of the 6 materials because these samples could not retain the moisture (water leaked from the bottom of the mold during compaction). For these materials, the values at optimum are interpreted as shown in Table 2-8. Water contents were measured by placing the entire mold and samples in the

oven at 110ºC for several days until the water content stabilized. For RAP, the oven temperature was set at 60ºC.

The specific gravities (G_s) in Figure 2-23 were calculated based on the specific gravities of the fine and coarse aggregate, and their percent composition in the blend as follows: G_s = (% fine + % coarse)/(% fine/$G_{s\ fine}$ + % coarse/$G_{s\ coarse}$) where $G_{s\ fine}$ and $G_{s\ coarse}$ are the apparent specific gravities of the fine and the coarse aggregate from Table 2-1. For the blends, the same methodology was used.

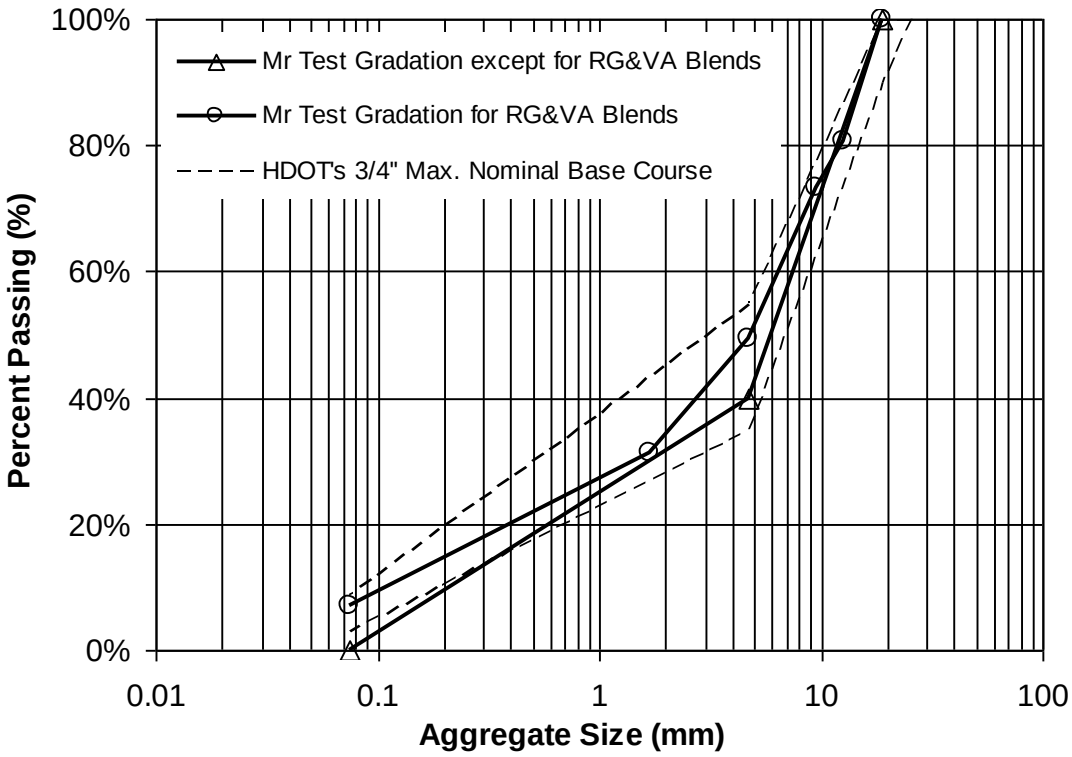

Figure 2-22 Sample gradation used for M_r test

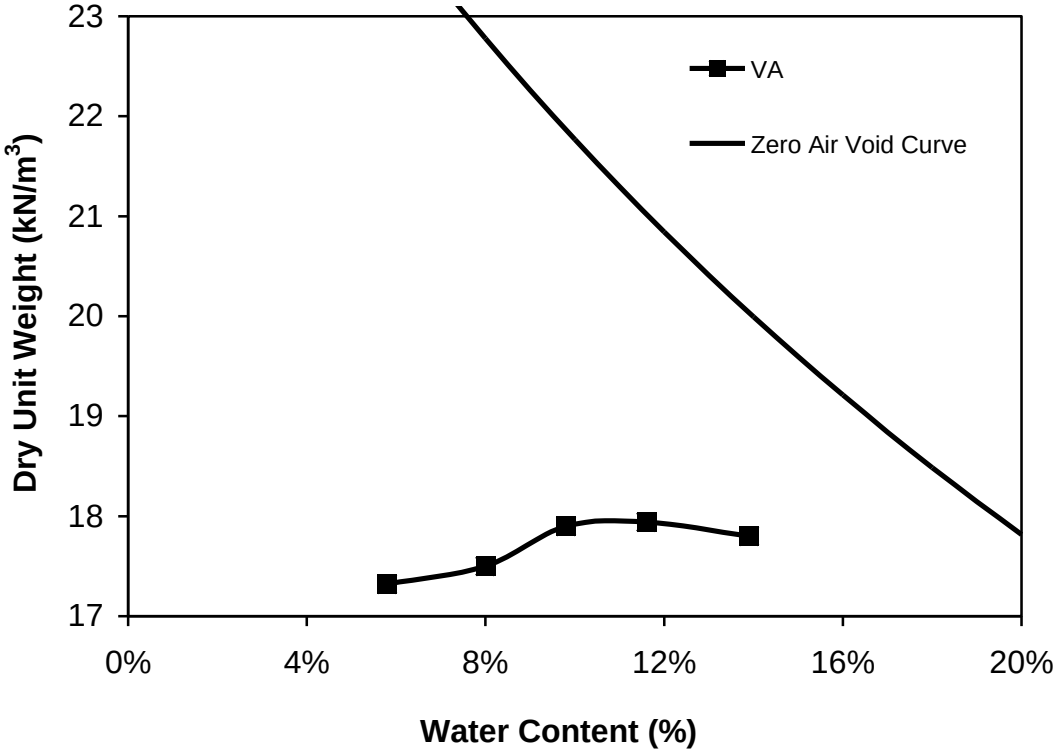

Figure 2-23a Compaction curve for VA (G_s = 2.85 for ZAV curve)

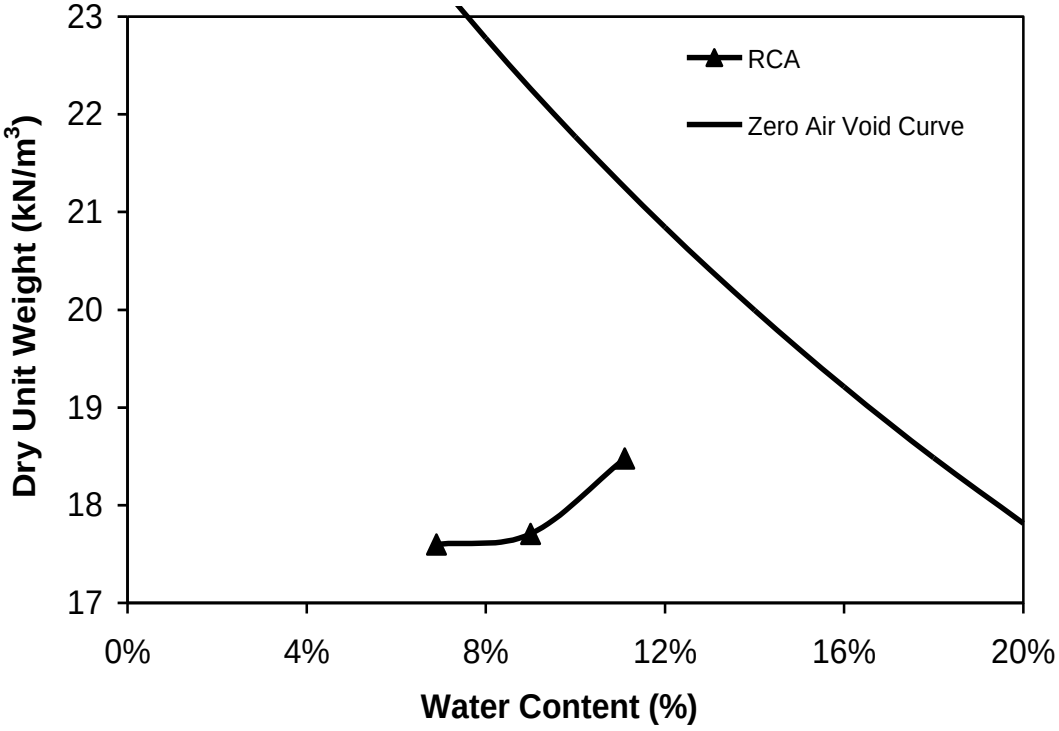

Figure 2-23b Compaction curve for RCA (G_s = 2.85 for ZAV curve)

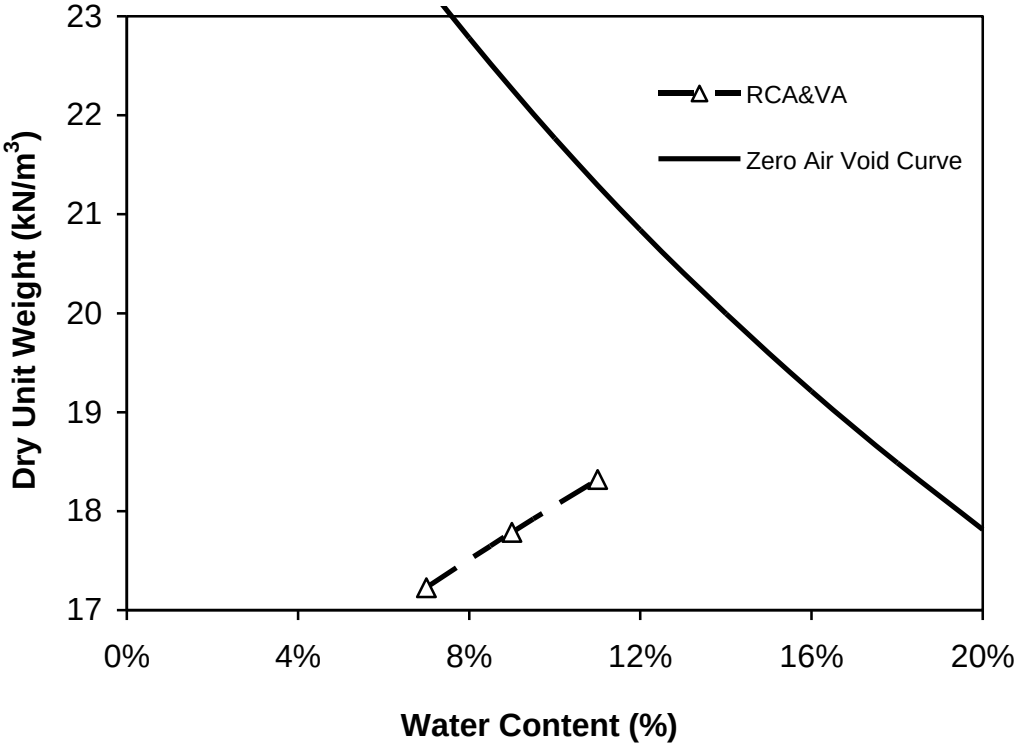

Figure 2-23c Compaction curve for RCA&VA (G_s = 2.85 for ZAV curve)

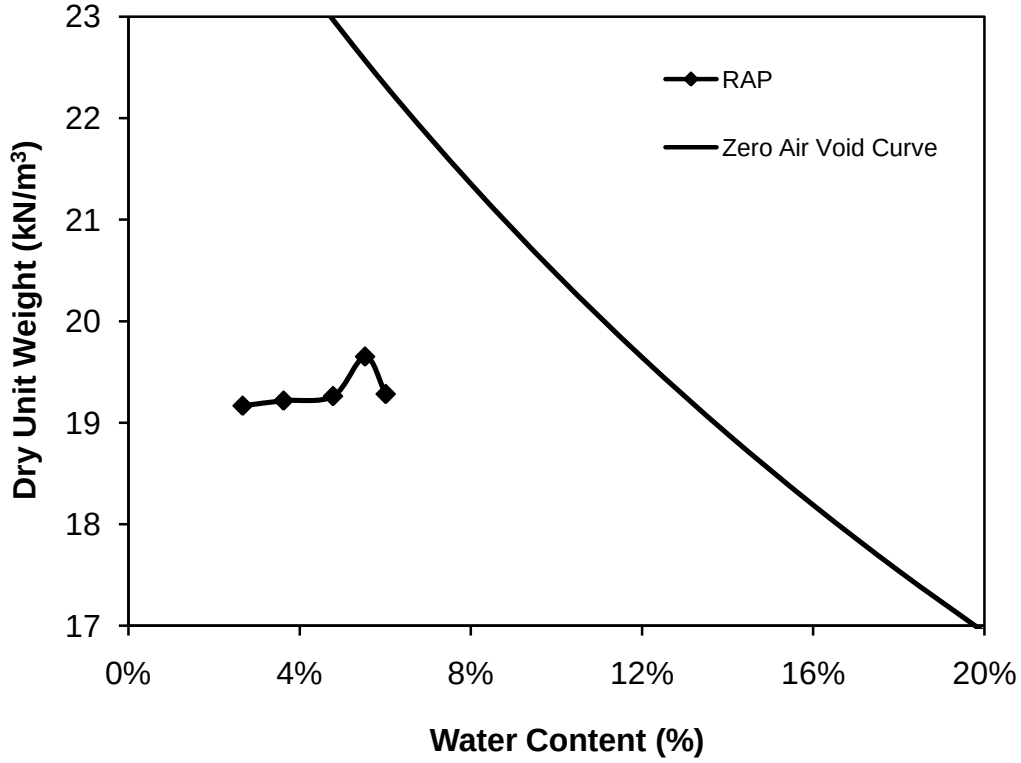

Figure 2-23d Compaction curve for RAP (G_s = 2.64 for ZAV curve)

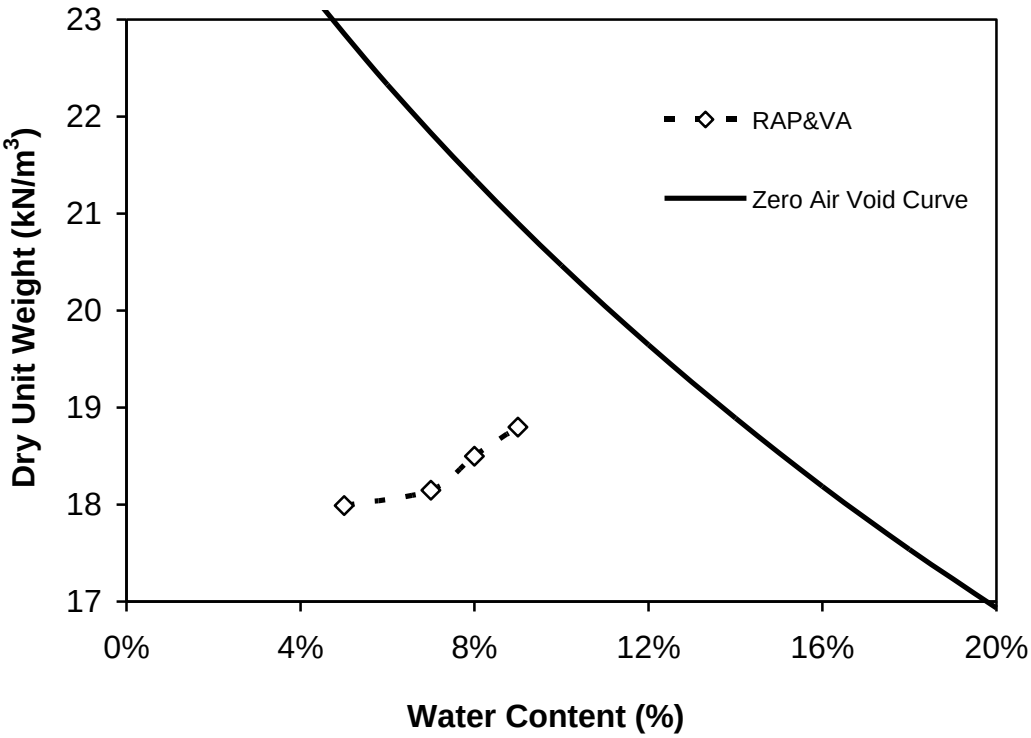

Figure 2-23e Compaction curve for RAP&VA (G_s = 2.74 for ZAV curve)

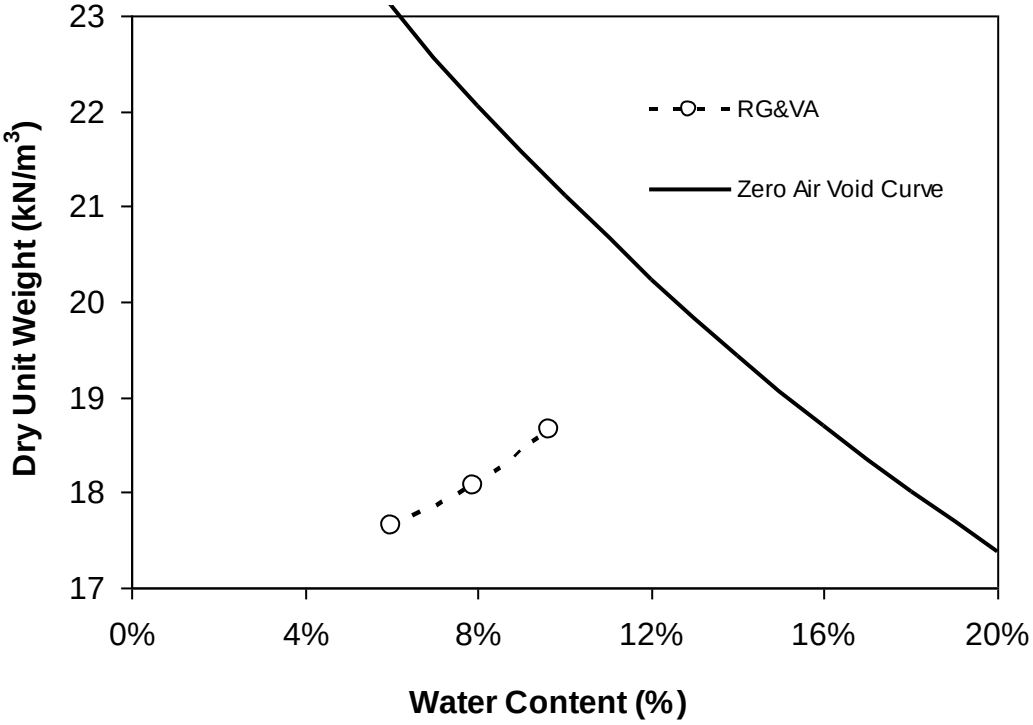

Figure 2-23f Compaction curve for RG&VA (G_s = 2.74 for ZAV curve)

Table 2-8 Water contents and dry densities of M_r test samples

Material	Target Water Content (%)	Water Content Before Test (%)	Water Content After Test (%)	Target Dry Density (kg/m^3)	Actual Dry Density (kg/m^3)
VA	8.8	8.7	8.4	1741	1743
	8.8	9.0	8.8	1801	1798
	8.8	9.5	8.4	1833	1821
	8.8	9.3	8.4	1833	1825
	10.8 (opt[1])	12.6	10.2	1741	1713
	10.8 (opt[1])	11.5	10.3	1833	1822
	12.8	14.0	11.2	1741	1723
	12.8	14.2	11.9	1822	1800
	12.8	13.2	11.3	1833	1827
RAP	4.5	4.3	4.2	1903	1907
	4.5	4.9	4.1	1903	1896
	4.5	5.5	4.5	2003	1984
	4.5	4.7	4.1	2003	1999
	5.5 (opt[1])	5.8	4.7	1903	1898
	5.5 (opt[1])	5.9	4.4	1903	1896
	5.5 (opt[1])	5.6	4.5	2003	2001
	5.5 (opt[1])	5.6	4.9	2003	2001
	6.5	6.7	5.4	1903	1899
	6.5	6.5	4.9	1903	1903
	6.5	5.8	4.8	2003	2016
	6.5	6.5	4.9	2003	2003
RAP&VA	7.0	7.5	6.5	1850	1841
	7.0	7.2	6.1	1850	1847
	7.0	7.3	6.5	1916	1911
	9.0 (opt[1])	9.7	7.7	1916	1904
	9.0 (opt[1])	9.6	7.7	1916	1906
	9.0 (opt[1])	9.3	7.5	2022	2017
	11.0	11.7	8.4	1916	1904
	11.0	11.6	8.5	2022	2011
RCA	9.1	9.4	8.6	1808	1803
	9.1	8.6	8.1	1884	1893
	11.1 (opt[1])	11.4	10.4	1808	1803
	11.1 (opt[1])	11.3	9.9	1884	1881
	13.1	14.7	11.3	1884	1858
RCA&VA	9.0	9.2	9.1	1813	1810
	9.0	9.2	9.0	1867	1864
	11.0 (opt[1])	11.3	9.9	1867	1862
	11.0 (opt[1])	11.4	10.0	1961	1954
	13.0	13.9	11.7	1961	1946
RG&VA	7.9	8.2	7.4	1841	1836
	9.6 (opt[1])	10.0	8.8	1901	1894
	9.6 (opt[1])	10.2	8.6	1901	1891
	9.6 (opt[1])	9.9	8.6	2028	2023
	9.6 (opt[1])	9.8	8.4	2028	2024
	11.0	11.4	9.8	1987	1980
	11.0	11.4	9.2	2028	2021
	13.0	14.1	9.5	2028	2008

Note1 opt = optimum water content corresponding to the interpreted maximum dry density

2.10.2.2 Sample Preparation

M_r test samples were prepared in accordance with AASHTO T307. Each sample was compacted using a vibratory hammer in a split mold with a target diameter and height of 100 mm and 203.2 mm, respectively. A total of 47 samples were tested. The sample target water contents and dry densities are shown in Table 2-8.

Steps to prepare the samples are as follows:

(1) Place a rubber membrane around the inside of the split mold with the aid of a vacuum. Place the split mold around the bottom platen on a concrete floor;

(2) Place a piece of filter paper on the top of the bottom platen;

(3) Add 1/6 of the required amount of moist aggregate into the split mold;

(4) Compact the aggregate using a vibratory hammer to the target depth;

(5) Repeat steps (3) and (4) 5 times until the desired total length of sample is reached;

(6) Place a piece of filter paper and top platen on top of the compacted sample;

(7) Apply a vacuum to the sample;

(8) Remove the split mold;

(9) Add a second membrane around the sample just in case the first membrane was punctured during compaction;

(10) Place sample, membranes and end platens in a triaxial test chamber and tighten the chamber tightly to the top and base of the triaxial cell using bolted steel rods with end threads;

(11) Align the triaxial chamber in the loading frame;

(12) Apply the desired confining pressure;

(13) Remove sample vacuum; and

(14) Perform M_r testing.

Figures 2-24 and 2-25 show some of the materials tested and the compaction apparatus, respectively.

Figure 2-24 Materials tested: RAP after M_r testing (top left), RG and VA blend after M_r testing (top right), 100% RCA before (bottom left) and after (bottom right) mixing with water but before M_r testing.

Figure 2-25 Sample preparation apparatus (left) and compaction density control (right)

2.10.2.3 M_r Test Procedure and Equipment

The two recent M_r test procedures are AASHTO T307 and NCHRP 1-28A. AASHTO T307 is less suited for weaker materials compared to NCHRP 1-28A. There are a total of 15 combinations of deviator and confining stresses in AASHTO T307 while there are 30 in NCHRP 1-28A. The AASHTO T307 test procedure was adopted because of the following:

1. the samples tested were not weak;
2. AASHTO T307 requires a shorter testing time; and
3. NCHRP 1-28A had not yet been adopted by AASHTO at the time these tests were conducted.

There are three stages in the M_r test:

1) conditioning - all samples were subjected to 500 cycles of a deviator stress of 95 kPa under a 105 kPa confining pressure to better simulate the events occurring between compaction and traffic loading and to reduce the effects of improper contact between the top platen and the specimen;

2) measuring stresses and strains to determine M_r – apply 100 cycles at each combination of confining and deviator stresses. M_r is calculated as the average of the ratios of the deviator stress to resilient strain for the 96th through 100th cycle; and

3) quick shear testing – shear the sample drained at a strain rate of 1% per minute to measure the failure deviator stress.

All M_r tests were run using IPC Global Limited's Universal Testing System 25 (de Vos, 2004) consisting of a hydraulic axial stress and a pneumatic confining stress loading systems, a computer-controlled data acquisition system (CDAS) and a personal computer. The CDAS provides both the servo-feedback loading control electronics, and the transducer data acquisition and timing functionality. The testing software is the UTS009 *Unbound Materials Resilient Modulus Test Software* by IPC Global Limited. The system is capable of applying repeated cycles of a haversine-shaped load pulse of 0.1s with a 0.9s rest period. The system has two external sample LVDTs that provide the sample deformation, and a system LVDT that is attached to the actuator that provides the system deformation.

Deformations measured by the system LVDT are always larger than those measured by sample LVDTs 1 and 2 since the system LVDT also measures system compliance in addition to sample deformation. Therefore, it is important to use the sample LVDTs when computing the M_r.

Figure 2-26, 2-27 and 2-28 show a sample ready for testing and the LVDT setup, the CDAS and a sample after M_r and quick shear testing, respectively.

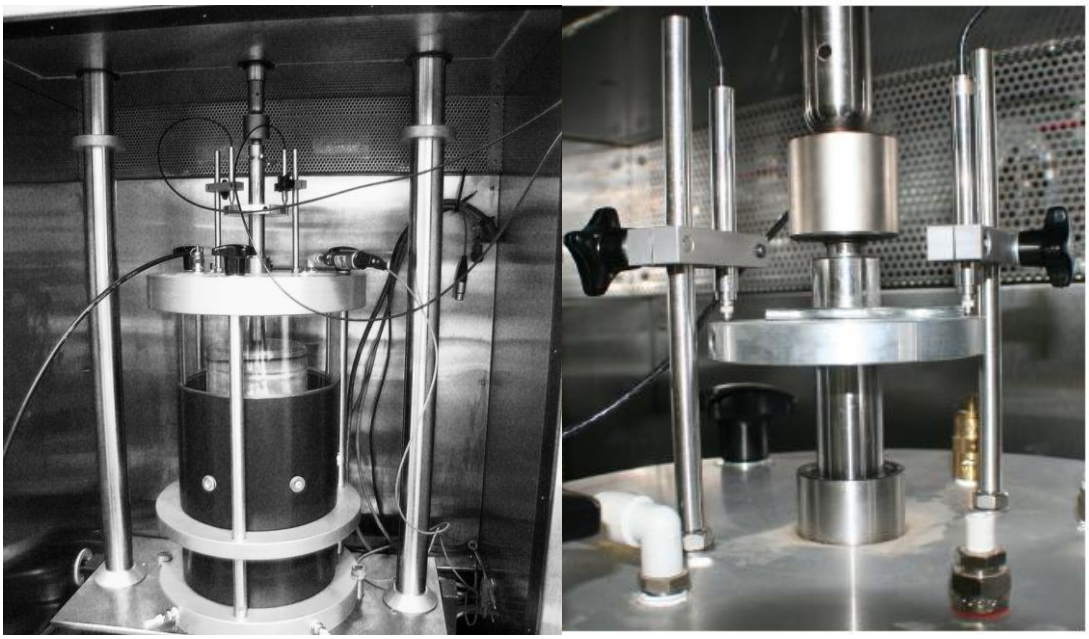

Figure 2-26 Sample ready for testing (left) and the LVDT setup (right)

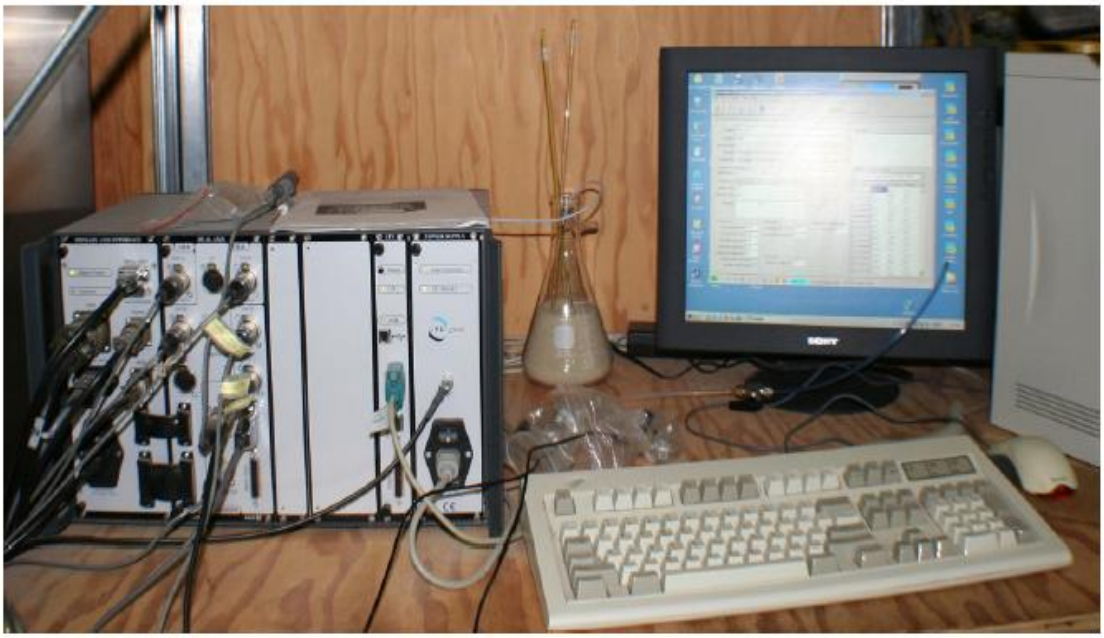

Figure 2-27 Computer-controlled data acquisition system

Figure 2-28 Sample after M_r and quick shear testing

Quality Control

Quality control on the following was made throughout the entire test program:

1) Dry density – The density should be within 3 percent of the target density per AASHTO T307. All samples met this requirement (Table 2-8). The critical measurement for controlling density is the sample volume since the weight can be accurately determined with a scale. Sample heights in the split mold were controlled using markings on the compaction rod (Figure 2-25). The various taped marks correspond to the desired compacted lift heights.

2) Water content - The water content should be within 1 percent of the target water content per AASHTO T307. The majority of the samples met this

requirement (Table 2-8). The water contents were measured before and after testing. The values after testing were always smaller because drainage was allowed during testing. The difference is more significant for the wetter samples.

3) Deformation measurements - The resilient deformation used for calculating M_r is the average measured by LVDTs 1 and 2. Their ratios were checked to see if they were within the range of 0.95 - 1.05. Satisfying this ratio is an indication of minimal eccentric loading on the sample during testing. All samples met this requirement.

2.10.3 FACTORS AFFECTING M_r

Observations on the various factors influencing M_r are reported in this section. The reasonableness of these observations can be considered as part of the quality control process.

2.10.3.1 Effect of Stress Level on M_r

The effect of confining and deviator stresses on the M_r of VA is presented in Figure 2-29a. Increases in both the confining and deviator stresses lead to higher M_r. It was observed that the rate of increase in M_r with increasing stress level is material specific (e.g., compare VA - Figure 2-29a with RG&VA - Figure 2-29b).

One advantage of using bulk stress only instead of separately using confining and deviator stresses in M_r models is its simplicity (only two parameters are required in the K-θ model). Note that $\theta = \sigma_d + 3\sigma_3$. Therefore, the K-$\theta$ model

assumes that the effect of increasing the confining stress by one unit of stress on M_r is identical to the effect of increasing the deviator stress by three units of stress, which is not always true. This is the main disadvantage of using bulk stress alone to model M_r.

2.10.3.2 Effect of Water Content on M_r

The effect of water content on M_r of VA is shown in Figure 2-30 for samples having similar dry densities. As the water content increased, the stiffness decreased for most materials, with only a few exceptions. Water content did not have a strong influence on M_r of RAP. This may be attributable to the fact that water content did not have a great effect on the compaction curve (Figure 2-23d).

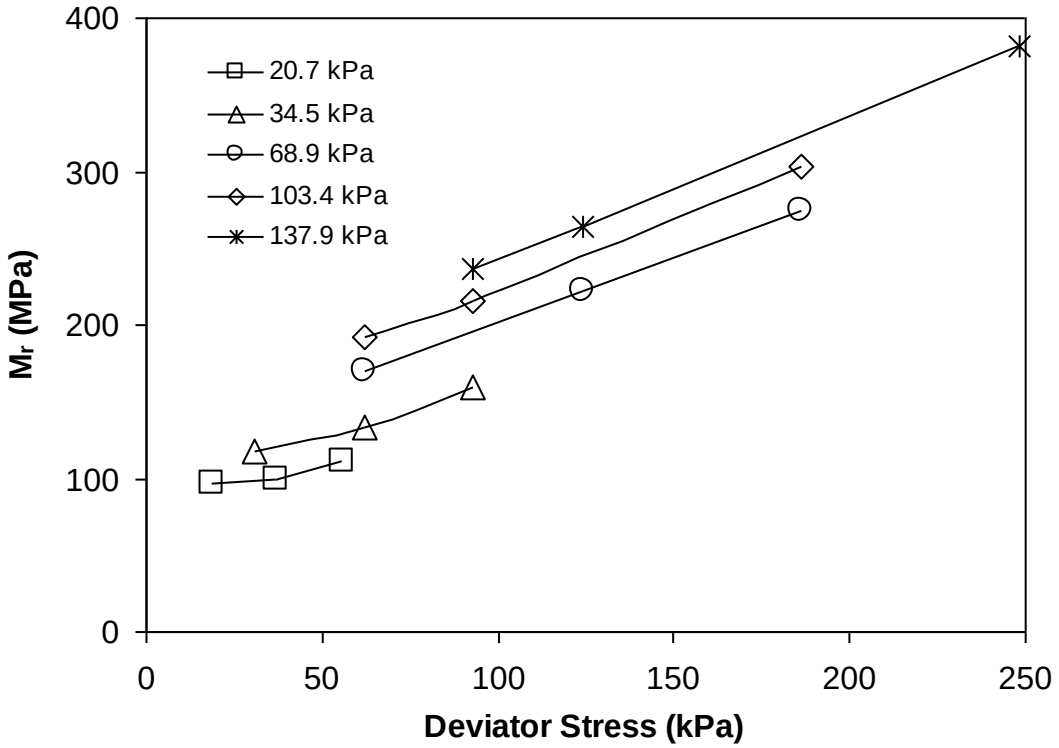

Figure 2-29a M_r as a function of stress level - VA (Legend - confining stress)

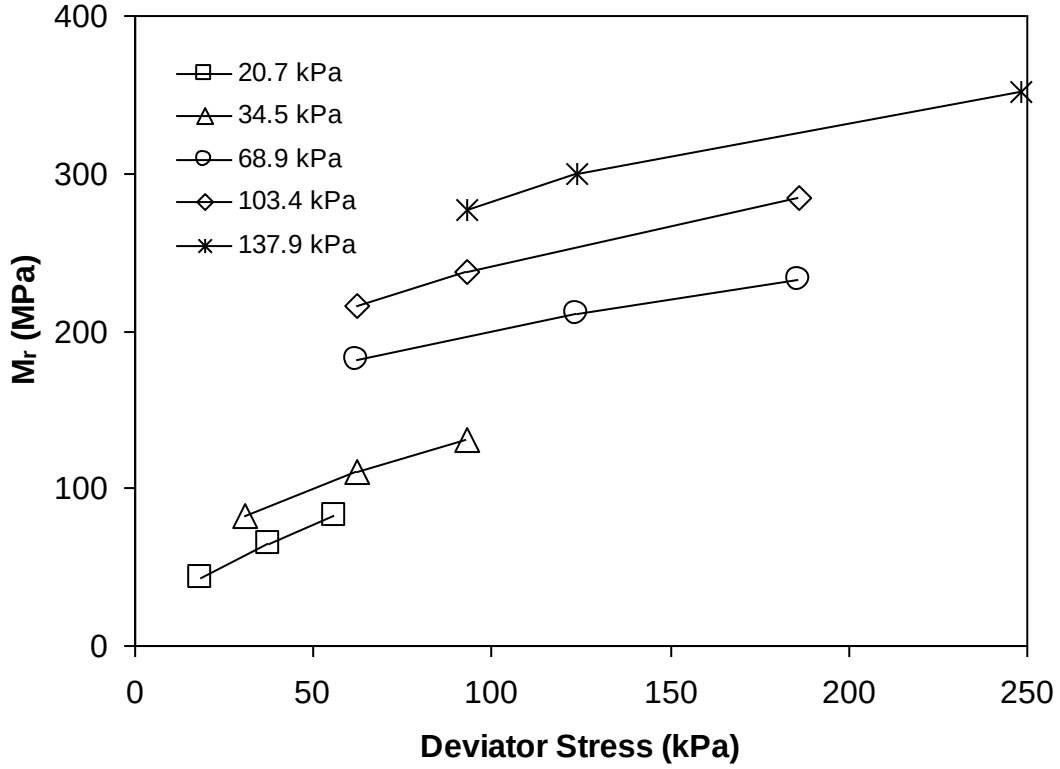

Figure 2-29b M_r as a function of stress level - RG&VA (Legend - confining stress)

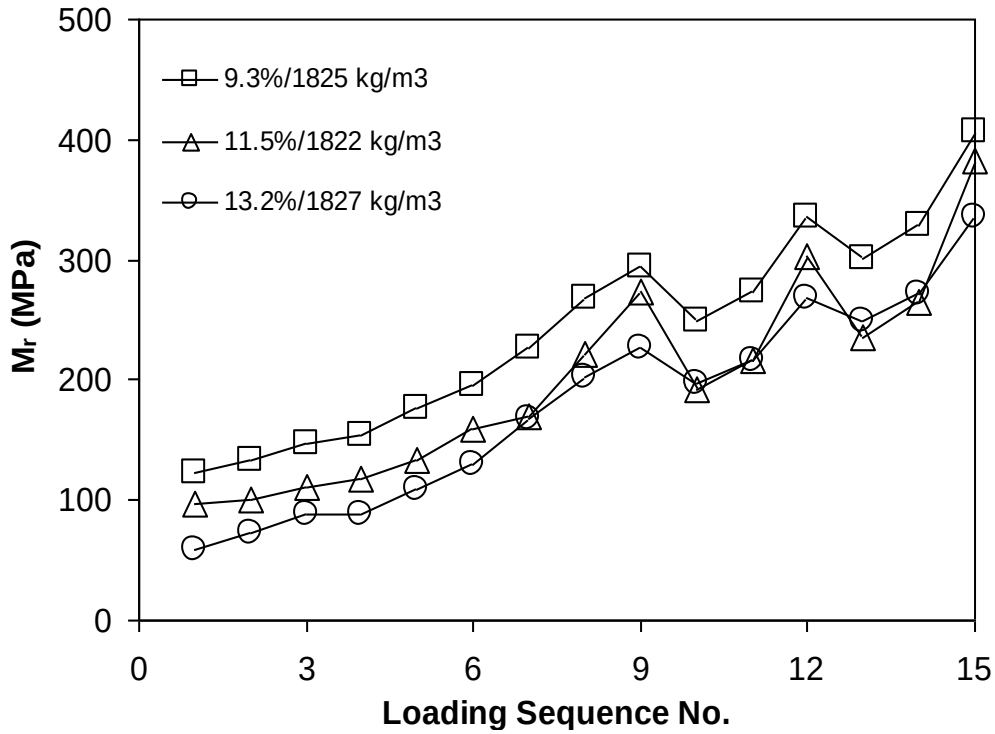

Figure 2-30 Effect of water content on M_r for VA (Legend - molding water content/dry density)

2.10.3.3 Effect of Dry Density on M_r

In general, M_r increased with increasing dry density. Figure 2-31 shows the effect of dry density on M_r of VA for samples having similar water contents. For RAP, dry density had little influence on M_r.

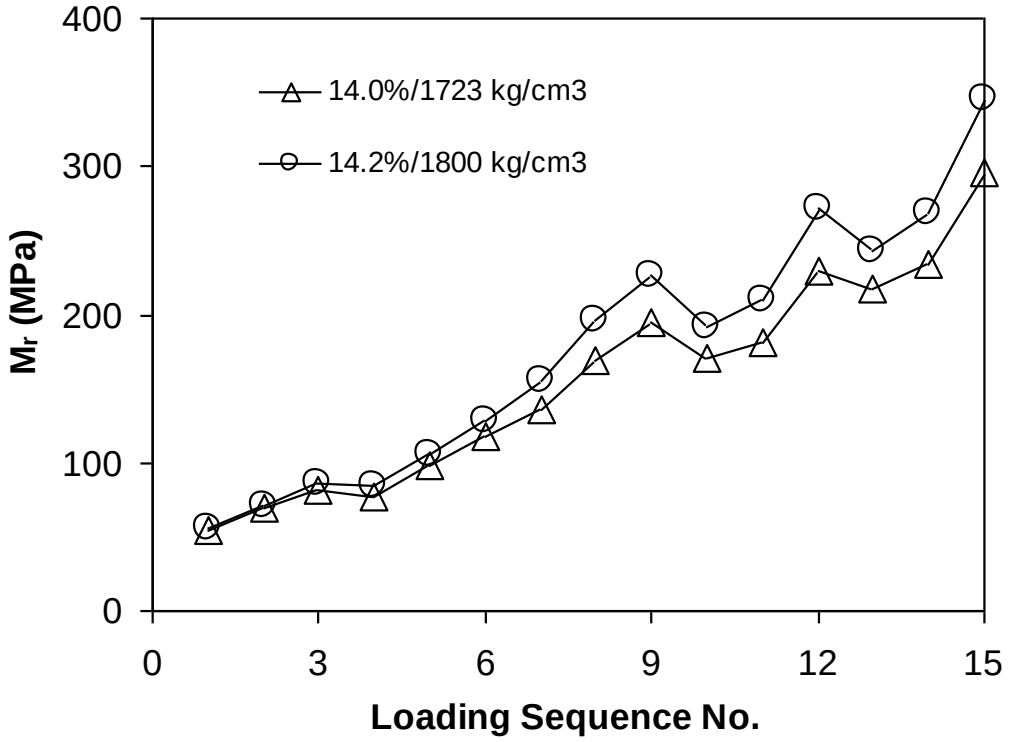

Figure 2-31 Effect of dry density on M_r for VA (Legend - molding water content/dry density)

2.10.4 M_r MODELING

Regression analysis is used to develop a relationship between two or more variables in such a way that one variable can be predicted by the other variable(s). The predicted variable is called the dependent variable (M_r in this case) while the other parameters are known as independent variables. In this research, ordinary least squares (OLS) regression analysis was performed with the aid of statistical software *SPSS Statistics GradPack* version 17.0 distributed by SPSS (Statistical Package for the Social Sciences) Inc.

2.10.4.1 M_r Modeling of Individual Samples

To study the effects of confinement and shear on M_r, values of k_i were first estimated for each sample using the two-parameter model by Seed et al. (1967) and the three-parameter model in the MEPDG (ARA, Inc. 2004).

$$M_R = k_1 p_a \left(\frac{\theta}{p_a} \right)^{k_2} \tag{2.2}$$

$$M_R = k_1 p_a \left(\frac{\theta}{p_a} \right)^{k_2} \left(1 + \frac{\tau_{oct}}{p_a} \right)^{k_3} \tag{2.3}$$

where θ = bulk stress, τ_{oct} = octahedral shear stress, p_a = atmospheric pressure and k_1, k_2, and k_3 are regression parameters The regression constants k_1 and k_2 in Equation 2.2 are summarized in Table 2-9 along with some descriptive statistics in Table 2-10. (Refer to Song, 2009 for detail plots of the data). The regression constants k_1, k_2 and k_3 in Equation 2.3 are also summarized in Table 2-9 along with some descriptive statistics in Table 2-11. The majority of the coefficients of determination, R^2, range from 0.95 to 0.99 for both Equations 2.2 and 2.3. Overall, the R^2 from Equation 2.3 is slightly larger than those from Equation 2.2.

While there are some negative k_3 values, they are mostly positive, indicating that M_r increased with increasing octahedral shear stress. One useful exercise is to understand the effects of saturation or water content and void ratio or dry density on k_i. These trends are useful when subsequently developing the two- and three-parameter models for each material dataset.

Table 2-9 Summary of regression parameters for Equations 2.2 and 2.3

Material	Target Water Content (%)	Water Content before Test(%)	Actual Dry Density (kg/m^3)	Equation 2.2			Equation 2.3			
				k_1	k_2	R^2	k_1	k_2	k_3	R^2
VA	8.8	8.7	1743	0.98	0.68	0.994	0.98	0.68	0.02	0.994
	8.8	9.0	1798	1.25	0.50	0.906	1.12	0.29	0.79	0.978
	8.8	9.5	1821	0.69	0.83	0.982	0.64	0.69	0.52	0.994
	8.8	9.3	1825	1.30	0.54	0.986	1.24	0.46	0.32	0.996
	10.8	12.6	1713	0.58	0.85	0.990	0.55	0.76	0.32	0.994
	10.8	11.5	1822	0.97	0.61	0.939	0.87	0.40	0.82	0.992
	12.8	14.0	1723	0.64	0.75	0.992	0.62	0.68	0.30	0.997
	12.8	14.2	1800	0.67	0.82	0.992	0.64	0.73	0.35	0.997
	12.8	13.2	1827	0.70	0.80	0.995	0.68	0.75	0.19	0.996
RAP	4.5	4.3	1907	1.73	0.52	0.991	1.71	0.50	0.11	0.993
	4.5	4.9	1896	1.33	0.68	0.982	1.32	0.67	0.05	0.982
	4.5	5.5	1984	1.58	0.50	0.904	1.41	0.28	0.88	0.985
	4.5	4.7	1999	1.43	0.50	0.906	1.26	0.28	0.87	0.987
	5.5	5.8	1898	1.54	0.59	0.992	1.53	0.57	0.04	0.992
	5.5	5.9	1896	1.69	0.53	0.990	1.66	0.49	0.13	0.992
	5.5	5.6	2001	1.87	0.50	0.974	1.78	0.41	0.35	0.989
	5.5	5.6	2001	1.69	0.53	0.987	1.64	0.47	0.24	0.993
	6.5	6.7	1899	1.48	0.58	0.973	1.39	0.46	0.45	0.990
	6.5	6.5	1903	1.83	0.51	0.990	1.83	0.51	0.00	0.990
	6.5	5.8	2016	1.48	0.62	0.980	1.41	0.53	0.99	0.989
	6.5	6.5	2003	1.81	0.52	0.995	1.81	0.52	0.00	0.995
RAP &VA	7.0	7.5	1841	1.58	0.59	0.970	1.62	0.64	-0.20	0.974
	7.0	7.2	1847	1.44	0.59	0.992	1.49	0.65	-0.22	0.997
	7.0	7.3	1911	1.40	0.58	0.967	1.34	0.50	0.31	0.975
	9.0	9.7	1904	1.13	0.58	0.980	1.08	0.48	0.38	0.992
	9.0	9.6	1906	1.21	0.67	0.989	1.25	0.73	-0.22	0.992
	9.0	9.3	2017	1.18	0.78	0.987	1.20	0.81	-0.11	0.989
	11.0	11.7	1904	0.95	0.73	0.975	0.90	0.60	0.47	0.987
	11.0	11.6	2011	0.84	0.95	0.988	0.86	1.00	-0.21	0.989
RCA	9.1	9.4	1803	1.45	0.55	0.991	1.43	0.52	0.09	0.992
	9.1	8.6	1893	1.72	0.60	0.967	1.60	0.45	0.54	0.990
	11.1	11.4	1803	1.17	0.71	0.990	1.21	0.76	-0.21	0.993
	11.1	11.3	1881	1.29	0.67	0.965	1.18	0.51	0.63	0.990
	13.1	14.7	1858	0.88	0.63	0.949	0.79	0.43	0.79	0.992
RCA &VA	9.0	9.2	1810	1.28	0.59	0.980	1.28	0.58	0.03	0.980
	9.0	9.2	1864	0.81	0.72	0.979	0.77	0.61	0.43	0.980
	11.0	11.3	1862	0.86	0.73	0.990	0.83	0.67	0.22	0.993
	11.0	11.4	1954	0.95	0.74	0.998	0.95	0.75	-0.04	0.998
	13.0	13.9	1946	0.52	1.00	0.956	0.50	0.93	0.29	0.959
RG &VA	7.9	8.2	1836	0.66	0.89	0.991	0.67	0.90	-0.05	0.991
	9.6	10.0	1894	0.66	0.74	0.971	0.62	0.61	0.47	0.986
	9.6	10.2	1891	0.71	0.80	0.976	0.66	0.66	0.51	0.991
	9.6	9.9	2023	0.68	0.86	0.954	0.62	0.65	0.77	0.984
	9.6	9.8	2024	0.76	0.85	0.992	0.76	0.84	0.04	0.992
	11.0	11.4	1980	0.57	0.90	0.990	0.57	0.90	-0.01	0.990
	11.0	11.4	2021	0.66	0.88	0.993	0.66	0.89	-0.03	0.993
	13.0	14.1	2008	0.56	0.89	0.958	0.52	0.75	0.54	0.967

Table 2-10 Summary of descriptive statistics for k_1 and k_2 in Equation 2.2

Material	Statistics	k_1	k_2
VA	Mean	0.86	0.71
	Standard deviation	0.27	0.13
	Coefficient of variation (CV)	0.31	0.19
	Range	0.64 -1.3	0.54 - 0.85
RAP	Mean	1.62	0.55
	Standard deviation	0.17	0.06
	Coefficient of variation (CV)	0.11	0.10
	Range	1.33 - 1.83	0.50 - 0.68
RAP&VA	Mean	1.22	0.68
	Standard deviation	0.25	0.13
	Coefficient of variation (CV)	0.21	0.19
	Range	0.84 - 1.58	0.58 - 0.95
RCA	Mean	1.30	0.63
	Standard deviation	0.31	0.06
	Coefficient of variation (CV)	0.24	0.10
	Range	0.88 -1.72	0.55 - 0.71
RCA&VA	Mean	0.88	0.76
	Standard deviation	0.27	0.15
	Coefficient of variation (CV)	0.31	0.20
	Range	0.52 -1.28	0.59 - 1.00
RG&VA	Mean	0.66	0.85
	Standard deviation	0.07	0.06
	Coefficient of variation (CV)	0.10	0.06
	Range	0.56 - 0.76	0.74 - 0.90

Table 2-11 Summary of descriptive statistics for k_1, k_2 and k_3 in Equation 2.3

Material	Statistics	k_1	k_2	k_3
VA	Mean	0.82	0.60	0.40
	Standard deviation	0.25	0.17	0.26
	CV[1]	0.30	0.29	0.65
	Range	0.55 - 1.12	0.29 - 0.75	0.02 - 0.82
RAP	Mean	1.56	0.47	0.34
	Standard deviation	0.20	0.11	0.37
	CV	0.13	0.23	1.08
	Range	1.26 - 1.83	0.28 - 0.67	0.00 - 0.88
RAP&VA	Mean	1.22	0.68	0.03
	Standard deviation	0.27	0.17	0.30
	CV	0.22	0.25	12.18
	Range	0.86 - 1.62	0.48 - 1.00	(-0.22) - 0.47
RCA	Mean	1.24	0.53	0.37
	Standard deviation	0.31	0.13	0.41
	CV	0.25	0.25	1.13
	Range	0.79 - 1.60	0.43 - 0.76	(-0.21) - 0.79
RCA&VA	Mean	0.87	0.71	0.19
	Standard deviation	0.28	0.14	0.19
	CV	0.33	0.20	1.03
	Range	0.50 - 1.28	0.58 - 0.93	(-0.04) - 0.43
RG&VA	Mean	0.64	0.78	0.28
	Standard deviation	0.07	0.12	0.33
	CV	0.11	0.16	1.16
	Range	0.52 - 0.76	0.61 - 0.90	(-0.05) - 0.77

1 Coefficient of variation

2.10.4.2 Two-Parameter M_r Modeling for Each Material Dataset

In Equation 2.2, M_r is expressed as a function of only the sample bulk stress. M_r can also be made a function of the sample water content and dry density by incorporating these parameters in k_1 and k_2. Several models have been developed using this idea where the water content (or saturation) and dry density (or void ratio) are referenced to the values at optimum (e.g., Ooi et al., 2004 and Archilla et al., 2007). With the test gradation however, an optimum value was not reached in 4 of the 6 compaction curves. Since the optimum only serves as a reference point, it is conceivable that the referencing can be made with respect to the zero air void (ZAV) curve instead.

Archilla et al. (2007) found that saturation and void ratio provided better correlation with resilient modulus than water content and dry density. Hence, k_1 and k_2 are expressed in terms of S_{zav} - S and e - e_{zav} as follows:

$$k_1 = a_1(S_{zav} - S) + a_2(e - e_{zav}) + a_3$$

$$k_2 = b_1(S_{zav} - S) + b_2(e - e_{zav}) + b_3 \qquad (2.4)$$

where S = degree of saturation of sample, S_{zav} = degree of saturation on the ZAV curve at the same dry density as the sample = 1, e = sample void ratio, e_{zav} = void ratio on the ZAV curve at the same water content as the sample, and, a_1, a_2, a_3, b_1, b_2 and b_3 are regression constants.

Figure 2-32 illustrates the relationship between the parameters S_{zav} - S and e - e_{zav} and the ZAV curve. Table 2-12 presents sample calculations for S_{zav} - S and e - e_{zav} for VA.

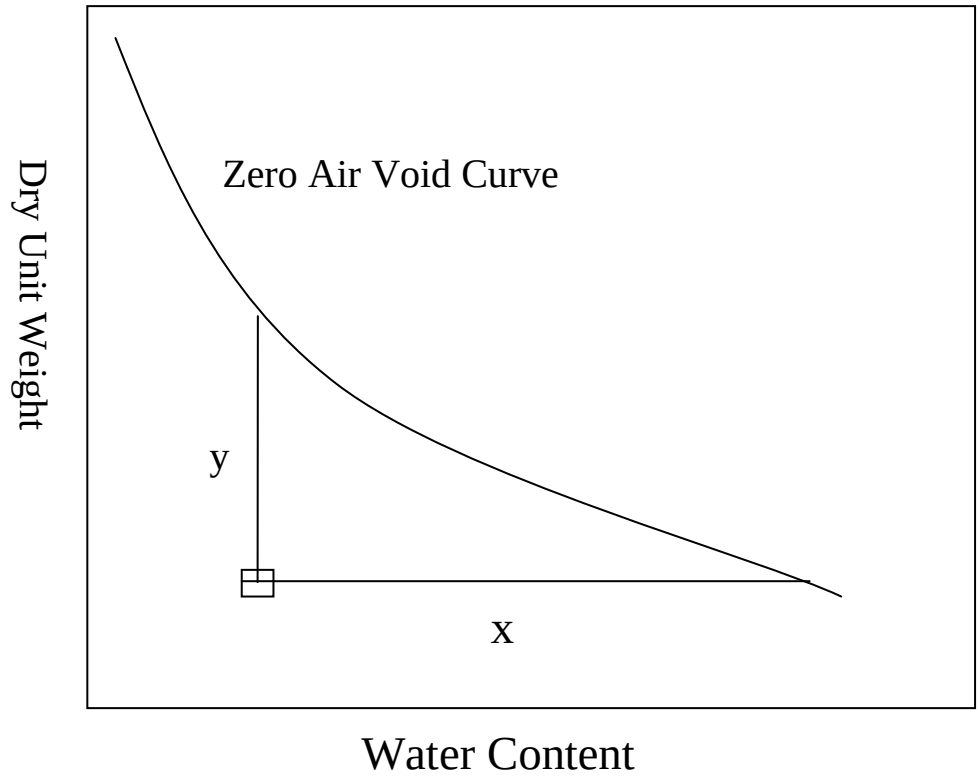

Figure 2-32 S_{zav} - S is related to x and e - e_{zav} is related to y

Table 2-12 Sample calculation of S_{zav} - S and e - e_{zav} for VA.

w (%)	γ_d (kN/m^3)	$e=G_s\gamma_w/\gamma_d-1$	$e_{zav}=wG_s$	e - e_{zav}	$S=wG_s/e$	S_{zav} - S
8.7%	17.1	0.64	0.25	0.39	0.39	0.61
9.0%	17.6	0.59	0.26	0.33	0.44	0.56
9.5%	17.9	0.56	0.27	0.29	0.48	0.52
9.3%	17.9	0.56	0.27	0.30	0.47	0.53
12.6%	16.8	0.66	0.36	0.30	0.54	0.46
11.5%	17.9	0.56	0.33	0.24	0.58	0.42
14.0%	16.9	0.65	0.40	0.26	0.61	0.39
14.2%	17.7	0.58	0.40	0.18	0.69	0.31
13.2%	17.9	0.56	0.38	0.18	0.67	0.33

Regression constants for VA are summarized in Table 2-13. The t-statistic for parameter b_1 was smaller than 2.0, indicating that b_1 is statistically insignificant. Hence it is not included in the table. Even though the t-statistic

for parameter b_3 is less than 2.0, it was not and should not be excluded. This is because excluding constants is likely to introduce a bias to the model.

Table 2-13 Regression results for VA using equations 4.2 and 4.4

Parameter	Estimate	Std. Error	t-statistics	95% Confidence Interval	
				Lower Bound	Upper Bound
a_1	2.68	0.37	7.28	1.95	3.40
a_2	-5.59	0.67	8.33	-6.91	-4.26
a_3	1.20	0.15	8.20	0.91	1.49
b_2	2.06	0.39	5.26	1.28	2.83
b_3	0.10	0.11	0.91	-0.12	0.32
R^2 =0.89					

Figure 2-33 shows a plot of the measured and predicted M_r for VA using equations 2.2 and 2.4. It can be seen that the correlation is quite good (R^2 = 0.92). For other materials, the regression constants are shown in Table 2-14.

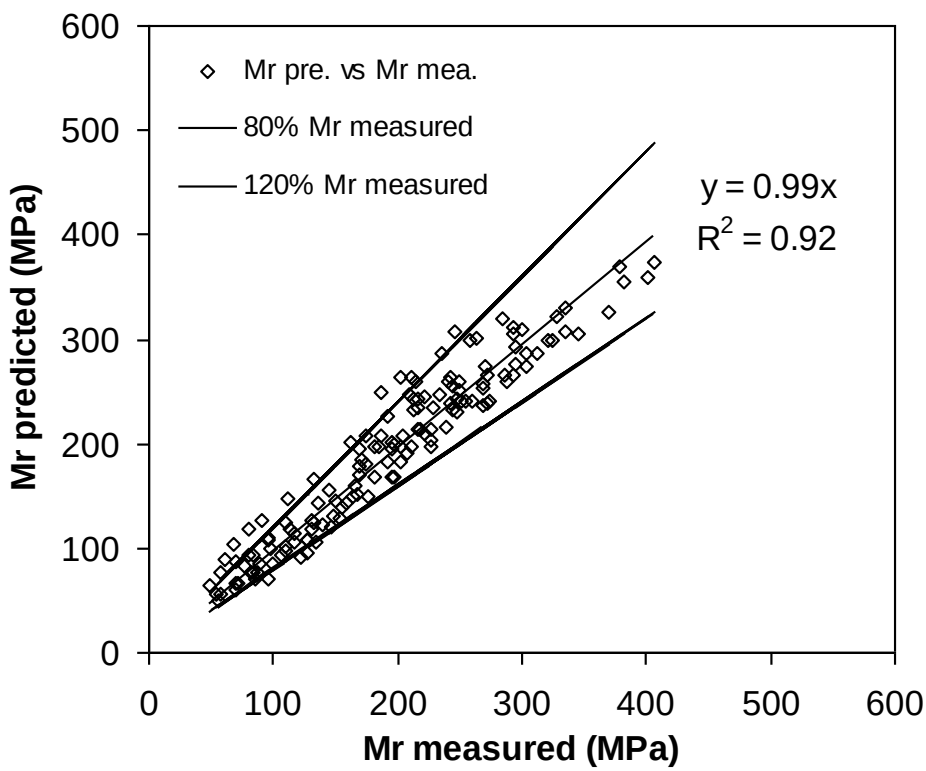

Figure 2-33 Measured and predicted M_r for VA using equations 2.2 and 2.4

Table 2-14 presents a summary of parameter estimates, t-statistics and R^2 for all materials tested. Except for the blends [RCA&VA (R^2 = 0.83), and RG&VA (R^2 = 0.84)], other materials had R^2 larger than or close to 0.90.

Table 2-14 Summary of parameter estimates, t-statistics and R^2 for two-parameter M_r model using equations 2.2 and 2.4

	VA		RCA		RCA&VA		RAP		RAP&VA		RG&VA	
Parameter	Estimate	t-stats	Estimate	t-stats	Estimate	t-stats	Estimate	t-stats	Estimate	t-stats	Estimate	t-stats
a_1	2.68	7.28	7.53	13.95	1.34	4.18	-0.51	3.27	0.88	3.28	4.58	5.88
a_2	-5.59	8.33	-8.40	10.07	[1]		[1]		[1]		-5.69	3.29
a_3	1.20	8.20	0.02	0.19[2]	0.36	3.09	1.88	19.62	0.91	8.06	0.002	0.04[2]
b_1	[1]		-0.80	4.91	-0.55	2.02	[1]		-0.37	2.45	-1.60	5.20
b_2	2.06	5.26	[1]		[1]		[1]		[1]		[1]	
b_3	0.10	0.91[2]	1.01	13.19	0.94	8.06	0.56	42.02	0.80	11.94	1.36	12.37
R^2	0.89		0.96		0.83		0.93		0.90		0.84	
# of points	144		80		96		193		128		112	

Note 1) When parameter estimates are not shown, it is because their t-statistics are less than 2.0 (not statistically significant). In this case, the models were re-estimated by omitting these statistically insignificant parameters.

2) Parameter estimates a_3 and b_3 were not excluded even when their t-statistics were less than 2.0, because eliminating them may result in a bias on k_1 and k_2.

Archilla et al. (2007) stated that a good model should have the following characteristics: (1) intuitively correct signs (i.e.; M_r increases with decreasing saturation, decreasing void ratio and increasing bulk stress); (2) parameters must be statistically significant at a prescribed confidence level (i.e.; t-statistics ≥ 2.0 for a 95% confidence level); (3) fitted model should satisfy the assumptions on which it is based; and (4) model should fit the data points well (i.e.; large R^2). These aspects were checked and found to be satisfied.

The two-parameter model can be easily extended to incorporate the percent recycled material (i.e.; %RCA or %RAP) using the results for 0% recycled material (i.e.; 100% VA), 50% blend and 100% recycled material. To accomplish this, the expressions for k_1 and k_2 are modified as follows:

$$k_1 = a_1(S_{zav} - S) + a_2(e - e_{zav}) + a_3\,(\%R) + a_4$$
$$k_2 = b_1(S_{zav} - S) + b_2(e - e_{zav}) + b_3\,(\%R) + b_4 \qquad (2.5)$$

where %R = percent recycled material, a_1, a_2, a_3, a_4, b_1, b_2, b_3, and b_4 are regression constants.

Again, some parameters are not statistically significant (t-statistics less than 2.0). After excluding them in a step-wise fashion, the regression parameters were re-estimated for RCA/VA blends and RAP/VA blends as summarized in Tables 2-15 and 2-16, respectively. Overall, the fit is quite good with coefficients of determination of 0.89 for RCA blends and 0.92 for RAP blends.

The signs were also checked to see if the trends are sensible. With these models, M_r increases with decreasing saturation, decreasing void ratio,

increasing bulk stress, increasing RAP content and increasing RCA content. It is quite surprising that M_r increases with increasing RAP content but this is probably due to: (1) RAP is made of Type A basalt; and (2) the water contents at which the RAP and RAP blend were tested are significantly lower than VA.

Table 2-15 Summary of regression constants of RCA and VA blends using equations 2.2 and 2.5

Parameter	Estimate	Std. Error	t-statistics	95% Confidence Interval	
				Lower Bound	Upper Bound
a_1	3.56	0.34	10.37	2.88	4.23
a_2	-3.35	0.48	7.04	-4.29	-2.42
a_3	0.28	0.02	11.93	0.23	0.32
a_4	0.15	0.07	2.07	0.01	0.29
b_1	-0.42	0.13	3.12	-0.68	-0.15
b_4	0.88	0.06	14.01	0.75	1.00
R^2 = 0.89, # of points = 320					

Table 2-16 Summary of regression constants of RAP and VA blends using equations 2.2 and 2.5

Parameter	Estimate	Std. Error	t-statistics	95% Confidence Interval	
				Lower Bound	Upper Bound
a_1	0.89	0.14	6.41	0.62	1.16
a_3	0.67	0.04	18.14	0.60	0.74
a_4	0.45	0.07	6.88	0.32	0.58
b_1	-0.89	0.10	9.09	-1.08	-0.70
b_2	0.72	0.16	4.58	0.41	1.03
b_4	0.92	0.04	20.84	0.83	1.00
R^2 =0.92, # of points = 464					

2.10.4.3 Three-Parameter M_r Modeling for Each Material Dataset

The same methodology used to develop the two-parameter models was employed to develop the three-parameter models. Using OLS regression, Equation 2.3 was combined with the following expressions for k_1, k_2 and k_3:

$$k_1 = a_1(S_{zav} - S) + a_2(e - e_{zav}) + a_3$$

$$k_2 = b_1(S_{zav} - S) + b_2(e - e_{zav}) + b_3 \qquad (2.6)$$

$$k_3 = c_1(S_{zav} - S) + c_2(e - e_{zav}) + c_3$$

where S, S_{zav}, e and e_{zav} have been defined previously and a_1, a_2, a_3, b_1, b_2, b_3, c_1, c_2 and c_3 are regression constants.

Regression results for VA using equations 2.3 and 2.6 are summarized in Table 2-17. The majority of the t-statistics are larger than 2.0, with c_3 being the only exception. Figure 2-34 shows a plot of the predicted versus measured M_r of VA using equations 2.3 and 2.6. For other materials, the regression constants and t-statistics are contained in Table 2-18. Except for an R^2 of 0.84 for RCA&VA, all other materials showed R^2 larger than 0.90.

Table 2-17 Regression results for VA using Equations 2.3 and 2.6

Parameter	Estimate	Std. Error	t-statistics	95% Confidence Interval Lower Bound	Upper Bound
a_1	5.53	0.61	9.03	4.32	6.75
a_2	-6.99	0.94	7.45	-8.85	-5.14
a_3	0.19	0.09	2.19	0.02	0.37
b_1	-4.15	0.90	4.62	-5.93	-2.38
b_2	5.79	1.39	4.16	3.04	8.54
b_3	0.91	0.13	7.18	0.66	1.16
c_1	4.37	2.02	2.16	0.36	8.37
c_2	-6.68	3.14	2.13	-12.89	-0.47
c_3	0.25	0.28	0.91	-0.29	0.80
R^2=0.96					

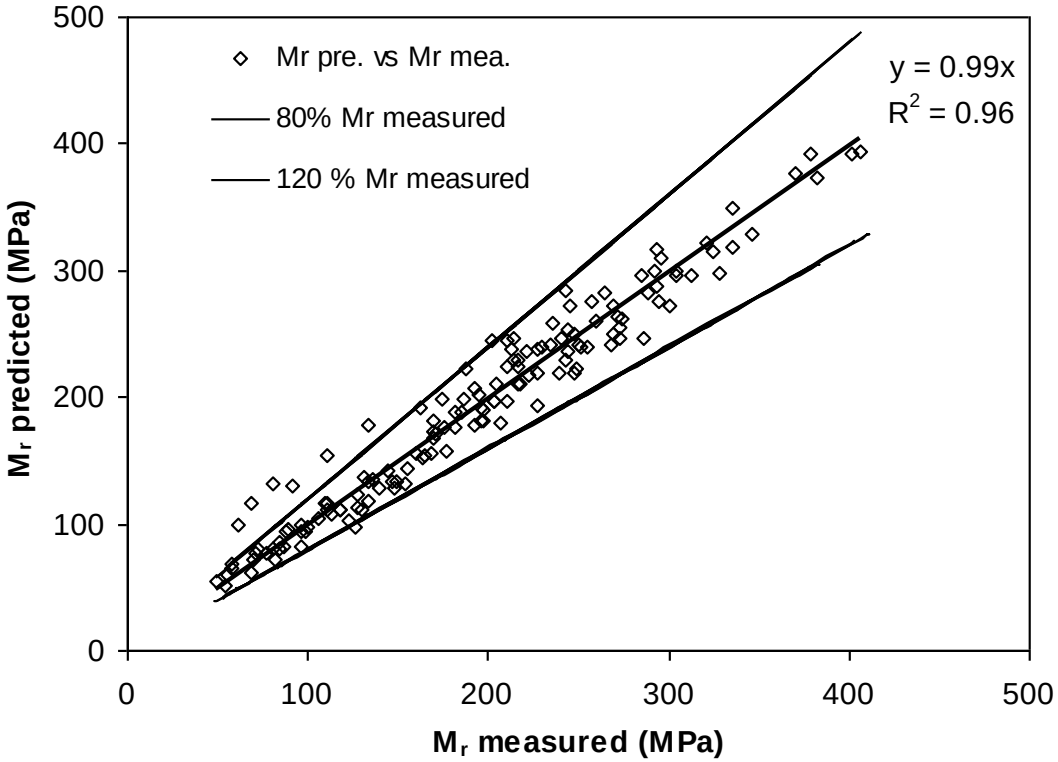

Figure 2-34 Measured and predicted M_r for VA using equations 4.3 and 4.6

Table 2-18 Summary of parameter estimates, t-statistics and R^2 for three-parameter M_r model using equations 2.3 and 2.6

	VA		RCA		RCA&VA		RAP		RAP&VA		RG&VA	
Parameter	Estimate	t-stats	Estimate	t-stats	Estimate	t-stats	Estimate	t-stats	Estimate	t-stats	Estimate	t-stats
a_1	5.53	9.03	5.87	6.26	1.23	4.51	-5.19	5.98	0.88	3.26	[1]	
a_2	-6.99	7.45	-5.47	3.27	[1]		8.48	5.85	[1]		[1]	
a_3	0.19	2.19	0.03	0.52[2]	0.39	4.02	2.80	10.77	0.91	8.03	0.67	25.86
b_1	-4.15	4.62	-2.21	3.09	[1]		[1]		-0.37	2.44	[1]	
b_2	5.79	4.16	3.51	2.86	[1]		[1]		[1]		[1]	
b_3	0.91	7.18	0.68	7.09	0.63	9.85	0.49	27.58	0.80	10.99	0.76	20.35
c_1	4.37	2.16	5.99	3.50	-1.26	6.10	4.18	4.05	[1]		2.81	2.36
c_2	-6.68	2.13	-13.45	4.59	[1]		-7.56	4.40	[1]		-5.57	2.36
c_3	0.25	0.91[2]	0.91	4.02	0.78	2.92	-0.60	1.93[2]	-0.01	0.12[2]	0.11	0.93[2]
R^2	0.96		0.98		0.84		0.95		0.90		0.94	
# of points	144		80		96		193		128		112	

Note 1) When parameter estimates are not shown, it is because their t-statistics are less than 2.0 (not statistically significant). In this case, the models were re-estimated by omitting these statistically insignificant parameters.

2) Parameter estimates a_3, b_3 and c_3 were not excluded even when their t-statistics were less than 2.0, because omitting them may result in a bias on k_1 k_2, and k_3.

The three-parameter model can be easily extended to incorporate the percent recycled material (i.e.; %RCA or %RAP) using the results for 0% recycled material (i.e.; 100% VA), 50% blend and 100% recycled material. To accomplish this, the expressions for k_1, k_2 and k_3 are expressed as follows:

$$k_1 = a_1(S_{zav} - S) + a_2 (e - e_{zav}) + a_3 (\%R) + a_4$$

$$k_2 = b_1(S_{zav} - S) + b_2 (e - e_{zav}) + b_3 (\%R) + b_4 \qquad (2.7)$$

$$k_3 = c_1(S_{zav} - S) + c_2 (e - e_{zav}) + c_3 (\%R) + c_4$$

where %R = percent recycled material as defined previously and a_1, a_2, a_3, a_4, b_1, b_2, b_3, b_4, c_1, c_2, c_3 and c_4 are regression constants.

The regression constants for RCA and VA blends, and RAP and VA blends are summarized in Tables 2-19 and 2-20, respectively. Parameters with absolute t-statistic values less than 2.0 were omitted unless they are constants. For RCA and VA, the t-statistic for b_3 was slightly less than 2 but was left in the model.

Table 2-19 Summary of regression constants for RCA and VA blends using equations 2.3 and 2.7

Parameter	Estimate	Std. Error	t-statistics	95% Confidence Interval	
				Lower Bound	Upper Bound
a_1	3.58	0.32	11.34	2.96	4.20
a_2	-3.43	0.44	7.71	-4.31	-2.56
a_3	0.18	0.05	3.46	0.08	0.28
a_4	0.18	0.07	2.55	0.04	0.32
b_1	-0.42	0.12	3.40	-0.67	-0.18
b_3	0.07	0.03	1.91	0.00	0.13
b_4	0.73	0.07	11.10	0.60	0.86
c_4	0.36	0.06	6.21	0.25	0.47
R^2=0.91, # of points = 320					

Table 2-20 Summary of regression results for RAP and VA blends using equations 2.3 and 2.7

Parameter	Estimate	Std. Error	t-statistics	95% Confidence Interval	
				Lower Bound	Upper Bound
a_1	2.82	0.44	6.48	1.97	3.68
a_2	-3.75	0.76	4.96	-5.23	-2.26
a_3	0.33	0.11	2.92	0.11	0.54
a_4	0.49	0.06	8.34	0.37	0.60
b_1	-3.19	0.54	5.90	-4.25	-2.12
b_2	4.78	0.96	4.97	2.89	6.67
b_3	0.49	0.13	3.64	0.23	0.76
b_4	0.83	0.07	11.71	0.69	0.97
c_1	4.50	1.34	3.37	1.87	7.13
c_2	-7.41	2.40	3.08	-12.13	-2.68
c_3	-1.17	0.33	3.50	-1.82	-0.51
c_4	0.28	0.17	1.67	-0.05	0.60
R^2=0.93, # of points = 464					

In general, the three-parameter model yielded higher R^2, while the two-parameter model has the advantage of being simpler and easier to apply. In addition, the predicted M_r using both the two- and three-parameter models generally falls within 80% to 120% of the measured values, indicative of a good predictive capability.

2.10.5 SUMMARY AND CONCLUSIONS

M_r tests were performed on VA, RAP, RCA, 50% RAP:50% VA, 50% RCA:50% VA, and 30% RG:70% VA, all having gradations that are close to HDOT's base course gradation requirements. Models that incorporate the effects of degree of saturation, void ratio, stress state and percent recycled material content were presented. The following findings and conclusions are offered:

- The M_r samples mostly conformed to HDOT's base course gradation except that they contained no fines. This is because of a lack of fines

in the samples (especially RAP) and as such, large amounts of recycled materials had to be collected in order to collect the required amount of fines. Possibly as a result, several of the materials tested do not exhibit the classical bell-shaped compaction curve.

- For the samples tested, M_r increased with increasing confining stress, increasing deviator stress, increasing bulk stress, decreasing water content and increasing density. M_r of RAP is relatively insensitive to changes in water content and dry density because the compaction curve was relatively flat to begin with.

- The M_r of the recycled materials tested is comparable to or even higher than that of the virgin aggregate.

- Two- and three- parameter models capable of incorporating the effects of saturation, void ratio, stress level and percent recycled material were developed. The majority of the predicted M_r fell within 80% to 120% of the measured values. It should be noted that these models were developed for the gradation tested. Even though Croney and Croney (1997) indicated that the grading has little influence on the modulus of crushed rock and crushed gravel, the applicability of these models to other gradations should be verified.

- In general, the three-parameter model yielded a higher R^2, but the two-parameter model has the advantage of being simpler and easier to apply.

2.11 PERMANENT DEFORMATION TEST AND SHAKEDOWN ANALYSIS

In this section, the following are presented: (1) a literature review on permanent deformation (PD); (2) PD test results for a virgin basaltic aggregate and three recycled materials using single- and multi-stage repeated load triaxial (RLT) tests; (3) models developed to capture the behavior of the tested materials in single-stage PD tests; and (4) the rationale and procedure for evaluating the results of a multi-stage PD test.

In single-stage PD testing, multiple samples are compacted to the same physical state and tested under the same confining pressure. Only one deviator stress is applied per sample but the deviator stresses vary from sample to sample. In a multi-stage PD test, only one sample is tested at a constant confining pressure. This sample is subjected to several deviator stresses increasing stepwise from low to high until it fails or collapses. A constant limited number of cycles (e.g., 1000) of each deviator stress is applied to the sample. Currently, there is no published procedure for determining the shakedown (border between acceptable and unacceptable behavior) limit from a multi-stage PD test. A procedure to identify the material shakedown limit in a multi-stage PD test is proposed. This procedure is then used to compare with results from single-stage PD testing to verify its predictive capability.

2.11.1 LITERATURE REVIEW

PD or rutting of the wearing, base and subbase courses is an important failure criterion that must be considered in pavement design. Rutting of

unbound base and subbase layers (UBL) is directly incorporated in the new Mechanistic-Empirical Pavement Design Guide or MEPDG (ARA, Inc. 2004). One way to analyze rutting is to use the concepts of shakedown theory.

Shakedown analysis was first applied to pavements by Sharp and Booker (1984). When the applied traffic-induced stress is below a certain threshold known as the shakedown limit, the material's PD stabilizes to a constant value with increasing load cycles. This represents a safe regime of applied loading. When the applied traffic load exceeds the shakedown limit, the deformation increases rapidly with increasing load cycles and eventually, leading to failure. Therefore, in shakedown limit-based rutting design, the applied stress must be smaller than the material shakedown limit, deduced from RLT testing.

Several studies have been previously performed on the PD behavior of RCA and RAP. These are summarized in Table 2-21. No study on the PD characteristics of RG was found.

Table 2-21 Recent PD studies on RCA and RAP

Reference	Country	Recycled Materials Tested	Highlights from Study
Van Niekerk et al. (2000)	Netherlands	RCA	Gradation and composition of the granular base are of secondary importance when compared to the influence of the stress conditions, water content and degree of compaction. Good-quality road bases can be built using RCA.
Aurstad and Hoff (2002)	Norway	RCA and RAP	Recycled materials show high PD resistance; RCA enjoys little improvement upon compaction, while the benefit of compacting RAP is more significant.
Mohammad et al. (2006)	USA	RAP	RAP shows similar PD resistance as crushed limestone.
Aurstad et al. (2006)	Norway	RCA	Friction angles were higher than virgin aggregate. RCA shows high stability and PD resistance.
Huurman and Molenaar (2006)	Netherlands	RCA	Shakedown limit of RCA and crushed masonry depends largely on degree of compaction.
Saeed (2008)	USA	RCA and RAP	PD resistance of RAP blends decrease with increasing %RAP; RCA and its blend is superior to RAP and its blend.

A literature review on PD and shakedown behavior of unbound granular materials (UGM) is summarized under the following general topics:

- Consideration of PD of UGM in pavement design (Section 2.11.1.1)
- Shakedown theory (Section 2.11.1.2)
- Factors affecting PD of UGM (Section 2.11.1.3)

- Modeling PD behavior and shakedown analysis (Section 2.11.1.4)

Previously, PD was controlled by limiting the applied stress in the UGM to an arbitrary fraction of the failure deviator stress. This limiting applied shear stress ratio is defined in Figure 2-35. A typical value of 0.7 was common in England (Brown and Dawson, 1992) and South Africa (Almássy, 2002). According to Tutumluer and Dawson (2004), this limiting value ranges between 0.6 and 0.7. For wet aggregate with fines (e.g. during spring thaw), Dawson et al. (2007) suggested that this limiting value should be lowered to 0.5 to 0.55 based on RLT testing. Shakedown limit analysis provides a more rational method of establishing the limiting applied shear stress and is discussed in Section 2.11.1.2.

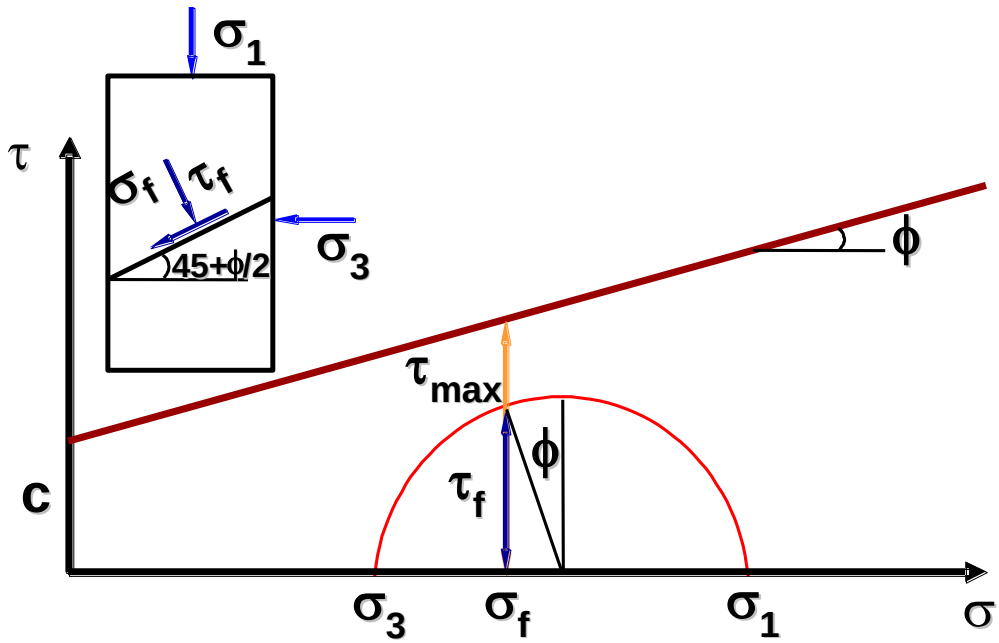

$$\textbf{\textit{Shear Stress Ratio:}}\ \frac{\text{Applied Shear Stress } (\tau_f)}{\text{Shear Strength } (\tau_{max})}$$

Figure 2-35 Schematic illustration of shear stress ratio criterion in pavement design (Tutumluer and Dawson, 2004)

2.11.1.1 Consideration of PD of UGM in Pavement Design

Stresses induced in a pavement system due to traffic loading are highest in the upper layers and diminish with depth (Figure 2-36). Consequently, higher quality and generally more expensive materials (base course) are used in the highly stressed upper layers, and lower quality and less expensive materials (subbase course) are used in the deeper layers of the pavement. This optimization of material usage minimizes construction costs (Christopher et al., 2006).

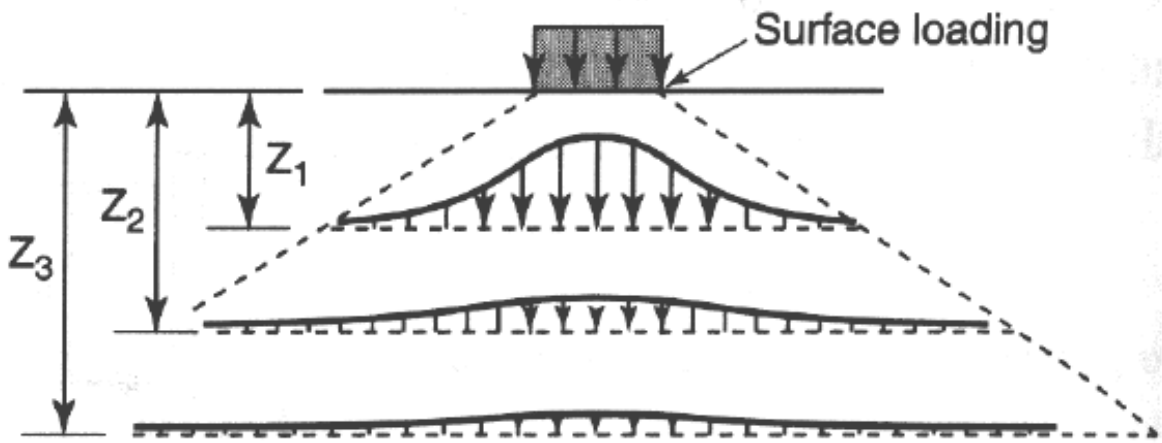

Figure 2-36 Attenuation of traffic induced stresses with depth (Christopher et al., 2006)

To study rutting, it is important to understand the stresses in pavement layers.

2.11.1.1.1 Stresses in Pavement UGM

Acting on a given element in a UGM are a set of complementary normal and shear stresses. It can be shown that for a given state of stress at a point, there are three mutually perpendicular planes known as principal planes on which the shear stresses are zero. Acting on these principal planes is a set of three principal stresses.

A moving wheel load imposes varying magnitudes of vertical, horizontal, and shear stresses in the UGM at different times. As traffic approaches and passes over a given point, rotation of principal stresses occurs as shown in Figure 2-37. A description of what a geomaterial element experiences as a wheel load approaches and passes is as follows:

- First, the applied vertical stress is lower than the applied horizontal stress when the wheel is far from the element.

- Second, the applied vertical stress becomes higher than the applied horizontal stress, when the wheel approaches the element.

- Third, the applied vertical and horizontal stresses reach their highest values when the wheel is right above the element. The applied vertical stress is still higher than the applied horizontal stress. Only during this instant are the vertical and horizontal stresses the major and minor principal stresses, respectively.

- The fourth and fifth scenarios are analogous to the second and first scenarios, respectively, as the wheel leaves the element.

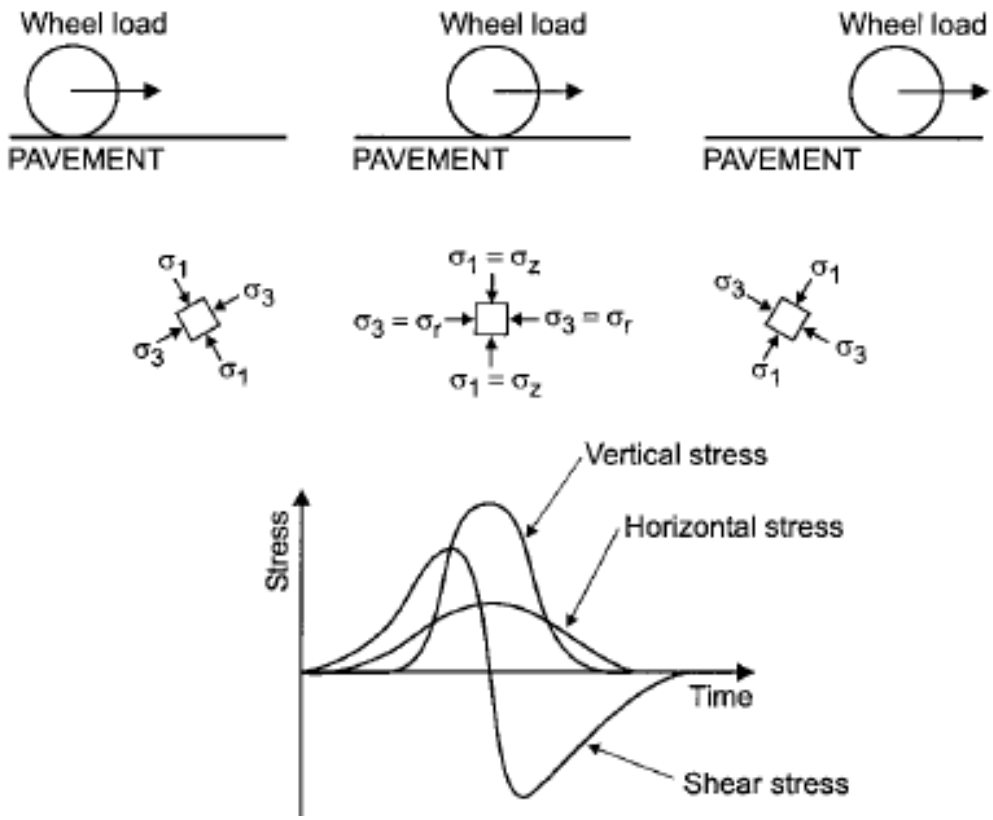

Figure 2-37 Stresses beneath rolling wheel load (Lekarp et al., 2000)

During traffic loading, the stresses consist of static and dynamic stress components. Static components of stress are attributable to self-weight and locked-in stresses induced during compaction and initial traffic loading. The dynamic stress component is due to traffic loading. It is common practice among pavement engineers to preclude the locked-in compaction-induced stresses. Figure 2-38 presents a series of load-unload-reload paths that can occur during compaction and initial trafficking, where $\sigma_v^{'}$ and $\sigma_h^{'}$ are vertical and horizontal effective stress, respectively.

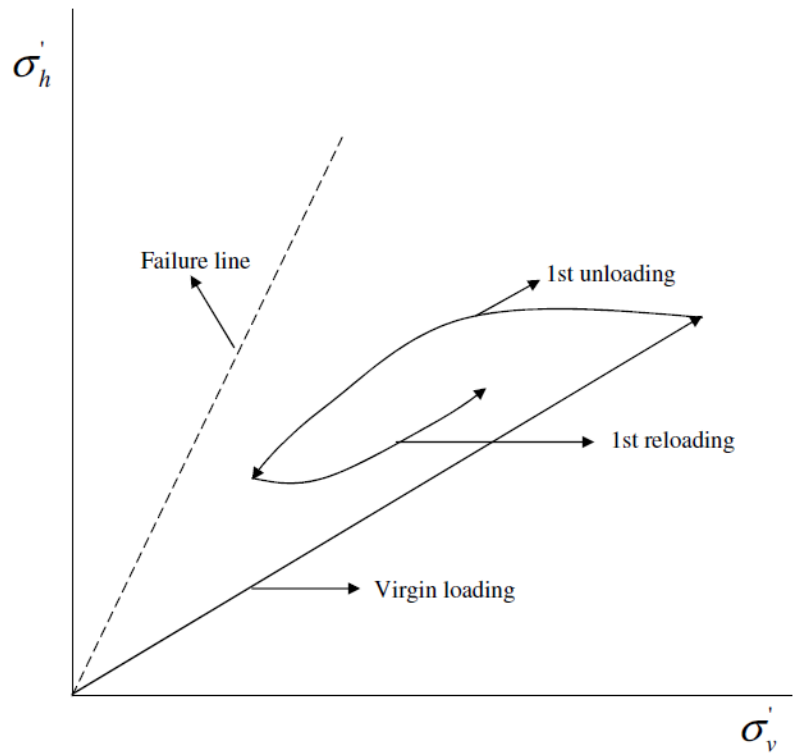

Figure 2-38 Field stresses during a load-unload-reload path (redrawn after Mayne and Kulhawy, 1982)

Arnold (2004) noticed the significance of locked-in lateral stress on pavement design and summarized previous research by Sowers et al. (1957); Uzan (1985); Selig (1987); Duncan and Seed (1986); and Almeida (1993). Selig (1987) found large lateral plastic strains at the bottom of a pavement granular layer during initial loading with the response rapidly approaching an elastic condition with subsequent loading. This suggests that tensile stresses occur in the first few cycles but are quickly cancelled out by the developed lateral locked-in stresses, resulting in a net horizontal compressive stress state. Selig concluded that the locked-in lateral stress is the most important factor limiting rutting of granular base, and suggested (as well as by Uzan, 1985) that it should be considered in mechanistic-based pavement design.

The at-rest coefficient of lateral earth pressure during virgin loading is related to the soil friction angle, ϕ, as follows (Jaky, 1944):

$$K_o = 1 - \sin\phi \qquad (2.8)$$

Equation 2.8 can be confirmed in the laboratory using a consolidometer that has the ability to measure lateral stress or a triaxial apparatus by measuring the lateral to vertical stress ratio when the axial and volumetric strains are equal. The value of K_o for normal consolidation should be distinguished from overconsolidation. For primary or first unloading as shown in Figure 2-38, K_o can be expressed as (Kulhawy and Mayne 1990)

$$K_o = (1 - \sin\phi)OCR^{\sin\phi} \qquad (2.9)$$

where

OCR = overconsolidation ratio = σ'_{vm} / σ'_v

σ'_{vm} = maximum past or preconsolidation pressure

σ'_v = current vertical effective stress.

Assuming the preconsolidation pressure remains unchanged, values of K_o for subsequent reload and unload cycles will be less than those during primary unloading.

Typically, bases and subbases are compacted during the pavement construction process, rendering these layers overconsolidated. However, it is

difficult to estimate the OCR during design because the compactive effort (or equipment) is seldom known until construction. As a result, the actual locked-in horizontal stress remains elusive to pavement engineers and is often estimated as (1 - sinϕ) $\sigma_v^{'}$, which is the value for virgin loading. Ignoring these locked-in stresses can have an impact on the pavement design.

2.11.1.1.1 Behavior of UGM in a PD Test

Fig. 2-39 presents a typical load-unload stress-strain cycle for a UGM. It is not retraceable upon removal of load. Instead, a hysteresis loop is formed. Two different strains are observed in this cycle: a resilient strain, which is recoverable after the load is removed, and a permanent or plastic strain, which can accumulate with additional load cycles. This permanent strain must be limited in design of pavements against rutting.

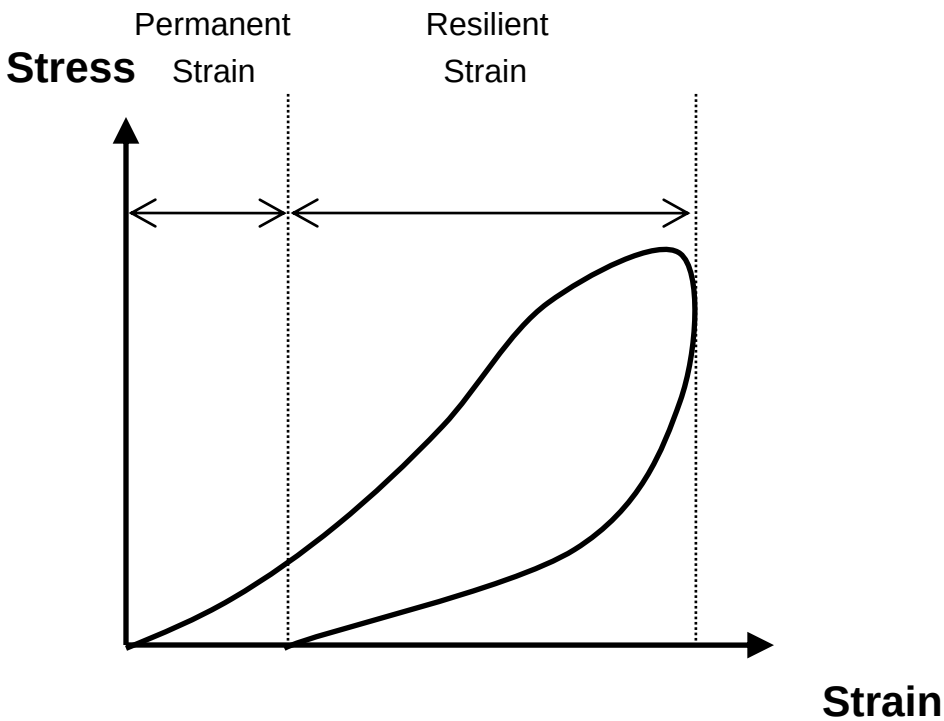

Figure 2-39 Hysteresis loop during a load-unload cycle in a RLT test on UGM

Based on Hertz contact theory, Werkmeister (2003) postulated that the resilient deformation is mainly attributable to the deformation of the individual grains. On the other hand, permanent deformation is primarily due to particle re-orientation. Mechanisms such as particle rotation and sliding play a big role during traffic loading. The most severe loading however, occurs during compaction, when particles can crush or grains can abrade. Consequently, grain fragmentation is more important during compaction and less during the service life of the pavement.

In the laboratory, PD is commonly measured using the constant confining pressure (CCP) RLT test. In this test, the stresses applied only mimic the in situ principal stresses directly beneath the center of the wheel load. It is unable to simulate rotation of principal stresses and the shear stresses induced during real traffic loading. In reality, the confining stress is not constant as in the CCP RLT test, but rather it is variable. More flexible stress paths can be simulated by using devices such as the FastCell, developed at the University of Illinois at Urbana-Champaign, a hollow cylinder apparatus (Chan, 1990) or a K-mold apparatus (Arnold, 2004). Applying a variable confining pressure (VCP) best mimics the conditions in the field. However, these are more expensive and difficult to perform and are used mostly as research tools.

2.11.1.1.2 Consideration of PD in Pavement Design

Rutting occurs not only in the wearing course but also in the unbound layers. For example, at the American Association of State Highway Officials (AASHO) road test in Ottawa, IL conducted between 1958 and 1960, the AC, base, subbase, and subgrade layers contributed 32%, 18%, 39%, and 11%, respectively, to the total rut depth (Christopher et al., 2006); i.e., about two-thirds of the rutting was in the unbound materials. In the Canterbury Accelerated Pavement Testing Indoor Facility (CAPTIF) pavement in Christchurch, New Zealand, the base layer contributed up to 70% of the total rut depth (Haddock et al., 2005).

Quite often used in the United States, the 1993 AASHTO method for pavement design is based on the full scale AASHO road test. In this method, rutting in unbound materials is related empirically to the elastic or resilient strain at the top of the subgrade (Christopher et al., 2006). As Monismith (2004) and Dawson et al. (2008) criticized, this method is based on a set of specific local environmental conditions and cannot be applied elsewhere as a *"one-for-all principal".*

In the MEPDG (ARA, Inc., 2004) approach, pavement design is accomplished by inputting the traffic load spectra, material properties and thickness, and environmental conditions. The MEPDG software performs a mechanistic analysis of the pavement and outputs stresses and strains. Then empirical relationships are used to relate the outputs to pavement distresses. The MEPDG software calculates the PD of each layer by subdividing them into small elements and then summing the total rut depth. It characterizes the PD

of unbound base, subbase, and subgrade materials using the Tseng and Lytton (1989) model (discussed later).

2.11.1.2 Shakedown Theory

Shakedown theory was originally developed to analyze the behavior of pressure vessels under cyclic thermal loads, and later metal surfaces under repeated rolling or sliding loads (Werkmeister, 2003). It has been used to describe the behavior of structures and more recently pavements under cyclic loading.

Two factors that influence material response to repeated loading are the stress levels and number of load applications (Dawson, 1999; Theyse, 2000; Khogali et al., 2007; Yang et al., 2008). At low levels of deviator stress, the deformation reaches an asymptotic value and becomes resilient as the number of cycles becomes very large. At high levels of deviator stress, PD continuously increases eventually leading to failure or collapse. This implies a critical stress level between stable and unstable conditions must exist. This critical stress level is termed the plastic shakedown limit.

According to Werkmeister (2003), a material's PD behavior can be categorized into one of the following three ranges as shown in Figure 2-40 and Figure 2-41:

Range A Applied load is smaller than the plastic shakedown limit, and the PD approaches a constant value with increasing number of load cycles. The

response then becomes entirely resilient. This behavior is termed plastic shakedown.

Range C Applied load is large and the sample fails quickly at low number of cycles. The deformation is predominantly plastic. Known as incremental collapse, this is an undesirable situation and should be avoided in pavement design.

Range B Applied load is larger than the plastic shakedown limit but is smaller than the plastic creep limit, which is the limit between incremental collapse and this intermediate behavior. A material in this range, also known as plastic creep, will eventually fail at a large number of load cycles.

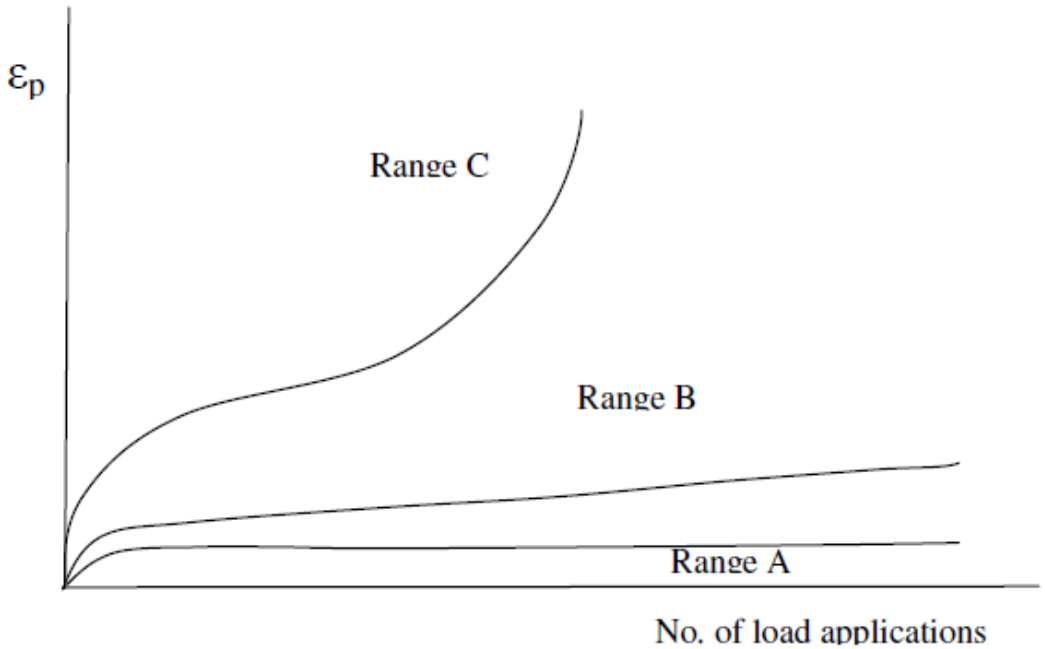

Figure 2-40 Shakedown ranges (Tutumluer and Dawson, 2004)

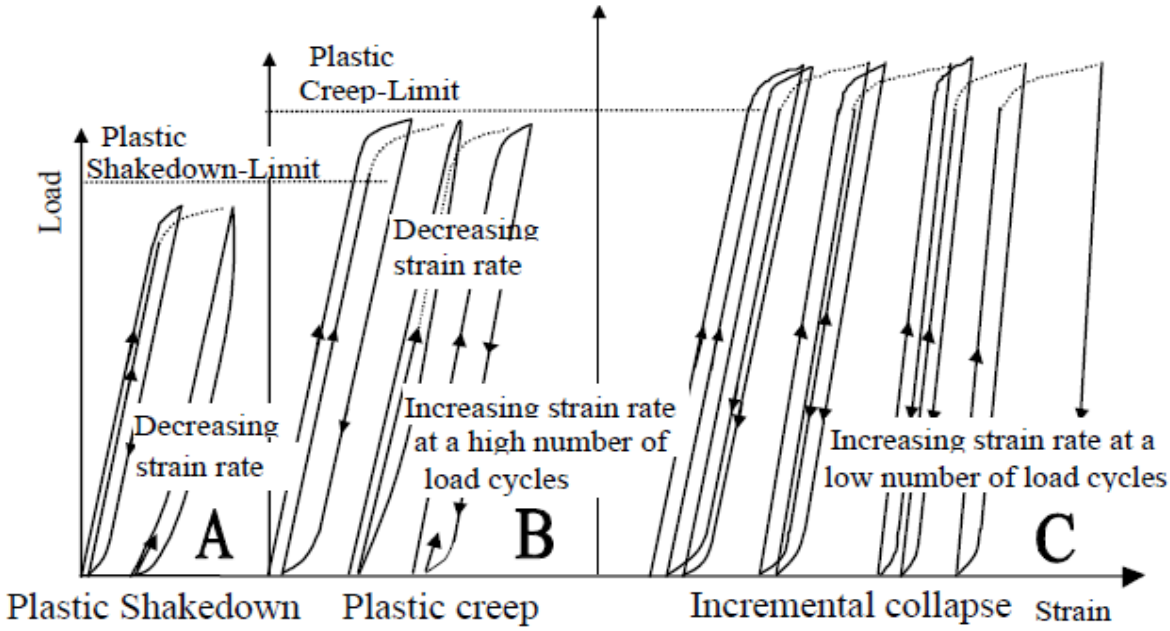

Figure 2-41 Shakedown behavior for UGM (Werkmeister, 2003)

The three different ranges can be distinguished by plotting the results as follows:

1) vertical permanent strain versus number of load cycles (Figure 2-40)

2) vertical permanent strain rate (vertical permanent strain divided by number of load cycles) on a log scale versus vertical permanent strain (Figure 2-42)

3) resilient strain versus number of load cycles (Figure 2-43). Alternatively, the resilient modulus could be plotted instead of resilient strain as the two are inversely related.

A description of how the behavioral ranges are distinguished is summarized in Table 2-22. The least ambiguous procedure to distinguish between the

three behavioral ranges is the permanent strain rate versus permanent strain plot.

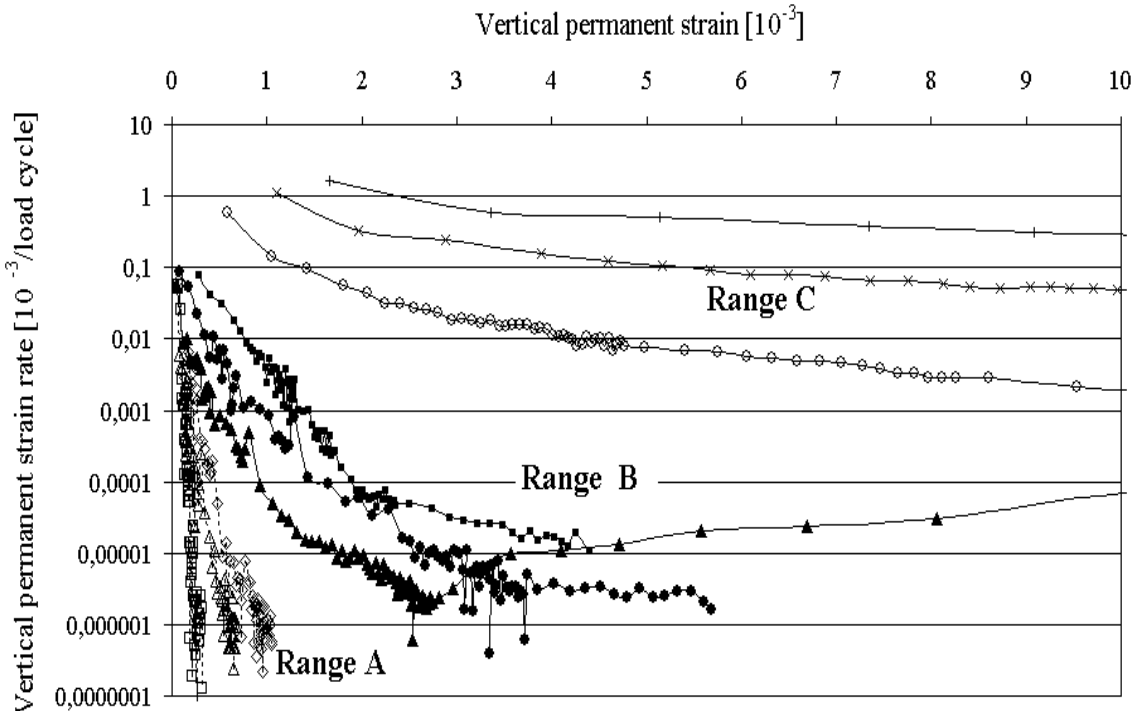

Figure 2-42 PD ranges by permanent strain rate (Werkmeister et al., 2004)

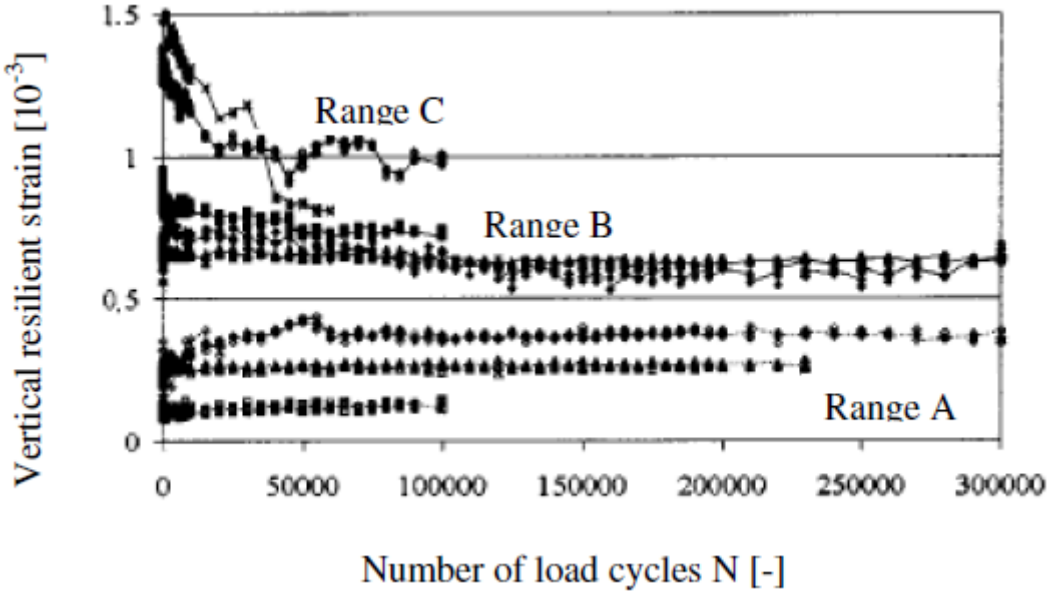

Figure 2-43 PD ranges by resilient strain (Werkmeister et al., 2004)

Table 2-22 Methods for distinguishing the various PD behavioral ranges

Plot	Range A (Shakedown)	Range B (Plastic Creep)	Range C (Incremental Collapse)
Permanent strain versus number of cycles (Figure 2-40)	Permanent strain approaches a constant value after a large number of load cycles	Permanent strain appears to approach a constant value but eventually increases asymptotically after a large number of load cycles; the latter may not be observed in a PD test with a limited number of cycles	Permanent strain increases asymptotically after a relatively low number of load cycles
Resilient modulus versus number of cycles (Figure 2-42)	Resilient modulus initially increases (modulus hardening) but approaches a constant after a large number of cycles	Slight decrease in resilient modulus (modulus softening) with increasing number of cycles	Large decrease in resilient modulus (modulus softening) with increasing number of cycles
Permanent strain rate versus permanent strain (Figure 2-43)	Permanent strain rate decreases linearly with increasing permanent strain	Permanent strain rate decreases linearly at first with increasing permanent strain followed by a flattening of the curve	Permanent strain rate decreases very slowly or not at all with increasing permanent strain or the permanent strain rate decreases with permanent strain followed by an increase

2.11.1.3 Factors affecting PD of UGM

Factors that can decrease a geomaterial's susceptibility to PD include (Lekarp et al., 2000; Dawson et al., 2000 and Cheung and Dawson, 2002):

1. higher relative density
2. lower water content or higher suction
3. higher preconsolidation pressure
4. higher confining stress
5. lower applied stress

6. smaller number of load cycles
7. more well-graded as opposed to a uniform gradation
8. lower fines content
9. more angular and rough particles as opposed to rounded and smooth
10. larger maximum particle size

2.11.1.4 Permanent Deformation Models

One objective of this research is to develop models to predict the PD at any number of cycles under a given stress level. The PD models available can be classified into three categories: (1) Models that relate permanent strain to number of cycles only (Table 2-23); (2) Models that relate permanent strain to stress level only (Table 2-24); (3) Models that relate permanent strain to both number of cycles and stress levels (Table 2-25).

Table 2-23 Models for estimating permanent strain as a function of the number of load cycles (modified after Hornych and El Abd, 2004)

Author	Relationship	Parameters
Barksdale [1972]	$\varepsilon_1^p = a + b\log(N)$	a, b
Khedr [1985]	$\frac{\varepsilon_1^p}{N} = A.N^{-b}$	A,b
Tseng and Lytton [1989]	$\varepsilon_1^P(N) = \varepsilon_0 \cdot e^{-\left(\frac{\rho}{N}\right)^{\beta}}$	ε_0, ρ, β
Sweere [1990]	$\varepsilon_1^p = a N^b$	a, b
Hornych et al. [1993]	$\varepsilon_1^{p*} = A\left(1-\left(\frac{N}{100}\right)^{-B}\right)$	ε_1^{p*} permanent axial strain after the first 100 cycles A, B
Vuong [1994]	$\varepsilon_1^p = \varepsilon_1^r\left(\frac{a}{b}\right)N^c$	ε_1^r resilient axial strain a, b, c
Wolff and Visser [1994]	$\varepsilon_1^p = (cN + a)\left(1 - e^{-bN}\right)$	a, b, c

Table 2-24 Models for estimating permanent strain as a function of the applied stress level (modified after Hornych and El Abd, 2004)

Author	relationship	Parameters
Lashine et al. [1971]	$\varepsilon_1^p = a\frac{q}{\sigma_3}$	a, σ_3 confining stress, q deviator stress
Barksdale [1972]	$\varepsilon_1^p = \frac{q/a\sigma_3^b}{1-\left[\frac{R_f.q.(1-\sin\phi)}{2(C.\cos\phi+\sigma_3\sin\phi)}\right]}$	a, b , R_f = ratio of applied deviator stress q to deviator stress at failure q_f. ϕ friction angle, C cohesion
Shenton [1974]	$\varepsilon_1^p = K\left(\frac{q_{max}}{\sigma_3}\right)^a$	K ,a , q_{max} maximum applied deviatoric stress
Lentz and Baladi [1981]	$\varepsilon_1^p = \varepsilon_{0,95S}\ln(1-q/S)^{-0,15} + \left[\frac{n(q/S)}{1-m(q/S)}\right]\ln(N$	$\varepsilon_{0,95S}$ axial strain at 95% of the deviatoric stress at failure, n , m slope of the failure line, S deviatoric stress at failure
Nishi [1994]	$\varepsilon_1^{p,ult} = k\frac{q^a}{p^b}$	k, a, b $\varepsilon_1^{p,ult}$ ultimate permanent axial strain
Lekarp and Dawson. [1998]	$\frac{\varepsilon_1^p(N_{ref})}{(L/p_0)} = a\left(\frac{q}{p}\right)^b$	a,b $\varepsilon_1^p(N_{ref})$: permanent strain after a reference number of cycles N_{ref} >100 $L = \sqrt{p^2+q^2}$ p_0 reference mean stress

Table 2-25 Models for estimating permanent strain as a function of the number of load cycles and applied stress level

Author	Relationship	Parameters
Pappin (1979)	$\varepsilon_s^p = f_n(N) L \left(\frac{q}{p}\right)^{2.8}$	ε_s^p permanent shear strain $f_n(N)$ shape function, depending on the number of cycles N, p mean normal stress $L = \sqrt{p^2 + q^2}$
Lentz and Baladi (1981)	$\varepsilon_1^p = \varepsilon_{0.95S} \ln(1 - q/S)^{-0.15} + \left(\frac{n(q/S)}{1 - m(q/S)}\right) \ln(N)$	$\varepsilon_{0.95S}$ axial strain at 95% of the deviator stress at failure, n model parameter m slope of the failure line S deviator stress at failure N number of loading cycles Note: this model is based on static load testing
Paute et al. (1988)	$\varepsilon_1^p = \frac{A\sqrt{N}}{\sqrt{N} + D}$	ε_1^p permanent strain after the first 100 cycles A,D parameter function of stress level
Paute et al. (1994)	$\varepsilon_1^p = f(N) \frac{\frac{q}{p + p^*}}{b\left(m - \frac{q}{p + p^*}\right)}$	ε_1^p permanent axial strain after the first 100 cycles b, p* model parameters m slope of failure line in p-q space f(N) function of the number of cycles N
Huurman (1997)	$\varepsilon_p(\mathrm{N}) = \mathrm{A} \cdot \left(\frac{N}{1000}\right)^B + C\left(e^{D\frac{N}{1000}} - 1\right)$	A, B, C, D, parameter function of the level of stress
Theyse (2000)	$PD = Q \cdot e^{dN} - A \cdot e^{-bN} - Q + A$ $PD = m \cdot N + a(1 - e^{-bN})$ $PD = m \cdot N + \frac{c \cdot N}{\left[1 + \left(\frac{c \cdot N}{a}\right)^b\right]^{1/b}}$	First two equations for stable state, and last for unstable state. PD (mm): vertical permanent deformation A, Q, a, b, c, d, m: stress dependent parameters
Gidel et al. (2001)	$\varepsilon_1^p(N) = \varepsilon_{10}^p \left(1 - \left(\frac{N}{N_0}\right)^{-B}\right) \left(\frac{L_{\max}}{P_a}\right)^n \frac{1}{\left(m + \frac{s}{p_{\max}} - \frac{q_{\max}}{p_{\max}}\right)}$	$L_{\max} = \sqrt{p_{\max}^2 + q_{\max}^2}$ p_a = 100 kPa, N_0 reference number of cycles, ε_{10}^p, B, n, m, s are parameters of the model.
Hornych and El Abd (2004)	$\varepsilon_1^p(N) = f(N) \left(\frac{L_{\max}}{P_a}\right)^n \frac{1}{\left(m + \frac{s}{p_{\max}} - \frac{q_{\max}}{p_{\max}}\right)}$	f(N) - adopt Sweere (1990) model or Hornych et al. (1993) model

From Table 2-23, Khedr (1985), Sweere (1990) and Vuong (1994) models are all a form of the power model. Since the power model is known to fit PD test data very well and since it is simple, it has formed the basis of f(N) in some of the models in Table 2-25.

Naturally, the third class of models is superior because it captures two of the most important factors that affect PD. Of the models in this class, there are two that model the stable (Range A) and unstable (Ranges B and C) PD behavior: (a) Theyse (2000) and (b) Huurman (1997) models. Theyse used separate equations to model the stable and unstable behaviors whereas Huurman proposed an all encompassing equation that is more elegant. In Table 2-25, Huurman used the power model in the first term of the equation below:

$$\varepsilon_p(\mathrm{N}) = \mathrm{A}\left(\frac{N}{1000}\right)^B + C\left(e^{D\frac{N}{1000}} - 1\right) \tag{2.10}$$

where:

ε_p(%) = permanent strain at load cycle N

N = number of cycles

e = base of natural logarithm (2.17828.....)

$$\mathrm{A} = \mathrm{a}_1\left(\frac{\sigma_1}{\sigma_{1\mathrm{f}}}\right)^{a_2} \quad \mathrm{B} = \mathrm{b}_1\left(\frac{\sigma_1}{\sigma_{1\mathrm{f}}}\right)^{\mathrm{b}_2} \quad \mathrm{C} = \mathrm{c}_1\left(\frac{\sigma_1}{\sigma_{1\mathrm{f}}}\right)^{\mathrm{c}_2} \quad \mathrm{D} = \mathrm{d}_1\left(\frac{\sigma_1}{\sigma_{1\mathrm{f}}}\right)^{\mathrm{d}_2}$$

a_1, a_2, b_1, b_2, c_1, c_2, d_1, d_2 are regression constants

σ_1 = major principal stress

$$\sigma_{1f} = \frac{(1+\sin\varphi)\cdot\sigma_{3f} + 2\cdot c\cdot\cos\varphi}{(1-\sin\varphi)}$$ major principal stress at failure

σ_{3f} = minor principal stress at failure

ϕ = angle of internal friction

c = cohesion

The first term describes a linear increase of permanent strain with number of load cycles on a log-log scale. The parameter A gives the permanent strain at 1000 cycles, and B gives the subsequent slope of the permanent strain with number of load cycles.

The unstable behaviour at high stress level cannot be described by the first term alone because the PD increases exponentially rather than linearly with load cycles. Hence, Huurman introduced the second term.

In this model, parameters A, B, C and D are stress dependent. The other models in Table 2-25 were not considered because (1) they require lateral strain, which was not measured (e.g. Pappin (1979) model) (2) there is insufficient details provided to fully define the model (e.g., ε_{10}^{p} in Gidel's (2001) model, and in many other models, it is not defined under what conditions are the failure deviator stresses measured); (3) they were published in a foreign language (e.g. Paute, 1994 model).

2.11.2 SELECTION OF CONFINING STRESS

To run the single- and multi-stage PD tests, a representative confining stress is needed. Its value depends on the: (1) pavement layer thickness; (2) material properties; (3) design traffic load; and (4) stress history of the unbound base course.

The confining stress for the PD tests was derived by assuming a pavement section consisting of 6 inches of asphalt concrete, overlying 8 inches of base course (friction angle ϕ = 45°) overlying subgrade. The confining stress at the middle of base course was determined by assuming that the base course is proof-rolled with a drum roller. From Clough and Duncan (1991), the locked-in lateral stress at a depth of 4 inches can easily reach 3 psi based on a friction angle of 45°. Thus, a horizontal stress of 3.0 psi or 21 kPa was adopted for all PD tests.

2.11.3 SELECTION OF DEVIATOR STRESSES FOR PD TESTING

In the absence of a standard for single-stage PD test in the United States, the strategy adopted was to select an arbitrary deviator stress corresponding to a fraction of the failure deviator stress. The deviator stress is then adjusted until both shakedown and incremental collapse is observed with the criterion that at least three deviator stresses be applied per material.

PD tests were performed on the following: (1) VA; (2) RCA; (3) 50% RCA:50% VA blend (RCA&VA); (4) RAP; and (5) 50% RAP:50% VA blend (RAP&VA). For all samples, the target physical states are optimum water

content and maximum dry density based on the modified Proctor test (AASHTO T180).

The test equipment and sample preparation method are identical to those for the resilient modulus tests as described in Section 2.10. As discussed previously, the external sample LVDTs provide the sample deformation while the system LVDT attached to the actuator provides the system deformation. The maximum range of the sample LVDTs is 10 mm corresponding to 5% vertical strain, which is inadequate for PD testing that involves larger strains. Therefore, in the PD tests, all deformations were measured using the system LVDT.

The PD test matrix is summarized in Table 2-26, along with the failure deviator stresses measured with the drainage valve open during test. Multi-stage PD test is even more obscure than the single-stage variety with specifications available only in Europe. The loading sequence for a multi-stage PD test on a blend of RCA&VA is given in Table 2-27 as an example.

All samples were conditioned by applying 500 cycles of a 95 kPa deviator stress at a confining stress of 105 kPa. This is similar to the conditioning specified in AASHTO T307 for resilient modulus testing of unbound base/subbase.

The maximum number of cycles in the single-stage PD tests and multi-stage PD tests are about 60,000 and 14,000, respectively. The single and multi-stage PD tests were terminated earlier if the samples failed.

Table 2-26 Single-stage PD test matrix and shear test results

Materials	Failure Deviator stress[1]	Applied Deviator stress	Deviator Stress Level	Deviator Stress Normalized with Confining Stress
	σ_{df} (kPa)	σ_d (kPa)	σ_d/σ_{df} (%)	σ_d/σ_3 -
VA	700	210	30%	10.0
		330	47%	15.7
		420	60%	20.0
		550	79%	26.2
		660	94%	31.4
RCA	800	240	30%	11.4
		400	50%	19.0
		560	70%	26.7
RCA&VA	580	174	30%	8.3
		290	50%	13.8
		406	70%	19.3
RAP	340	204	60%	9.7
		238	70%	11.3
		272	80%	13.0
		340	100%	16.2
RAP&VA	340	102	30%	4.9
		170	50%	8.1
		238	70%	11.3

Note 1 Triaxial testing was performed on the compacted specimen under a confining stress of 21 kPa. A shear rate of 1%/minute was adopted.

Table 2-27 Multi-stage PD test load sequence for RCA&VA

Number of Cycles N -	Applied Confining Stress σ_3 (kPa)	Applied Seating Stress - (kPa)	Applied Deviator Stress [1] σ_d (kPa)	Deviator Stress Level[3] σ_d/σ_{df} (%)
500[2]	105	10	95	16%
0-1000	21	5	29	5%
1000-2000	21	5	58	10%
2000-3000	21	5	87	15%
3000-4000	21	5	116	20%
4000-5000	21	5	145	25%
5000-6000	21	5	174	30%
6000-7000	21	5	203	35%
7000-8000	21	5	232	40%
8000-9000	21	5	261	45%
9000-10000	21	5	290	50%
10000-11000	21	5	319	55%
11000-12000	21	5	348	60%
12000-13000	21	5	377	65%
13000-14000	21	5	406	70%
14000-15000	21	5	435	75%
15000-16000	21	5	464	80%
16000-17000	21	5	493	85%
17000-18000	21	5	522	90%
18000-19000	21	5	551	95%
19000-20000	21	5	580	100%

Notes
1 This load sequence is not the same for all materials.
2 500 cycles were applied to condition all samples, consistent with AASHTO T 307 for resilient modulus testing of unbound base/subbase. These cycles are not included in the cycle count in column 1.
3 Ratio of applied deviator stress to the failure deviator stress.

2.11.4 PD TEST RESULTS

2.11.4.1 Target Sample Water Content and Dry Density

The target and actual molding water contents and dry densities are listed in Table 2-28 for each applied deviator stress level. The water contents of the samples after testing were consistently smaller than those before testing as drainage was permitted during the test. All samples have water contents and dry densities within 1.4% of the target values.

Table 2-28 Water content and dry density for single-stage PD tests

Materials	Deviator Stress Level	Target Water Content	Water Content before Test				Water Content after Test	Target Dry Density	Dry Density before Test			
	$\sigma_d/\sigma_{d,f}$ (%)	$\omega_{desired}$ (%)	ω_{before} (%)	Mean (%)	COV -	Deviation from Mean (%)	ω_{after} (%)	ρ_d kgm^{-3}	ρ_d kgm^{-3}	Mean kgm^{-3}	COV -	Deviation from Mean (%)
VA	30%	10.8%	11.5%	10.9%	5.2%	5.3%	10.7%	1833	1821	1831	0.5%	-0.5%
	47%	10.8%	11.3%			3.5%	9.5%	1833	1825			-0.3%
	60%	10.8%	11.1%			1.6%	9.5%	1833	1828			-0.2%
	79%	10.8%	10.6%			-2.9%	9.7%	1833	1836			0.3%
	94%	10.8%	10.1%			-7.5%	9.5%	1833	1845			0.7%
RCA	30%	11.0%	10.8%	11.4%	5.3%	-5.3%	9.9%	1884	1887	1877	0.5%	0.5%
	50%	11.0%	11.4%			0.0%	10.6%	1884	1877			0.0%
	70%	11.0%	12.0%			5.3%	10.2%	1884	1867			-0.5%
RCA&VA	30%	11.0%	12.4%	12.2%	2.6%	1.9%	11.0%	1867	1844	1848	0.3%	-0.2%
	50%	11.0%	11.8%			-3.0%	11.0%	1867	1854			0.3%
	70%	11.0%	12.3%			1.1%	11.1%	1867	1845			-0.1%
RAP	60%	5.6%	5.6%	5.6%	0.9%	-0.4%	4.6%	2003	2003	2003	0.0%	0.0%
	70%	5.6%	5.6%			-0.4%	4.5%	2003	2003			0.0%
	80%	5.6%	5.6%			-0.4%	4.2%	2003	2003			0.0%
	100%	5.6%	5.7%			1.3%	4.5%	2003	2001			-0.1%
RAP&VA	30%	9.0%	9.4%	9.7%	2.6%	-2.8%	9.0%	1916	1909	1904	0.2%	0.2%
	50%	9.0%	9.9%			2.4%	7.5%	1916	1900			-0.2%
	70%	9.0%	9.7%			0.3%	7.7%	1916	1904			0.0%

2.11.4.2 Behavioral Ranges from Single-Stage PD Tests

Plots of permanent strain and resilient modulus versus number of cycles, and permanent strain rate versus permanent strain are presented in Figure 2-44 through Figure 2-48 for all materials subjected to single-stage PD testing.

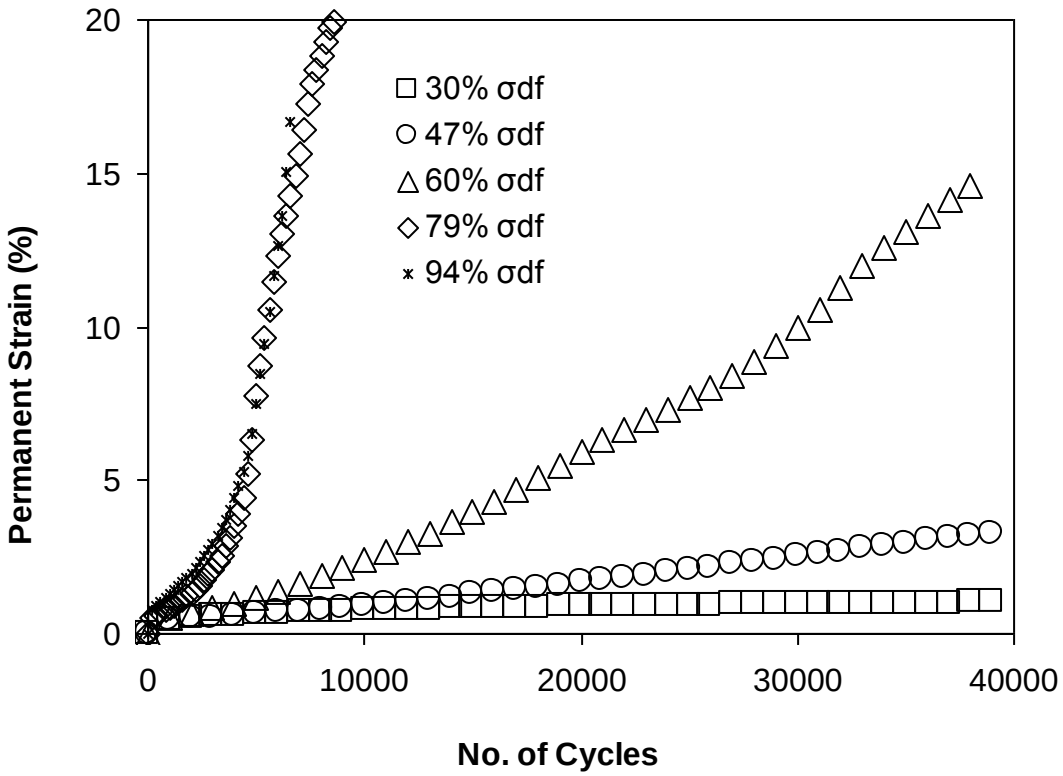

Figure 2-44a Permanent strain versus N at different deviator stress levels for VA

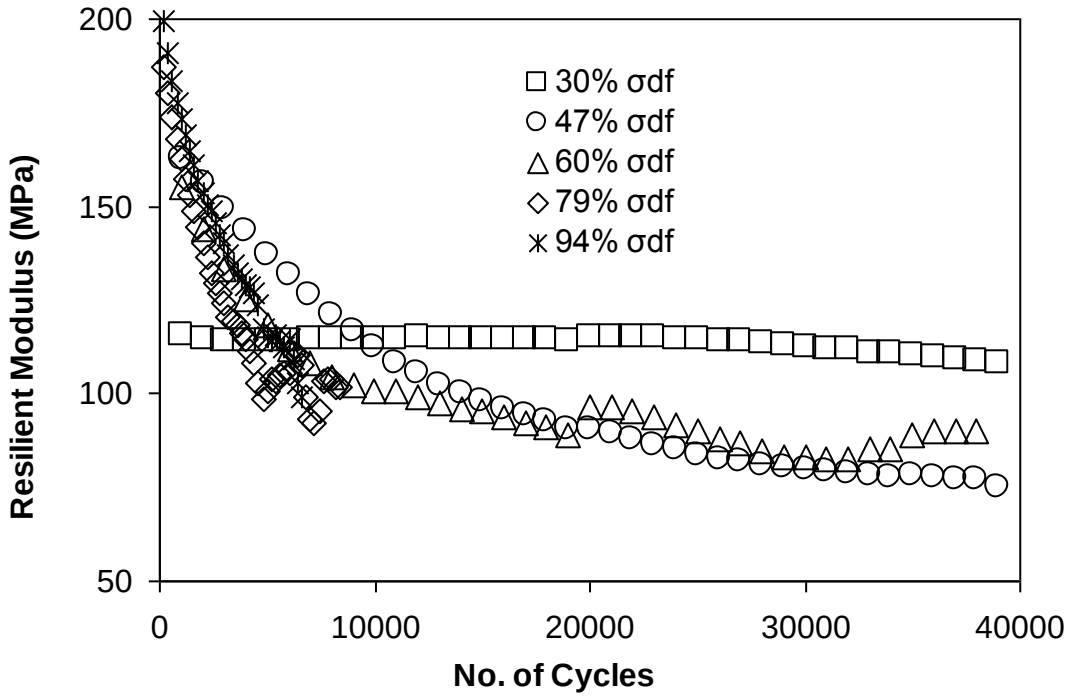

Figure 2-44b Resilient moduli versus N at different deviator stress levels for VA

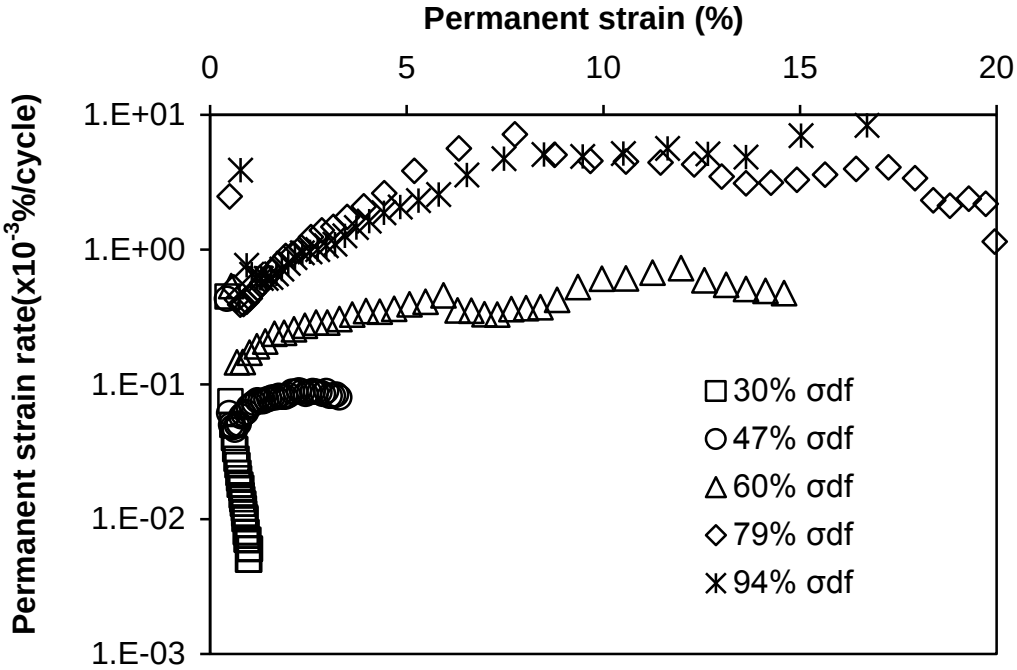

Figure 2-44c Permanent strain rate versus permanent strain at different deviator stress levels for VA

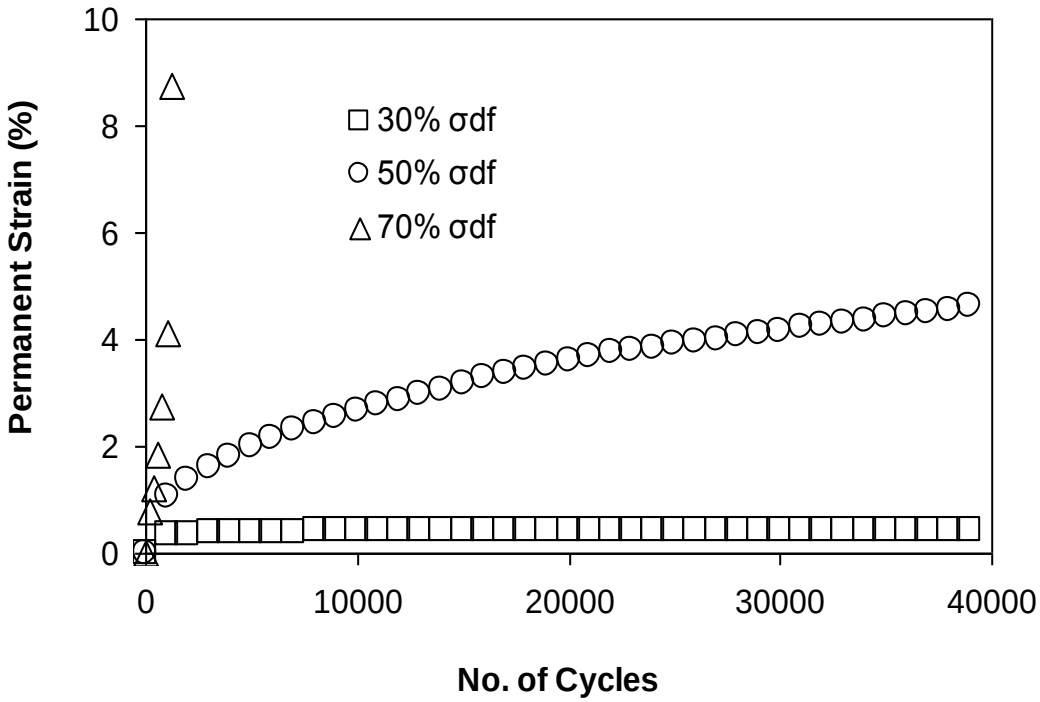

Figure 2-45a Permanent strain versus N at different deviator stress levels for RCA

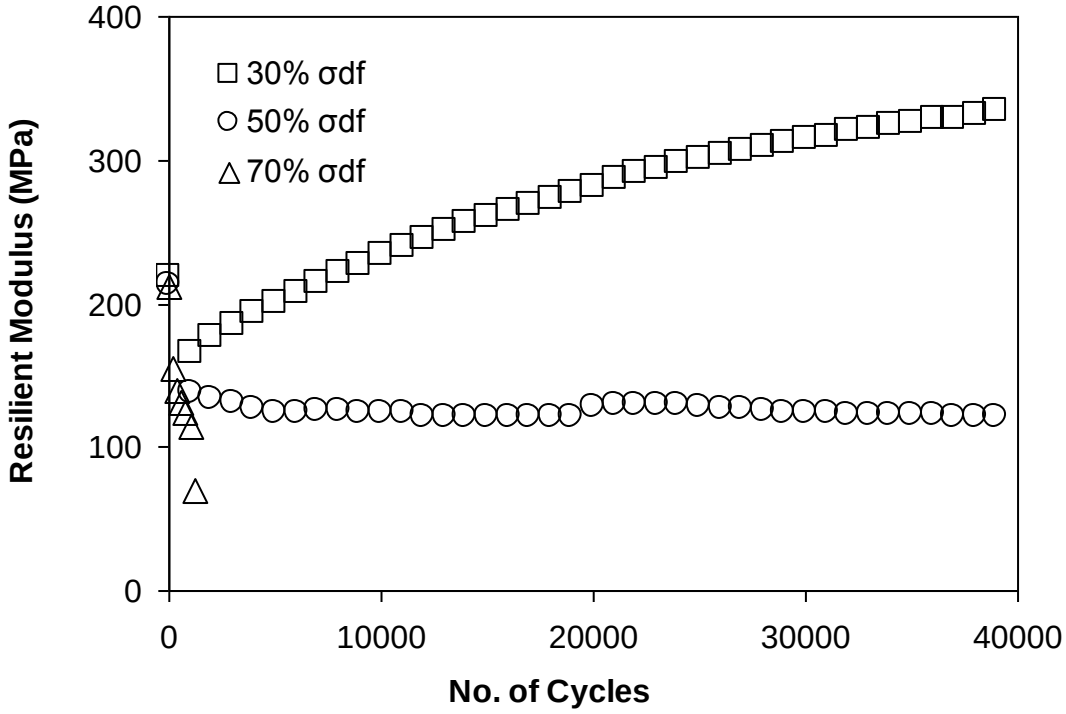

Figure 2-45b Resilient moduli versus N at different deviator stress levels for RCA

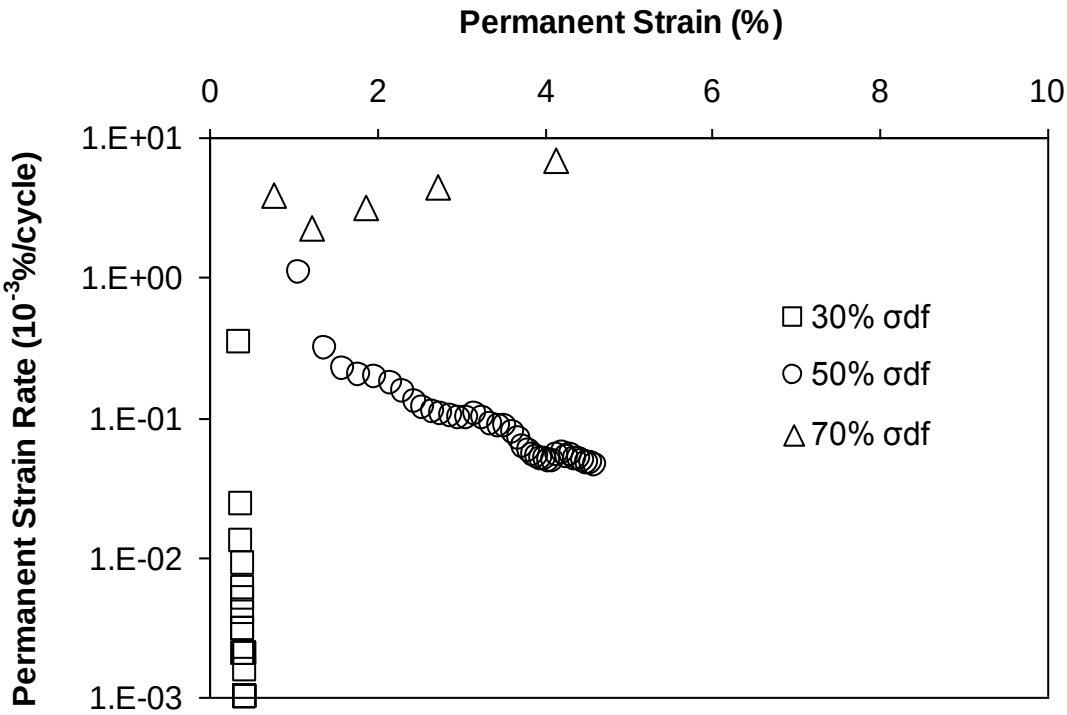

Figure 2-45c Permanent strain rate versus permanent strain at different deviator stress levels for RCA

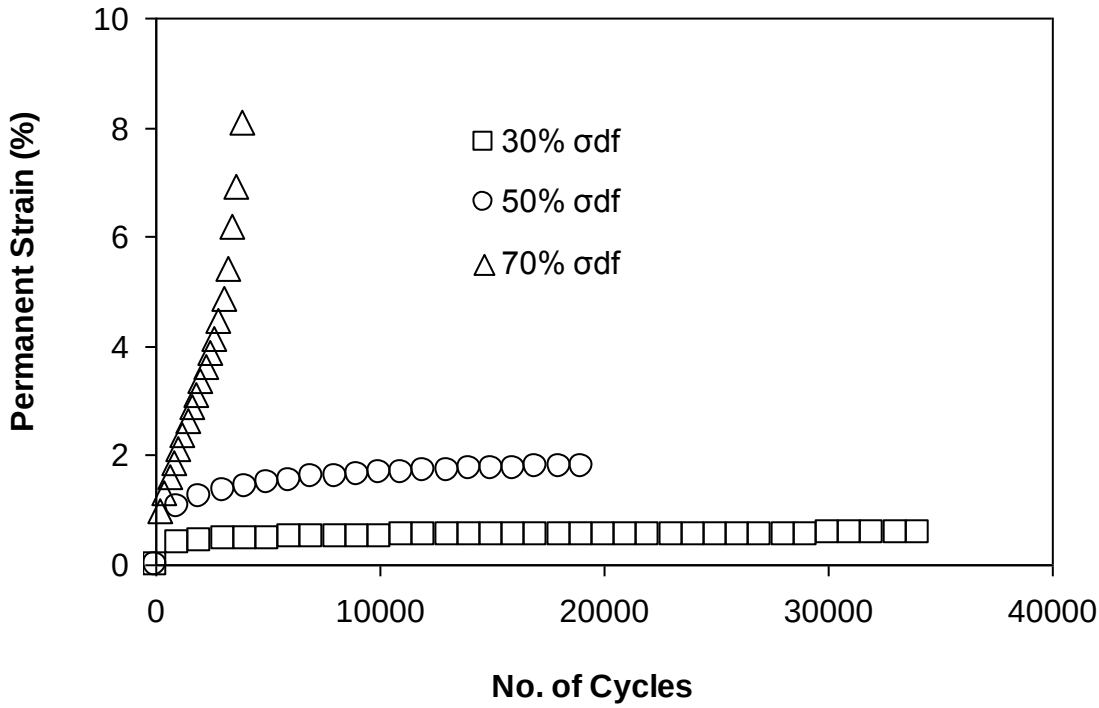

Figure 2-46a Permanent strain versus N at different deviator stress levels for RCA&VA

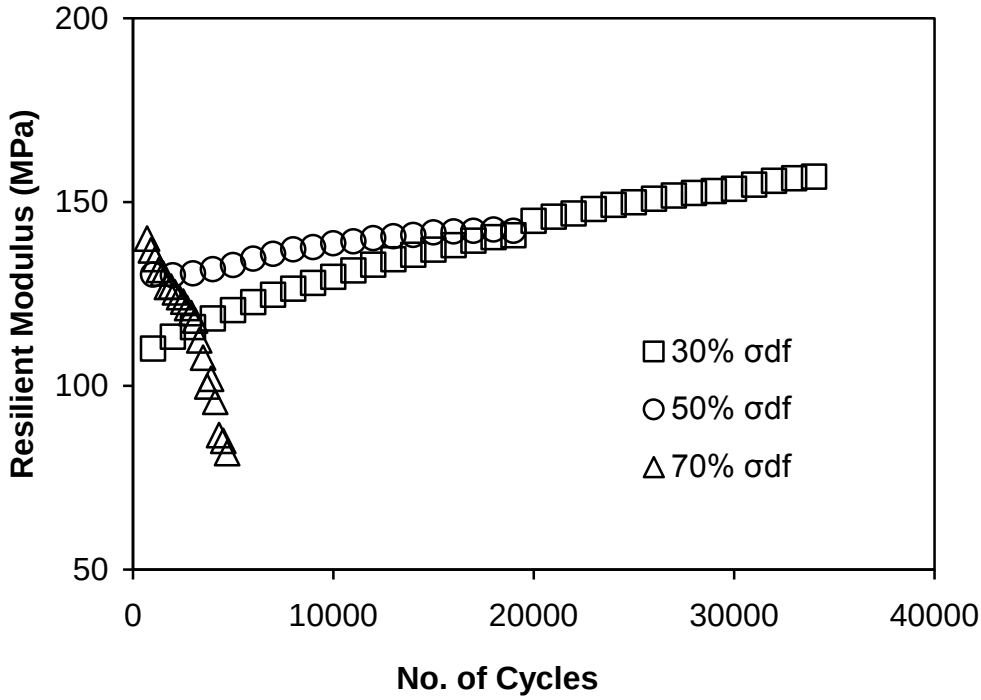

Figure 2-46b Resilient moduli versus N at different deviator stress levels for RCA&VA

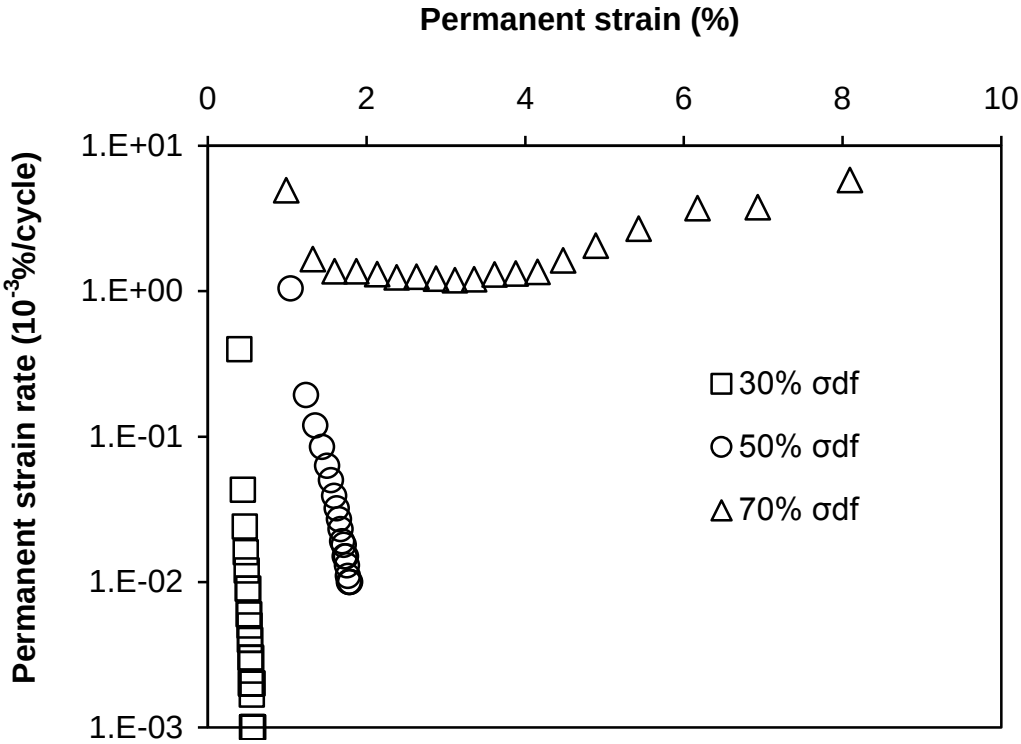

Figure 2-46c Permanent strain rate versus permanent strain at different deviator stress levels for RCA&VA

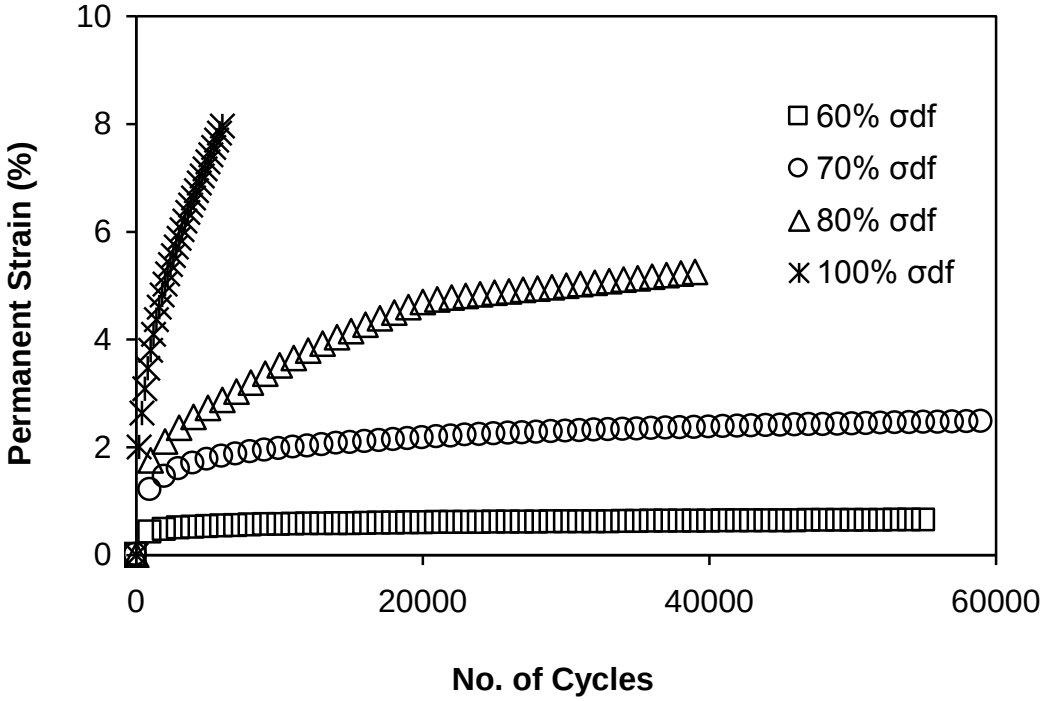

Figure 2-47a Permanent strain versus N at different deviator stress levels for RAP

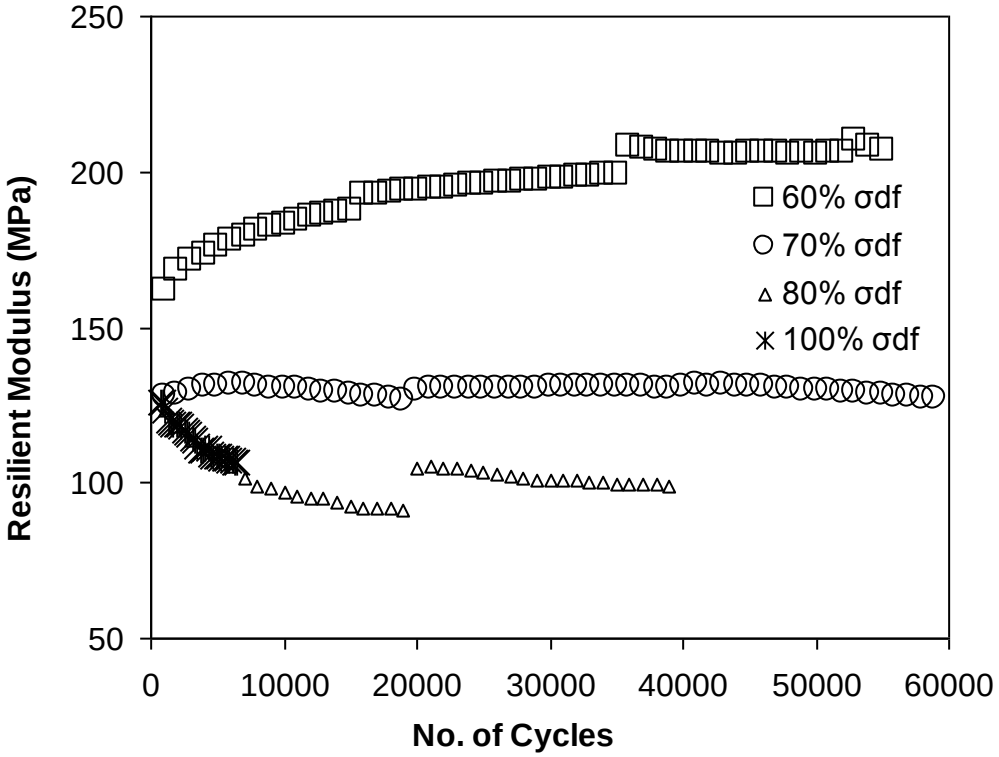

Figure 2-47b Resilient moduli versus N at different deviator stress levels for RAP

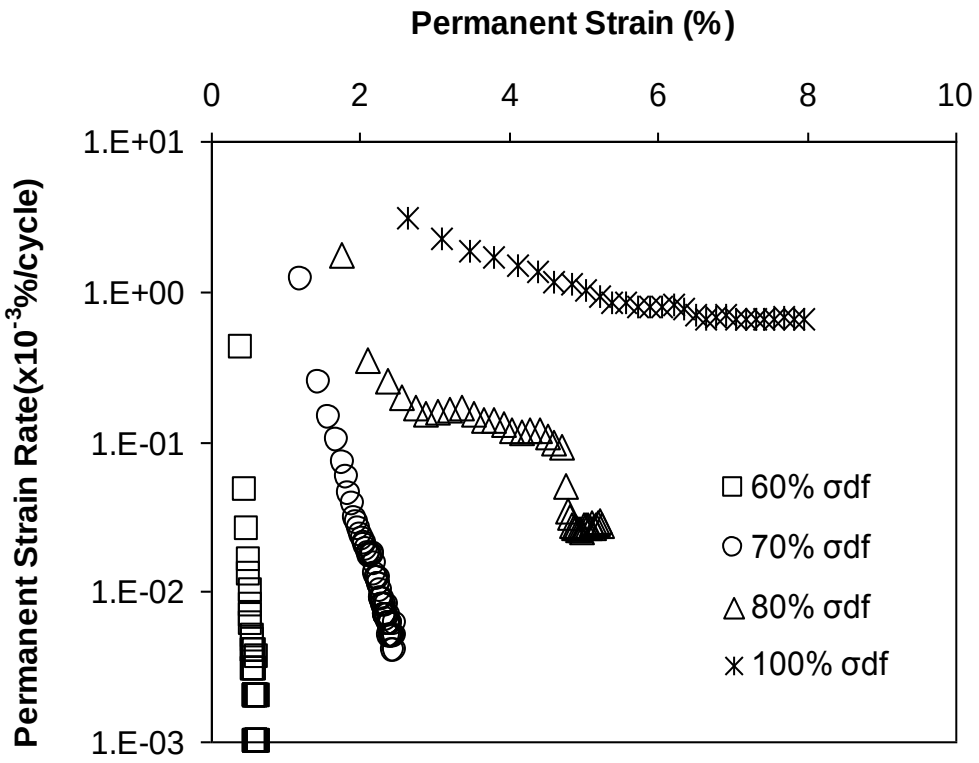

Figure 2-47c Permanent strain rate versus permanent strain at different deviator stress levels for RAP

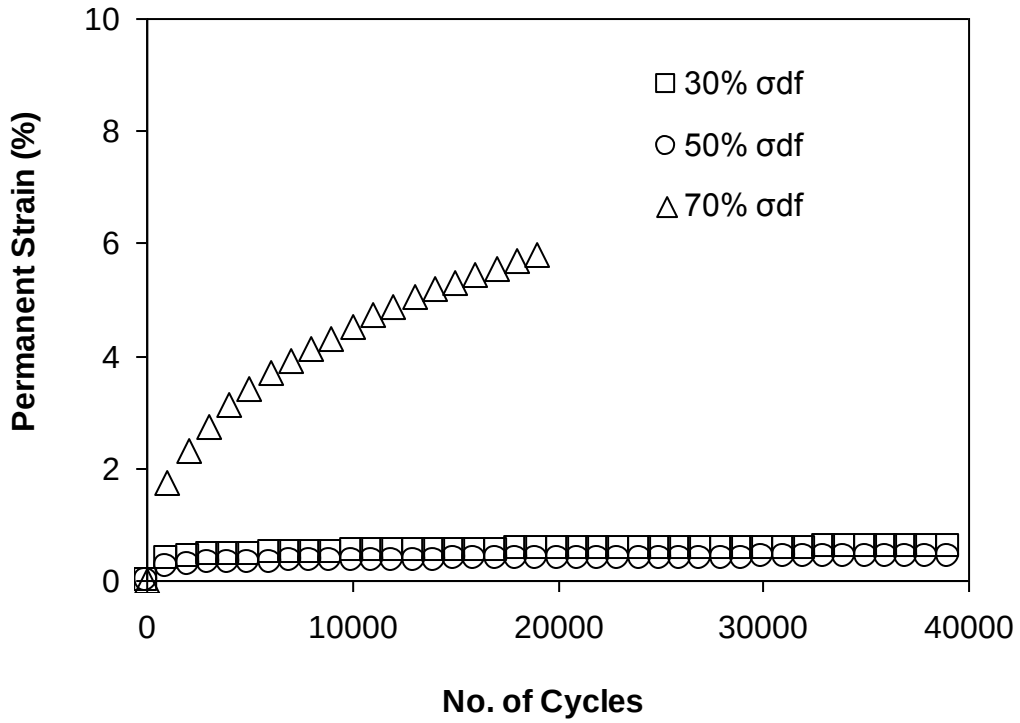

Figure 2-48a Permanent strain versus N at different deviator stress levels for RAP&VA

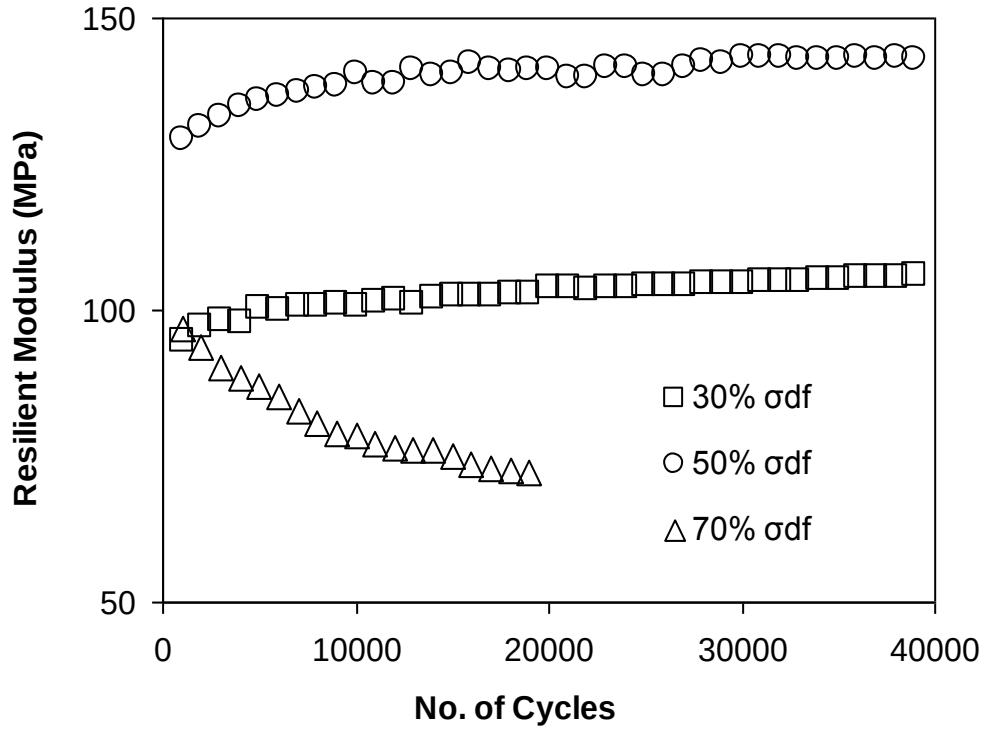

Figure 2-48b Resilient moduli versus N at different deviator stress levels for RAP&VA

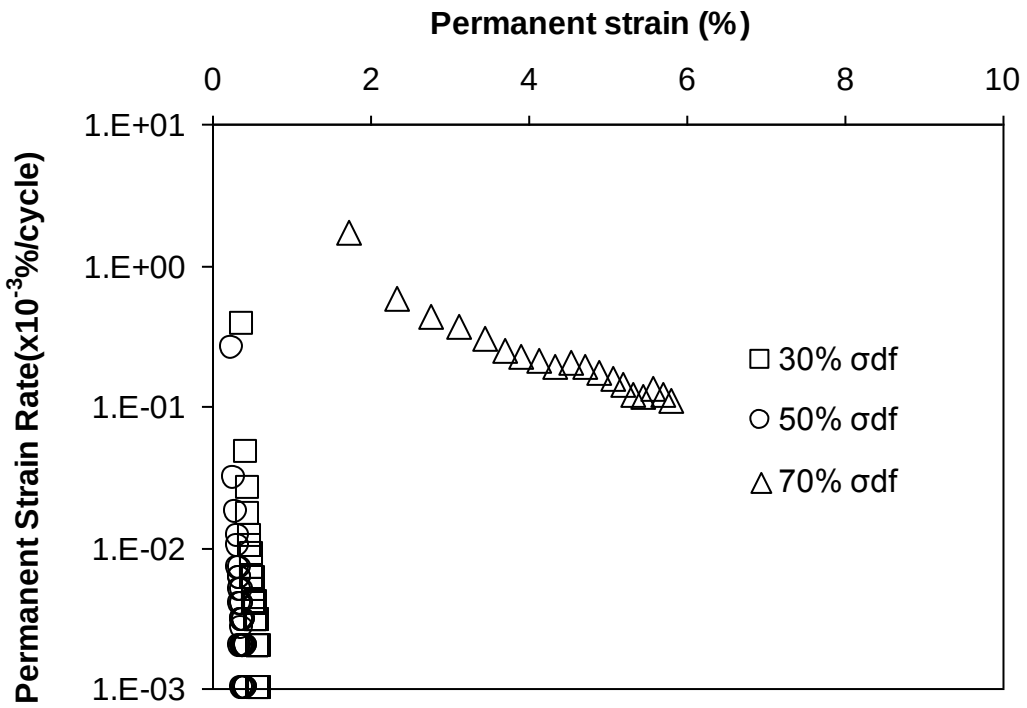

Figure 2-48c Permanent strain rate versus permanent strain at different deviator stress levels for RAP&VA

The behavioral ranges for all materials tested are also summarized in Table 2-29.

Table 2-29 Behavioral ranges based on a single-stage PD testing

Material	Deviator Stress Level	Number of Load Cycles at End of Test	Behavioral Ranges [1]	Range of Plastic Shakedown Limit
	σ_d/σ_{df}	N	-	-
	(%)	-	-	(kPa)
VA	30%	39600	A	210-330
	47%	39600	B	
	60%	38400	C	
	79%	8200	C	
	94%	6800	C	
RCA	30%	39400	A	240-400
	50%	39400	B	
	70%	1200	C	
RCA&VA	30%	34400	A	290-406
	50%	19800	A	
	70%	4400	C	
RAP	60%	54200	A	238-272
	70%	59200	A	
	80%	39600	B	
	100%	6000	C	
RAP&VA	30%	39200	A	170-238
	50%	39200	A	
	70%	19800	B	

Note
1 A: plastic shakedown; B: plastic creep; C: incremental collapse. Behavioral range classification based on plots of permanent strain rate versus permanent strain.

Plastic shakedown

Plastic shakedown was observed in all the materials. From Figures 2-44a through 2-48a, the maximum permanent strains were generally less than 2%, and do not increase much with number of cycles.

From Figures 2-44b through 2-48b, it can be observed that the resilient modulus increases slightly or remains constant during shakedown.

From Figures 2-44c through 2-48c, the permanent strain rates decreased linearly with permanent strain during shakedown.

Incremental Collapse

Incremental collapse was observed in VA, RCA, RCA&VA and RAP but not in the RAP&VA samples.

From Figures 2-44a through 2-48a, the permanent strain increases asymptotically with increasing number of cycles with failure occurring at a relatively small number of load cycles.

During incremental collapse, the resilient modulus decreased or the resilient strain increased with increasing number of load cycles. This is contradictory to the trend of decreasing resilient strain with increasing number of load cycles published by Werkmeister et al. (2003). Two notable differences exist between their tests and the ones performed herein. Their samples were subjected to a loading frequency of 5Hz instead of 1Hz and their confining stresses are about 3 times higher than the value used in our test program (21kPa). At high load frequencies, there is a question as to whether the material will: (1) behave in a drained fashion; a more undrained behavior generally implies a stiffer response; and (2) have time to rebound due to viscous effects.

From Figures 2-44c through 2-48c, it can be observed that the permanent strain rate initially decreased. Then, it tended to a constant or increased slightly when the sample failed.

Plastic Creep

This intermediate behavior can be observed only with the permanent strain rate versus permanent strain plots of Figure 2-44c through 2-48c. This behavior is not observed in the other plots, because a large number of load cycles are required for failure to occur. Thus, the permanent strain rate versus permanent strain plot is least ambiguous for characterizing the various behavioral ranges.

2.11.4.3 Models for Single-Stage PD Tests

Historically, the power law model by Sweere (1990 - see Table 2-23) has been used widely to model PD test results because it is known to capture shakedown behavior well (Dawson 2008). The model is as follows:

$$\varepsilon_p = AN^B \qquad (2.11)$$

where ε_p(%) = permanent strain, N = number of cycles and A and B are regression parameters.

When Equation 2.11 is used to fit the PD test data, the power law model provided excellent fits to the data overall. The model parameters for the materials tested are summarized in Table 2-30. It can be seen that the coefficients of determination, R^2, are all above 0.91.

Equation 2.11 relates permanent strain to number of cycles only. When parameters A and B are plotted against deviator stress level (σ_d/σ_{df}) for VA, as shown in Figures 2-49a and b, respectively, it can be seen that both A and B vary with deviator stress levels. In light of this observation, it would be advantageous to develop permanent strain models that vary with both number of cycles and stress level.

Table 2-30 Power law model parameters for all materials tested

Materials	Applied Deviator Stress	Deviator Stress Level	Parameter A	Parameter B	R^2
	σ_d (kPa)	σ_d/σ_{df} (%)	- -	- -	- -
VA	210	30%	0.095	0.225	0.999
	330	47%	0.002	0.692	0.941
	420	60%	1.0E-04	1.089	0.971
	550	79%	2.0E-06	1.781	0.945
	660	94%	7.0E-05	1.350	0.914
RCA	240	30%	0.258	0.051	0.941
	400	50%	0.062	0.409	0.999
	560	70%	0.003	1.009	0.961
RCA&VA	174	30%	0.230	0.089	0.970
	290	50%	0.354	0.167	0.974
	406	70%	0.003	0.926	0.946
RAP	204	60%	0.239	0.090	0.985
	238	70%	0.493	0.148	0.982
	272	80%	0.181	0.323	0.985
	340	100%	0.226	0.408	0.999
RAP&VA	102	30%	0.177	0.116	0.995
	170	50%	0.109	0.129	0.998
	238	70%	0.105	0.408	1.000

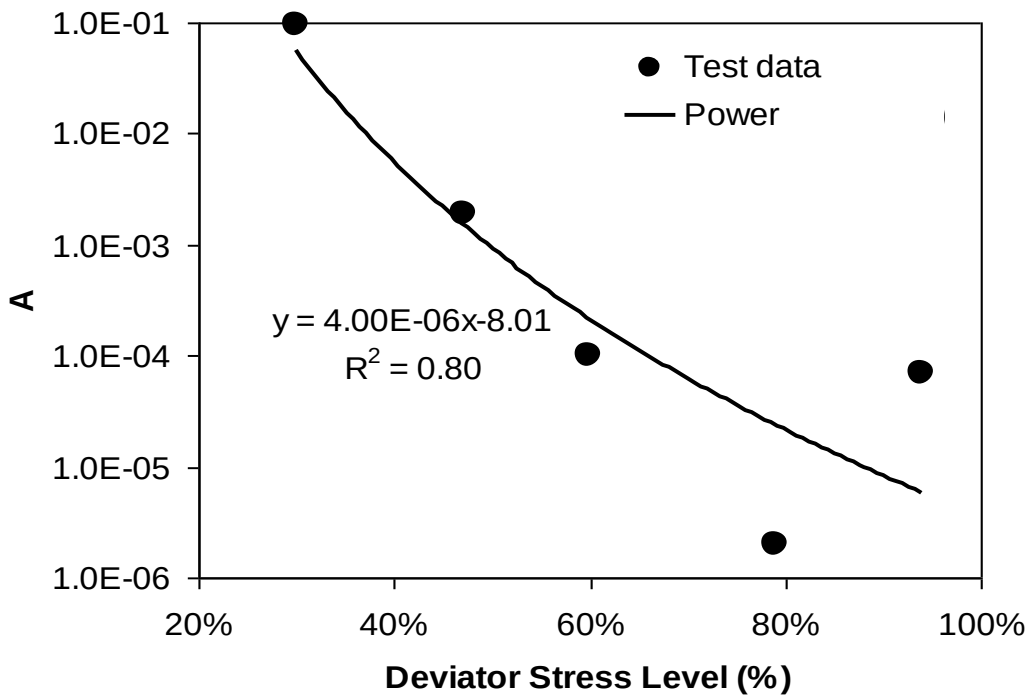

Figure 2-49a Power law model parameters A versus deviator stress level for VA

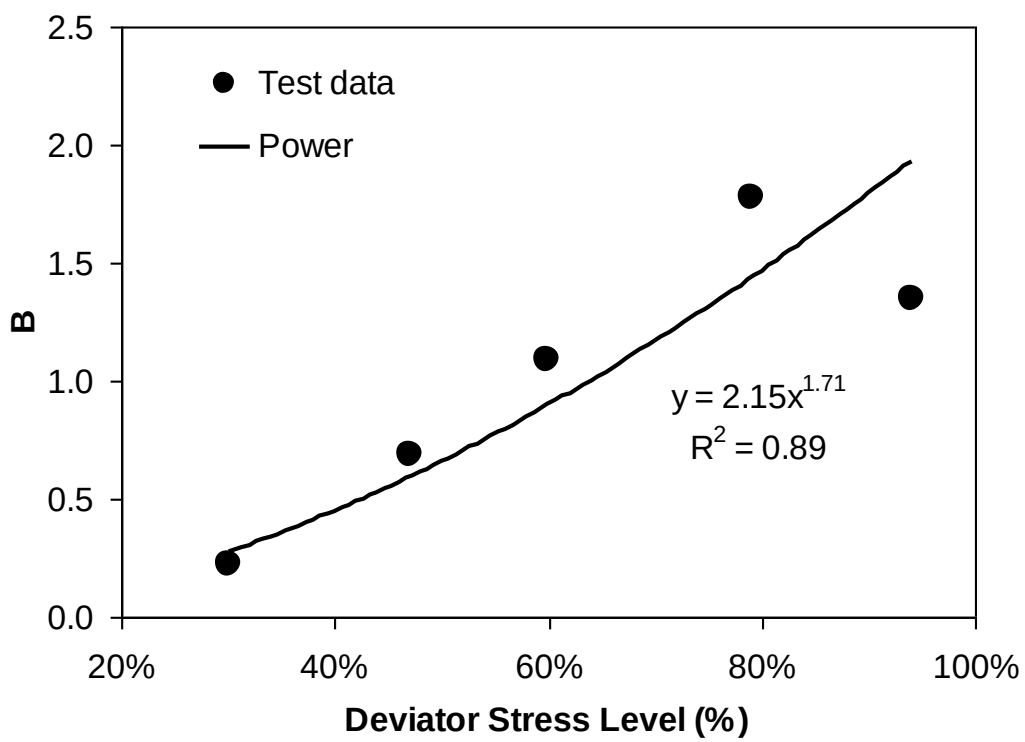

Figure 2-49b Power law model parameters B versus deviator stress level for VA

In addition to the Huurman (1997) model, another model that relates permanent strain to both number of cycles and stress levels is the Tseng and Lytton (1989) model. These two models were evaluated because: (1) they involve only one equation; and (2) they are both mathematically capable of modeling behavioral ranges varying from shakedown to incremental collapse. Also, the Tseng and Lytton (1989) model has been adopted in the MEPDG.

The Huurman model is presented first. The regression constants for this model (Equation 2.10) for all the materials tested are summarized in Table 2-31. This table shows that except for VA, the parameters c_1 and d_1 are all zero indicating that the second term in the Huurman (1997) model is zero. For VA, although the parameters c_1 and d_1 are not zero, their t-statistics are smaller than 2.0 (Table 2-32), indicating that the second term in the Huurman model is statistically insignificant and should be discarded.

Table 2-31 Summary of regression constants for the Huurman model

$$\varepsilon_p = A\left(\frac{N}{1000}\right)^B + C\left(e^{D\left(\frac{N}{1000}\right)} - 1\right)$$

Material	a_1	a_2	b_1	b_2	c_1	c_2	d_1	d_2
VA	0.008	1.623	1.850	1.320	1.8E-05	1.986	0.688	2.314
RCA	0.046	2.179	9.630	4.756	0.0E+0	4.097	0.0E+0	4.532
RCA&VA	0.031	1.606	6.290	5.401	0.0E+0	4.098	0.0E+0	4.532
RAP	0.035	4.311	0.534	1.843	0.0E+0	7.008	0.0E+0	4.452
RAP&VA	0.039	2.949	21.500	11.461	0.0E+0	5.230	0.0E+0	3.610

Table 2-32 Parameter estimates and t-statistics for VA using the Huurman model

Parameter	Estimate	Std. Error	t-statistics	95% Confidence Interval	
				Lower Bound	Upper Bound
a_1	0.008	0.002	4.120	0.004	0.012
a_2	1.623	0.476	3.412	0.689	2.557
b_1	1.850	0.135	13.685	1.584	2.115
b_2	1.320	0.156	8.468	1.014	1.626
c_1	1.800E-05	0.003	0.005	-0.006	0.006
c_2	1.986	373.466	0.005	-731.329	735.301
d_1	0.688	24.163	0.028	-46.757	48.133
d_2	2.314	71.608	0.032	-138.291	142.920

Without the second term, the first term of the Huurman model reverts to the power model. The data was re-analyzed using the power model and the regression constants for all materials are summarized in Table 2-33. The parameter estimates and t-statistics for VA as an example are summarized in Table 2-34. The t-statistics for all materials are all larger than 2.0, indicating statistical significance.

Table 2-33 Summary of regression constants for the first term of the Huurman model

$$\varepsilon_p = A\left(\frac{N}{1000}\right)^B$$

Material	a_1	a_2	b_1	b_2
VA	0.007	1.846	1.9708	1.218
RCA	0.046	2.179	9.630	4.756
RCA&VA	0.031	1.606	6.290	5.401
RAP	0.035	4.311	0.534	1.843
RAP&VA	0.039	2.949	21.500	11.461

Table 2-34 Parameter estimates and t-statistics for the first term of the Huurman model for VA

Parameter	Estimate	Std. Error	t-statistics	95% Confidence Interval	
				Lower Bound	Upper Bound
a_1	0.007	0.001	4.888	0.004	0.009
a_2	1.846	0.411	4.493	1.039	2.653
b_1	1.971	0.132	14.949	1.712	2.230
b_2	1.218	0.134	9.060	0.954	1.482

A comparison of the predicted and measured permanent strain as a function of number of cycles and deviator stress levels for VA is shown in Figure 2-50a. Figure 2-50b shows a comparison of the predicted and measured permanent strain with respect to a 1:1 line. It is observed that the first term of the Huurman model or the power model, is able to capture the data at low deviator stresses well. At high deviator stress levels where the material incrementally collapses, the fit is not as good. This makes sense since the power model captures only shakedown behavior well.

The Huurman model utilizes σ_{1f} as one of its parameters. However, σ_{1f} is sensitive to the molding water content and suction, etc. and can be highly variable especially when partially saturated. To avoid reliance on a parameter that can be so widely divergent, an alternative form of the stress ratio term $\left(\frac{\sigma_1}{\sigma_3}\right)$ instead of $\left(\frac{\sigma_1}{\sigma_{1f}}\right)$ was also investigated, where σ_3 is the confining stress. This model is termed the modified Huurman model.

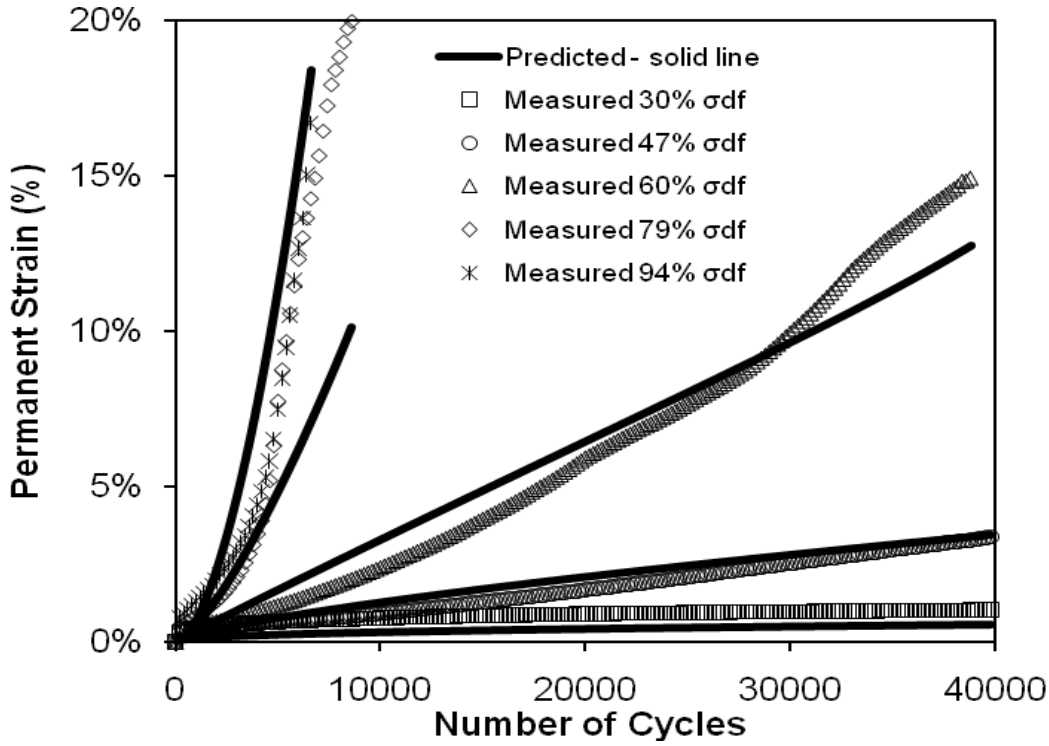

Figure 2-50a Predicted versus measured PD using first term of the Huurman model

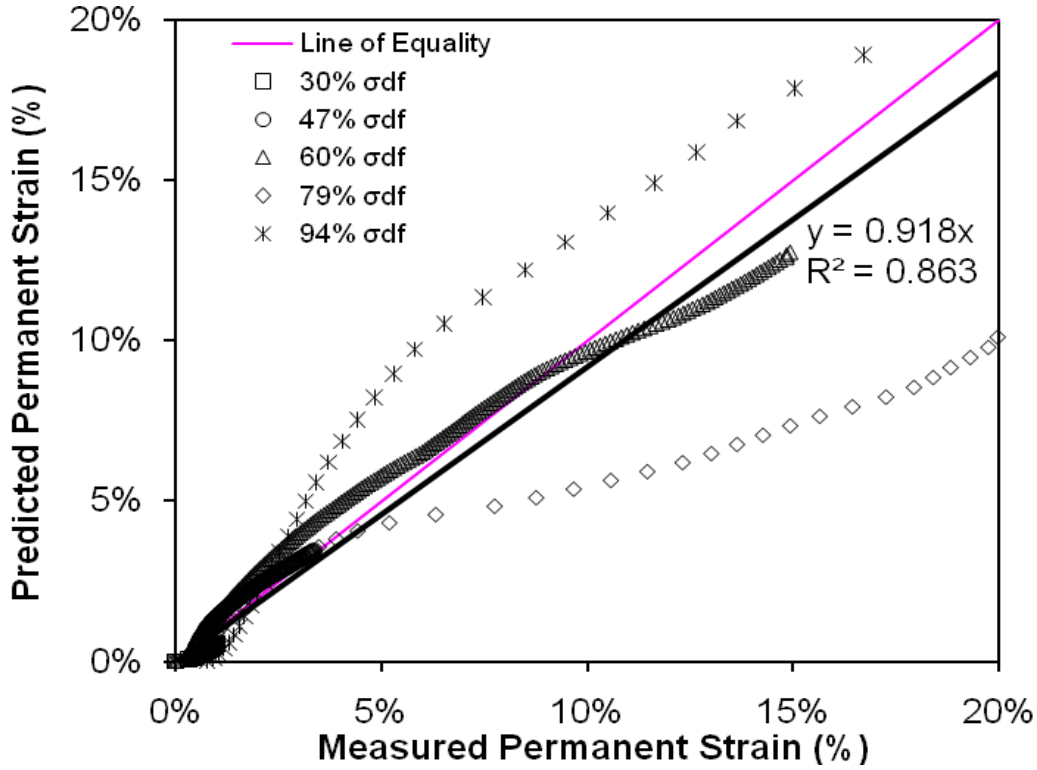

Figure 2-50b Predicted versus measured PD using first term of the Huurman model

When regression analysis was performed to derive the eight regression constants for the materials tested, again only the first term of the modified Huurman model was statistically significant. These four regression constants are summarized in Table 2-35. The parameter estimates and t-statistics for VA as an example are summarized in Table 2-36. (Note a_1 is a necessary parameter and cannot be discarded even though the t-statistic is 0.787.) The majority of the t-statistics for all material types are larger than 2.0, indicating statistical significance.

Table 2-35 Summary of regression constants for the first term of the modified Huurman model

$$\varepsilon_p = A\left(\frac{N}{1000}\right)^B$$

Material	a_1	a_2	b_1	b_2
VA	9.56E-06	1.85	0.03	1.22
RCA	1.47E-05	2.20	3.99E-07	4.61
RCA&VA	1.47E-04	1.60	8.18E-08	5.42
RAP	1.65E-07	4.31	2.83E-03	1.84
RAP&VA	2.33E-07	4.45	7.61E-08	6.19

Table 2-36 Parameter estimates and t-statistics for the first term of the modified Huurman model for VA

Parameter	Estimate	Std. Error	t-statistics	95% Confidence Interval	
				Lower Bound	Upper Bound
a_1	9.559E-06	1.215E-05	0.787	-1.430E-05	3.342E-05
a_2	1.846	0.411	4.493	1.039	2.653
b_1	0.027	0.011	2.416	0.005	0.048
b_2	1.218	0.134	9.060	0.954	1.482

A comparison of the predicted and measured permanent strain for VA is shown in Figure 2-51.

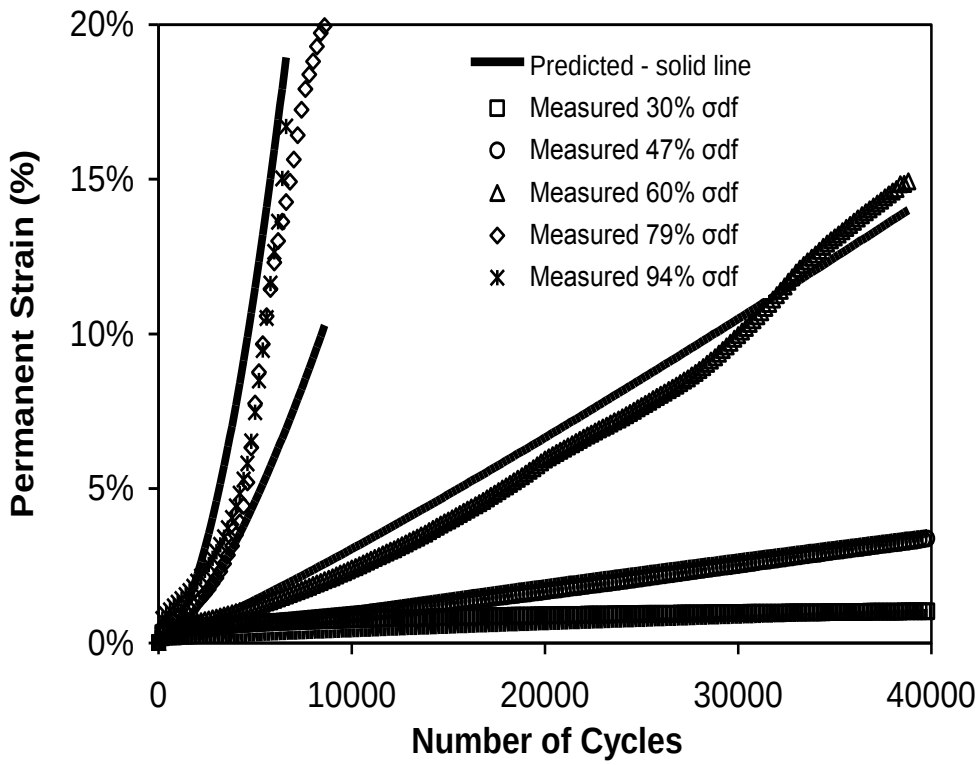

Figure 2-51a Predicted versus measured PD using the first term of the modified Huurman model

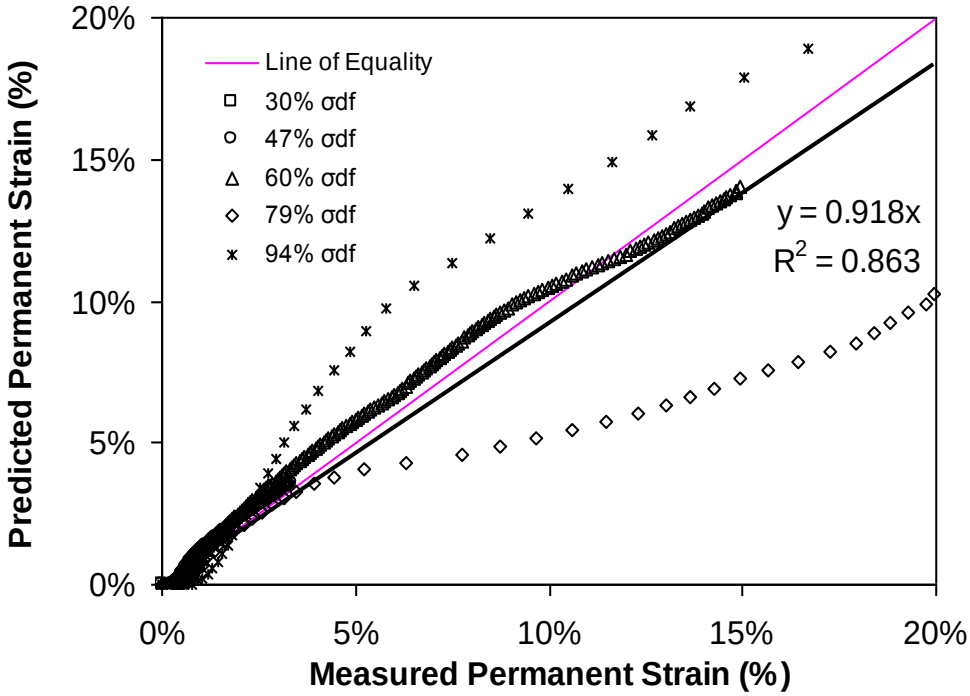

Figure 2-51b Predicted versus measured PD using the first term of the modified Huurman model

The Tseng and Lytton (1989) model was also evaluated by correlating its three parameters (A, B and C) with stress level in a power law format. This way, the model can predict PD as a function of N and stress level. The modified Tseng and Lytton (1989) model is as follows:

$$\varepsilon_p = Ae^{-\left(\frac{B}{N}\right)^C} \tag{2.12}$$

where A = $a_1\left(\frac{\sigma_1}{\sigma_3}\right)^{a_2}$, B = $b_1\left(\frac{\sigma_1}{\sigma_3}\right)^{b_2}$, C = $c_1\left(\frac{\sigma_1}{\sigma_3}\right)^{c_2}$, e = base of natural logarithm (2.17828…) and a_1, a_2, b_1, b_2, c_1, and c_2 are regression constants.

During non-linear regression, the exponential term became either very large or very small leading to convergence issues. As a result, further investigation on the use of this model was abandoned.

Regression results for all the materials tested using the first term of the Huurman and modified Huurman models are summarized in Table 2-37.

Table 2-37 Summary of the bias (slope) and coefficient of determination for the models evaluated

Material	First Term of the Huurman Model		First Term of the Modified Huurman Model	
	Slope	R^2	Slope	R^2
VA	0.918	0.863	0.918	0.863
RCA	1.000	1.000	1.000	1.000
RCA&VA	0.992	0.983	0.992	0.983
RAP	0.988	0.966	0.988	0.966
RAP&VA	0.978	0.966	0.975	0.961

The slope represents the bias of the prediction model and the R^2 represents the degree of scatter (or variability) of the data in relation to the model. Three indicators can be used to evaluate the models: (1) bias; (2) variability; and (3) simplicity. In terms of bias and variability, the first term of the Huurman model is just a little better off than the first term of the modified Huurman model. In terms of simplicity, the modified Huurman model requires less laboratory work since it does not require determination of the failure principle stress.

2.11.4.4 Multi-Stage PD Tests

Multiple single-stage PD tests must be conducted to determine the shakedown limit. Disadvantages of single stage PD tests include: (1) There may be variability among the individual samples which can adversely influence the interpretation of the shakedown limit; and (2) Performing multiple tests requires a significant amount of time. In light of these shortcomings, it may be worth considering multi-stage PD tests.

Multi-stage PD tests were also performed to verify whether they provide shakedown limits that are consistent with the single-stage PD tests on multiple samples. Standards are available in Europe to perform single- and multi-stage PD tests but not in the United States. In the European standard (CEN EN 13286-7), both the confining and deviator stresses vary in multi-stage PD testing. A loading frequency between 0.2 and 10 Hz is permitted. In the US, multi-stage PD testing was recently performed by Saeed (2008) as part of NCHRP Project 598. Saeed recommended a multi-stage PD test load sequence in which the confining stress is a constant (103.4 kPa) and the load

frequency is 1 Hz (0.1s load pulse with a 0.9s rest period). The number of load cycles in NCHRP Report 598 was used in this study. Details of the load sequence for the multi-stage PD tests are as follows:

1. The confining stress was kept constant throughout the test (21 kPa) and selected to be consistent with the value used in resilient modulus and single-stage PD tests. This allows a proper comparison of the shakedown limit from both single- and multi-stage tests to be made.

2. The deviator stress encompassed those used in the single–stage tests and were varied over a wide range to capture plastic shakedown through incremental collapse. A thousand load cycles of each deviator stress were applied as recommended in NCHRP Report 598.

2.11.4.5 Multi-Stage PD Test Results and Analysis

Results of multi-stage PD tests are presented in Table 2-38 in terms of the stress ratio at permanent strains of 1%, 2%, 5% and 10%. From these results, the VA and RCA are superior in terms of resistance to PD since they are able to sustain the highest stress ratios at a given permanent strain. It is quite surprising that the 50% RCA:50% VA did not fare as well as the unblended ingredients. However, clearly, the RAP and its blend are most susceptible to PD. This may be attributable to the fact that the asphalt caused the particles to deform within themselves more readily. It should be noted that the deviator stress increments applied are not consistent for each material type. This is because the increments were chosen to be between 5 to 15% of the failure deviator stresses, which are quite variable (Table 2-26).

Table 2-38 Summary of stress ratios at different permanent strains in multi-stage permanent deformation tests.

Material	Stress Ratio (σ_1/σ_3) at the following Permanent Strains			
	1%	2%	5%	10%
VA	32.4	32.4	37.6	37.6
RCA	31.4	35.2	35.2	35.2
50% RCA:50% VA	16.2	18.9	20.3	21.7
RAP	15.6	17.2	20.4	22.0
50% RAP:50% VA	9.1	10.7	12.3	12.3

Notes:

1) σ_1 = major principal stress = deviator stress + σ_3.
2) σ_3 = minor principal stress.

A big uncertainty in multi-stage PD tests is the determination of the shakedown limit. A method is proposed below, followed by a comparison of its predictive capability with those from single-stage PD test results.

When the results are plotted in terms of resilient modulus (at 200 cycle intervals) versus number of cycles (Figure 2-52 shows the results for RCA), an interesting observation is made. At a low constant deviator stress (≤ 400 kPa), the resilient moduli increased with increasing number of cycles indicative of modulus hardening during shakedown. At high constant deviator stresses (> 400 kPa), the resilient moduli decreased with increasing number of cycles (modulus softening) indicative of Range B and C behavior. Alternatively, the plot could be made in terms of resilient strain versus number of cycles except that the slope changes would be in reverse.

Only the curve for RCA is shown in Figure 2-52 for brevity. Curves for all other materials tested have similar trends. Based on this sudden switch in the resilient modulus trend, it is rational to assume that:

1) a deviator stress of 400 kPa is a lower bound for the shakedown limit of RCA under a confining pressure of 21 kPa; and
2) a deviator stress > 400 kPa is indicative of either plastic creep (Range B) or incremental collapse (Range C) of the RCA under a confining pressure of 21 kPa.

The behavioral range limits for all other materials tested are summarized in Table 2-39. Based on these limits, the behavioral range of the single-stage samples are evaluated and also summarized in the same table. It can be seen that 14 predictions out of 18 are correct (78% reliability). Possible reasons why the agreement is not perfect include: (1) variability among the single- and multi-stage samples; and (2) the number of cycles per deviator stress and number of deviator stresses are limited in a multi-stage test. However, considering these differences, the success rate is noteworthy and multi-stage PD testing can provide an economical alternative to characterize the PD behavior of geomaterials. Additional testing is needed to further validate this procedure. To facilitate this, a standard test load sequence is needed. The one proposed by Saeed (2008) presents a good starting point with perhaps a suggestion that the confining stress should be representative of the field pavement section to be studied.

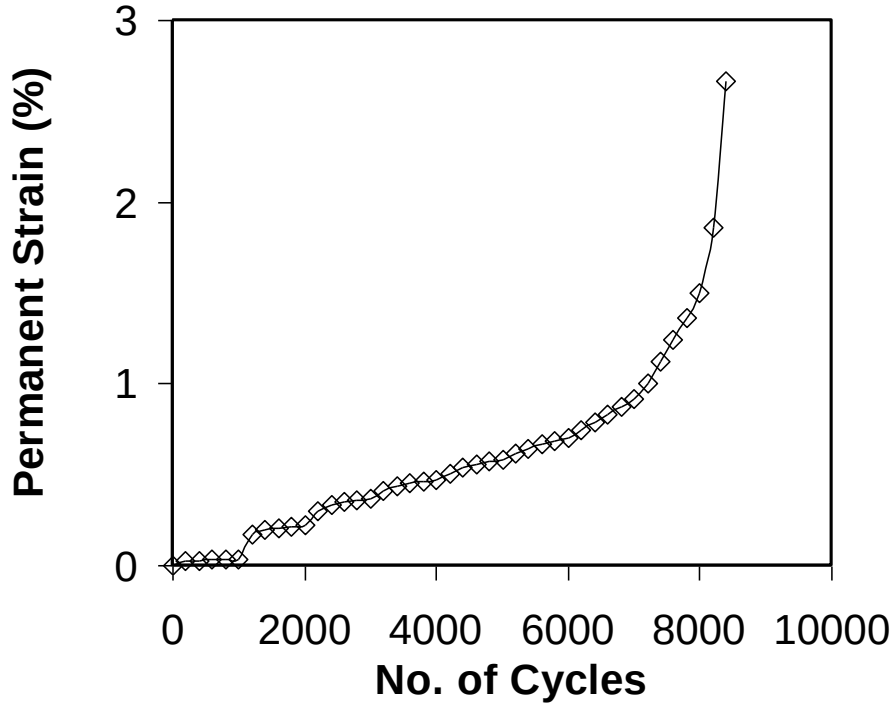

(a)

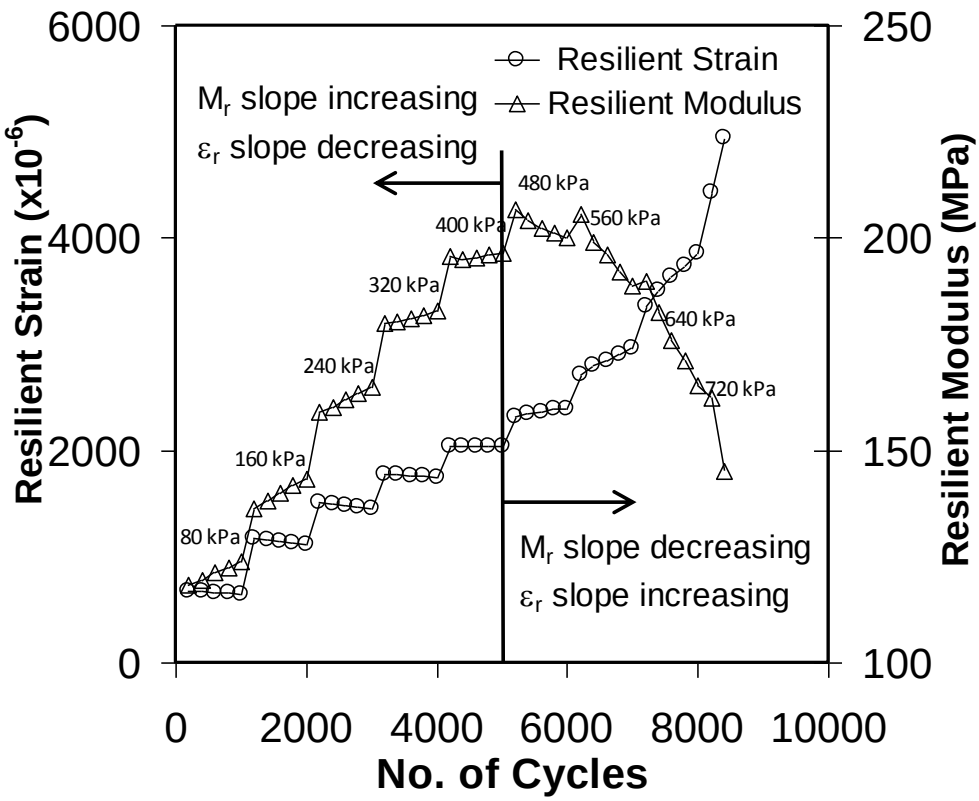

(b)

Figure 2-52 Multi-stage permanent deformation test results for recycled concrete aggregate (RCA): (a) Permanent strain versus number of cycles and (b) Resilient modulus/strain versus number of cycles. Deviator stresses are notated in figure.

Table 2-39 Behavioral ranges based on a single- and multi-stage PD testing.

Material	Single-Stage Tests			Multi-Stage Tests		
	Deviator Stress in Single-stage Tests σ_d (kPa)	Range of Plastic Shakedown Limit based on Single-stage Tests (kPa)	Behavioral Ranges based on Single-stage Tests[1]	Lower Bound Shakedown Limit based on Multi-stage Tests (Range A) (kPa)	Predicted Single-stage Sample Behavioral Range Using Multi-Stage Test Results	Accuracy
VA	210	210-330	A	217	A	√
	330		B		B/C	√
	420		C		B/C	√
	550		C		B/C	√
	660		C		B/C	√
RCA	240	240-400	A	400	A	√
	400		B		A	x
	560		C		B/C	√
50% RCA:50% VA	174	290-406	A	174	A	√
	290		A		B/C	x
	406		C		B/C	√
RAP	204	238-272	A	204	A	√
	238		A		B/C	x
	272		B		B/C	√
	340		C		B/C	√
50% RAP:50% VA	102	170-238	A	102	A	√
	170		A		B/C	x
	238		B		B/C	√

Note: 1) Behavioral range classification based on plots of permanent strain rate versus permanent strain. A= plastic shakedown; B = plastic creep; C = incremental collapse.

2.11.5 SUMMARY AND CONCLUSIONS

A confining stress of 21 kPa was used for all single- and multi-stage PD tests conducted on VA, RCA, RCA&VA, RAP and RAP&VA. The following summary and conclusions are offered:

- No agreed upon set of specifications for measuring PD have been established in the United States.

- The MEPDG combines the results of a mechanistic analysis of the various pavement layers with empirical pavement distress relationships to compute the incremental damage over time. The plastic deformation of each layer is summed and compared to the allowable value based on the rutting criteria.

- Upon application of a moving wheel load, a pavement element is subjected to a rotation of principal stresses. This rotation is not captured by regular CCP RLT test, but may be captured by more advanced VCP RLT tests.

- Pavement stresses consist of overburden pressure, compaction-induced locked-in stresses and traffic induced stresses. The compaction-induced locked-in stresses are difficult to determine and seldom addressed in pavement design.

- A direct dependency between the shear strength and PD resistance does not exist. PD is a function of the number of load cycles, confining and

deviator stresses, water content, density, stress history, stress paths, gradation and particle angularity and roughness.

- Three possible behavioral ranges are possible in a PD test. They include (a) plastic shakedown (Range A); (b) plastic creep (Range B); and (c) incremental collapse (Range C). The limit between plastic shakedown and plastic creep is known as the plastic shakedown limit. The limit between plastic creep and incremental collapse is known as the plastic creep limit.

- When interpreting single-stage PD test results, it is least ambiguous to use the vertical permanent strain rate versus permanent strain plot to distinguish between the behavioral ranges. This is because Range B behavior cannot be easily observed when plotting results in terms of number of cycles since a very large number of cycles are sometimes required to eventually collapse the sample.

- In single stage PD testing, modulus hardening was observed during plastic shakedown and modulus softening during plastic creep and incremental collapse. The latter is contradictory to trends observed by Werkmeister et al. (2004). The difference can be explained as follows: their samples were subjected to a much higher loading frequency (5Hz instead of 1Hz). At high load frequencies, the material tends to behave in a more undrained fashion leading to a stiffer resilient response. Also, there is inadequate time for the sample to recover from viscous effects.

- Ideally, UGM should be designed to limit the applied loads to less than the shakedown load, wherein the growth of plastic strains level off or shakes down as the UGM adapts to the applied loads.

- At low deviator stress levels, the power law model predicts the permanent strain in single-stage PD tests well.

- The Huurman and modified Huurman models were evaluated using the test data. The second term of these two models was found to be statistically insignificant. Neglecting the second term reverts them to the power model. It should be noted that these models were developed for the gradation tested and the applicability of these models to other gradations should be verified

- It was observed that the plastic shakedown limit and plastic creep limit at constant confining stress can be determined by a series of single-stage PD tests. However, there may be inherent variability among samples and they require a considerable amount of time to test. Alternatively, the plastic shakedown limit may be discerned by conducting one multi-stage PD test.

- Based on the unique switch in the resilient modulus trend, multi-stage PD tests can be used to interpret the shakedown limit for a material at a given confining stress. A procedure is proposed based on the fact that the resilient modulus increases under low deviator stresses and decreases when the deviator stresses are high or exceeds the shakedown limit.

When applied to the materials tested, the multi-stage test predicted correctly the behavior of single-stage-test samples 78% of the time. Possible reasons why the agreement is not perfect include variability among the single- and multi-stage samples and the number of cycles per deviator stress and number of deviator stresses are limited in a multi-stage test.

- Additional research is needed to further validate this procedure. To facilitate this, a standard test load sequence is needed. The one proposed in NCHRP Report 598 presents a good starting point. The deviator stress intervals should be small enough to allow all three behavioral ranges to be captured and the load frequency slow enough for the sample to drain and recover. One more suggestion is that the confining stress be representative of the field pavement section to be studied.
- Based on multi-stage PD tests results presented in terms of stress ratios at various permanent strain levels, the VA and RCA are superior in terms of resistance to PD as compared to RAP. This may be attributable to the fact that the asphalt caused the particles to deform within themselves more readily. This may be a potential concern and may require a limitation on the amount of RAP allowed in the unbound layers.

CHAPTER 3 ASSESSING THE COMPACTABILITY OF RECYCLED CONCRETE AGGREGATE AND RECLAIMED ASPHALT PAVEMENT

In this chapter, the characteristics of RCA and RAP during compaction in two 4-foot-high, 3-foot-diameter, 3/16-inch-thick wall cross-linked polyethylene bins (supplied by Chemtainer Industries, Inc. of Keaau, Hawaii) were studied. Their compactability was assessed using (a) the nuclear gauge and Time Domain Reflectometry (TDR) to measure the dry density and water content after compaction; (b) the GeoGauge and Portable Falling Weight Deflectometer (PFWD) to measure the stiffness of the soils after compaction; and (c) FlexiForce® electrical sensors to estimate the compaction-induced lateral pressures exerted by the RAP and RCA. It should be noted that in this chapter, the RAP and RCA were tested neat; i.e., without blending.

3.1 BACKGROUND AND OBJECTIVES

3.1.1 Nuclear Gauge

The nuclear gauge (Figure 3-1) rapidly measures the in-place density and moisture content of geomaterials by imparting low amounts of radiation. The most effective mode of testing geomaterials is the direct transmission mode, where the radiation source is inserted into a drilled hole. It can be lowered to a maximum depth of 12 inches but in these experiments, a penetration depth of 6 inches was adopted as this corresponds to the lift thickness.

Two different types of radiation sources are used: (1) Cesium 137 that emits gamma rays consisting of streams of photons. These photons collide with the geomaterial causing some photons to lose energy, which inhibits detection by the

gauge. The density is determined using an inverse relationship with the amount of photons that reach the detector. The density measured is the moist density; and (2) Americium-beryllium isotope that emits neutrons to measure the moisture content, which is determined by detecting the amount of hydrogen atoms present in the geomaterial. The neutron detector only senses “slow” neutrons. When the neutrons collide with most soil particles, they are reflected with minimal energy loss since these particles are much heavier than the neutrons. When the neutrons collide with elements having a similar mass such as the nuclei of hydrogen atoms present in water, the neutrons slow down and are counted by a detector, which translates this number to a moisture content.

Unlike the Cesium 137 isotope, the Americium-beryllium isotope is not lowered into the ground but remains in the gauge. The nuclear gauge only measures moisture content to a limited depth. 98% of the neutrons counted are above this depth of measurement. The depth of measurement is dependent on the moisture content as follows (Troxler Electronic Laboratories, Inc., 2009):

$$\text{Depth (inches)} = 11 - 0.17W \tag{3.1}$$

where W (lbs) = weight of water in 1 cubic foot of geomaterial = $w.\gamma_d = \gamma - \gamma_d$, w = water content, γ = moist unit weight and γ_d = dry unit weight. The higher the moisture content, the smaller is the depth of penetration. The nuclear gauge then calculates the dry unit weight as follows.

$$\gamma_d = \gamma - W \tag{3.2}$$

Figure 3-1 Troxler nuclear moisture/density gauge model 3450 used in the experiments

3.1.2 Time Domain Reflectometry

Developed at Purdue University and distributed by Durham Geo Slope Indicator, the time domain reflectometry (TDR) instrument used is the Moisture and Density (M+D) Indicator MDI-2000 Series. The TDR system consists of a personal data assistant (PDA), pulse generator, coaxial cable, probes to create an inner and outer conductor, coaxial head and a template to guide the probes when driven into the ground. Other components that came with the TDR include:

- standard Proctor mold and collar
- 9-inch tall, 4-inch diameter cylindrical compaction mold
- Center rod guide

- Non-conductive base

The TDR method also provides the in-situ dry density and moisture content. By passing an electromagnetic pulse through four multi-rod probes driven into the geomaterial, the dielectric constant and bulk electrical conductivity of the geomaterial are measured. These two parameters are used to calculate the density and moisture content using relationships established by Siddiqui and Drnevich (1995). Figure 3-2 shows the TDR set-up.

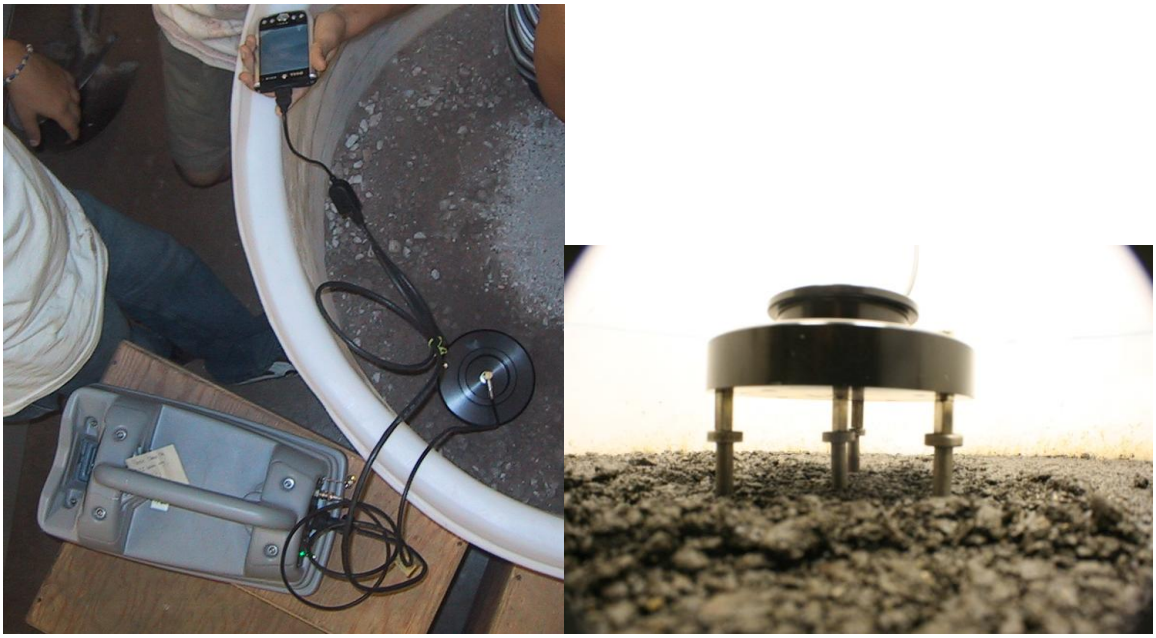

(a) (b)

Figure 3-2 Time Domain Reflectometry test set-up (a) round coaxial head connected to the TDR gauge which is operated using a PDA and (b) multi-rod probes below the coaxial head

3.1.3 GeoGauge

Supplied by Humboldt Manufacturing Company, the GeoGauge (Figure 3-3) is used to non-destructively and expediently measure the in place stiffness of a geomaterial. An annular foot extends from the bottom center of the GeoGauge and is the portion of the device that is in contact with the ground. The GeoGauge

applies a vibrating force at 25 steady state frequencies ranging from 100 to 196 Hz to produce small displacements on the geomaterial. The GeoGauge measures the force imparted to the surface and the resulting surface velocity, which can be integrated to obtain displacement, as a function of time. The stiffness, force divided by deflection, is determined at each frequency and the average is displayed. From the stiffness, the elastic modulus of the geomaterial can be estimated.

Figure 3-3 GeoGauge device

3.1.4 Portable Falling Weight Deflectometer (PFWD)

Developed by Keros Technology and Carl Bro Pavement Consultants of Denmark, the Portable Falling Weight Deflectometer (or PFWD – see Figure 3-4) can be used to measure the in place stiffness of geomaterials. A mass is dropped from a particular height and causes the circular footing to deflect. A geophone measures the acceleration, which can be integrated twice to obtain the

displacement. The impact force is measured using a load cell. The stiffness and elastic modulus are estimated based on the force and displacement.

Figure 3-4 Portable falling weight deflectometer

3.1.5 FlexiForce® Electrical Sensors

Manufactured by Tekscan, Inc., FlexiForce® electrical sensors were used to estimate the compaction-induced lateral pressures exerted by the RAP and RCA against the bin walls. The active sensing area, consisting of a force sensing resistor in an electrical circuit, is located at the end of the sensor (Figure 3-5). Each sensor is connected to a transmitter, which sends the measured signal wirelessly to a main hub that is connected to a computer.

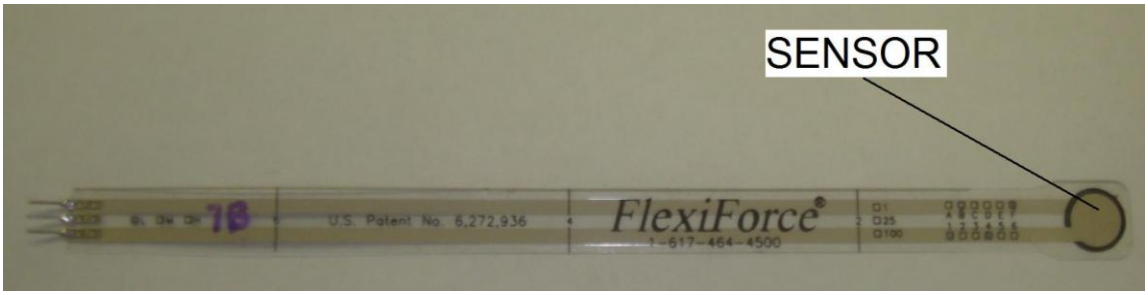

Figure 3-5 FlexiForce® sensor

3.1.6 Objectives

The main objectives of this experiment are to:

1) Determine the applicability of the nuclear gauge and TDR to measure the dry density and moisture content of RAP and RCA. The nuclear gauge detects water by detecting hydrogen atoms present in water. However, hydrogen is also present in asphalt, a component of RAP, and in cement paste, a component of RCA. This research will shed light on the reliability of the nuclear gauge when used with RCA and RAP. TDR has been used for decades in the agricultural industry to measure the volumetric water content of soils. More recently, a new version of this technology has been devised to measure the dry density and gravimetric water content. This instrument has not been used extensively on RAP and RCA and is investigated herein.
2) Determine the applicability of the Portable Falling Weight Deflectometer and GeoGauge in measuring the stiffness of RAP and RCA. There has been a push by pavement engineers to assess the compactability of geomaterials using stiffness instead of dry density and water content with the advent of the MEPDG (ARA, Inc., 2004). One of the key input parameters in the design of pavements using the MEPDG is the resilient

modulus or stiffness. The capability of these two instruments to provide the stiffness of RCA and RAP is assessed.

3) Estimate the compaction-induced lateral pressures of RAP and RCA. Compaction typically results in lateral pressures that are significantly above the normally consolidated at-rest values. These measurements will show the magnitude of the compaction-induced lateral pressures. Comparisons will then be made with values predicted from theory.

3.2 EXPERIMENTAL SET-UP

The experimental set-up is described in four sections. The first section discusses the material characteristics. The second is on calibrating the instruments that were used in the experiments. The third describes the bin set-up, installation of force sensors, compaction equipment and process, and measurements made in the polyethylene bins. The fourth focuses on post-compaction measurements as a function of time.

3.2.1 Materials

As discussed in Chapter 2, the RAP and RCA were obtained from Grace Pacific Corporation's quarry in Makakilo on the island of Oahu, Hawaii where RAP is stockpiled by gradation; one pile for 3/4 inch minus RAP and another for 3/8 inch minus RAP. The RCA was all crushed to one gradation.

To ensure that representative samples were taken from the stockpile, samples were obtained from mid-height below the surficial aggregate since samples at the bottom of the pile tend to be coarser.

3.2.1.1 Gradation

For the bin experiments, particles larger than ¾ inch were removed because their presence could locally influence the results of the various tests. Figure 3-6 shows the gradations for the RAP and RCA that were used in the experiments in this chapter. The RAP consisted of a blend of the ¾- and 3/8-inch minus fraction and contained little to no fines. It was not possible to create a 100% RAP blend that meets the HDOT base-course gradation because the RAP was crushed to two very uniform sizes. After removing the ¾-inch plus material, the RCA gradation met HDOT's 0.75-inch maximum nominal untreated base course gradation requirements while RAP did not.

3.2.1.2 Classification

According to the USCS, the RAP and RCA in Figure 3-6 are classified as GP (poorly-graded gravel) and GW (well-graded gravel), respectively. According to the AASHTO classification, both the RAP and RCA are classified as A-1-a.

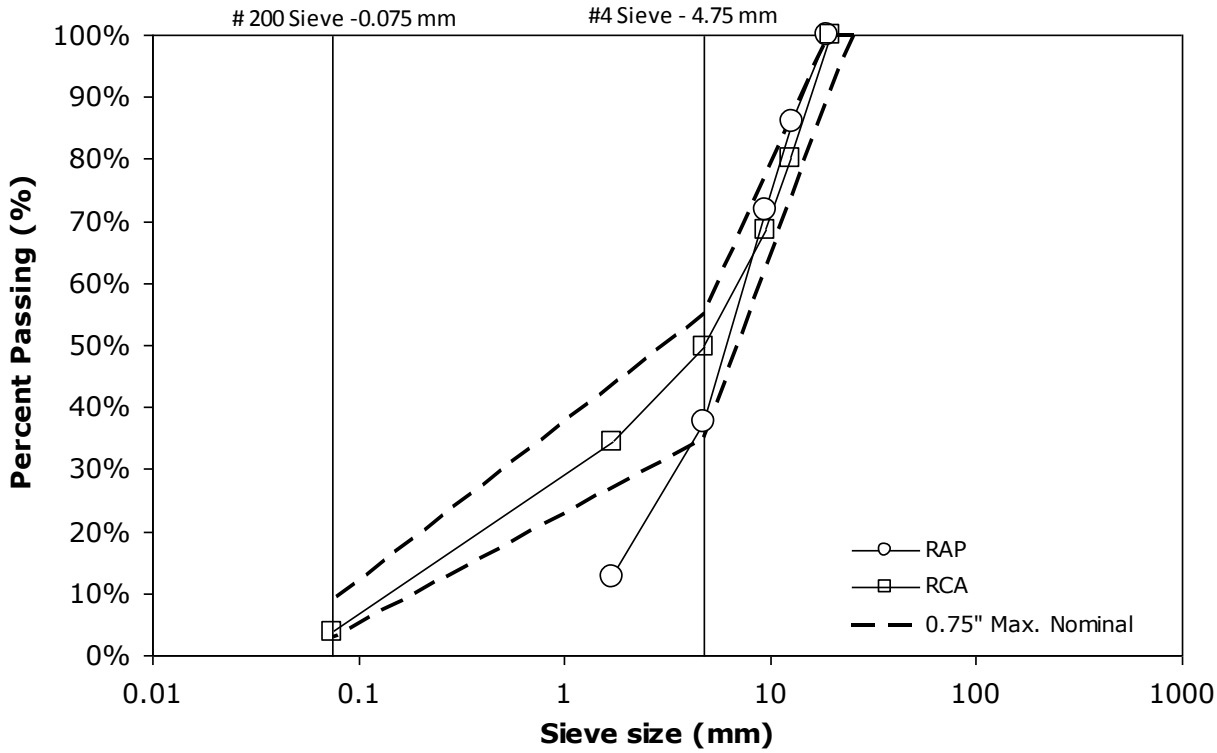

Figure 3-6 Comparison of grain size distribution of RAP and RCA with HDOT specification requirements for 0.75-inch

3.2.1.3 Compaction Curve

RAP and RCA were compacted in accordance with the Modified Proctor Test (ASTM D1557 – Method C). In both RCA and RAP, water was not readily absorbed by the materials especially with the wetter samples, wherein water was observed to seep from the bottom of the mold. This problem was more pronounced with RAP since it has a lower absorption and contained very little fines. With RCA at higher moisture contents, water sometimes collected at the surface. Figures 3-7 and 3-8 show the compaction curves for RAP and RCA, respectively.

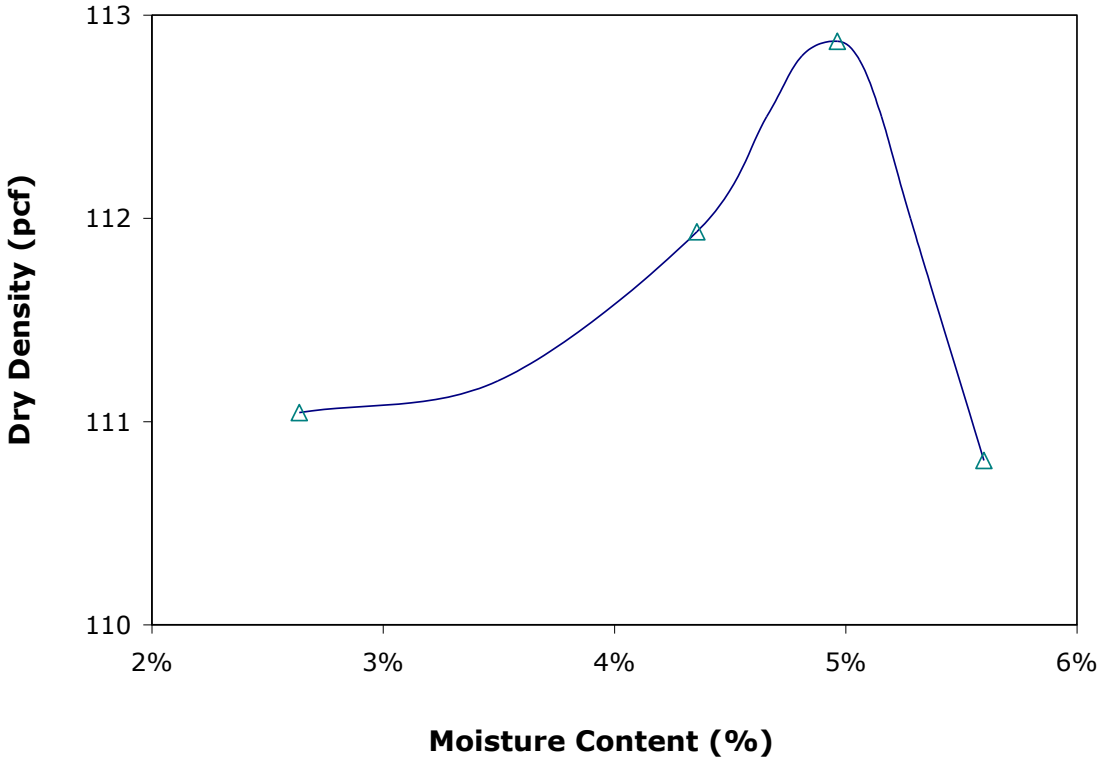

Figure 3-7 RAP compaction curve

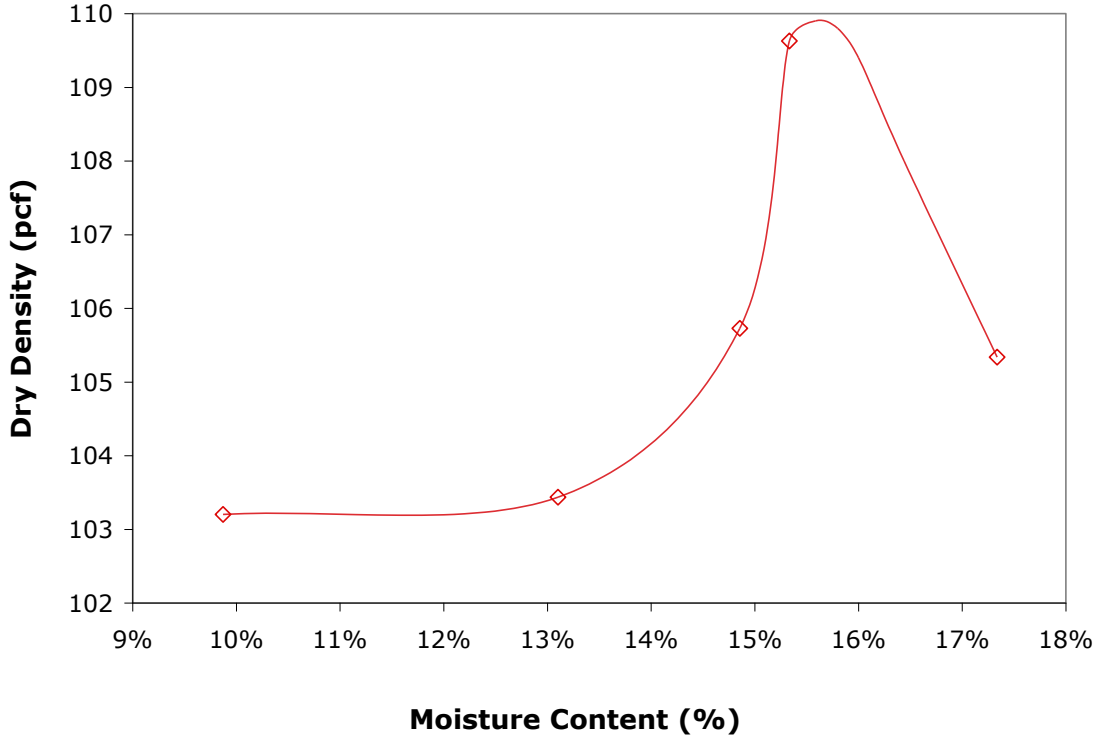

Figure 3-8 RCA compaction curve

3.2.1.4 Friction Angle

Selvarajah (2009) determined the friction angles of RAP and RCA used in these experiments in a direct shear box having a diameter of 2.4 inches (61.4 mm). Due to the limited size of the shear box, Selvarajah used gradations that were parallel to the ones shown in Figure 3-6 with a maximum size of 0.2 inches (4.75 mm). Several researchers have found that a finer parallel gradation gave similar friction angles to the same geological material with a coarser gradation provided the mineralogy, hardness of grains, particle shape, and particle roughness do not vary with particle size (Varadarajan et al., 2006, Varadarajan et al., 2003, Verdugo and de la Hoz, 2007, Cambio and Ge, 2007). Direct shear tests were conducted on samples compacted to a density and moisture content similar to the density that the materials were compacted to in the bin experiments. Based on Selvarajah's data, it was inferred that the friction angle of RCA and RAP were 50.7˚ and 42.8˚, respectively. These values are within 3 degrees of Rathje et al.'s (2002) values.

The friction angle of RCA is larger than that of RAP. This can be attributed to the fact that RCA particles have rough surfaces, which require more load to move the particles relative to each other. Also, hydration of cement in RCA may bind the particles and hinder their movement. On the other hand, the RAP particles are more likely to slip within themselves because of the asphalt binder.

3.2.2 Calibration of Instruments

Calibration offsets increase the accuracy of the nuclear gauge's readings. According to the Troxler Operator's Manual (2009), there are three types of offsets that can be used: wet density offset, trench offset, and moisture offset. The wet density offset should be used when the density does not range between 70 to 170 pcf. A trench offset should be provided when using the nuclear gauge within two feet of a vertical wall or structure. The moisture offset should be used on geomaterials containing hydrogen atoms present in a form other than water. To calculate the moisture offset factor, k, the following equation is used

$$k = \frac{\%w_{lab} - \%w_{gauge}}{100 + \%w_{gauge}} \times 1000 \qquad (3.3)$$

where $\%w_{lab}$ = water content in % measured using an oven and $\%w_{gauge}$ = water content in % measured using the nuclear gauge. Attention should be paid to the sign of the moisture offset factor.

On each day prior to using the nuclear gauge, it was necessary to run a standard count to ensure the gauge readings are reliable. Also, before obtaining readings in the bin, a trench offset is obtained.

The TDR and FlexiForce® Sensors were calibrated prior to use. The effect of three varying drop heights on stiffness was investigated prior to use of the PFWD. It was found that the various drop heights yielded similar stiffness values. It is expected that stiffness non-linearity will manifest in softer geomaterials rather than in the stiffer base/subbase type of materials that are addressed in this research.

3.2.3 Bin Set-up and Compaction

FlexiForce® sensors were attached to the inside wall of the bins at 0.25, 1.25 and 2.25 feet above the bottom to measure the compaction-induced lateral stress. In addition, a fourth sensor was placed at the bottom center of the bin to measure the vertical stress. The sensors were attached using scotch tape but care was made not to scotch tape the sensing element itself. The sensors and transmitters connected to the sensors are shown in Figure 3-9.

The cylindrical bins were marked every six inches to coincide with the intended lift thickness. Figure 3-10 shows a profile view of the bin used in the experiments.

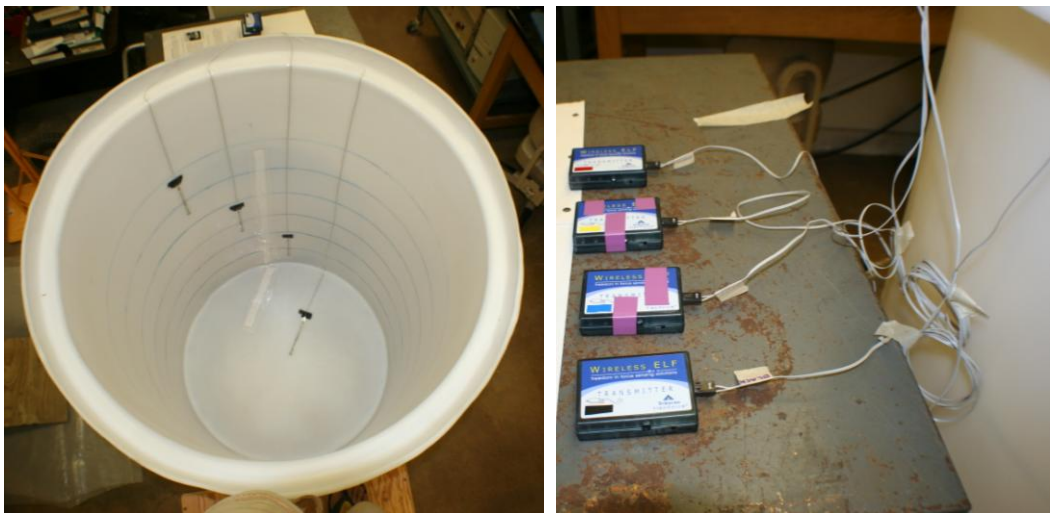

Figure 3-9 Sensors attached to bin (Left) and sensors connected to transmitters (Right)

Figure 3-10 Profile view of bin

Prior to compaction, the desired amount of material per lift was weighed and the water content measured. Values of dry density and water content from the nuclear gauge and TDR can then be compared to these “true” values. The recycled material and water were thoroughly combined in a concrete mixer as shown in Figure 3-11.

Figure 3-11 Electric concrete mixer used to blend RAP with water and RCA with water

The moist material was then poured into the bins and compacted using a Bosch Brute Breaker Hammer Model 11304 accessorized with an 8-inch by 8-inch steel tamper plate (Figure 3-12). A 2 ½-foot diameter, ¾-inch thick wood base was used between the compactor and the geomaterial to spread the compactive force over a wider area and to create a flat finished surface.

The RAP and RCA were compacted in six 6-inch lifts yielding a finished height of three feet. After each lift was compacted, GeoGauge, PFWD, nuclear gauge and TDR tests were performed in that order. The rationale for this sequence is to work from the least to the most destructive tests in the interest of sample preservation. Figure 3-13 shows a plan view of the bin and the respective test areas. At least five readings of dry density and water content for the nuclear gauge and TDR tests and five for the Geogauge and PFWD stiffness were recorded for each layer and for the top lift during post-compaction testing.

Figure 3-12 Bosch hammer with tamper plate and wood base

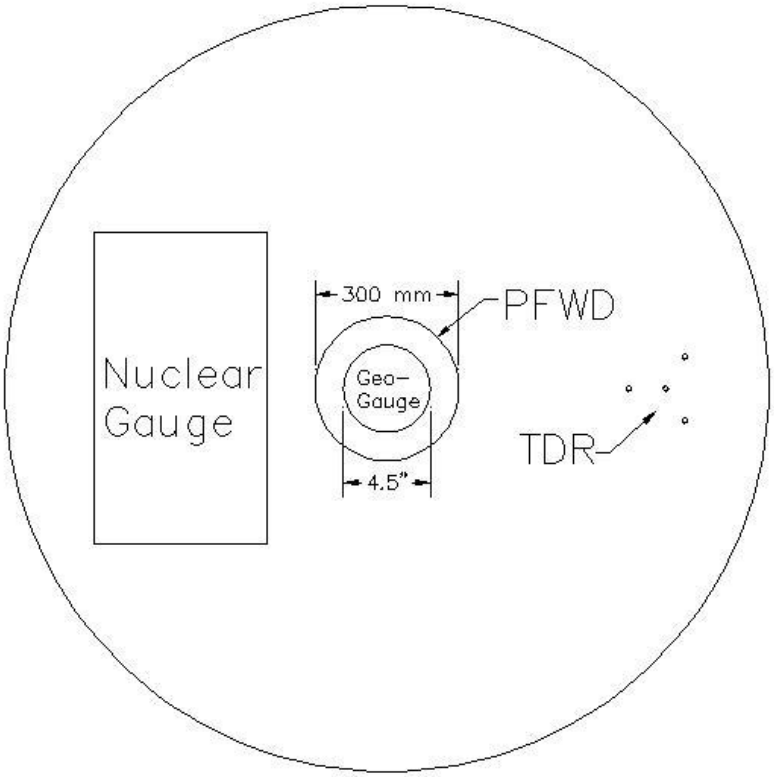

Figure 3-13 Plan view of test locations in bin

Dial gauges were attached to the outside wall of the bins at one and two feet above ground (Figure 3-14) to: (1) measure the bin wall deflections as the

material was compacted; (2) assess if any post-compaction deflections would occur as a result of creep; and (3) allow for more accurate volumes to be calculated when estimating the in-place densities. Sandbags were placed at the base of the dial gages to aid stability. The dial gauges were read after each lift and also periodically for about two months after reaching the three-foot height.

Figure 3-14 Dial gauges

A list of instruments used and the desired measurements are summarized below.

Instrument	Measurement
Nuclear Moisture Density Gauge	Moisture Content and Density
Time Domain Reflectometry	Moisture Content and Density
GeoGauge	Stiffness/Elastic Modulus
Portable Falling Weight Deflectometer	Stiffness/Elastic Modulus
FlexiForce® Sensors	Lateral Pressure
Dial Gages	Wall Deflection

3.2.4 Post-compaction Measurements

Another phase of this experiment was to evaluate if the properties changed or the material crept with time over a post-compaction period of approximately two months. Table 3-1 summarizes the tests performed and the times of testing.

Table 3-1 Experiment timeline

Instrument	**Days after compaction when readings were taken**	
	RAP	RCA
Nuclear Gauge/TDR/ GeoGauge/PFWD/ FlexiForce® Sensors	0	0
	5	5
	11	9
	15	-
	25	19
	43	37
	63	57
FlexiForce® Sensors	85	77

For the nuclear gauge test, it was attempted to use the same direct transmission hole when testing the top lift during this period except if the hole caved in, in which case, a new one was created.

For the TDR test, the probes were driven and left in place immediately after compaction for the entire post-compaction duration.

3.3 DENSITY EVALUATION USING NUCLEAR GAUGE AND TIME DOMAIN REFLECTOMETRY

3.3.1 Introduction

The sand cone and rubber balloon methods for determining in situ dry unit weight and moisture content require drying samples in an oven. Consequently, they do not provide instantaneous moisture content readings, which is an important element in earthwork construction. Two methods that instantaneously determine the dry unit weight and moisture content include the nuclear gauge (ASTM D6938) and TDR (ASTM D6780).

3.3.1.1 Previous Studies on the Nuclear Gauge on RCA and RAP

The applicability of the nuclear gauge on RCA and RAP has been investigated by Rathje et al. (2002). They found that the RCA moisture content from the nuclear gauge was about 20% larger than oven dried values while the RAP moisture content readings from the nuclear gauge were almost three times the oven dried readings (Rathje et al., 2002). This can be attributed to the fact that hydrogen atoms can be found not only in water but also in the cement and possible admixtures in RCA and in the asphalt in RAP (Rathje at al., 2002).

3.3.1.2 Previous Studies on Time Domain Reflectometry

Previous studies on the use of TDR on RAP and RCA were not found. Instead this section focuses on the background theory, calibration of the TDR and the test procedure. In the TDR method, an electromagnetic wave pulse is sent through probes embedded in a geomaterial. Reflections of the pulse caused by the top of the tested material and by the end of the probe are recorded using an oscilloscope. The oscilloscope plot is then used to provide the apparent

dielectric constant (K_a) and bulk electrical conductivity (EC_b) of the geomaterial. Topp et al. (1980) discovered the famous relationship between K_a and volumetric water content (θ) that initially facilitated its use in mostly agricultural applications.

$$\theta = 4.3 \times 10^{-6} K_a^3 - 5.5 \times 10^{-4} K_a^2 + 2.92 \times 10^{-2} K_a - 5.3 \times 10^{-2} \quad (3.4)$$

Applicable to a large number of different soils in the field, this relationship was established on the basis that large differences exist between K_a for soil solids and K_a for water, and that K_a for wet soil depends largely on the volumetric moisture content. Then Siddiqui and Drnevich (1995) of Purdue University developed relationships between the apparent dielectric constant (K_a) and bulk electrical conductivity (EC_b) with water content and with dry unit weight that made the TDR useful for geotechnical applications.

Apparent Dielectric Constant

According to Drnevich et al. (2003), the apparent dielectric constant is the real portion of the complex dielectric permittivity. The imaginary portion takes into account the electrical loss while the real portion represents the amount of energy stored in the material. Only the real portion is relevant in determining moisture content and dry unit weight.

A typical waveform is shown in Figure 3-15. Two reflections are observed: one when the pulse first contacts the soil surface and another when the pulse reaches the tip of the probe. K_a is measured using the following equation

$$K_a = \left(\frac{L_a}{L_p} \right)^2 \quad (3.5)$$

where L_p = length of center probe that is in the soil and L_a = apparent length = scaled horizontal distance between the first and second reflections (Yu & Drnevich, 2002).

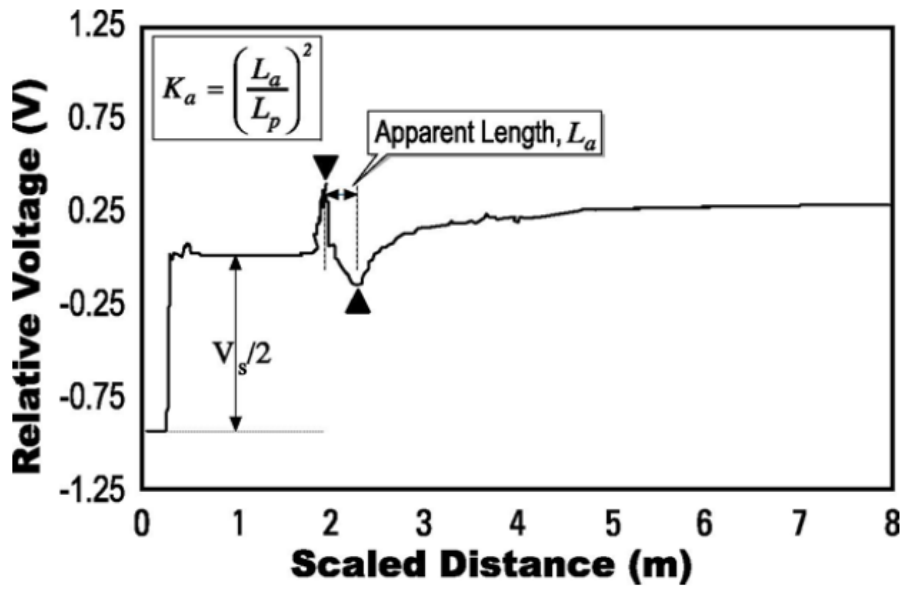

Figure 3-15 Parameters to determine K_a (Durham Geo Slope Indicator, 2003)

As an alternative to Equation 3.5, Drnevich et al (2003) proposed the following square root relationship between θ and K_a as equivalent to Topp's equation:

$$\theta = b\sqrt{K_a} + a \tag{3.6}$$

provided constants *a* and *b* had values of 0.1841 and 0.1181, respectively. However, Abdulla et al. (1988) and Ponizovsky et al. (1999) determined that soil density also influences the dielectric constant. This led Siddiqui (1995) to combine the gravimetric moisture content and dry densities in the following equation:

$$\sqrt{K_a}\,\frac{\rho_w}{\rho_d} = a + bw \tag{3.7}$$

where ρ_d = soil dry density, ρ_w = density of water and a and b are constants.

Bulk Electrical Conductivity

In principle, the electrical conductivity (EC_b) is the property of a material that causes an electrical signal to dissipate as it travels through that material. Therefore, the TDR signals are attenuated due to a material's EC_b, which can also be measured using the same waveform for determining K_a as follows (Yu & Drnevich, 2002 – see Figure 3-16):

$$EC_b = \frac{1}{C}\left(\frac{V_s}{V_f} - 1\right) \tag{3.8}$$

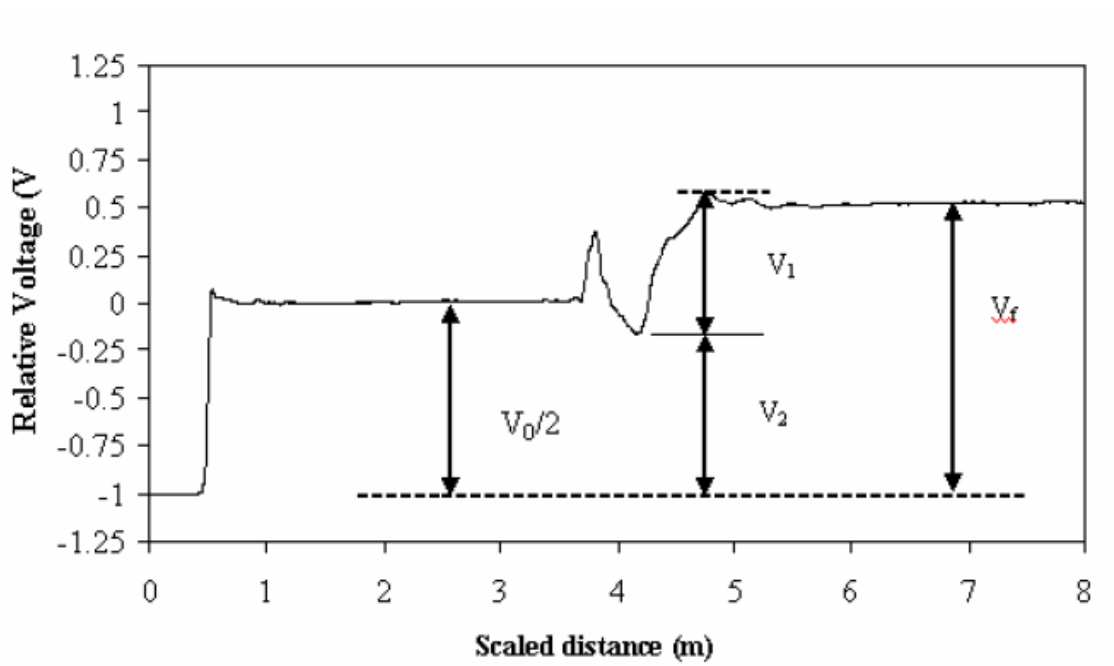

Figure 3-16 Parameters to determine EC_b (Yu and Drnevich, 2004)

where V_s = source voltage = two times the step voltage, V_f = final voltage level and C is based on how the probes are configured as follows:

$$C = \frac{2\pi L_p R_s}{\ln\left(\frac{d_o}{d_i}\right)} \tag{3.9}$$

where R_s = internal resistance of the pulse generator, d_o = outside diameter of the conductor, and d_i = inside diameter of the conductor (Giese and Tiemann, 1975).

Yu and Drenvich (2004) proposed the following empirical relationship between EC_b, moisture content and dry density:

$$\sqrt{EC_b} \cdot \frac{\rho_w}{\rho_d} = c + dw \tag{3.10}$$

where c and d are constants.

Calibration

Prior to using the TDR, the equipment should be calibrated for each geomaterial that it will be used on. Calibration for RAP and RCA was facilitated by running Proctor Tests. The standard TDR equipment includes a 4-inch diameter compaction mold. However, the gradation of RAP and RCA precluded the use of a 4-inch diameter mold because greater than 20% of the material is retained on the 3/8-inch sieve. Method C of ASTM D1557, which allows more than 20% retained on the 3/8-inch sieve and less than 30% retained on the ¾- inch sieve, had to be used, but this method requires a 6-inch-diameter compaction mold. Therefore, such a mold with a non-conductive base had to be custom ordered from the manufacturer to perform the calibration.

During compaction, a regular steel base was used. During calibration, the base was switched to the non-conductive variety as shown in Figure 3-17. Then, a plastic guide was attached to the top of the mold to help direct the driving of a rod in the middle with the aid of a rubber mallet or non-steel hammer. The plastic guide is removed and the top edge of the mold is cleaned to ensure proper

electrical contact between the mold and mold collar. The mold collar is then placed on the mold followed by the coaxial head ensuring that the center rod is in contact with the center of the coaxial head (see Figure 3-17 right)

Figure 3-17 Center rod guide and non-conductive base (Left) and coaxial head and mold collar on compaction mold (Right)

For each compaction sample, K_a and EC_b are measured and recorded. Calibration constants *a* and *b* can be found using Equation 3.7 by plotting $\sqrt{K_a}\frac{\rho_w}{\rho_d}$ against water content (Figure 3-18). The slope and y-intercept are *b* and *a*, respectively. Constant *a* is related to the dry density and apparent dielectric constant of the geomaterial while *b* is related to the dielectric constant of the pore fluid (Drnevich et al., 2003).

Constants *c* and *d* are obtained by plotting $\sqrt{EC_b}\frac{\rho_w}{\rho_d}$ against water content (Figure 3-19). The slope and y-intercept are *d* and *c*, respectively. The constant *c* is related to the dielectric conductivity and dry density while *d* is related to the material type and pore fluid properties (Drnevich et al., 2003).

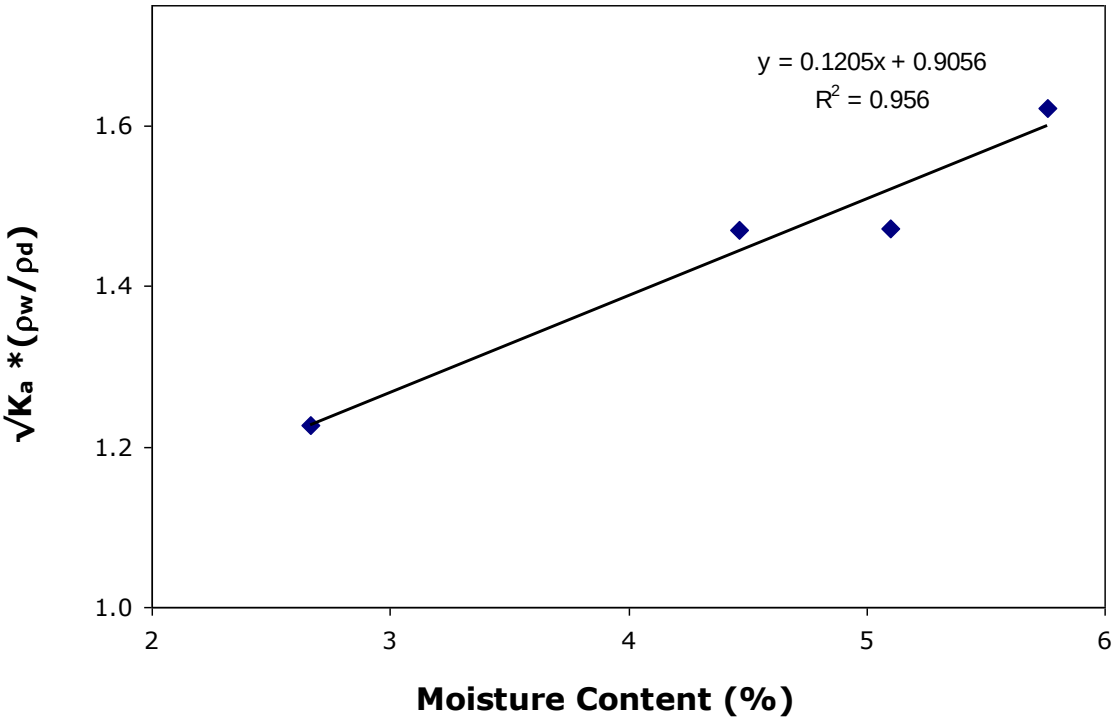

(a)

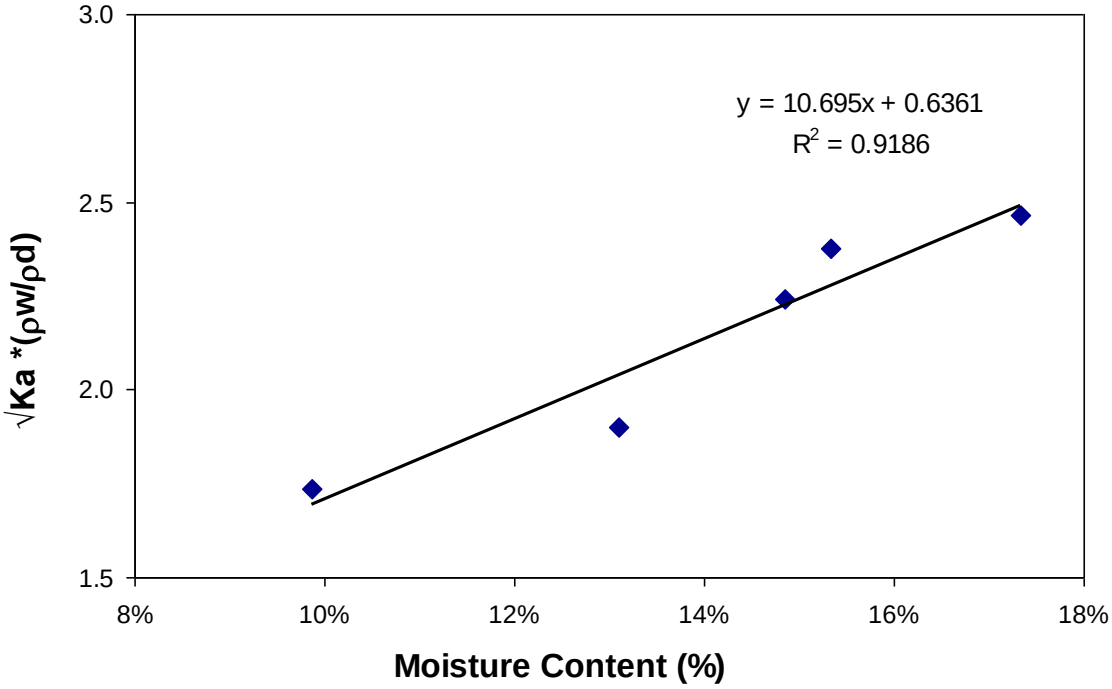

(b)

Figure 3-18 Constants a and b for (a) RAP and (b) RCA

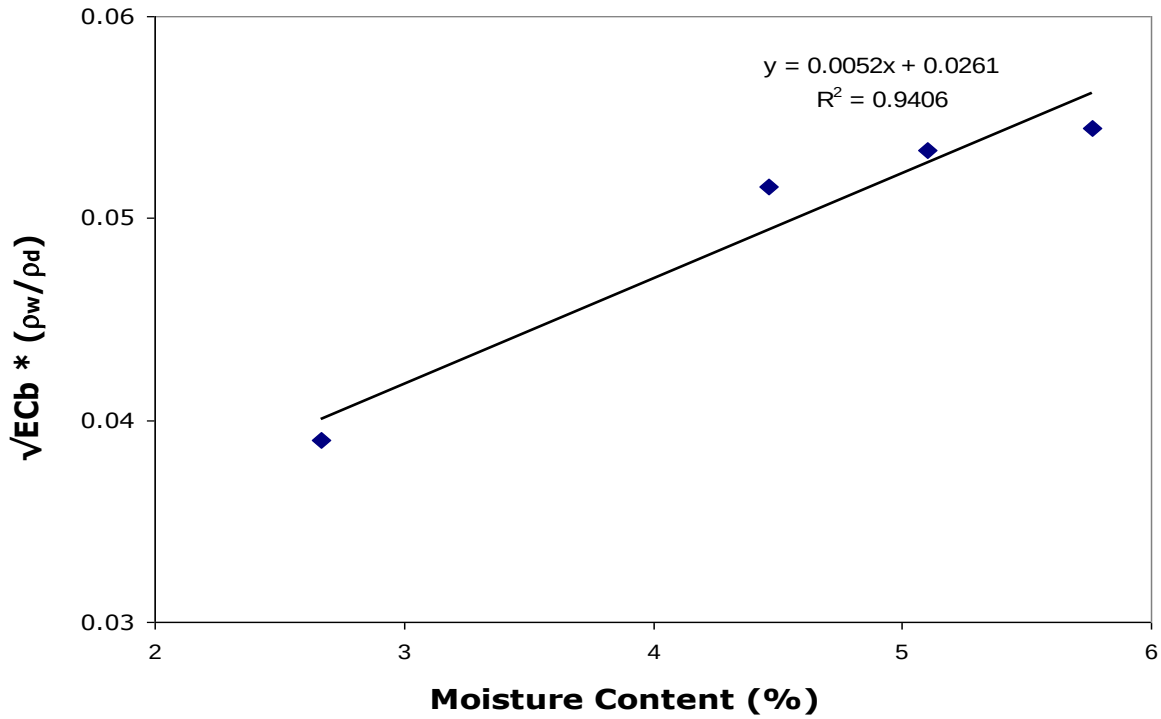

(a)

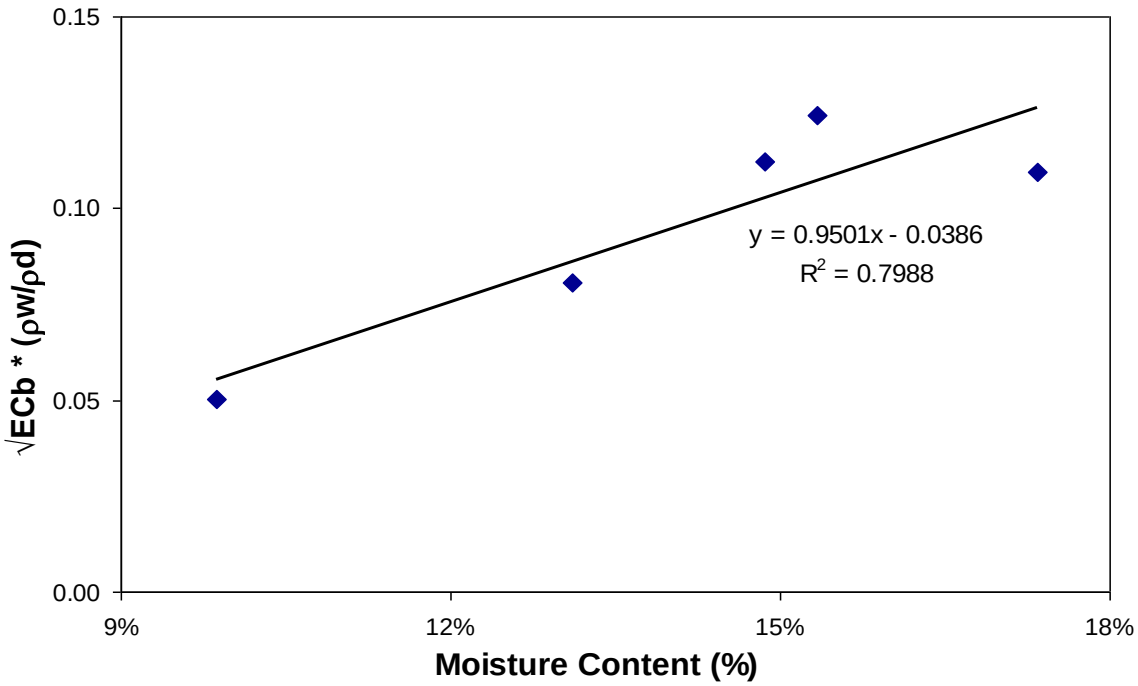

(b)

Figure 3-19 Constants c and d for (a) RAP and (b) RCA

From equations 3.7 and 3.10, it can be seen that E_{cb} and K_a are related as follows (Drnevich et al., 2003):

$$\sqrt{EC_b} = \frac{b \cdot c - a \cdot d}{b} \frac{\rho_d}{\rho_w} + \frac{d}{b} \sqrt{K_a} \tag{3.11}$$

which has the same form as:

$$\sqrt{EC_b} = f + g\sqrt{K_a} \tag{3.12}$$

Therefore, *f* is related to constants *a*, *b*, *c*, *d* and dry density. Even though *f* is related to dry density, it is referred to as a constant by Yu and Drnevich (2004). Constant *g* is related to *b* and *d*. By plotting $\sqrt{\boldsymbol{EC_b}}$ against $\sqrt{\boldsymbol{K_a}}$ (Figure 3-20), the slope and y-intercept are *g* and *f*, respectively.

Table 3-2 summarizes the calibration constants for different types of soils. According to Yu and Drnevich (2004), values of *a* are typically between 0.7 and 1.85 and values of *b* are typically between 7 and 12. Typical values for *c, d, f,* and *g* have not yet been determined (Runkles et al., 2006).

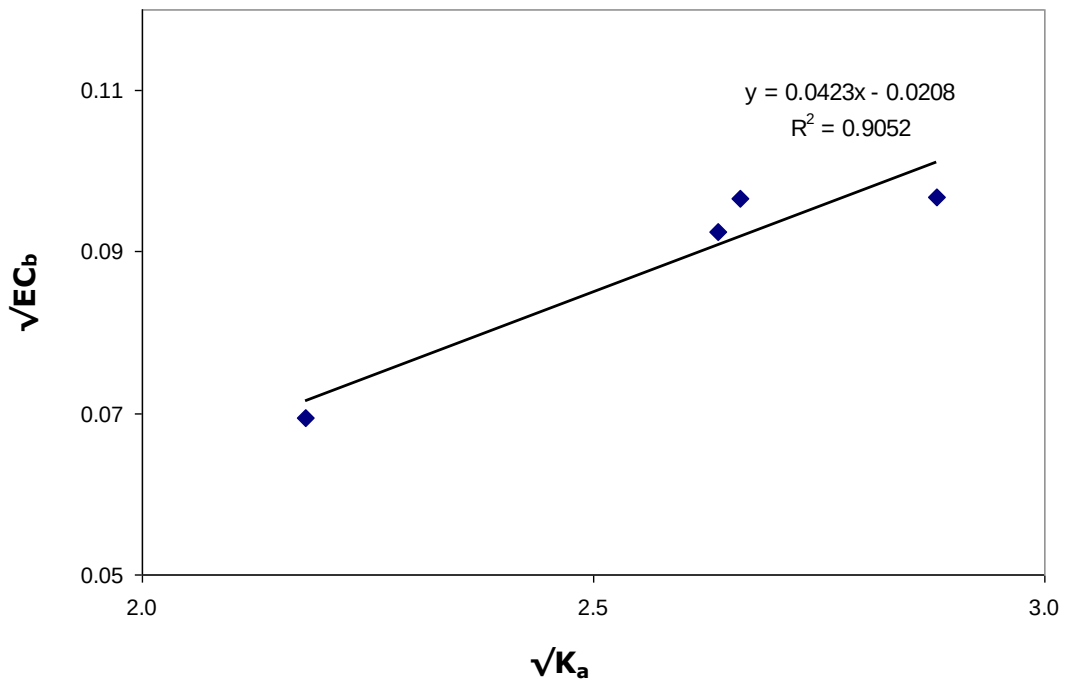

(a)

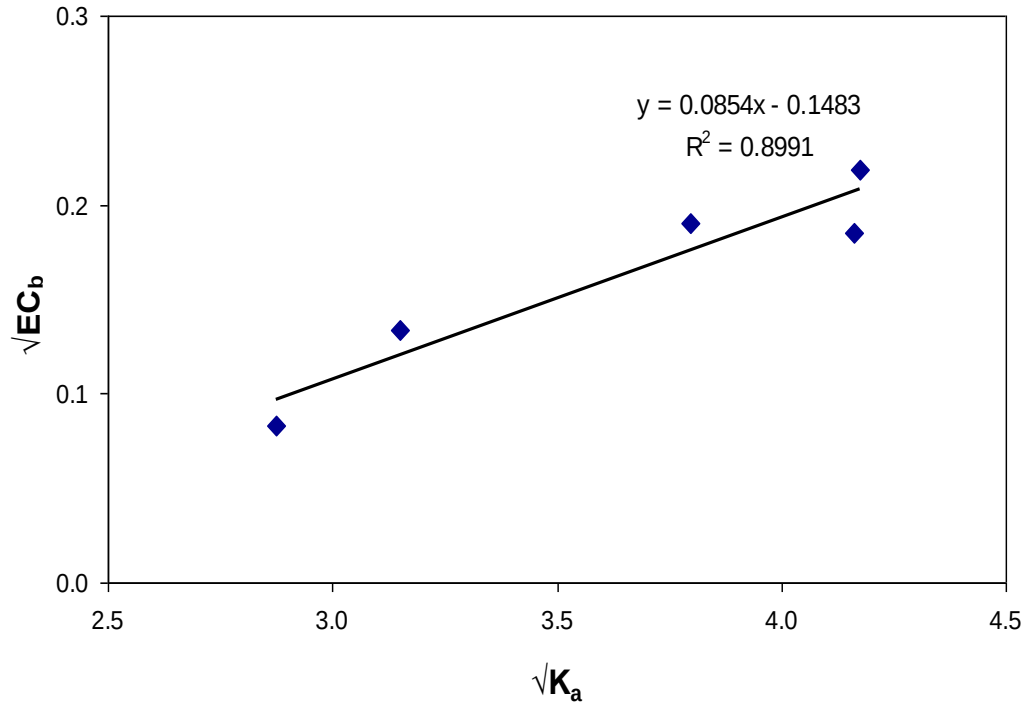

(b)

Figure 3-20 Constants f and g for (a) RAP and (b) RCA

Table 3-2 Summary of TDR calibration constants

	USCS Classification	a	b	c	d	f	g	Reference
Ottowa Sand	SP	0.93	9.21	-	-	-	-	Drnevich et al., 2003
Florida Sands (Max)	SP	1.080	10.15	0.0593	0.801	0.0285	0.0836	Runkles et al., 2006
Florida Sands (Min)	SP	0.875	7.48	0.0036	0.149	-0.0923	0.0210	
Ottowa Sand (Illinois)	SP	1.03	7.83	-	-	-	-	Durham, 2005
Sandy Soil (Florida)	SP	1	8.45	-	-	-	-	
Brown County Clay (Ohio)	CL	0.91	8.84	-	-	-	-	
Glacial Till (Indiana)	SM	1.02	9.06	-	-	-	-	
Loess (Mississippi)	ML	1.21	7.95	-	-	-	-	
Lean Clay (Mississippi)	CL	1.3	7.93	-	-	-	-	
Buckshot Clay (Mississippi)	CH	1.22	10.97	-	-	-	-	

Calibration Constants Determined in this Study

Table 3-3 summarizes the constants for RAP and RCA obtained in this study.

Table 3-3 Soil specific calibration constants for this study

	USCS Classification	a	b	c	d	f	g
RCA	GP	0.6361	10.695	-0.0386	0.9501	-0.1483	0.0854
RAP	GW	0.905	12.06	0.026	0.5213	-0.02	0.0422

For the most part, the calibration constants for RCA and RAP are comparable to values in the literature. Constant *a* for RCA was slightly outside the typical range of values.

Knowing the calibration constants a, b, c and d, and combining equations (3.7) and (3.10), the dry density and moisture content can be estimated as follows (Siddiqui and Drnevich, 1995):

$$w = \frac{c\sqrt{K_a} - a\sqrt{EC_b}}{b\sqrt{EC_b} - d\sqrt{K_a}} \tag{3.13}$$

$$\boldsymbol{\rho_d = \frac{d\sqrt{K_a} - b\sqrt{EC_b}}{ad - cb}\rho_w} \tag{3.14}$$

Test Procedure

There are two methods for running the TDR tests (ASTM D6780) - the Two-Step and One-Step Method. In the Two-Step Method, the soil is tested in situ. The second step is to calibrate the TDR. This is performed by excavating a sample quickly and testing it in a mold on site so as to minimize drying.

In the One-Step Method, the calibration is performed in the laboratory prior to TDR testing in the field. The name “One Step Method” is not accurate because there are really two steps to this procedure. What the “one step” refers to is that there is only one step in the field; the calibration is performed in the laboratory. The One Step Method is followed in this research.

Steps to run the TDR test in the field are as follows:

(a) Drive four spikes in a coaxial configuration using the guide provided (Figure 3-21 left);

(b) Remove the guide (Figure 3-21 right);

(c) Place the coaxial head on the four probes ensuring good contact between them (Figure 3-2b);

(d) Connect the PDA to the TDR which in turn is connected to the coaxial head (Figure 3-2a); and

(e) Measure K_a. It will be explained later on that EC_b is not used at all in the field test.

Figure 3-21 Template (Right) and probes inserted in RAP (Left)

Field measurements (denoted with subscript *f*) of K_a ($K_{a,f}$) must be adjusted for temperature differences that exist between the laboratory calibration and the field measurements. The adjusted value is typically standardized to 20ºC. Therefore, the field value $K_{a,f}$ is corrected as follows:

$$K_{a,20^{\circ}C} = K_{a,f} \times TCF \tag{3.15}$$

where TCF = temperature correction factor using the following equations:

$$TCF = 0.97 + 0.0015T_{test,^{\circ}C} \quad \text{for a cohesionless geomaterial}$$

$$TCF = 1.10 - 0.005T_{test,^{\circ}C} \quad \text{for a cohesive geomaterial.}$$

These equations are applicable if the testing temperature, $T_{test,^{\circ}C}$, is between 4 and 40ºC. Then $EC_{b,adj}$ is determined using $K_{a,20^{\circ}C}$ as follows:

$$EC_{b,adj} = (f + g \cdot K_{a,20^{\circ}C})^2 \tag{3.16}$$

where *f* and *g* are determined from Figure 3-20. Then, the water content and dry density are calculated as follows:

$$w = \frac{c\sqrt{K_{a,adj}} - a\sqrt{EC_{b,adj}}}{b\sqrt{EC_{b,adj}} - d\sqrt{K_{a,adj}}} \tag{3.17}$$

$$\boldsymbol{\rho_d = \frac{d\sqrt{K_{a,adj}} - b\sqrt{EC_{b,adj}}}{ad - cb}} \tag{3.18}$$

It can be seen that the EC_b measured in the field is not used at all in the calculation of dry density and moisture content. For this experiment, no temperature adjustment factor was applied because the calibration and bin measurements were performed in the soils laboratory at the same temperature and using the same water source (tap water).

3.3.2 Test Results

3.3.2.1 Actual Dry Density

The actual dry density per lift was calculated using the measured wall deflections. An equation for the deflected bin wall was derived by using the two deflection measurements and by assuming the following boundary conditions: slope and deflection at the bottom and the slope at the top of the bin = zero.

The six deflected profiles after compaction of the six different RCA lifts are shown in Figure 3-22. It can be seen that the deflected profiles for lifts 2 through 6 are almost identical. The deflections after compacting Lift 1 are much smaller. Only the figure for RCA is presented. The deflected profile for RAP is not shown because the dial gauges were accidentally kicked during compaction.

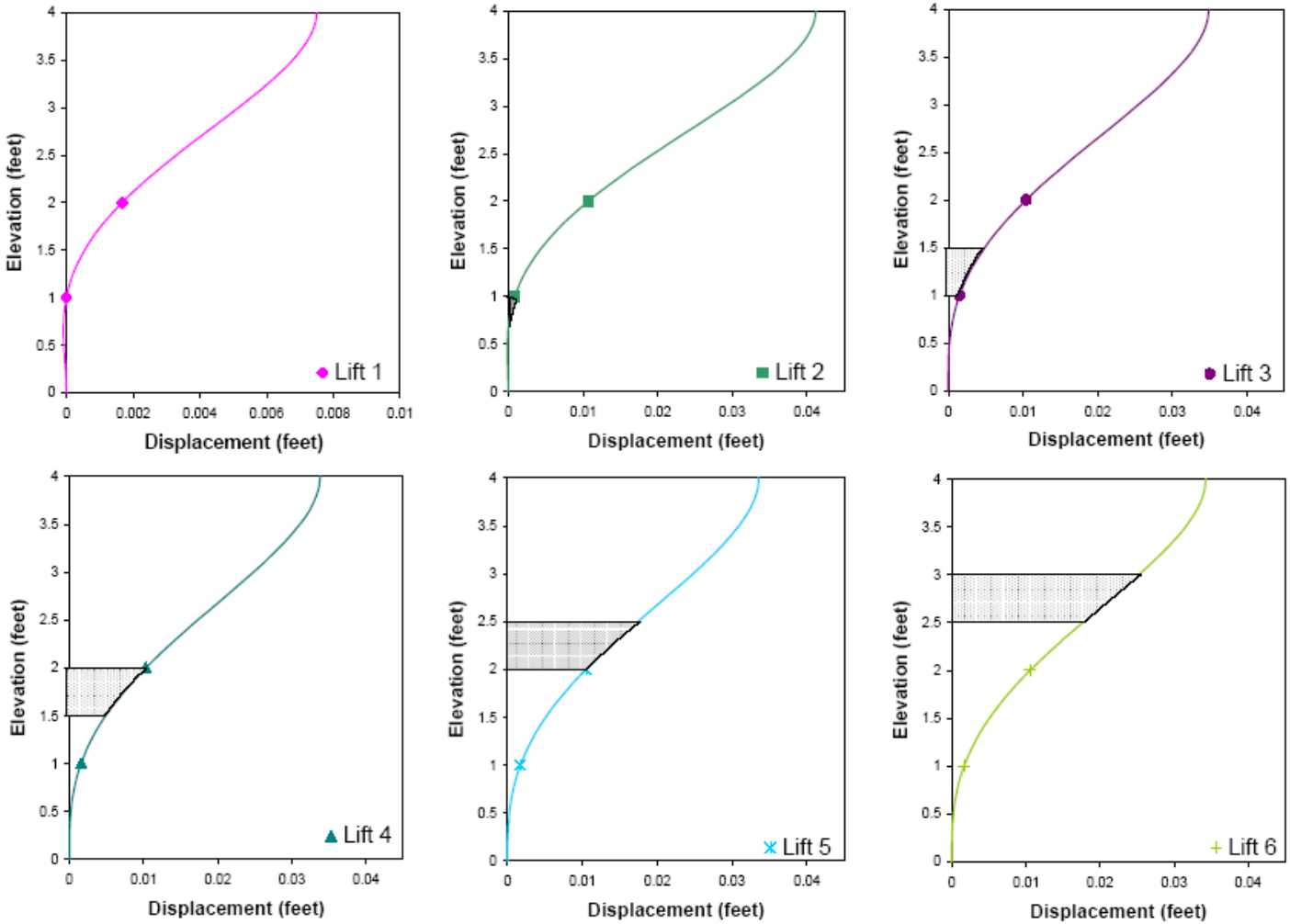

Figure 3-22 Deflection profile based on dial gauge readings

To determine the dry densities for each lift, the respective equations for the defected wall profiles were integrated to determine each lift volume. The dry densities can be determined with precision because the actual material weight was determined and the moisture content measured for each lift.

3.3.2.2 Measured Moisture Content

The nuclear gauge and TDR moisture contents for RAP and RCA are plotted versus the actual values in figures 3-23 and 3-24, respectively. The overall average ratios of the nuclear gauge/oven dry and TDR/oven dry moisture contents are summarized in Table 3-4. Over the six lifts, the nuclear gauge over-predicted the moisture contents of RCA and RAP on average by 14% and 55%, respectively, as compared to the oven dried values. TDR moisture contents for RAP are on average higher than the oven dried values by 5% while TDR moisture contents for RCA are 14% lower than the oven dried moisture contents.

Table 3-4 Moisture content summary

	w_{NG}/w_{OVEN}			w_{TDR}/w_{OVEN}		
	average	standard deviation	COV (%)	average	standard deviation	COV (%)
RAP	1.55	0.17	0.11	1.05	0.08	0.08
RCA	1.14	0.09	0.08	0.86	0.04	0.05

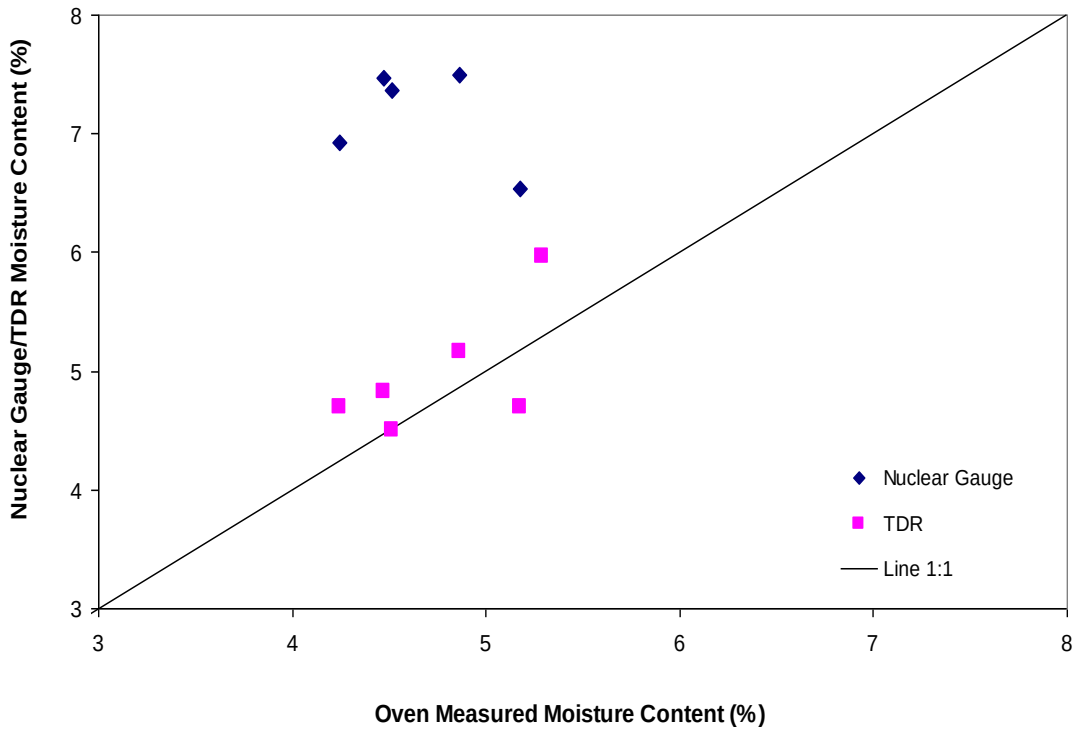

Figure 3-23 RAP moisture content comparison

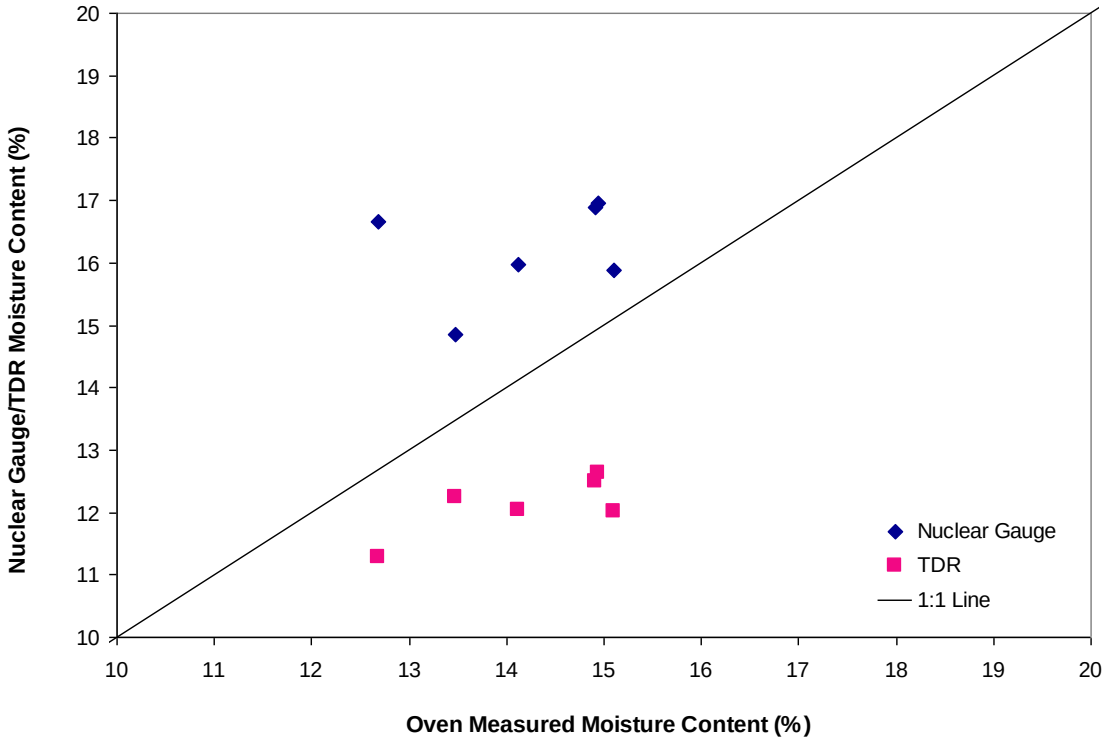

Figure 3-24 RCA moisture content comparison

3.3.2.3 Measured Dry Density

The nuclear gauge and TDR dry density for RAP and RCA are plotted versus the actual values in figures 3-25 and 3-26, respectively. Table 3-5 summarizes the average of the ratios of the measured dry densities with the actual values along with some statistics. For RAP, the nuclear gauge and TDR points hover around the 1:1 line indicating that the measured dry unit weights are on average close to the actual. For RCA, the nuclear gauge dry unit weights are on average close to the actual values but the TDR dry unit weights are relatively constant.

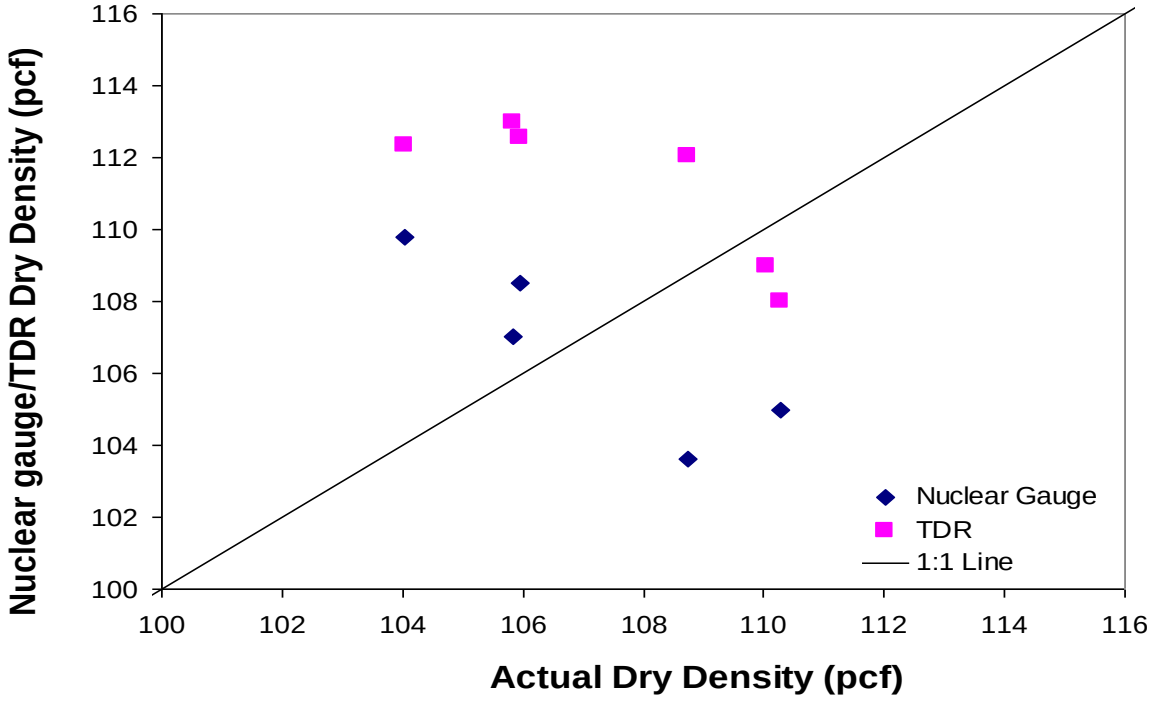

Figure 3-25 RAP dry density comparison

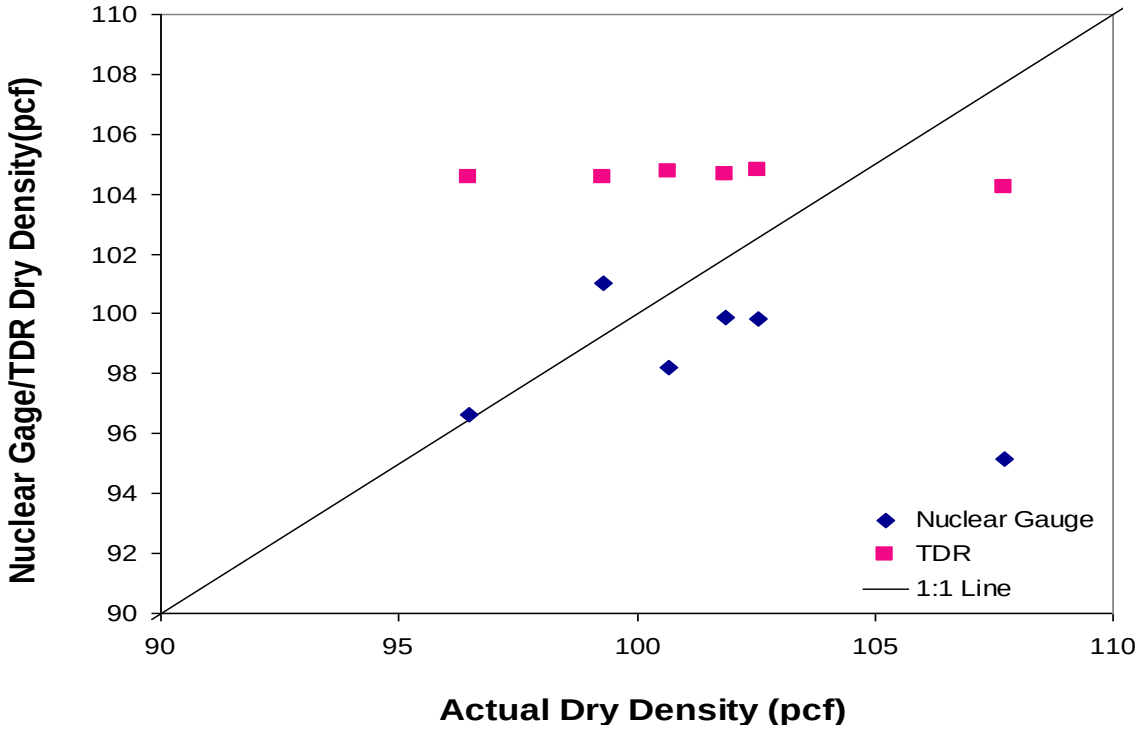

Figure 3-26 RCA dry density comparison

Table 3-5 Dry density summary

	$\gamma_{dNG}/\gamma_{dACTUAL}$			$\gamma_{dTDR}/\gamma_{dACTUAL}$		
	average	standard deviation	COV (%)	average	standard deviation	COV (%)
RAP	1.00	0.05	0.05	1.03	0.04	0.04
RCA	0.97	0.05	0.05	1.01	0.04	0.04

Due to the TDR's poor prediction of the dry unit weight of RCA, an attempt was made to mathematically recreate the RCA compaction curve using the TDR calibration constants and equations 3.12, 3.13 and 3.14. The following expression for dry density as a function of moisture content can be derived:

$$\gamma_d = \frac{f\gamma_w}{w(d - bg) + c - ag} \tag{3.19}$$

From Figure 3-27, it is observed that equation 3-19 cannot recreate a classical bell-shaped compaction curve for all practical ranges of moisture content (i.e; $d\rho_d/dw$ can never be zero to yield a maximum ρ_d).

3.3.2.4 Post-Compaction Moisture Content and Density

Following compaction of the top lift, the RCA and RAP were tested to see if the moisture content and density changed with time.

Moisture Content

With respect to the variation of moisture content with time, the following observations are offered:

1. The Nuclear Gauge consistently provided higher moisture contents than the TDR (Figure 3-27 and 3-28).

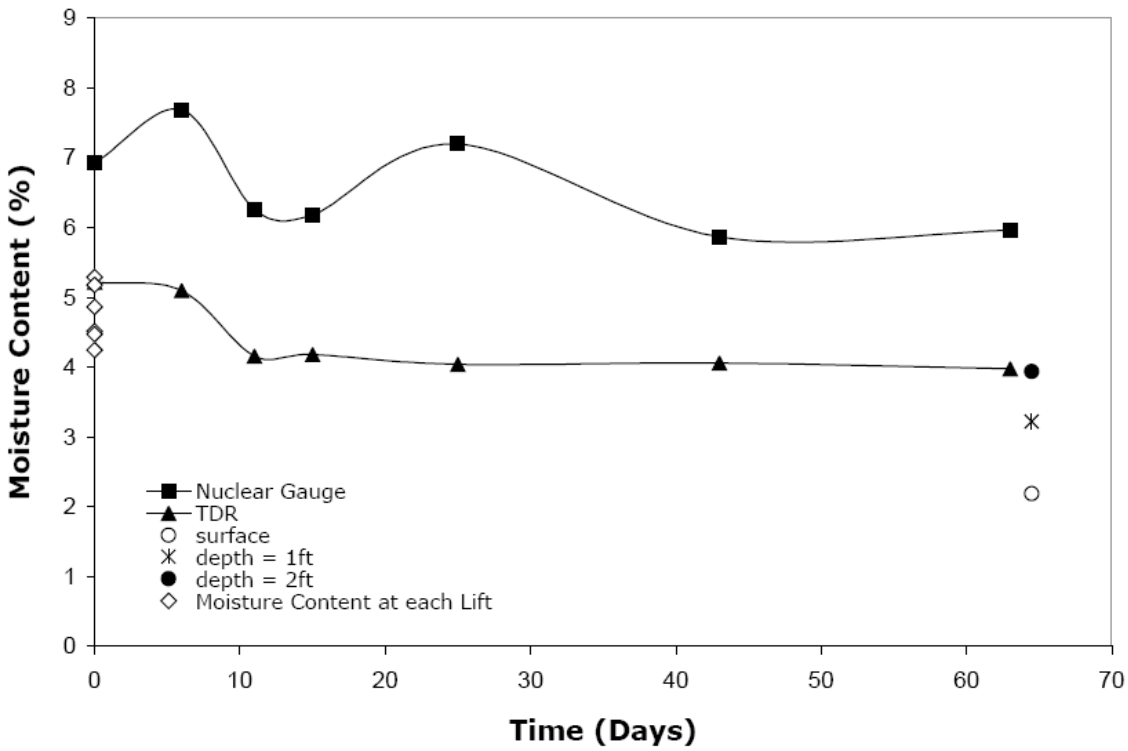

Figure 3-27 RAP moisture content versus time

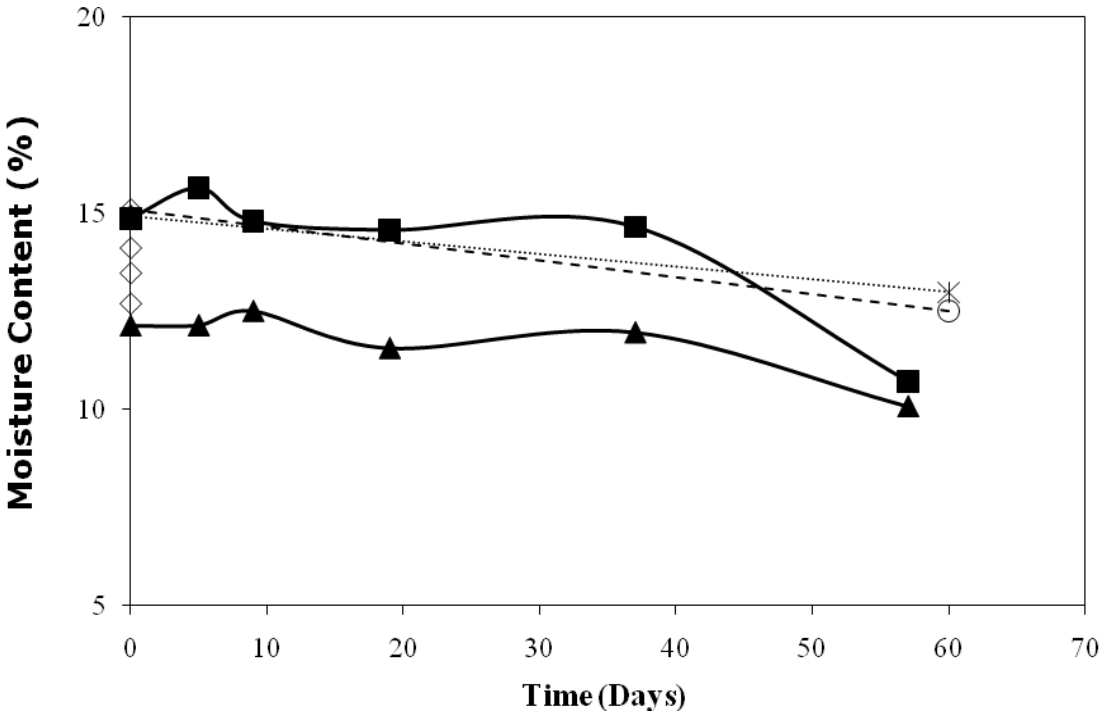

Figure 3-28 RCA moisture content versus time

2. After 63 days, the RAP oven dried moisture contents are lower than those during compaction. The fact that RAP has a low absorption, contained less fines and standing water was observed at the bottom of the bin when it was emptied suggests that water flowed down from the top. Evaporation was minimized by covering the bins with lids as shown in Figure 3-29.

Figure 3-29 Bin covered with lid

3. The RCA moisture content appeared relatively constant for the first 37 days (Figure 3-28). Thereafter, both the Nuclear Gauge and TDR registered a drop in moisture content. The oven-dry moisture content also dropped slightly after the 57-day post-compaction period. No standing water was observed at the bottom of the bin when it was emptied. Again, the bin was covered with a lid during the post-compaction period. If the lid was effective in minimizing evaporation, the drop in moisture content may be a result of hydration in the RCA since the crushing process most likely exposed unhydrated cement leading to additional pozzolanic reaction upon wetting (water was added during mixing).

Density

With respect to the change of dry unit weight with time, the following observations are offered:

1. Ten days after compaction, both the nuclear gauge and TDR dry densities for RAP remained relatively constant (Figure 3-30).

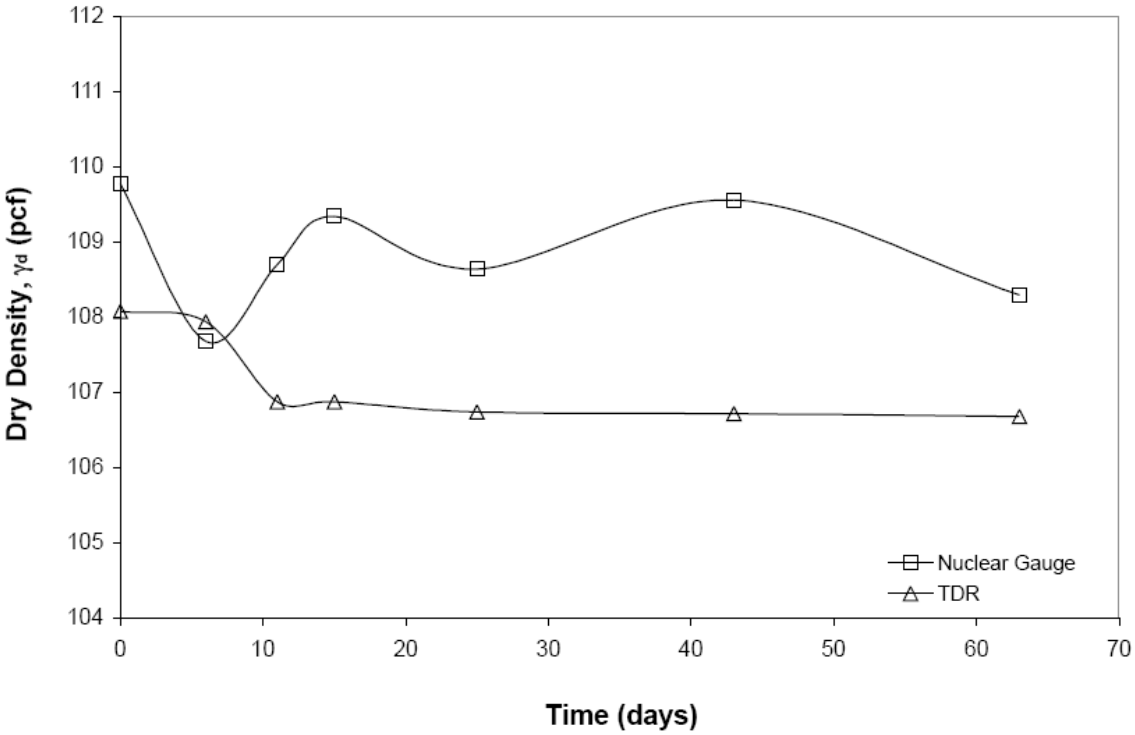

Figure 3-30 RAP dry density versus time

2. Figure 3-31 shows that the TDR dry density for RCA remained constant throughout the entire post-compaction period while the nuclear gauge dry density increased with time over the same period. The dial gauges did not register any bin wall movements for both RAP and RCA during the post-compaction period. Thus, the dry density should theoretically not change. Based on this, the nuclear gauge dry density values for RCA over time are questionable.

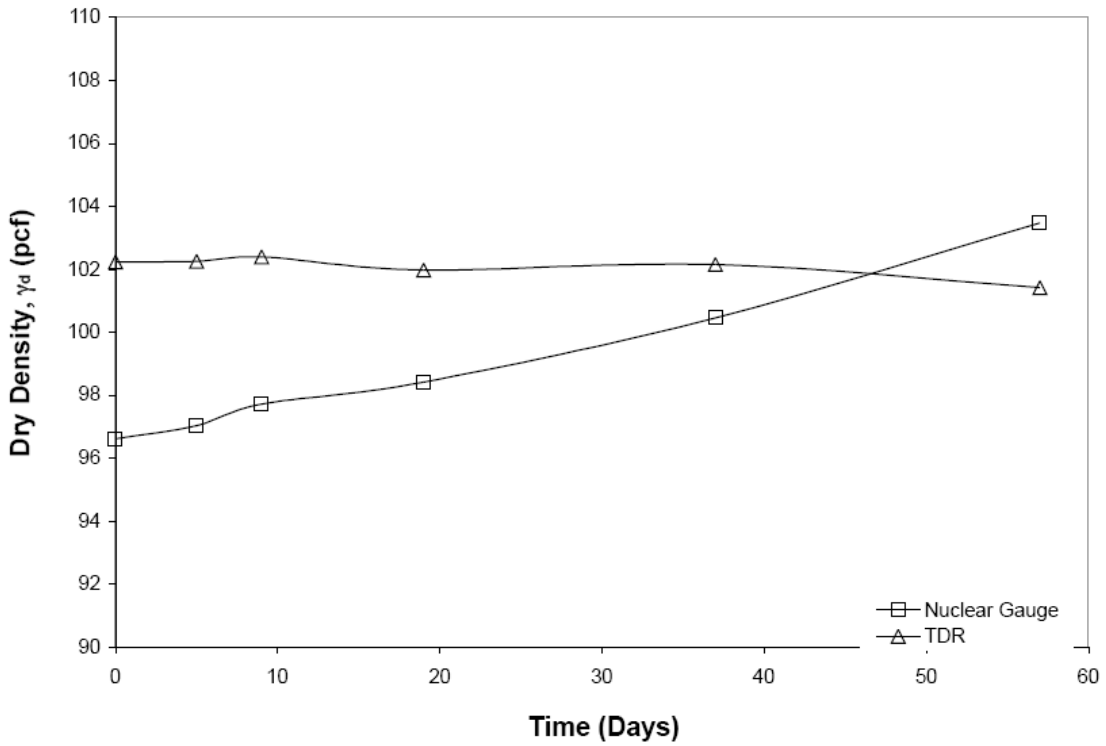

Figure 3-31 RCA dry density versus time

3.3.3. Summary and Conclusions

The objectives of this chapter were to: (a) compare the nuclear gauge and TDR methods of estimating moisture content and dry density of RAP and RCA with actual values by compacting these materials in six 6-inch-thick lifts in 3-foot diameter bins; (b) assess the variation of moisture content and dry density in the top lift over a post-compaction period of two months; and (c) assess if the materials crept during the post compaction period by monitoring the bin wall movements with time. The following conclusions are offered:

1. The nuclear gauge consistently provided higher moisture contents than actual for both RAP and RCA. This can be attributed to the fact that in addition to being present in free water, hydrogen atoms also exist in the cement paste in RCA and in asphalt in RAP. This suggests the need for nuclear offsets to be calibrated prior to use with these materials. The nuclear gauge moisture offset factors are estimated to be -23.3 and -13.8 for RAP and RCA, respectively.
2. The dry density from the nuclear gauge on average appears relatively reliable. However, this may be fortuitous because the nuclear gauge actually provides a measure of the moist unit weight. The dry unit weight is then derived using the overly predicted moisture content.
3. The TDR water contents for RAP and dry densities for RAP and RCA seemed reasonably accurate on average. However, the TDR water contents for RCA were underpredicted.
4. Attempts to replicate a bell-shaped compaction curve using the experimentally-derived calibration constants and the formulation published by Yu and Drnevich (2004) were not successful. This limitation poses a question as to whether the TDR is able to overall yield reliable results and its formulation should be re-evaluated.
5. With respect to the variation of moisture content with time, the following observations are offered:
    a. The nuclear gauge consistently provided moisture contents higher than the TDR.

b. The moisture content of the top lift in RAP initially decreased with time. After 11 days, the moisture content remained constant.

c. The RAP oven dried water contents after 2 months are lower than those at the end of compaction due to downward flow of water since RAP contained little fines, does not have a high absorption and standing water was observed at the bottom of the bin when it was emptied. During the post compaction period, the bins were covered with lids to minimize evaporation.

d. The RCA moisture content appeared relatively constant for the first 37 days. Thereafter, both the Nuclear Gauge and TDR registered a drop in moisture content. Oven-drying also indicated that the moisture content decreased during the post-compaction period. The fact that there was no standing water observed at the bottom of the RCA bin suggests there was little downward flow. The decrease in moisture content suggests that hydration of the water added during compaction due to pozzolanic reaction most likely occurred during this period.

6. With respect to the change of dry unit weights with time, the following observations are offered:

a. The nuclear gauge dry density for RAP is higher than the TDR dry density.

b. Ten days after compaction, both the nuclear gauge and TDR dry densities for RAP remained relatively constant.

c. The TDR dry density for RCA remained constant throughout the entire post-compaction period while the nuclear gauge dry density increased

with time. The dial gauges did not register any bin wall movements for both RAP and RCA during the post-compaction period. Thus, the dry density should theoretically not change. Based on this, the nuclear gauge dry density values over time are questionable.

3.4 STIFFNESS EVALUATION USING PORTABLE FALLING WEIGHT DEFLECTOMETER AND GEOGAUGE

3.4.1 Introduction

Traditionally, quality control/quality assurance of earthwork compaction is based on dry density and moisture content. However, with the advent of the MEPDG, there has been a recent push to use stiffness instead of dry density and moisture content. Dry density and moisture content are not engineering properties; they provide little insight on the material's deformation characteristics. On the other hand, the stiffness of the base, subbase and subgrade are increasingly recognized as being important input parameters for determining the thickness of pavement sub-layers.

The California Bearing Ratio and plate load tests have been utilized to measure the strength or stiffness of a geomaterial for use in pavement design. However, these tests require large reaction forces and cumbersome equipment (Kim et al. 2007) making them time consuming to perform. There are several portable devices that can be used to provide a measure of a geomaterial's surface stiffness. They can be divided into three categories. The first category consists of impact devices that actually penetrate into the ground. They include:

1. Clegg Impact Hammer (Steinert et al., 2005);
2. Dynamic Cone Penetrometer (Illinois Department of Transportation, 2005); and
3. PANDA dynamic cone penetrometer (Langton, 1999).

The second category consists of devices that send a shock wave to the ground. The stiffness is calculated based on load and displacement measurements (using velocity transducers or accelerometers). These devices include:

1. Loadman portable falling weight deflectometer (Steinert et al., 2005);
2. German Dynamic Plate (Alshibli et al., 2005);
3. PRIMA 100 portable falling weight deflectometer or PFWD (Steinert et al., 2005, Alshibli et al., 2005);
4. Dynaplaque II (Ruban, 2002);
5. Portable Seismic Property Analyzer (Celaya and Nazarian, 2006); and
6. GeoGauge (Humbolt Manufacturing Co., 2007).

According to Tutumluer (2004), the first two devices rely on physics (height and weight of the drop load) to estimate the force rather than a load cell, which led Tutumluer to conclude that they are deficient in accuracy.

A third category consists of burying sacrificial sensors in the compacted ground to monitor the growth in amplitude of pressure waves. Once the growth ceases, the compaction is considered complete and the next lift can proceed. An example of this device is the Soil Quality Indicator (SQI).

This section focuses on two devices from the second category: the PRIMA 100 PFWD and GeoGauge to measure the stiffness of RAP and RCA in the bin experiments.

3.4.2 Literature Review

Density and Stiffness

According to Fiedler et al. (2000) and Ooi and Pu (2003), there is no direct relationship between dry unit weight and stiffness. A material having a particular dry unit weight can have two values of stiffness. In addition, the maximum stiffness does not necessarily occur at the maximum dry density in compacted cohesive soils; they can occur dry of optimum (Lenke et al, 2001 and Ooi & Pu, 2003). In general, the stiffness decreased as the moisture content increased and the dry density decreased.

PFWD

Developed by Keros Technology and Carl Bro Pavement Consultants of Denmark, the Prima 100 PFWD consists of a falling mass that impacts a load plate, which in turn deforms into a geomaterial. The mass is dropped by pressing a release trigger seen in Figure 3-32 (left). The mass falls along a guide pole onto rubber buffers seen in Figure 3-32 (right). A load cell in the instrument measures the force that is imparted by the falling mass and a geophone measures the surface velocity. The PFWD can be accessorized with up to three additional geophones to measure the ground response. If all three geophones are used, then the offset of the geophones with respect to the center geophone are typically 207 mm and 407 mm (8 and 16 inches). Additional geophones were not used in these experiments.

Figure 3-32 PFWD release trigger (Left) and drop weight, rubber buffers, velocity transducer (Right)

There are several falling mass, drop height and plate diameter configurations. The three falling mass choices include 22, 33 and 44 lbs (10, 15, 20 kg). The drop heights range between 0.4 and 33.5 inches (10 to 850 mm). The choices of plate diameters

include 3.9, 7.9, and 11.8 inches (100, 200, 300 mm) (Steinert et al., 2005). In these experiments, the following were used: a 22-lb-mass, a 66-cm-drop height and a 300-mm-diameter load plate.

The elastic modulus is calculated from the solution for the deflection of a uniformly loaded circular plate on a linear elastic half space (Florin, 1959) as follows:

$$E_{PFWD} = \frac{2(1-\nu^2)\sigma \times R}{\delta_c} \tag{3.20}$$

where $\sigma =$ applied stress, R = plate radius, ν = Poisson's ratio of the geomaterial, δ_c = deflection at the center of the plate.

Steinhert et al. (2005) studied the effect of repeated drops on the stiffness at one location. They found that the first measurement was typically smaller than subsequent measurements, and recommended that the first value should not be included in the final stiffness average. They also studied the effects of the plate size and drop weight and found that when using the 15 or 20 kg drop weight, the stiffness did not change very much with different plate diameters.

Lin et al. (2006) also studied the effect of varying drop heights on stiffness. Using four drop heights and two plate diameters, they found that the different drop heights had very little effect on stiffness.

To determine the quality of the PFWD results, Fleming et al. (2001) suggested that the deflection-time history of each drop be assessed. Figure 3-33 shows that a high quality test should have no deflection at time zero, should increase to a maximum value followed by a decrease, and should have little to no deflection at the end of the pulse.

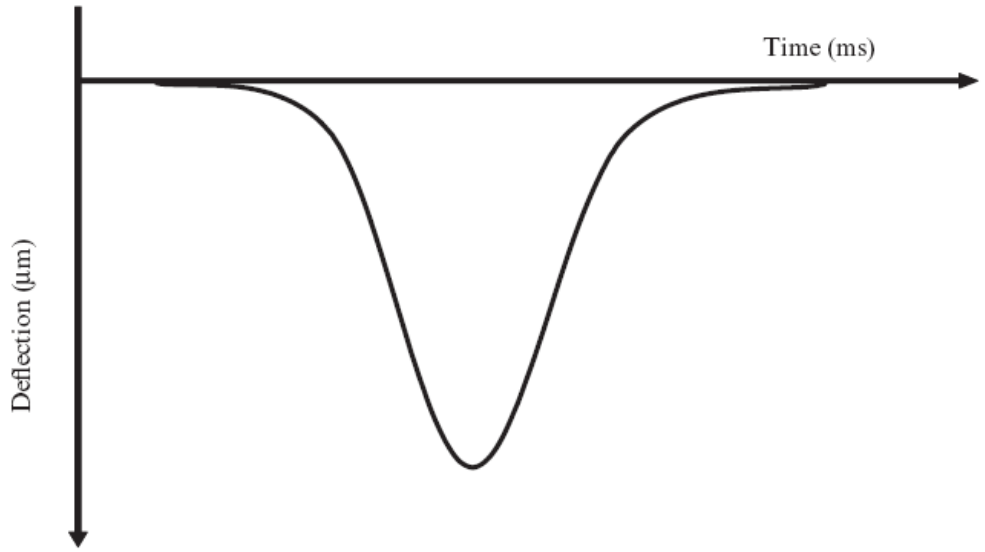

Figure 3-33 High quality PFWD reading (Fleming et al., 2009)

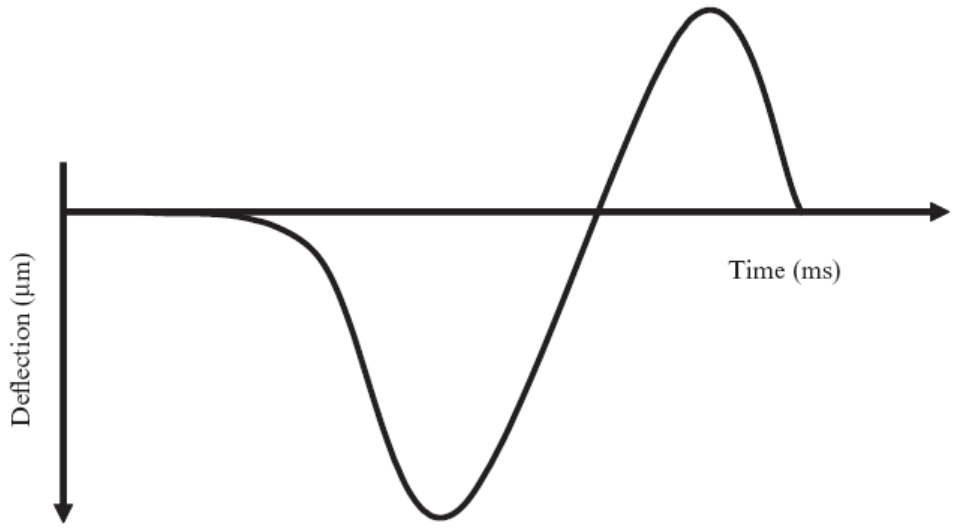

Figure 3-34 High rebound PFWD reading (Fleming et al., 2009)

Figure 3-34 shows the deflection at the end of the pulse going in an opposite direction instead of returning to zero. This type of signal can be obtained if the instrument bounces off the ground upon impact or if there is excess water in the geomaterial. .

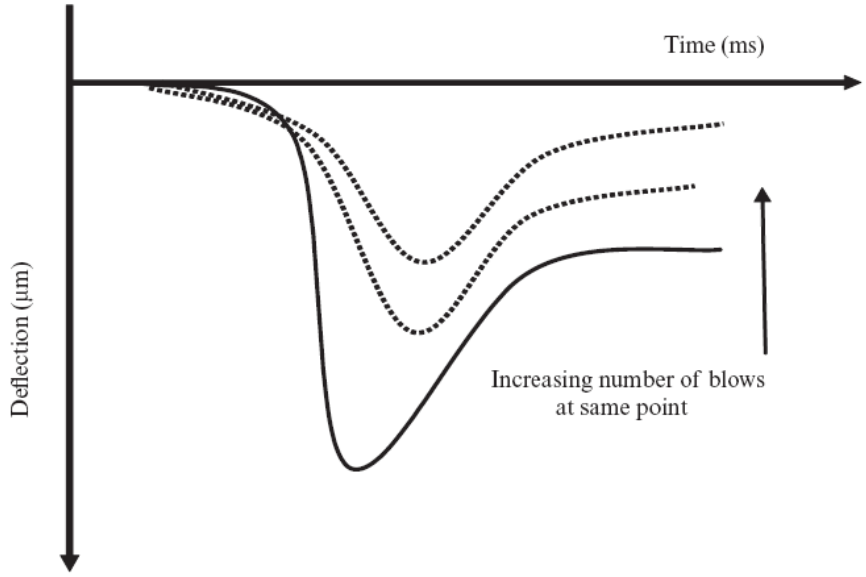

Figure 3-35 Effect of subsequent PFWD drops (Fleming et al., 2009)

Figure 3-35 shows the changes in the deformation-time histories upon successive drops at the same spot. Both the maximum deflection and the final deflection decrease with increasing number of blows.

The above graphs provide a means of evaluating which readings should or should not be used. For the bin experiments, each PFWD drop was plotted. For example, Figure 3-36 contains a plot of a series of readings obtained for the first RCA lift. Among the six drops, it can be seen that the first drop should be considered erroneous. During the second drop, the instrument may have bounced off the ground. Drops 3 through 6 are considered valid.

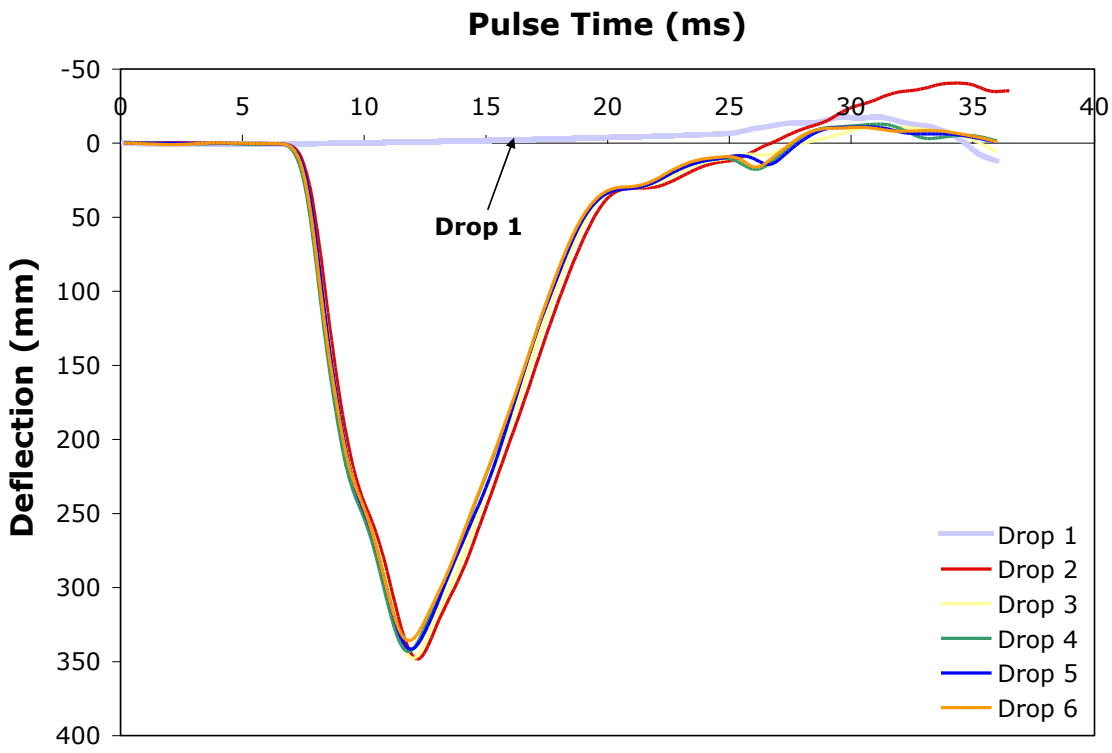

Figure 3-36 RCA PFWD test quality assessment

GeoGauge

The GeoGauge was developed by the FHWA and the U.S. Department of Defense Advanced Research Programs Administration based on the principles of a U.S. military device for detecting land mines using acoustic and seismic detectors. According to Fiedler et al. (1998), the same theory and technology employed in this device can be used to assess the compaction of earthworks.

The GeoGauge is 11 inches in diameter and 10 inches tall. It is placed on a geomaterial by means of a ring-shaped foot that protrudes from the bottom center (Figure 3-37).

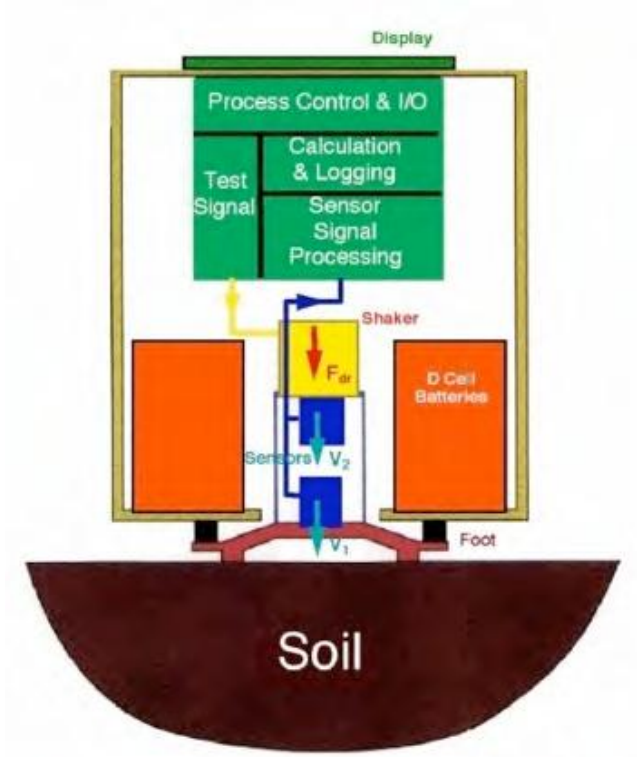

Figure 3-37 Schematic of GeoGauge (GeoGauge User Guide, 2007)

The foot has an outer diameter of 4.5 inches, an inner diameter of 3.5 inches and a thickness of 0.5 inches and is powered by six D-cell batteries. In the GeoGauge is an electro-mechanical shaker, that is set to vibrate at 25 different frequencies varying from 100 to 196 Hz. The vibrations cause very small displacement (about 0.0005 inches). At each frequency, the stiffness (K) of the material is determined from the force in the load cell and the displacement from the transducers. Then the elastic modulus is computed as follows (Egorov, 1965):

$$E = K\frac{(1-\nu^2)}{1.77R} \tag{3.21}$$

where E = elastic modulus, K = Geogauge stiffness, R = radius of ring shaped foot (2.25 inches) and ν = Poisson's Ratio. It is important to have at least 60% of the area of the foot in direct contact with the geomaterial. Each test takes about 1.5 minutes.

Previous Studies on Cement Stabilized Soils

Using the Prima 100 PFWD and GeoGauge, Abu-Farsakh et al. (2004) measured the stiffness of a mixture of clay and either two or four percent cement for about 2 weeks. In general, the elastic modulus increased to a maximum because of cementation and decreased thereafter. One reason cited for the decrease is shrinkage cracks.

Alshibli et al. (2005) performed a similar study on the stiffness over a period of time, using 2, 4, 6 or 8 percent cement and clay. Similar trends were found in this and the previous study where the stiffness of the material measured by the GeoGauge and PFWD decreased after a certain point probably also due to shrinkage cracks. It is interesting to note that field measurements are typically made immediately after compaction and before shrinkage cracks have had a chance to form.

Zone of Influence

Associated with the PFWD and GeoGauge is a zone of influence or the depth in the geomaterial at which the imparted stress becomes negligible. If the geomaterial below a layer that is being tested has a different stiffness and falls within the zone of influence, then the PFWD or GeoGauge will provide a composite stiffness value. Therefore it is important to establish the zone of influence for both instruments so that the modulus can be associated with the appropriate lift thickness. There have been several studies to determine the zone of influence.

Nazzal (2002) determined the zone of influence for both the PFWD and GeoGauge in two test boxes that were 36 inches wide, 72 inches long and 36 inches deep, one box containing compacted clay and the other compacted Florolite, more commonly known as plaster of Paris. The clay had a smaller stiffness than the Florolite. In his experimental set-up, a 9- to 12-inch-deep, 12-inch-diameter plastic cylindrical mold was placed at the center of the test box. Then, the material was compacted around the plastic cylindrical mold. The plastic cylindrical mold was subsequently removed leaving a cylindrical opening. Then the material to be tested is compacted with a standard Proctor hammer in the cylindrical void. After each layer was compacted, the PFWD and GeoGauge were used to determine the stiffness of each layer. The variation of stiffness versus elevation was plotted and Nazzal estimated the zone of influence by determining the depth at which the stiffness began to level off. Nazzal's results are shown in Table 3-6. It should be noted that the PFWD tests were conducted using a base diameter of 8 inches (about 200 mm) and a drop weight of 22 lb (10 kg). The drop height used in his study was not stated.

Sawangsuriya et al. (2002) determined the zone of influence of the GeoGauge in a 1.2 m x 1.2 m x 1.2 m box. Their procedure was similar to Nazzal's. They used three different materials with different stiffnesses. Three different sized cylindrical molds were placed in the middle of the box. The results of Sawangsuriya's experiments are also summarized in Table 3-6.

Table 3-6 Summary of zone of influence from the literature

Instrument	Test Configuration (Material Tested)	Zone of Influence (in)	Author (Date)
GeoGauge	36 inches wide, 72 inches long and 36 inches deep (Clay and Florolite)	7.5-8	Nazzal (December 2002)
PFWD	36 inches wide, 72 inches long and 36 inches deep (Clay and Florolite)	10.5 - 11	Nazzal (December 2002)
GeoGauge	4 feet x 4 feet x 4 feet box (Medium sand, crushed lime rock and mixture of plastic beads with sand)	5 – 10	Sawangsuriya et al. (January 2002)

3.4.3 Quality Control

Both the PFWD and GeoGauge were placed at the center of the bins to achieve an axi-symmetric loading configuration. Extra care was taken to ensure good contact with the surface. If the surface was not level, then a thin layer of fines from the geomaterial tested was sprinkled on the surface. Fleming et al. (2007) indicated that a thin layer of sand on an unleveled surface improved contact between the bottom of the instrument and the geomaterial, which in turn improved modulus readings. However, if the sand layer is too thick, then the readings can be low.

Also, care was taken to ensure that the instruments were not seated on large particles, which can yield erroneously high moduli. The GeoGauge was run before the PFWD since the PFWD exerts a larger strain on the material. At each lift and on each day post-compaction that the GeoGauge or PFWD were used, a minimum of 5 readings were made. All the raw deflection-time histories from the PFWD were plotted and

evaluated for quality. If the number of PFWD readings are less than 5, it implies that some data were omitted based on the deflection-time histories. Typically at least 5 readings were obtained per lift except for the first two lifts of RAP.

3.4.4 Test Results

The GeoGauge's and PFWD's default value of Poisson's ratio is 0.35. Based on high quality tests on granular soils reported by Lade (2005), the Poisson's ratio ranged from 0.17 to 0.26 with an average value of 0.2. Since RCA and RAP are also granular, a Poisson's ratio of 0.2 was adopted in this study.

3.4.4.1 Elastic Modulus During Compaction

Figures 3-38a and 3-39a plot the moduli versus depth for RAP and RCA, respectively along with interpreted trendlines. The average moduli and some statistics for RAP and RCA are summarized in tables 3-7 and 3-8, respectively. It is observed that the scatter (coefficients of variation) is much larger in the GeoGauge results than the PFWD.

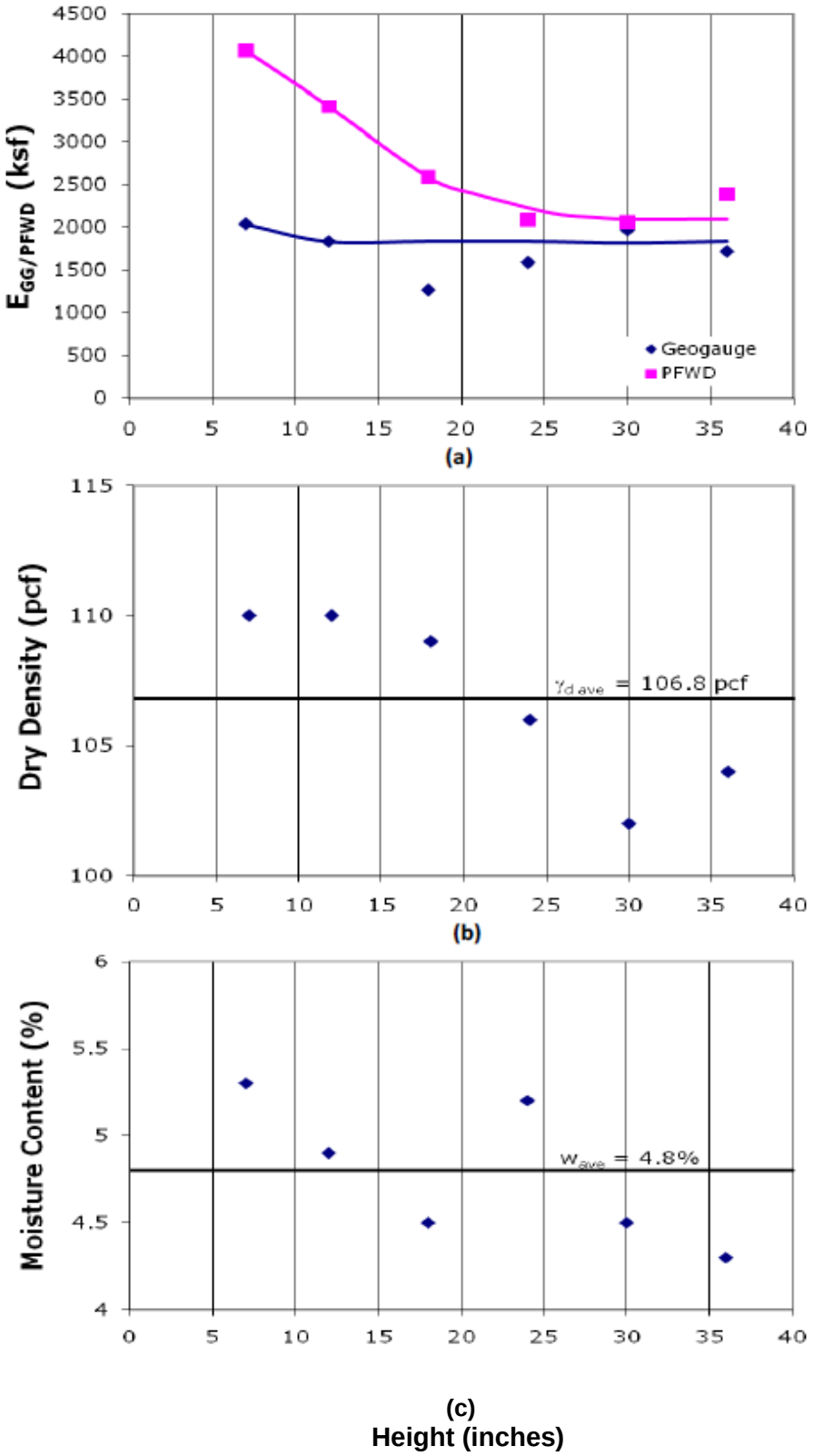

Figure 3-38 RAP stiffness, dry density and moisture content versus height

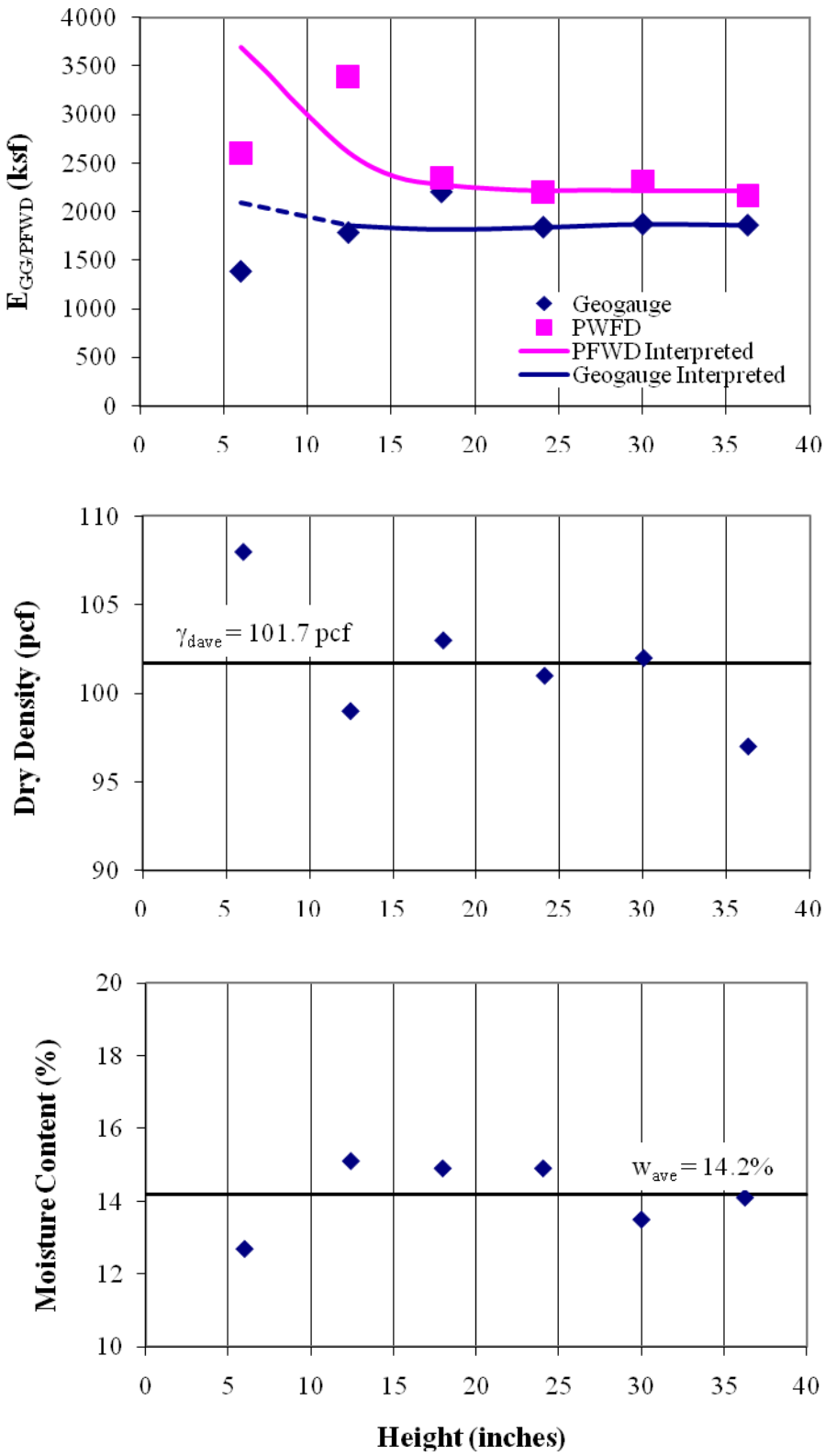

Figure 3-39 RCA stiffness, dry density and moisture content versus height

Table 3-7 RAP stiffness for each lift

		PFWD			GG		
Lift	Depth (in)	E_{avg} (ksf)	COV (%)	No. of Readings	E_{avg} (ksf)	COV (%)	No. of Readings
1	7	4073.2	2.5	4	2039.5	1.82	3
2	12	3413.7	0.9	3	1832.9	2.16	4
3	18	2584.7	1.43	5	1261.0	2.98	5
4	24	2082.4	2.76	10	1585.2	2.41	5
5	30	2051.5	1.08	7	1967.4	3.91	5
6	36	2382.6	0.72	6	1713.3	3.27	5

Table 3-8 RCA stiffness for each lift

		PFWD			GG		
Lift	Depth (in)	E_{avg} (ksf)	COV (%)	No. of Readings	E_{avg} (MPa)	COV (%)	No. of Readings
1	6	2597.7	1.27	5	1381.5	4.82	5
2	12.43	3389.4	0.92	5	1783.1	7.03	5
3	18	2347.2	1.27	5	2204.4	3.36	5
4	24.08	2203.0	3.71	5	1839.0	3.67	5
5	30.03	2307.7	1.55	5	1871.9	2.88	5
6	36.3	2161.3	0.39	4	1860.8	1.58	5

In general, the stiffness was highest in the lowest lift. Then, it decreased towards a constant value. Also, the PFWD consistently yielded higher moduli than the GeoGauge. This is unexpected because the GeoGauge imparts smaller strains than the PFWD and is expected to yield larger moduli. This trend has also been observed by Abu-Farsakh et al. (2004) and Alshibli et al. (2005) in cement-stabilized soils. The nature of the loading (annular versus circular and vibratory versus impact) and the zones of influence for the two instruments are dissimilar (Table 3-6). Also, the geomaterial may be cemented. The result is a trend in a complex problem that is difficult to rationalize and should make an interesting further study.

In Figure 3-38a, the change in RAP moduli with depth using the PFWD is much more dramatic than with the GeoGauge. The GeoGauge moduli seem to be relatively constant after the first lift while the PFWD moduli became constant only after the third

lift. An attempt was made to keep the dry density and water content constant in each lift (Figures 3-38b, 3-38c, 3-39b and 3-39c) but inevitably, some scatter could not be avoided. The fact that the GeoGauge stiffness became constant more rapidly than the PFWD can be explained as follows: the zone of influence of the GeoGauge is smaller than that for the PFWD (Table 3-6). Hence, the PFWD stiffness is more affected by the concrete floor in lifts that extend higher than during GeoGauge testing.

In Figure 3-39a, there are two moduli outliers - the GeoGauge modulus in lift one (6-inch depth) and the PFWD modulus in lift two (12-inch depth). These outliers cannot be explained alone by the variation in the dry unit weight and water content. It can only be theorized that the deviation may be attributed to a seating problem of the instruments.

3.4.4.2 Post Compaction Measurements

Figures 3-40 and 3-41 show the variation of moduli with time for RAP and RCA, respectively. In Figure 3-40, the modulus of RAP continually increased with time. This may be because the moisture content of RAP decreased over the duration of the experiment due to a downward percolation of water as shown in Figure 3-27.

In Figure 3-41, the modulus of RCA increased to a peak at about 20 days and then decreased. The initial increase is consistent with a reduction in moisture content and hydration of cement. It is postulated that the subsequent decrease is caused by shrinkage cracking, which was also observed by Abu-Farsakh et al. (2004) and Alshibli et al. (2005) in cement stabilized soils.

Table 3-9 and 3-10 summarize the average post-compaction moduli for the top lift, the coefficients of variation and the total number of readings. Again, the coefficients of variation again are much larger with the GeoGauge than with the PFWD.

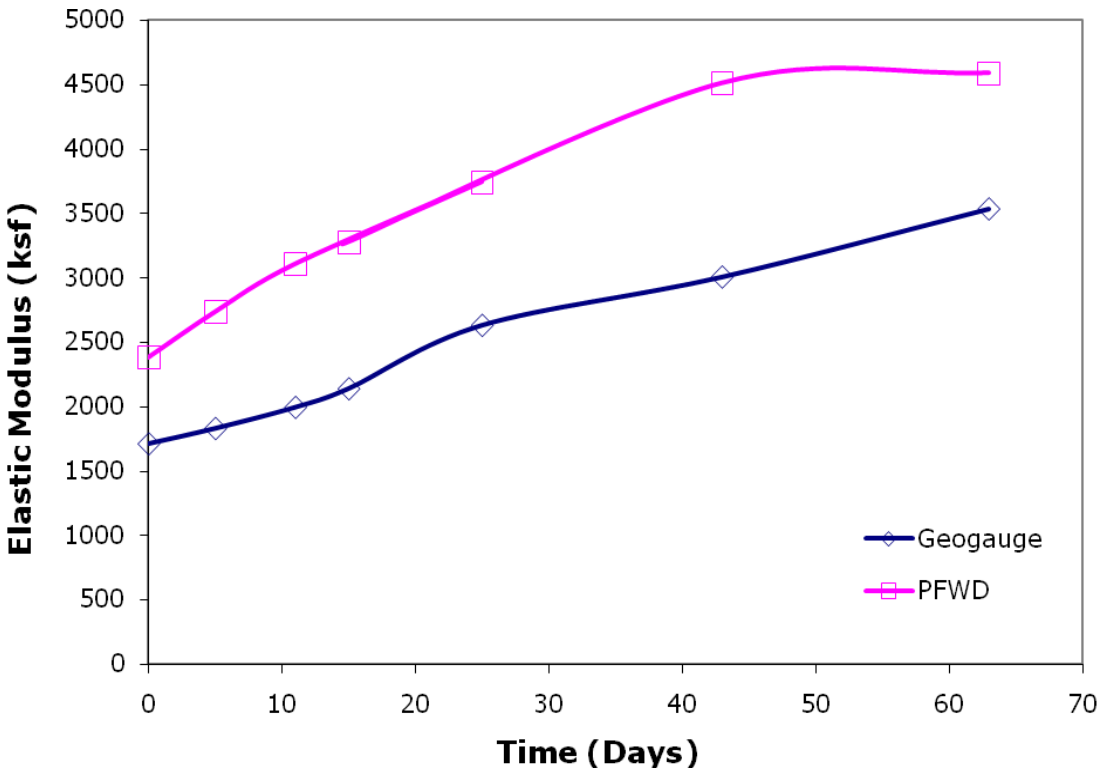

Figure 3-40 RAP elastic modulus versus time

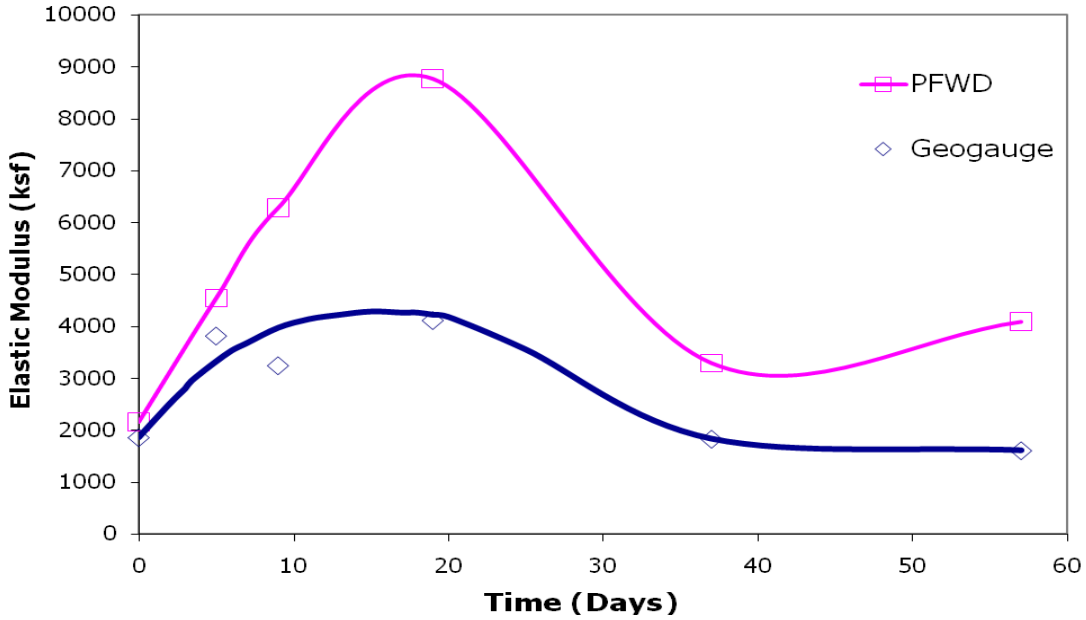

Figure 3-41 RCA elastic modulus versus time

Table 3-9 Variation of RAP stiffness with time

	PFWD			GG		
Days	E_{avg} (ksf)	COV (%)	No. of Readings	E_{avg} (ksf)	COV (%)	No. of Readings
0	2382.6	0.72	6	1713.29	3.27	5
5	2735.7	0.9	4	1831.92	2.09	4
11	3107.6	0.07	3	1995.54	2.71	5
15	3745.0	0.89	5	2139.83	2.56	5
25	3279.5	1.39	3	2631.38	2.1	5
43	4510.8	1.12	4	3005.79	2.8	4
63	4589.3	1.36	8	3533.02	1.32	4

Table 3-10 Variation of RCA stiffness with time

	PFWD			GG		
Days	E_{avg} (ksf)	COV (%)	No. of Readings	E_{avg} (ksf)	COV (%)	No. of Readings
0	2161.3	0.39	4	1860.8	1.58	5
5	4542.5	0.25	5	3816.7	3.45	5
9	6278.6	1.24	4	3245.6	2.16	6
19	8763.5	0.26	5	4114.3	0.99	4
37	3294.4	2.8	5	1832.6	2.24	5
57	4088.3	0.67	5	1610.2	2.09	5

3.4.4.3 Correlation Between PFWD and GeoGauge Stiffness

Figures 3-41 and 3-42 compare the moduli obtained from the PFWD and GeoGauge.

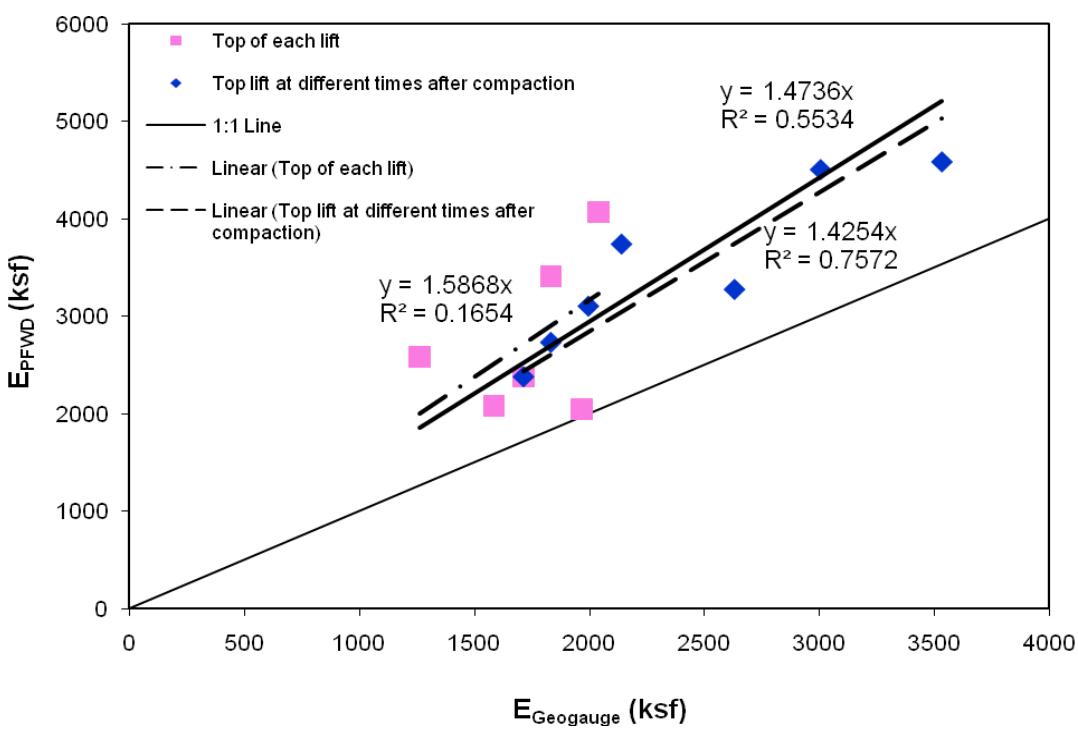

Figure 3-42 RAP PFWD and GeoGauge modulus comparison

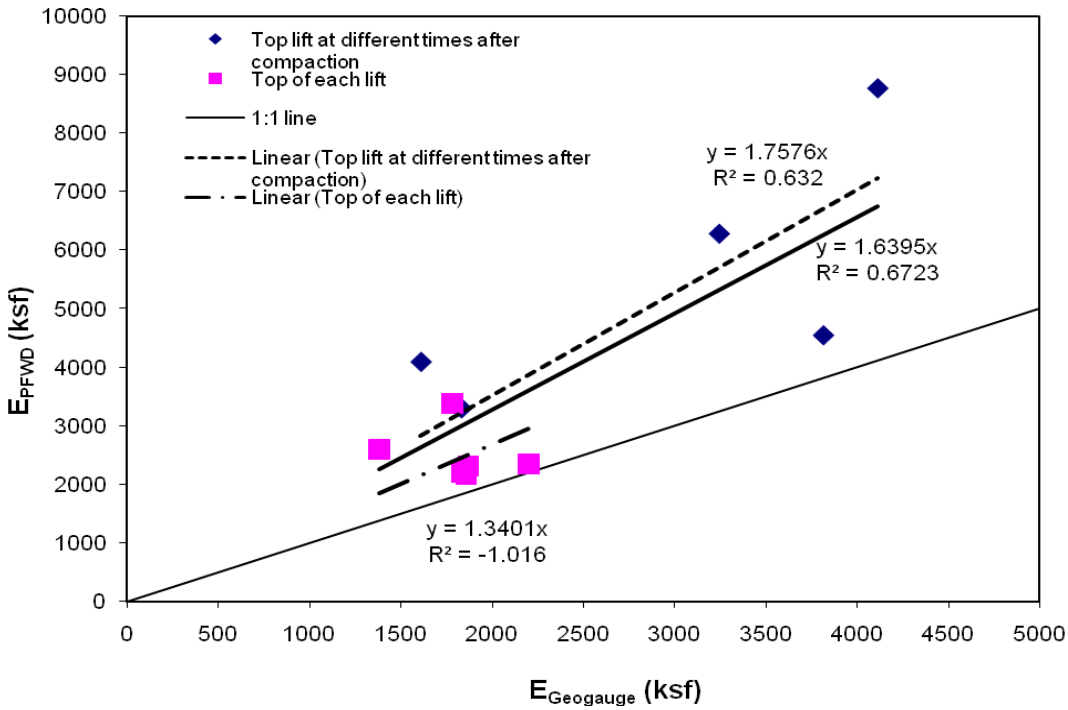

Figure 3-43 RCA PFWD and GeoGauge modulus comparison

It is evident that there is little correlation between the PFWD and GeoGauge measured in the six different lifts (R^2 = 0.16 and -1.02 for RAP and RCA, respectively). The PFWD and GeoGauge post-compaction moduli measured at the top lift correlated better with less scatter (R^2 = 0.76 and 0.63 for RAP and RCA, respectively). If the as-compacted and post-compaction moduli were combined into the same dataset, the R^2 for RAP and RCA were 0.55 and 0.67, respectively.

3.4.5 Summary and Conclusions

In this section, the objectives were to: (a) measure the PFWD and GeoGauge moduli of RAP and RCA in each of the six lifts as the material is compacted in 3-foot-diameter polyethylene bins; (b) assess the variation of the moduli of the top lift over a post-compaction period of two months; and (c) determine if there is a correlation between the PFWD and GeoGauge moduli of RAP and RCA. The following conclusions are offered:

1. The PFWD consistently provided higher moduli than the GeoGauge for RAP and RCA.
2. The PFWD gave more repeatable moduli than the GeoGauge (PFWD moduli coefficients of variation were lower). This may be because the quality of the PFWD results can be assessed using displacement-time histories.
3. It is important to consider the zone of influence when interpreting PFWD and GeoGauge moduli. That the GeoGauge stiffness became constant more rapidly than the PFWD is attributable to the influence of the concrete floor extending further up with the PFWD than with the GeoGauge.
4. With respect to the variation of stiffness with time:
    a. The RAP stiffness increased over the 2 month post-compaction period probably due to a drop in the moisture content as water percolated downwards with time.
    b. The RCA stiffness increased to a peak and subsequently decreased. The initial increase in stiffness is due to pozzolanic reaction in the RCA. The subsequent drop in stiffness may be attributed to shrinkage cracks in the RCA, which has also been observed in other studies on cement-stabilized soils.
5. There is a stronger correlation between the PFWD and the GeoGauge moduli after compaction than during compaction. In general, correlation in the six compacted lifts was non-existent.

3.5 EARTH PRESSURES

3.5.1 Introduction

The lateral earth pressure coefficient, K, relates the horizontal (σ_h') and vertical (σ_v') effective stresses as follows:

$$K = \frac{\sigma'_h}{\sigma'_v} \tag{3.22}$$

For a normally consolidated material, the at-rest earth pressure coefficient ($K_{o\ nc}$) can be approximated by the following relationship (Jaky, 1944):

$$\boldsymbol{K_{o\,nc} = 1 - \sin\phi} \tag{3.23}$$

where ϕ is the effective friction angle of the soil. Equation 3.23 is used extensively to estimate the horizontal stresses in the base, subbase and subgrade when designing pavements using the MEPDG (ARA, Inc., 2004). However, these pavement layers are typically proof-rolled in the field. Compaction induces preconsolidation. During primary unloading, the overconsolidated at-rest earth pressure coefficient ($K_{o\ oc}$) can be approximated as follows (Kulhawy and Mayne, 1990):

$$\boldsymbol{K_{ooc} = (1 - \sin\phi)OCR^{\sin\phi}} \tag{3.24}$$

where OCR is the overconsolidation ratio = σ_{vm}'/σ_v' and σ_{vm}' = preconsolidation stress. Since OCR is always greater than 1 for overconsolidated geomaterials, $K_{o\ oc}$ is always greater than $K_{o\ nc}$. One of the objectives of this experiment was to measure the compaction-induced lateral earth pressure of RAP and RCA in the bins and to investigate the effects of compaction on the value of $K_{o\ nc}$.

3.5.2 Literature Review

3.5.2.1 Rankine Active and Passive Lateral Earth Pressure Coefficients

Rankine (1857) developed the following expressions for the active (K_a) and passive (K_p) earth pressure coefficients

$$K_a = \frac{1 - \sin\phi'}{1 + \sin\phi'} \tag{3.25}$$

$$K_p = \frac{1 + \sin\phi'}{1 - \sin\phi'} \tag{3.26}$$

Rankine's equations 3.25 and 3.26 apply when there is no friction between the soil and wall and when the failure surface is planar (Figure 3-44). However, studies have shown that the failure surface is typically curved and approaches that of a logspiral. There is no simple equation for the logspiral active and passive pressure coefficients. They can be estimated using tables and figures from the geotechnical literature.

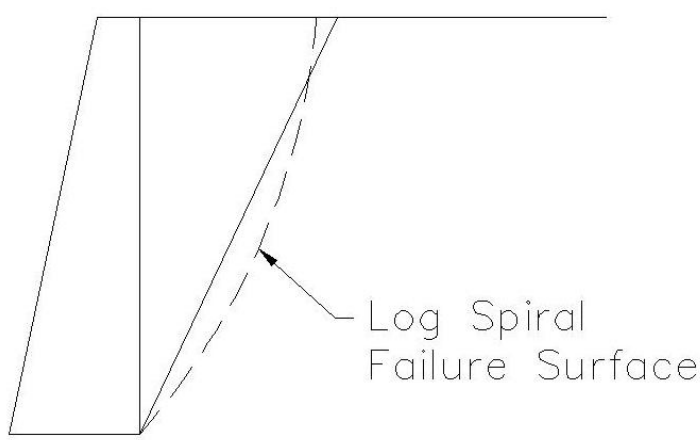

Figure 3-44 Planar and logspiral failure surfaces (Clough & Duncan, 1991)

3.5.2.2 Stresses in Silos

Retaining wall problems are typically plane strain; i.e.; they are long in the out-of-plane direction unlike in a bin, where the problem is axi-symmetric. To calculate the vertical and lateral pressures in the bins, theories for estimating pressures on a silo wall can be used. Janssen's (1895) and Reimbert and Reimbert's (1976) theories were developed for the design of silos to store grains, coals, cement, etc. These theories apply to any shaped silos and type of ensiled material.

Janssen's (1895) Theory

Figure 3-45 shows a schematic of the stresses acting on an element of material of thickness dz in a silo. Let σ_v = vertical stress at depth z and $\sigma_v + d\sigma_v$ = vertical stress at depth z + dz. The lateral stress $\sigma_h = K\sigma_v$. The shear stress $\tau = \mu\sigma_h = \mu K\sigma_v$ where μ = friction coefficient between the wall and the ensiled material.

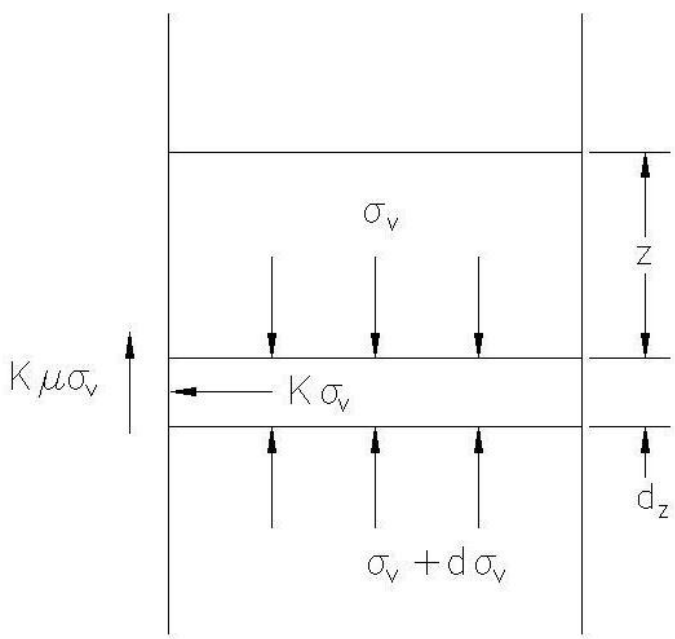

Figure 3-45 Forces in a silo (Janssen, 1895)

Resolving forces in the vertical direction yields:

$$A(\sigma_v + d\sigma_v) + \mu K \sigma_v P dz = \gamma A dz + A\sigma_v \tag{3.27}$$

where P = silo perimeter and A = silo cross-sectional area. Rearranging yields the following first order differential equation:

$$\frac{d\sigma_v}{dz} = \gamma - \left(\frac{K\mu P}{A}\right)\sigma_v \tag{3.28}$$

Solving the differential equation, σ_v and σ_h can be derived as follows:

$$\sigma_v = \frac{\gamma D}{4K\mu}\left[1 - e^{\frac{-4K\mu z}{D}}\right] \tag{3.29}$$

$$\sigma_h = K\sigma_v = \frac{\gamma D}{4\mu}\left[1 - e^{\frac{-4K\mu z}{D}}\right] \tag{3.30}$$

where D = silo diameter. It can be seen from equations 3.29 and 3.30 that as z →∞, σ_v → $\frac{\gamma D}{4K\mu}$ and σ_h → $\frac{\gamma D}{4\mu}$. It should be noted that Janssen's theory assumes that the lateral earth pressure coefficient, K, remains constant throughout the entire depth.

Reimbert and Reimbert's (1976) Theory

The main difference between Janssen's theory and Reimbert and Reimbert's (1976) theory is that Reimbert and Reimbert assumed a curved variation of wall friction with depth based on stress measurements on silo walls. σ_v and σ_h for Reimbert and Reimbert's theory are as follows:

$$\sigma_v = \gamma z\left[\frac{1}{1 + \frac{4Kz\mu}{D}}\right] \tag{3.31}$$

$$\sigma_h = \frac{\gamma D}{4\mu}\left[1 - \frac{1}{\left(1 + \frac{4Kz\mu}{D}\right)^2}\right] \tag{3.32}$$

It can be seen from Equation 3.31 that as z →∞, $\sigma_v \rightarrow \frac{\gamma D}{4K\mu}$ and $\sigma_h \rightarrow \frac{\gamma D}{4\mu}$; i.e.; identical to Janssen's theory. By dividing Equation 3.32 by 3.31, it can be shown that the lateral earth pressure coefficient, σ_h/σ_v, initially decreases with depth followed by an increase (Reimbert and Reimbert, 1976). In summary, the Janssen and Reimbert and Reimbert silo theories yield the same vertical and lateral pressures at large depths. The difference between these two theories is in the variation of the stresses at shallow depths.

3.5.3 Sensors

The bin wall earth pressures were measured using A201 FlexiForce® electrical sensors manufactured by Tekscan, Inc. The sensor is 0.008 inches thick, 0.55 inches wide and 7.75 inches long. Located at one end, the sensing area is 0.375 inches in diameter. The other end of the sensor is a 3-pin male connector. The center pin is inactive. The outer portion of the sensor is made of polyester while the conductive traces are silver. The sensor is extremely flexible and can conform to many different shaped surfaces, making them ideal for use on the circular bin walls.

Each sensor is connected to a transmitter. The transmitters send the data to a hub wirelessly. The hub is connected to the USB port of a computer. The Wireless Economical Load and Force (WELF) software reads the information from each transmitter and coverts it to a load based on the calibration factor.

3.5.3.1 Calibration

Calibration of the sensors was performed prior to the experiments. To calibrate the sensors, a known weight is placed on the sensing element and the sensor resistance output is determined and plotted. This is repeated using a number of known weights over a range that resembles the forces that will be encountered during the experiment. It is also important to recalibrate the sensors if they are not used for a long period of time.

3.5.3.2 Set Up

Four sensors were used in each bin (Figure 3-46).

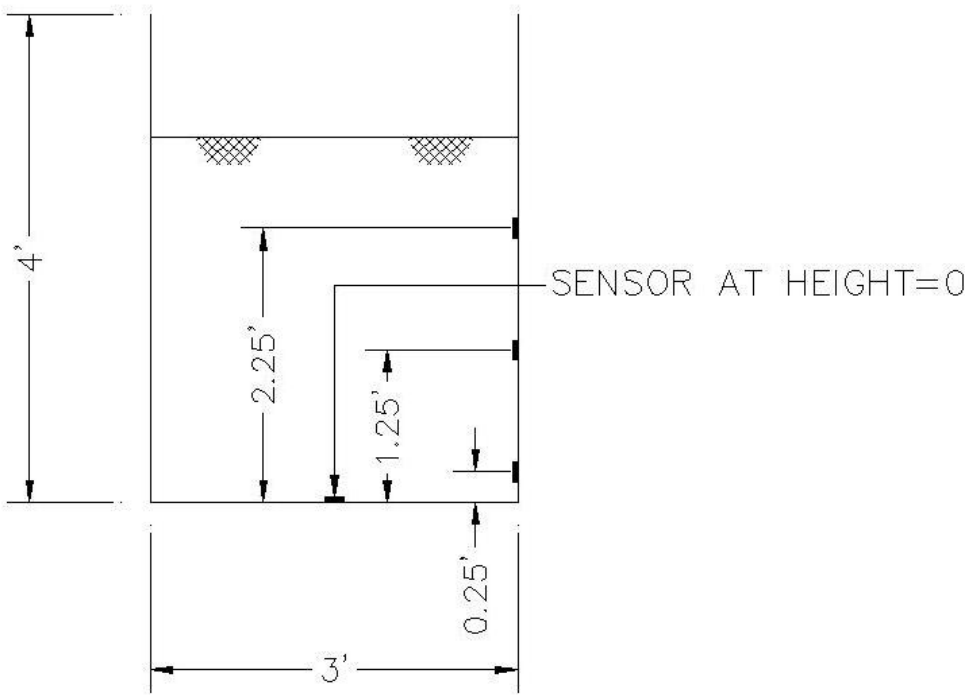

Figure 3-46 Sensor locations

One sensor was placed at the bottom center of the bin to measure the vertical stress. Three sensors were placed along the wall of the bins (at 0.25, 1.25, and 2.25 feet above the bottom) to measure the horizontal pressures. The sensors at 1.25 feet in both bins

did not work during the experiments despite the fact that extreme care was taken when compacting adjacent to a sensor.

It was found that the accuracy of the sensor readings stabilized with time. Therefore, the sensors were left on during the entire compaction phase of the experiment and the earth pressure is estimated based on the “long-term” sensor readings.

3.5.4 Test Results

3.5.4.1 Dial Gauge Readings

Figure 3-22 shows the RCA bin wall displacements obtained from dial gauge readings. Dial gauges were placed at one and two feet above the bottom of the bin. Based on the dial gauge readings and with the aid of the wall movement to height ratios from Clough and Duncan (1991) to distinguish active from at-rest behavior, it was found that the movements were small enough that the bin walls can be considered to be in an at-rest state. The RAP bin wall dial gauges were inadvertently dislodged during the experiment. In light of the movements observed in the RCA bin, at-rest conditions were also assumed for RAP.

3.5.4.2 Interface Friction Angle

The interface friction angle between soil and the cross-linked polyethylene wall, δ, was estimated using Koerner’s (1998) recommended efficiency of 0.56 for high-density polyethylene (HDPE) geomembrane/concrete sand interface defined as follows:

$$E = \frac{\tan\delta}{\tan\phi} \tag{3.33}$$

A literature search for the efficiency of CLPE was not successful. Based on measured friction angles of 50.7° and 42.8° for RCA and RAP (Selvarajah, 2009), the interface

friction angles were calculated to be 34.4° and 27.4° corresponding to μ of 0.68 and 0.52 for RCA and RAP, respectively.

3.5.4.3 Depth vs. Vertical Stress

Figures 3-47 and 3-48 present σ_v in the RAP and RCA bins, respectively. The lines represent σ_v calculated assuming free-field conditions ($\sigma_v = \gamma z$), Reimbert and Reimbert's and Janssen's theories. The measured σ_v at a depth of 3 feet is also plotted for comparison. This plot shows that σ_v from silo theories are less than the free-field values because wall friction reduces σ_v. The measured σ_v in both the RAP and RCA were close to the free-field σ_v, but larger than σ_v calculated using Janssen's and Reimbert and Reimbert's theories. This suggests that the value of μ is much smaller than estimated and that silo theories do not have to be considered in this experiment.

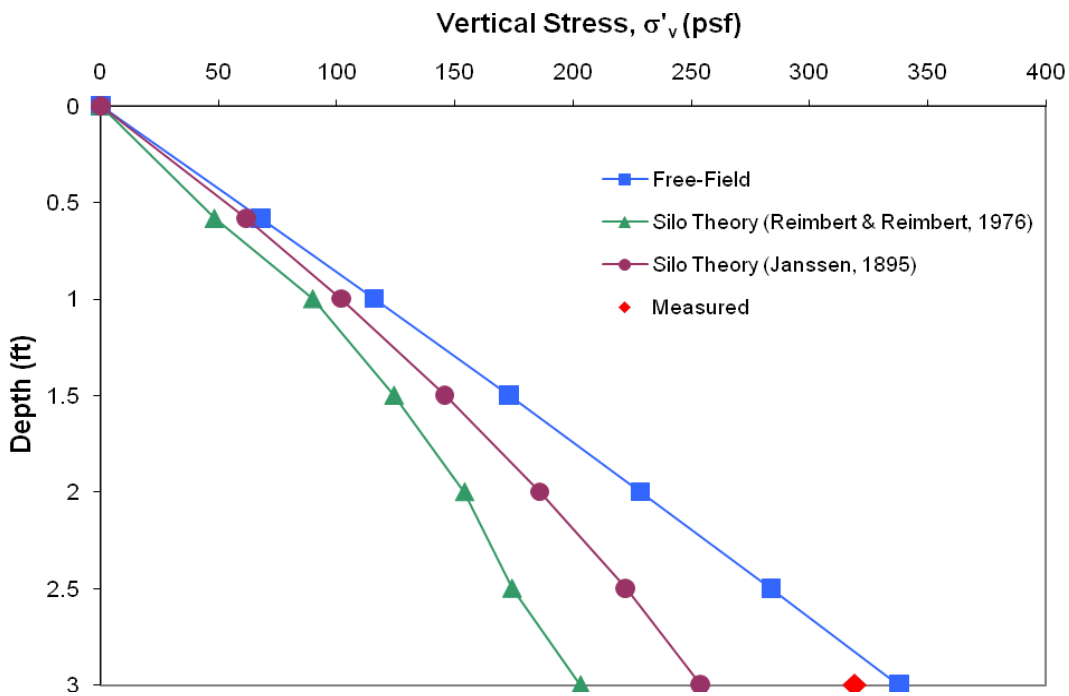

Figure 3-47 Vertical stress versus depth for RAP

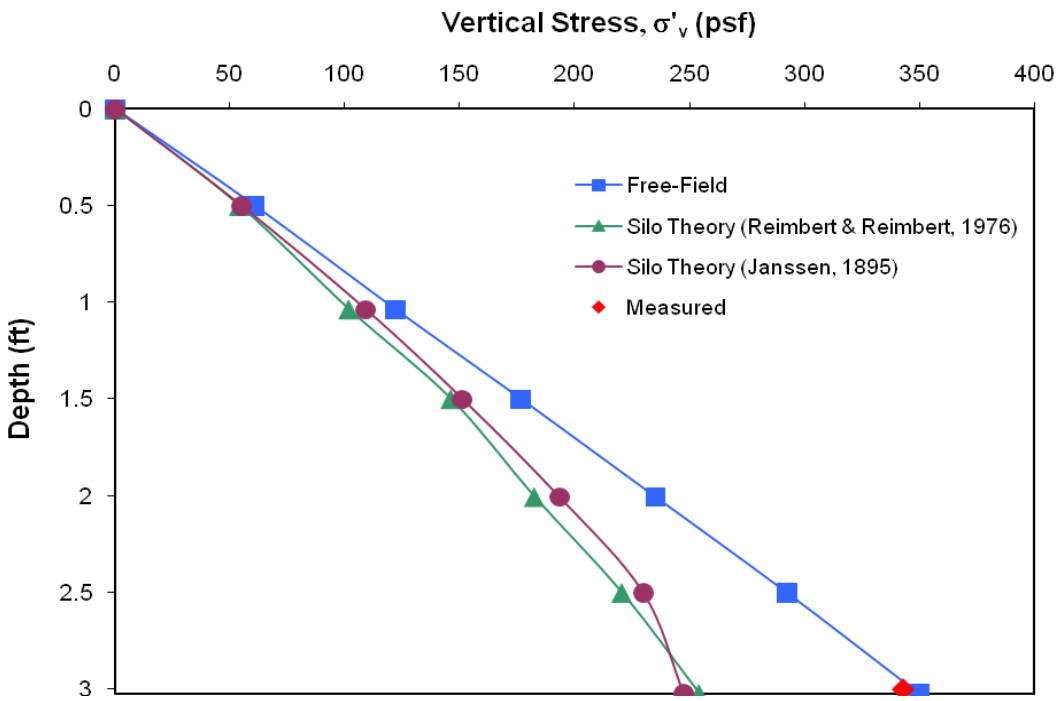

Figure 3-48 Vertical stress versus depth for RCA

3.5.4.4 Depth vs. Lateral Pressure

Figures 3-49 and 3-50 present σ_h in the RAP and RCA bins, respectively. The graph includes the upper passive and lower active limits of horizontal stress calculated using logspiral lateral pressure coefficients. These two lines represent the extreme limits between which, the data must lie. Also shown are the free-field at-rest, Janssen's and Reimbert and Reimbert's σ_h. These three curves were determined assuming $K = K_{o\ nc}$ (Jaky, 1944). The measured σ_h at depths of 0.75 and 2.75 feet are also shown. Measured values of σ_h are much higher than the theoretical ones. This can be attributed to the effects of compaction as explained in Section 2.11.1.1.1. For RAP, the calculated compaction-induced K_o (= $\sigma_{h\ measured}/\sigma_{v\ free\ field}$) varied from about 2.6 (at 0.75 ft depth) to 0.53 (at 2.75 ft depth), which are about 8.2 and 1.7 times the normally consolidated K_o value, while this ratio is about 0.8 for RCA at both depths, which is about 3.5 times the normally consolidated K_o value.

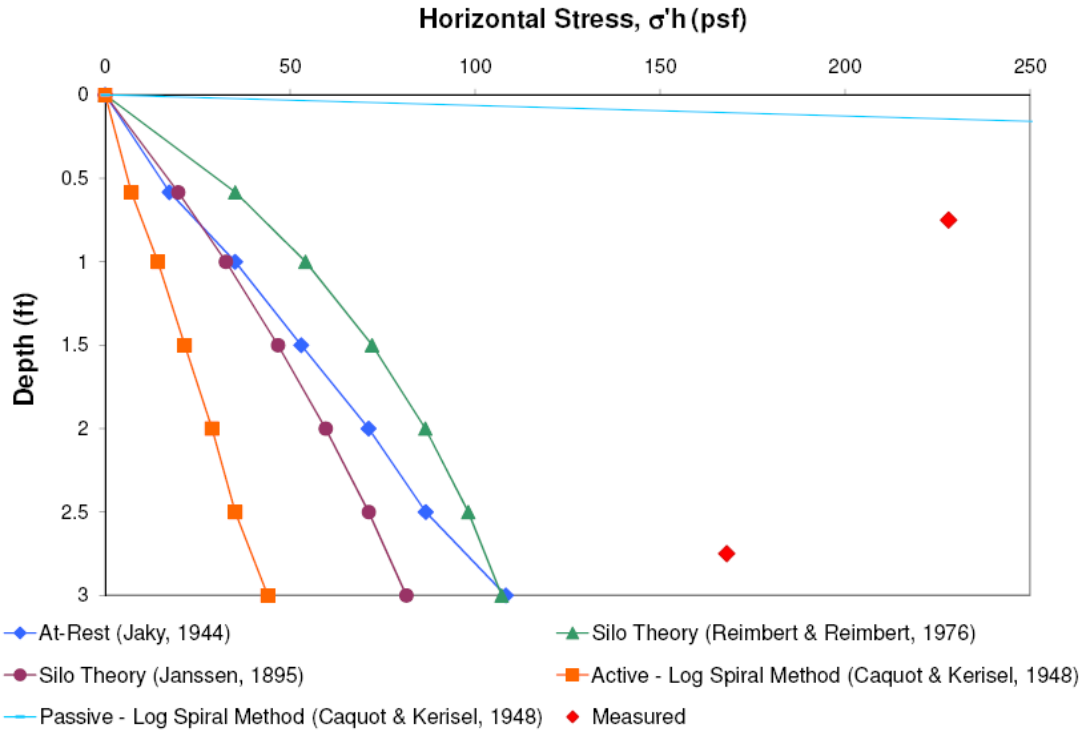

Figure 3-49 Depth versus lateral stress for RAP

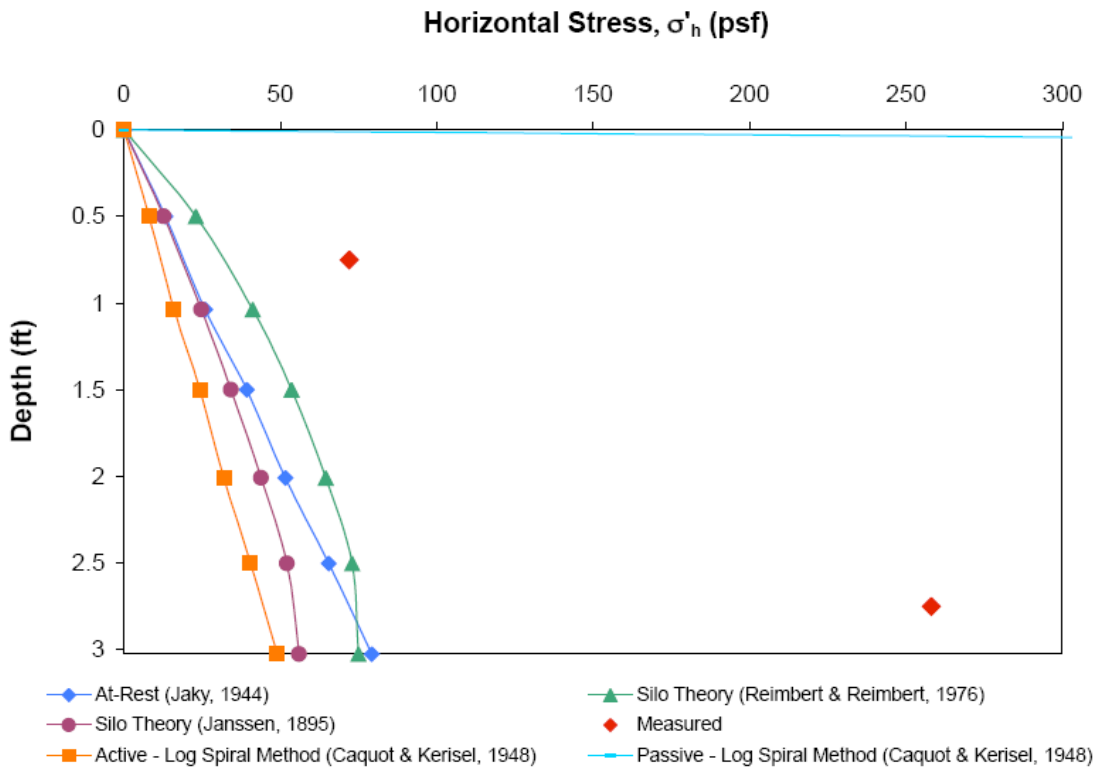

Figure 3-50 Depth versus lateral stress for RCA

It can be seen that the free-field at-rest stresses plot between the Reimbert and Reimbert's and Janssen's lateral pressures. Reimbert and Reimbert's σ_h is higher than the free field, while Janssen's σ_h is lower than the free field.

3.5.5 Summary and Conclusions

The objectives of this section were to compare the measured earth pressures with theory so as to determine the impact of compaction on the lateral stresses. The following summary and conclusions are offered:

1. The measured σ_v at the bottom of the bin was similar to the free-field but higher than σ_v calculated using silo theories. Based on this observation, the effects of wall friction is insignificant in these bins.
2. Dial gauge readings from Figure 3.22 show that the wall movements are negligible and that at-rest conditions prevail.
3. Compaction significantly increased the locked-in lateral stress from its normally consolidated at-rest value as the measured lateral stresses are much higher than theoretical values calculated assuming at-rest conditions. For RAP, the calculated compaction-induced ($K_o = \sigma_{h\ measured}/\sigma_{v\ free\ field}$) varied from about 2.6 (at 0.75 ft depth) to 0.53 (at 2.75 ft depth), which are about 8.2 and 1.7 times the normally consolidated K_o value, while this ratio is about 0.8 for RCA, which is about 3.5 times the normally consolidated K_o value.

CHAPTER 4 POTENTIAL FOR TUFA PRECIPITATION WITH CRUSHED CONCRETE CONTAINING COARSE BASALTIC AND FINE CORALLINE SAND AGGREGATES

4.1 INTRODUCTION

Reuse of crushed recycled concrete aggregate (RCA), derived from demolition of existing Portland Cement Concrete (PCC) structures and pavements, as road base and subbase course and as backfill has significant environmental and economical benefits. They include reduction in waste disposal in landfills and preservation of natural resources by reduced mining of virgin aggregate, thereby leading to more sustainable construction practices. Despite its advantages, RCA performance-related issues that need to be addressed include asbestos and lead paint contamination, high pH, sulfate attack, alkali-silica reaction, alkali-carbonate reaction and formation of tufa, which is a calcite or calcium carbonate ($CaCO_3$) precipitate that has the ability to clog drainage systems and filter fabrics. The focus of this study is on tufa formation. Clogged systems can lead to water retention and generation of large excess pore pressures especially when used below a roadway. According to Gupta and Dollimore (2002), tufa formation "is due to excess dissolution of calcium ions ……. caused by absorption of carbon dioxide into the aqueous solution."

Based on a survey of the various state departments of transportation (Gupta and Kneller, 1993), tufa-related problems of varying degrees have been reported in Iowa, Kansas, Maryland, Minnesota, Ohio, Pennsylvania and West Virginia. Consequently,

many of these states limit the percent of RCA in unbound pavement layers. Interestingly, not all states report such problems.

Use of RCA in highway projects as a base/subbase in the continental USA and abroad has been gaining popularity. The state of Hawaii Department of Transportation (HDOT) is considering utilizing RCA in its projects. The RCA coarse aggregate in Hawaii is basalt while the fine aggregate is commonly coralline sand. This study investigates whether tufa will precipitate when RCA containing such an aggregate mixture reacts with carbonic acid in rainwater in an accelerated testing environment.

4.2 LITERATURE REVIEW

Based on laboratory and field studies, Snyder and Bruinsma (1996) agreed with Michigan DOT's suggestion that calcium ion concentration tests can be used to quantify the precipitate potential of RCA, but no benchmark criterion was available then. Bruinsma et al. (1998) indicated that the amount of calcite precipitate is influenced by (a) the contact time of the drainage water with the aggregate; and (b) the aggregate surface area; i.e., aggregates with more fines, which have a larger surface area, have a higher precipitation potential.

Gupta and Kneller (1993), Dollimore et al. (2000) and Gupta and Dollimore (2002) applied thermal analysis and X-ray diffraction (XRD) test to establish the portlandite [$Ca(OH)_2$], dolomite [$CaMg(CO_3)_2$] and calcite [$CaCO_3$] content in RCA from Ohio. Dollimore et al. (2000) concluded that the calcium content from the carbonate components of the aggregate affects calcite deposition while the small quantities of

portlandite from the cement paste "would not seem to make this material a significant factor in calcite precipitation."

Gupta and Dollimore (2002) asserted that "in general, good quality cement does not produce tufa." Rather, tufa may be produced from "processed fine aggregates of dolomitic or calcitic origins" as the RCA tested from Ohio consisted mostly of dolomite and calcite. Based on leaching tests of RCA in acidic water (CO_2 in water), their studies evaluated the leachate concentration of magnesium and calcium ions using Inductive Coupled Plasma-Atomic Emission Spectroscopy (ICP-AES). Their studies confirmed previous work (e.g., see Drever, 1988) which indicated that in the dolomite/calcite equilibrium,

$$CaMg(CO_3)_2 + Ca^{2+} = 2\ CaCO_3 + Mg^{2+}$$

A ratio of $Mg^{2+}/\ Ca^{2+} > 0.6$ will favor tufa ($CaCO_3$) precipitation in the presence of carbonate in rainwater. Based on this, they recommended that leachates should have a Mg^{2+}/Ca^{2+} ratio of less than 0.6 for RCA to be used as base/subbase course. This last recommendation pertains to dolomitic-based RCA.

A literature review has not revealed any studies on the tufa precipitate potential of RCA containing coarse basaltic and fine coralline sand aggregates. Basalt typically has a composition by weight of 45 - 55% of SiO_2, 2 – 6% of total alkalis (Na_2O, K_2O), 0.5 – 2% of TiO_2, 5 - 14% of FeO, 5 – 12% of MgO, ~10% of CaO and 13% or more of Al_2O_3. Pyroxene, olivine and plagioclase are the most common minerals. The fine coralline sand aggregate is predominantly calcium carbonate.

4.3 CHEMISTRY OF TUFA

Tufa exists in nature from the precipitation of calcium ions and dissolved CO_2 in natural waters.

$$Ca^{2+}(aq) + CO_3^{2-}(aq) \leftrightarrow CaCO_3(\downarrow)$$

The source of the carbonate ions is typically CO_2 in the air, which dissolves in rain or natural water to form carbonic acid, H_2CO_3.

$$CO_2 + H_2O \leftrightarrow H_2CO_3$$

Carbonic acid disassociates to form mostly bicarbonate ions:

$$H_2CO_3 \leftrightarrow H^+ + HCO_3^-$$

Bicarbonate ions increase the solubility of the calcium ions (Gupta and Dollimore, 2002).

Possible sources of Ca^{2+} in the RCA from Hawaii include Portland cement, basalt and/or coralline sand. Cement is manufactured by crushing clay and limestone together and then firing it in a kiln. The end product consists mostly of calcium silicates and aluminates. Calcium hydroxide or portlandite is one of the bi-products of cement hydration. Portlandite is not very soluble in water. In fact, its solubility decreases with increasing alkalinity. Since concrete is naturally alkaline, it is unlikely that the calcium ions in tufa will come from cement. Instead, Gupta and Dollimore (2002) suggest that the calcium ions are derived primarily from the aggregate, which is predominantly dolomite in their state of Ohio.

For tufa to precipitate, one of the following three conditions must exist (Gupta and Dollimore, 2002): (a) change in pH leading to a change in solubility; (b) evaporation; (c) change in temperature to cause freezing and thawing.

4.4 CHARACTERIZATION OF THE AS-RECEIVED RCA

Samples of RCA were obtained from a paving contractor on the island of Oahu, Hawaii. A petrograhic description of the RCA is made based on visual observation of thin sections. X-ray fluorescence (XRF) tests were conducted on the as-received RCA to determine its elemental composition.

4.4.1 Petrographic Description of the RCA

Standard-size (25 x 40 mm) rectangular, polished petrographic thin sections (thickness 30 microns) of the RCA samples were made to enable a petrographic description and in-situ micro-analytical analysis to be made. The RCA is composed of angular basalt fragments, 5-15 mm in size, embedded in a matrix of predominantly fine (0.1-0.5 mm) coralline sand and cement. Visually estimated proportions are 60-70 modal percent basalt, 10-15 percent sand and 10-15 percent cement.

The angular basaltic fragments are compositionally and texturally typical of Hawaiian lava flows and feeder dikes, as quarried in a few locations on the island of Oahu. Most fragments are olivine-phyric basalts with a very fine-grained to microcrystalline massive groundmass consisting of plagioclase microphenocrysts, opaque titanomagnetite and less abundant calcic clinopyroxenes. Less common are feeder-dike derived, slightly coarser grained diabase fragments, which contain similar mineralogy but with a coarser groundmass consisting of euhedral magnetites and plagioclase laths with a very strong

lattice preferred orientation. Despite more than a million years of exposure to the tropical climate, they have undergone little to moderate degrees of low-temperature hydrous alteration, preserving most phenocryst and groundmass minerals.

The fine aggregate sand is predominantly composed of well-rounded, biogenic micritic carbonate fragments such as fragments of corals and bivalves, with some subrounded basalt fragments, typical of beach deposits. The cementitious matrix was not studied petrographically.

4.4.2 Elemental Composition of the RCA

The basic principle of the XRF is to bombard the sample with X-ray. The sample fluoresces with X-ray peaks at characteristic energies depending on its elemental composition. Major elements are analyzed by the methods outlined in Norrish and Chappell (1977).

XRF was performed using a Siemens SRS-303AS wavelength dispersive X-ray spectrometer, having a Rh X-ray source at 60 kV and 45 mA. Powdered RCA sample is mixed with lithium metaborate, ignited at 900°C and cast into a glass disk. Major element data are reported as weight of oxides in percent. Results of duplicate XRF tests conducted on the as-received RCA are summarized in Table 4-1. Compared with average compositional values for basalt published by Blyth and de Freitas (1984), the RCA contains significantly more CaO. According to Marske et al. (2008), basalt from the Kilauea eruption on the Island of Hawaii has around 10 - 12% CaO. Slight variation in the CaO content was observed in the older volcanoes; e.g. the basalt from a quarry in Makakilo on the island of Oahu, was found to contain 8.4% CaO on average based on

XRF testing (sample size = 36). This implies that 12 – 16% of the calcium is from the cement and/or fine aggregate (coralline sand which is predominantly $CaCO_3$) used in the manufacture of concrete in Hawaii.

Table 4-1 X-ray fluorescence test results on the as-received RCA showing the major elements reported in terms of weight of oxides in percent

Material	Composition (%)					
	SiO_2	CaO	Al_2O_3	Fe_2O_3	MgO	Na_2O
RCA Sample	**39.3**	**24.1**	**11.6**	**10.8**	**6.48**	**1.78**
Makakilo (Oahu) Basalt Measured	**47.8**	**8.4**	**13.6**	**14.1**	**8.10**	**3.10**
Published Average for Basalt from the Kilauea eruption on the Island of Hawaii (Marske et al.,	**50.7**	**10.7**	**13.3**	**12.2**	**7.60**	**2.20**
Published Average for Basalt (Blyth and de Freitas, 1984)	**49.1**	**9.0**	**15.7**	**5.4**	**6.20**	**3.10**

4.5 LEACHING EXPERIMENT

Leaching tests were performed by soaking two sets of the RCA aggregate in rain water for over three months. In the first set, CO_2 gas was bubbled through the rain water and aggregate for 95 days in an attempt to facilitate the formation of tufa on an accelerated basis. Serving as a control, the second set was identical to the first except no CO_2 was bubbled through. Rain water rather than distilled water was used to simulate as closely as possible the actual environment in the pavement base and/or subbase course.

The aggregate was housed in a soil triaxial test chamber having an acrylic cylindrical wall (Figure 4-1). A geotextile was placed at the bottom of the aggregate to prevent any tufa and fines from draining out when periodically collecting the rainwater leachate for testing. Five kilograms of aggregate was used in each test chamber and the aggregate compositions and gradations were varied as summarized in Table 4-2.

Figure 4-1 Test setup for bubbling CO_2 through RCA soaked in rain water. CO_2 is fed through the bottom of each test chamber. It then bubbles up through the aggregate solution and exits at the top of the chamber into a hose that feeds into the large plastic container filled with water

Table 4-2 Aggregate used in leaching tests and test objectives

Sample #	Aggregate	Gradation	Test Objective
1	100% virgin basaltic aggregate	HDOT subbase	Tests 1, 2 and 3 – to study the effect of percent RCA on tufa formation
2	50% RCA:50% VA	HDOT subbase	
3	100% RCA	HDOT subbase	
4	100% RCA	Coarser than subbase	Tests 3, 4 and 5 – to study the effects of gradation on tufa formation
5	100% RCA	Finer than subbase	
6	90% RCA and 10% fly ash	HDOT subbase	Tests 3 and 6 – To study the effects of fly ash on mitigating tufa

Chambers 1, 2 and 3 contained aggregate meeting HDOT's gradation requirement for subbase (Figure 4-2) but the percent ratio of virgin basaltic aggregate/RCA was varied from 100/0 to 50/50 to 0/100. Chambers 4 and 5 contained 100% RCA, the latter and former being coarser and finer than HDOT's subbase gradation (Figure 4-2). Chambers 3, 4 and 5 allow the effects of gradation on tufa formation to be studied. Chamber 6 is similar to Chamber 3 except 10% flyash was added to evaluate the effectiveness of fly ash in mitigating tufa formation as suggested by Gupta and Kneller (1993).

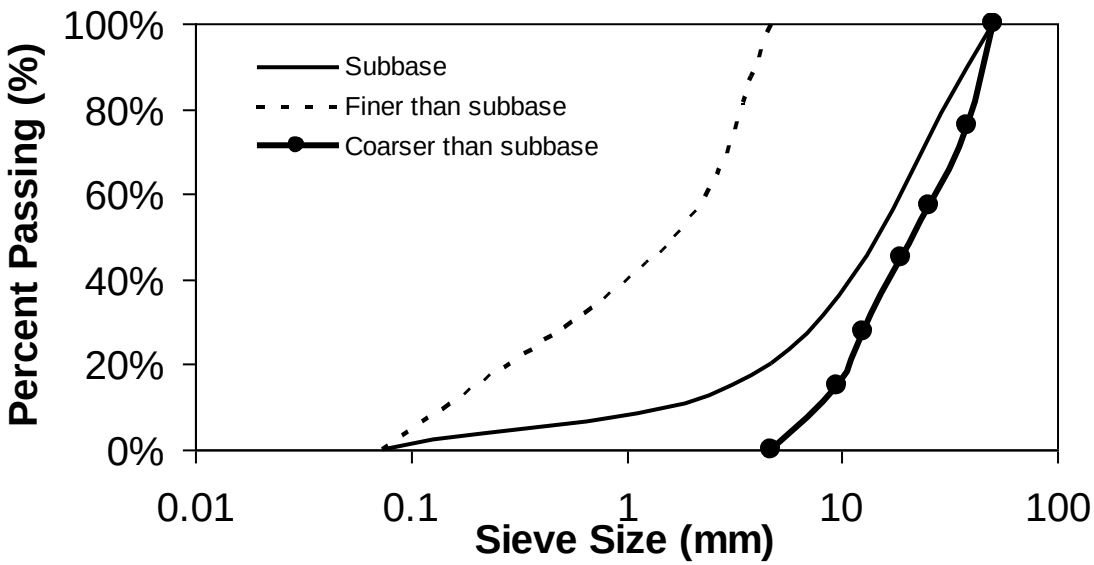

Figure 4-2 State of Hawaii Department of Transportation's subbase gradation along with the gradations finer and coarser than the subbase gradation used in the leaching experiments

A total of 21 23-kg-tanks of CO_2 were used over the 95-day test period.

4.6 DISCUSSION OF TEST RESULTS

Both sets of rainwater leachate, with and without CO_2 bubbling, were subjected to pH and ICP-AES testing.

4.6.1 pH of the Leachate

Over the 95-day test duration, pH of the leachate was measured using a Milwaukee pH600 pH meter with a resolution of 0.1. On the day of each measurement, the pH meter was attuned using a calibration solution (PINPOINT^{TM}) at a pH of 7. pH values are summarized in figures 4-3a and 4-3b for the leachate with and without CO_2 bubbling, respectively. In Figure 4-3a, the last two readings for Chamber 5 (100% RCA finer than subbase) and the last reading for Chamber 6 (90% RCA with 10% fly ash) were not obtained because the leachate was depleted. The aggregate in these two chambers are finer and have a higher surface area resulting in a greater rate of reaction and faster depletion of the leachate. Evaporation and leakage also played a part but the rates should be fairly similar among the various test chambers. Additional rain water was not supplemented during the tests.

Prior to mixing with aggregate, the pH of the rain water alone was 7.6. Immediately after mixing with RCA but prior to CO_2 bubbling, the pH increased to between 11.4 and 12.3 (time = 0 days – off the scale in Figure 4-3a) except for 100% basalt, where the pH was 7.7. One day after CO_2 was introduced, the pH dropped and eventually stabilized at about 6.2 to 6.4 (for the 100% basalt, the pH varied between 5.8 and 6.0).

For the aggregate without CO_2 bubbling, the pH dropped slightly from their initial values. However, the solution remained highly basic (pH between 11 and 12). pH values for the 100% basalt sample ranged from 7.5 to 8.2.

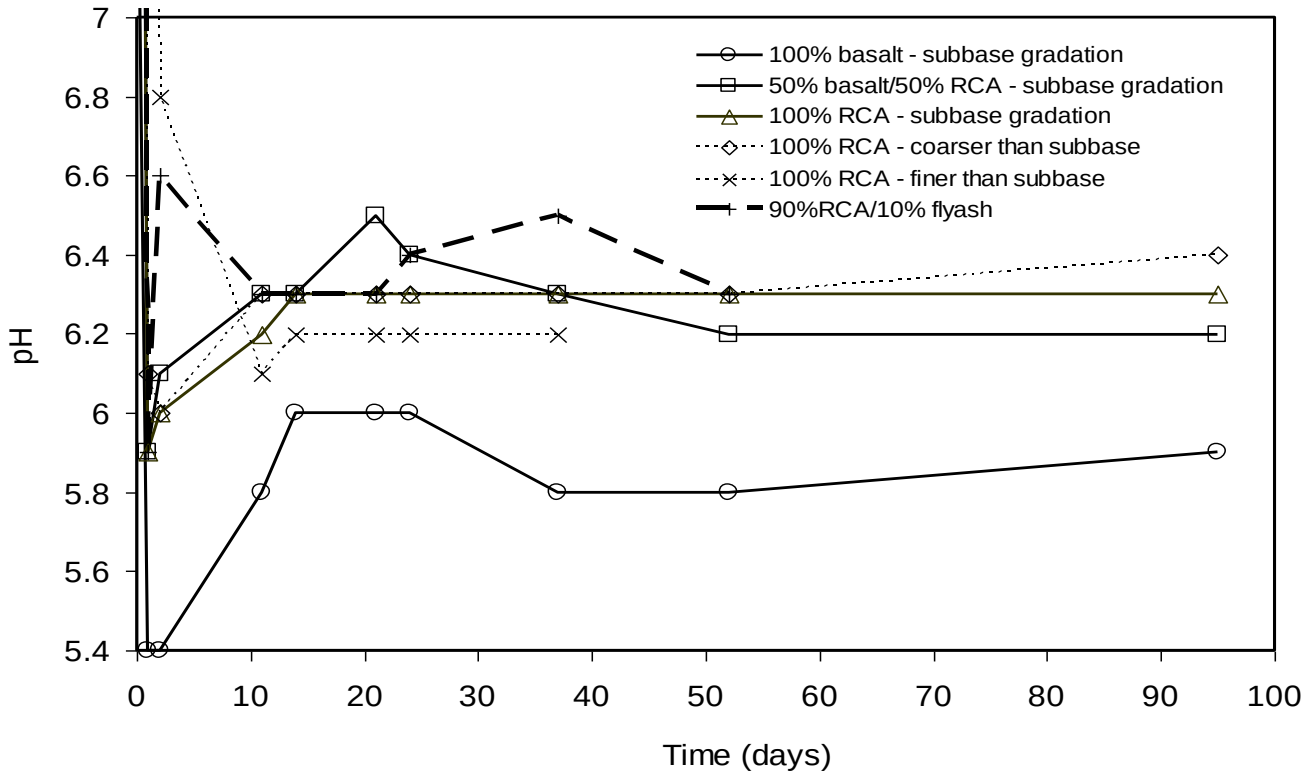

(a)

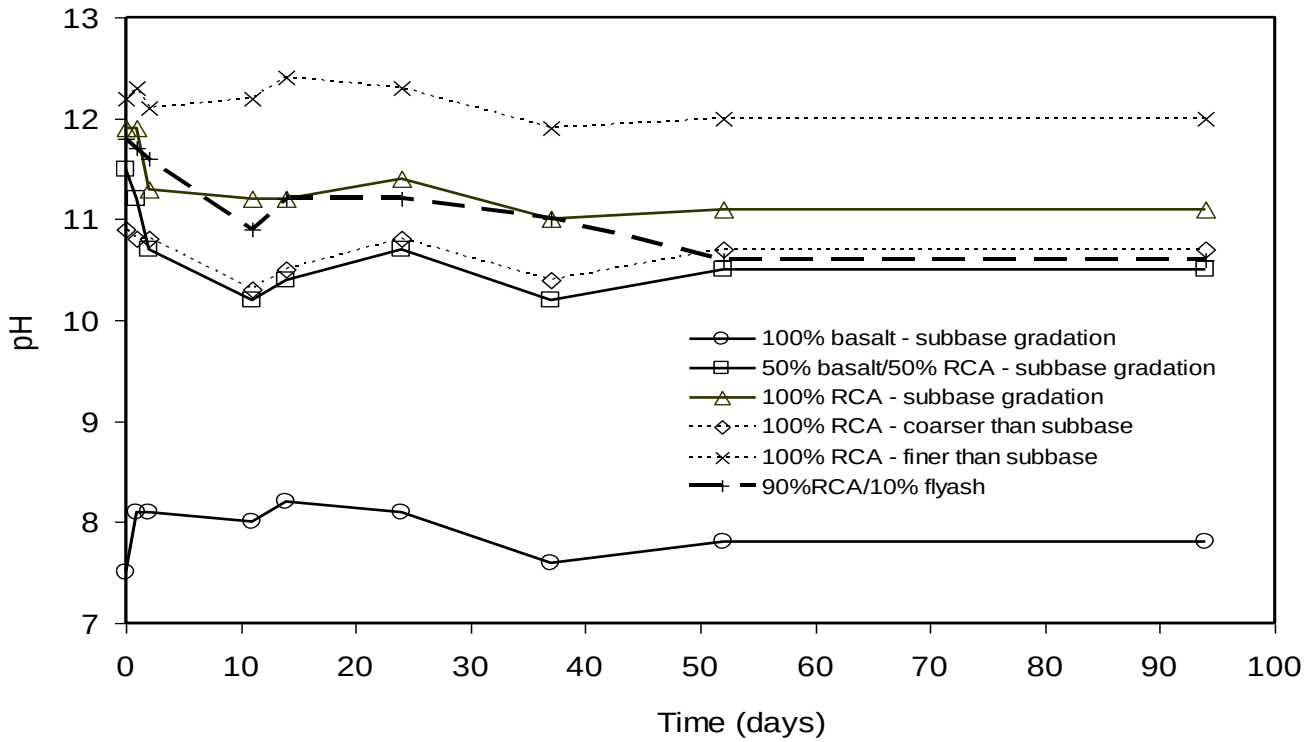

(b)

Figure 4-3 pH of leachate (a) with and (b) without CO_2 bubbling versus time

4.6.2 ICP-AES Tests on Leachate

ICP-AES tests were conducted throughout the course of the experiment to measure the Ca^{2+} and Mg^{2+} ions in the RCA leachate. Using a Vista-MPX CCD Simultaneous ICP-OES manufactured by Varian, Inc., an aerosol of the leachate is first humidified with argon gas and atomized with a plasma torch. This excites the electrons present in the leachate, which then emits light energy at specific wavelengths that are unique depending on the elemental composition. A spectrometer measures the intensity of the light energy, which can then be correlated to the concentration of that element.

Figures 4-4 and 4-5 show the variation of Ca^{2+} and Mg^{2+} concentrations with time in the leachate with and without CO_2 bubbling, respectively. From these figures, the following are observed:

1) The Ca^{2+} and Mg^{2+} with CO_2 bubbling are significantly higher than those without bubbling.

2) With CO_2, the Ca^{2+} and Mg^{2+} concentrations increased with increasing RCA content (Figs. 4-4a-c).

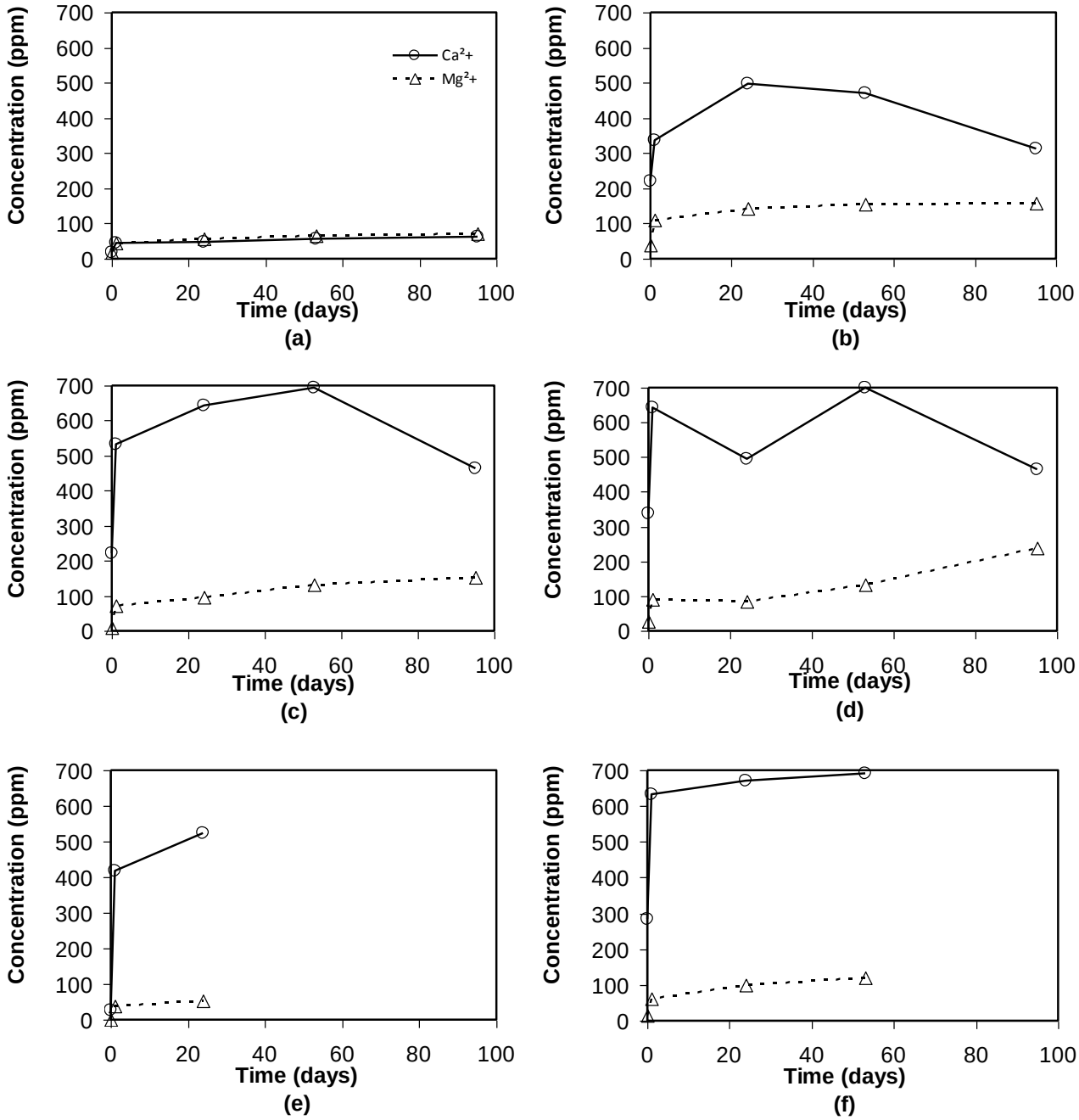

Figure 4-4 Ca^{2+} and Mg^{2+} ion concentration in the leachate with CO_2 bubbled through versus time. (a) 100% virgin basaltic aggregate – subbase gradation; (b) 50% RCA and 50% virgin basaltic aggregate – subbase gradation; (c) 100% RCA - subbase gradation; (d) 100% RCA – coarser than subbase gradation; (e) 100% RCA – finer than subbase gradation and (f) 90% RCA (subbase gradation) and 10% flyash

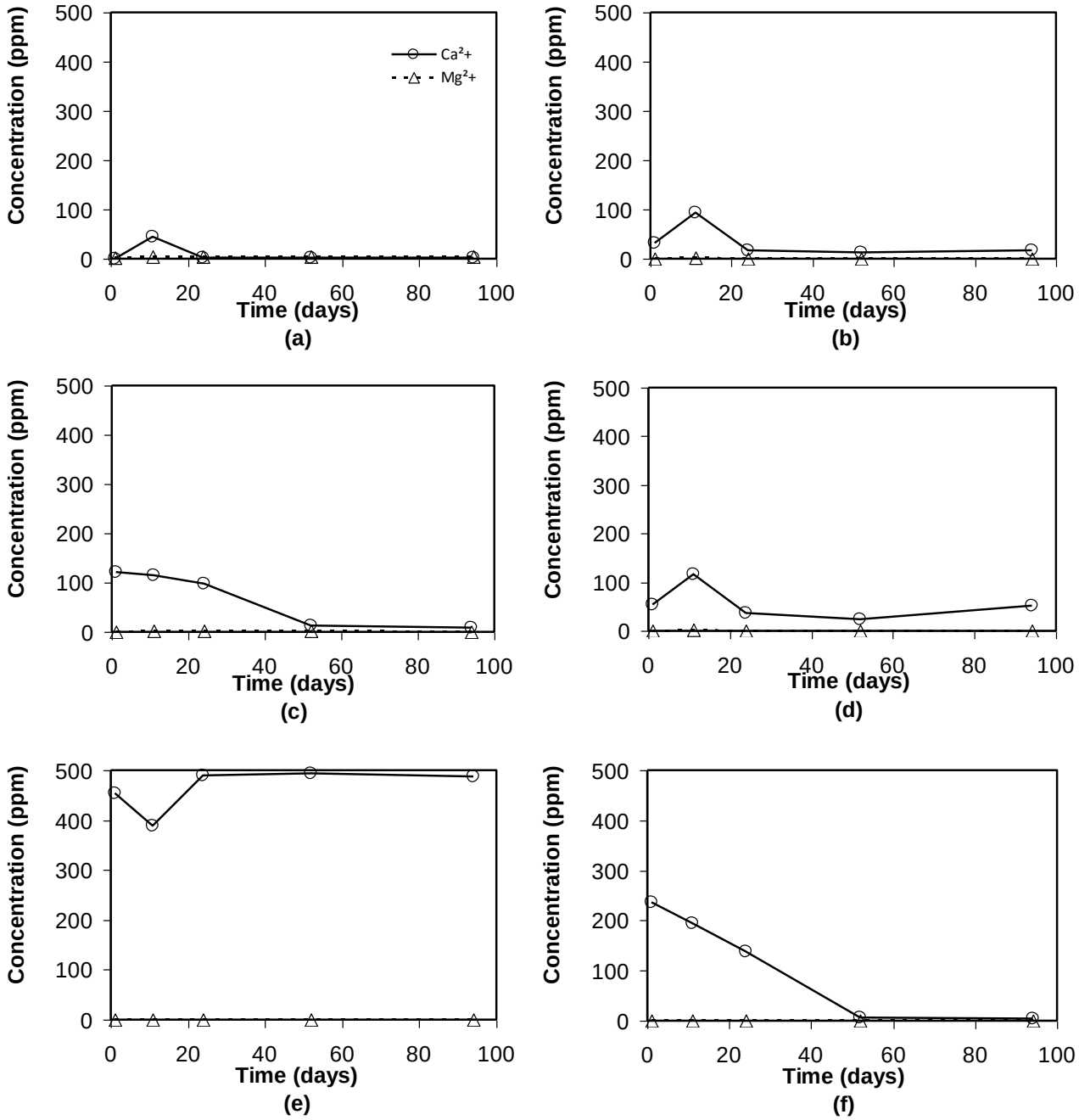

Figure 4-5 Ca^{2+} and Mg^{2+} ion concentration in the leachate without CO_2 bubbled through versus time. (a) 100% virgin basaltic aggregate – subbase gradation; (b) 50% RCA and 50% virgin basaltic aggregate – subbase gradation; (c) 100% RCA - subbase gradation; (d) 100% RCA – coarser than subbase gradation; (e) 100% RCA – finer than subbase gradation and (f) 90% RCA (subbase gradation) and 10% flyash

3) With CO_2, the Mg^{2+} concentrations increased with time at a very slow rate. In contrast, the Mg^{2+} ion concentration in similar experiments performed on an RCA containing a slag and dolomitic aggregate from Ohio increased very rapidly to 620 ppm within 5 days (Figure 4-6 after Gupta and Dollimore, 2002). Since dolomite ($CaMg(CO_3)_2$) contains an abundance of Mg^{2+} ions and since the solubility of $MgCO_3$ (3.5×10^{-8}) is an order of magnitude higher than that of $CaCO_3$ (3.8×10^{-9}), the Mg^{2+} ions will preferentially remain in solution while the Ca^{2+} ions will combine with the CO_3^{2-} ions to precipitate as tufa (Gupta and Dollimore, 2002). However, XRF tests indicate that the percent MgO is only about a quarter of CaO in the RCA (Table 4-1).

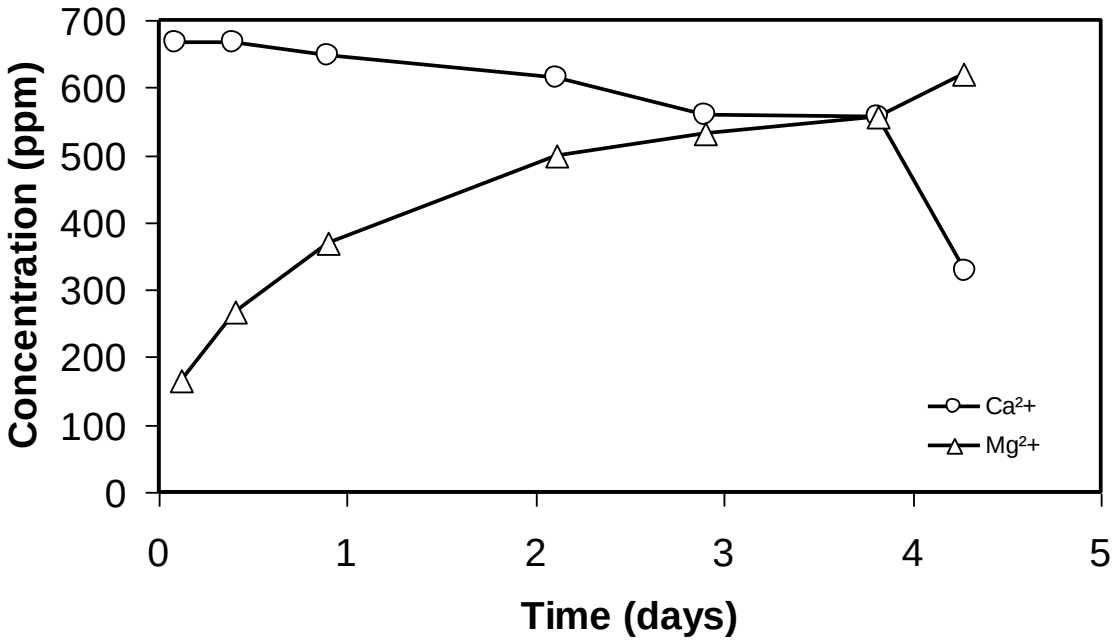

Figure 4-6 Ca^{2+} and Mg^{2+} ion concentration in the leachate of a RCA sample from Ohio containing slag with CO_2 bubbled through versus time (after Gupta and Dollimore, 2002)

4) With CO_2, the Ca^{2+} ion concentration in the RCA leachate increased initially and then generally decreased after 53 days. After 95 days, the Ca^{2+} ion concentration was still significant (465 ppm in Figures 4-4c and 4-4d) suggesting that the Ca^{2+} ions have a tendency to remain in solution rather than precipitating. In contrast, the Ca^{2+} ion concentration in similar experiments performed on an RCA containing a slag and dolomitic aggregate from Ohio dropped to 330 ppm within 5 days (Figure 4-6). The leachate from this RCA had a Mg^{2+}/Ca^{2+} ratio of 0.57 suggesting that this RCA had a marginal potential to precipitate tufa. The tendency for the Ca^{2+} and Mg^{2+} ion concentrations to equilibrate so quickly after 5 days of CO_2 bubbling, as compared to the Hawaiian RCA whose curves did not crisscross even after 95 days, suggests that the basaltic RCA has a lower tendency for tufa precipitation than the dolomitic RCA.

5) Dollimore and Gupta (2002) indicated that for tufa to precipitate, one of the following conditions must exist: (a) change in pH; (b) evaporation; or (c) freeze/thaw or temperature change. Evaporation and freezing results in a reduction in water and an increase in the concentration of the mineral ions, which then leads to precipitation. In this experiment, CO_2 was bubbled till the leachate was almost completely depleted. This is analogous to complete evaporation whereby the concentration of mineral ions should have been the highest towards the end to facilitate any tufa precipitation.

4.6.3 Characterization of the RCA Aggregate before and after Leaching Experiment

Tests were conducted on the RCA before and after CO_2 bubbling. They include:

(a) X-ray diffraction (XRD); and

(b) Scanning electron microscopy (SEM) with energy dispersive spectroscopy (EDS) capability on thin sections of RCA. Prior to the leaching experiment, a piece of RCA was split into two. One half was used to prepare a thin section immediately, which represents the aggregate before the leaching experiment. The other half was placed in Chamber 3. After 3 months of CO_2 bubbling, the same piece of aggregate was removed and another thin section was prepared to represent the aggregate after the leaching experiment.

4.6.4 XRD Test Results

XRD was performed on pulverized samples of the RCA before and after the leaching experiment using a Scintag Model PAD V X-ray diffraction machine. The powder was mounted in a sample holder, which was then placed in a goniometer. A scanning rate of 1 degree per minute was used. Scan angles ranged from 2 to 90 degrees.

Using a 45kV, 40 mA power supply to heat up a copper filament, X-rays generated were fed through a beryllium window filter before impacting the sample at an angle. A detector, chilled using liquid nitrogen, received the X-rays after reflection from the sample. The results consist of peak intensities for various values of 2θ, where θ is the angle of incidence of the X-ray on the sample. Using Bragg's law, θ can be related to the inter-atomic spacing (d) of the crystals that exist in the RCA as follows:

$$\boldsymbol{d = \frac{n\lambda}{2Sin\theta}} \qquad (4.1)$$

where λ = wavelength (1.54054Å for this test) and n is an integer. The peak intensities are plotted versus 2θ for the RCA before and after the experiment in Figure 4-7a and 4-

7b, respectively. It is observed that the “after” XRD test results are almost identical to those before the experiment.

In both results, the three dominant peaks detected include calcite ($CaCO_3$), augite ($Ca(Fe,Mg)Si_2O_6$) and plagioclase ($CaAl_2Si_2O_8$). Published inter-atomic spacings (Joint Committee on Powder Diffraction Standards, 1983) for these minerals are in close agreement with measured values. For calcite, published and measured values of d are 3.035Å and 3.021Å, respectively, for augite d = 2.999Å and 2.991Å, respectively, and for plagioclase, d = 3.20Å and 3.196Å, respectively. While augite and plagioclase are the two more common minerals in basalt, the calcite crystals showed a high intensity, probably because of the presence of coralline sand (mostly calcite), which is used as fine aggregate in the RCA. However, the similarity of figures 4-7a and 4-7b plus the fact that the calcite peak is not overwhelming in the “after” sample suggests that tufa has not formed in appreciable quantities.

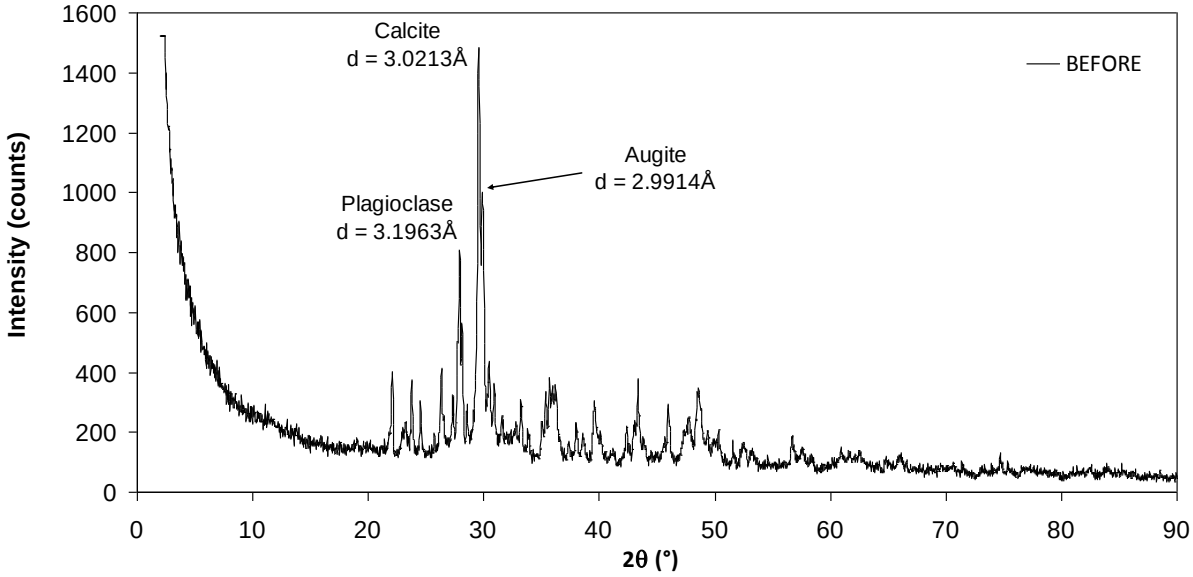

(a)

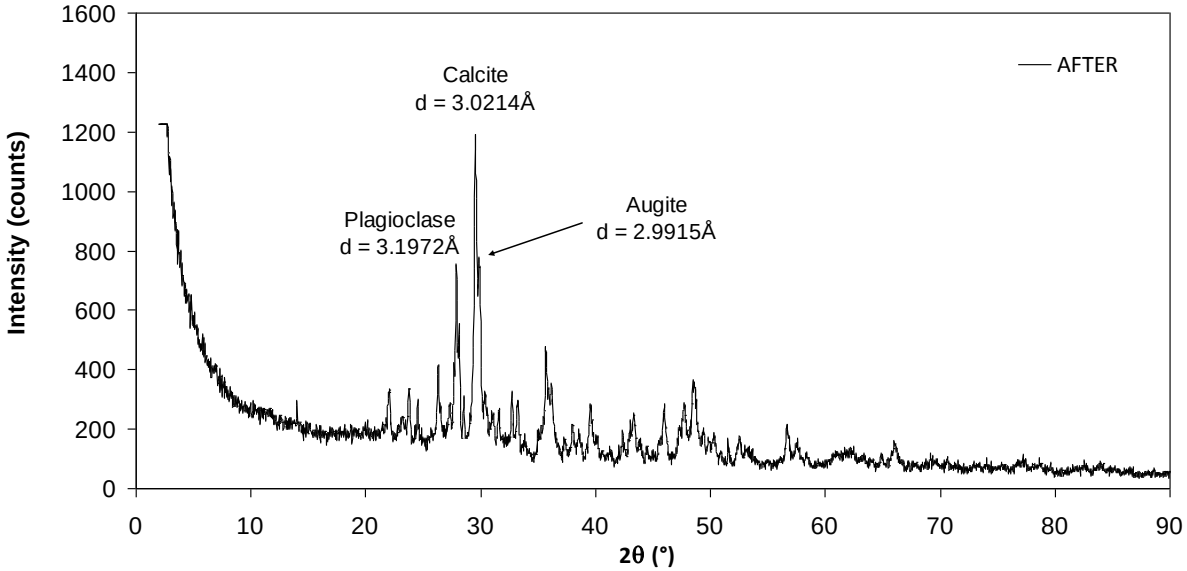

(b)

Figure 4-7 X-ray diffraction results of pulverized RCA (a) before; and (b) after CO_2 bubbling through

Though not among the top few peaks, olivine [$(Fe,Mg)_2SiO_4$] was also detected (d = 2.81Å) among the top 20 peaks of the XRD. Olivine was petrographically observed in thin sections of large coarse aggregate pieces. XRD was performed on pulverized concrete. Since it was easier to crush cement and fine aggregate rather than the coarse aggregate, this may explain why olivine was less prominent in the XRD.

4.6.5 SEM with EDS Test Results

Thin sections of RCA before and after CO_2 bubbling were observed using SEM with EDS capability. Magnified images of the thin sections were captured using a JEOL JXA-8500F SEM by bombarding the samples with high energy electrons. The electron beam diameter is smaller than 1 micron with an acceleration potential of 15 keV and a spectrum current of 15 nanoamps. The electrons interact with the nuclei of the

elements generating secondary electrons (SE), backscatter electrons (BSE) and X-rays. The BSE are used to provide an enlarged image of the sample; e.g., a large deflection with little energy transfer is characteristic of a nucleus having a large mass and vice versa.

The SEM images before and after the leaching experiment are shown in figures 4-8a and 4-9a, respectively. Images around a void were selected because should any reaction occur, it would most likely be on the periphery rather than in the interior of the sample. It is consistently observed that the perimeter of the void of the “before” sample is smooth and regular while that of the “after” sample appears rough and jagged. This suggests that some chemical reaction has occurred in the sample periphery. However, the quantity of the reaction product or precipitation in the void periphery during the course of the leaching experiment is insignificant considering the scale as shown in the figures.

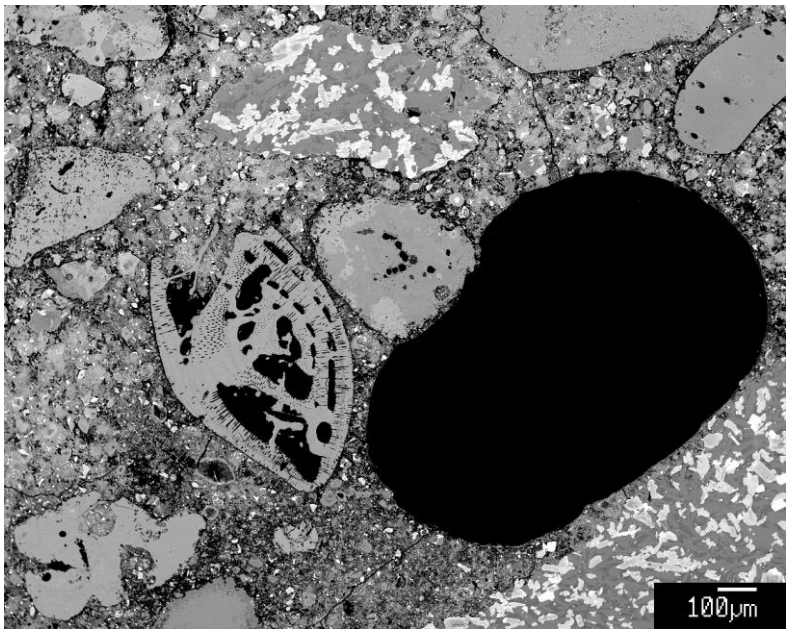

(a)

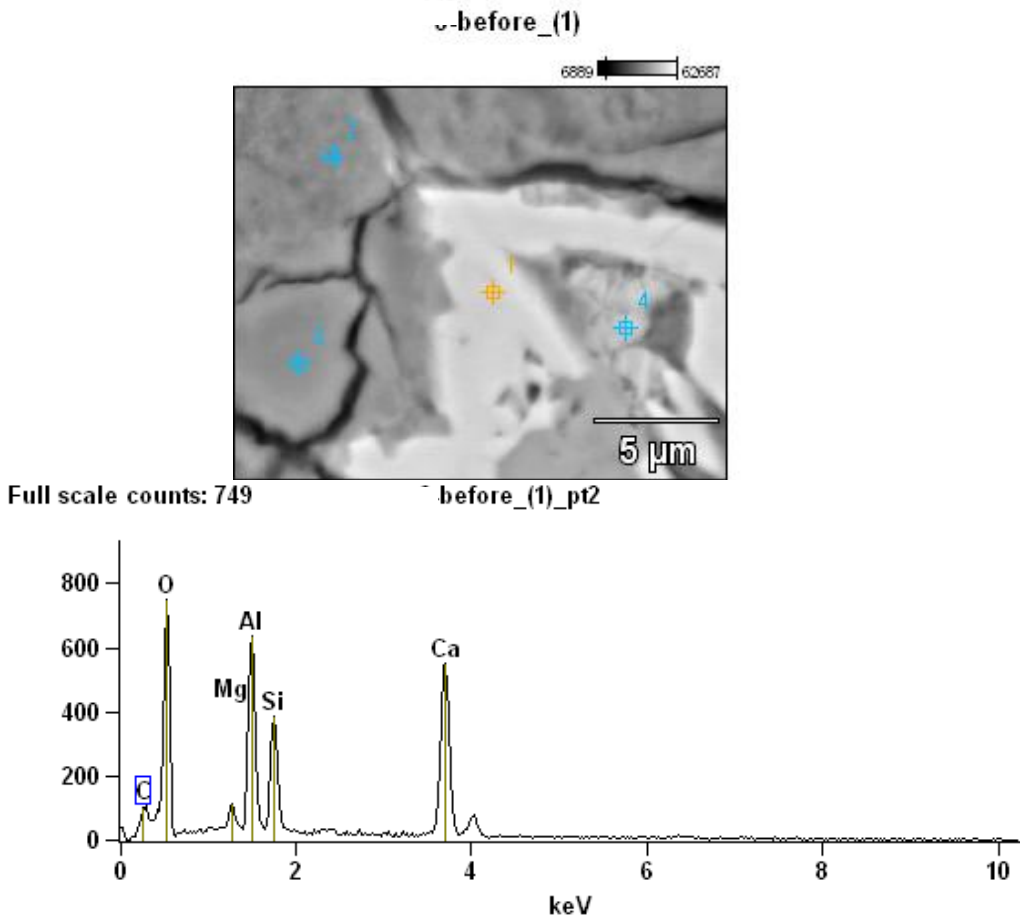

(b)

Figure 4-8 (a) SEM image of an interior void in RCA sample and (b) EDS test results for RCA before CO_2 bubbling

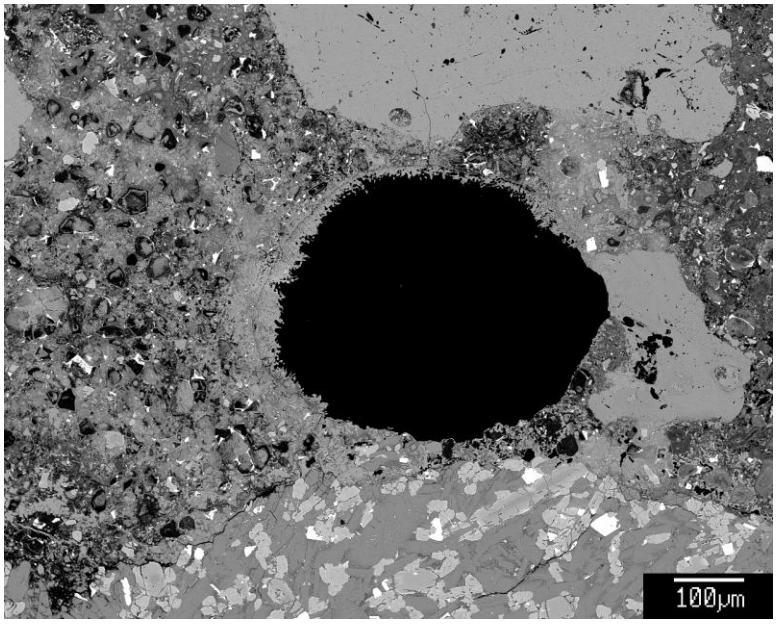

(a)

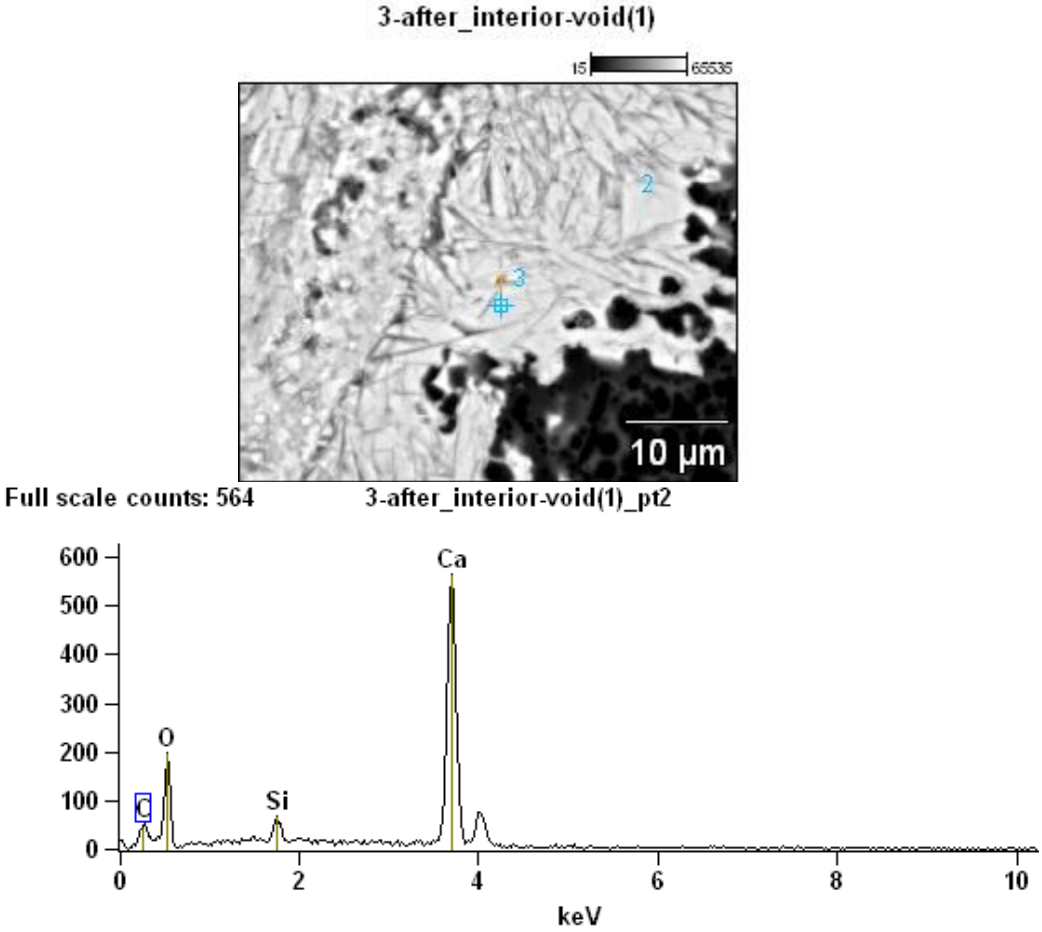

(b)

Figure 4-9 (a) SEM image of an interior void in RCA sample and (b) EDS test results for RCA after CO_2 bubbling

The EDS results, before and after CO_2 bubbling, are shown in Figures 4-8b and 4-9b, respectively. The principles of the EDS are similar to XRF. The elements detected in the concrete portion of the “before” sample (Figure 4-8b) consist of elements typically found in concrete such as Ca, Al, Si and O, consistent with the calcium silicates and aluminates in cement. The elements in the basalt portion are not shown for brevity. The elements detected near the perimeter of the void in the “after” sample (Figure 4-9b), however, consist primarily of Ca and O with little Si and no Al. Carbon is used as a backing during the EDS and therefore it will show up regardless of whether any carbon is present chemically. Thus, it is possible that the reaction product formed in the void is calcium carbonate or tufa. Since only trace amounts were detected by the SEM, it could not be practically sampled and analyzed using XRD for further confirmation.

4.6.6 Sample Observation after Leaching Experiment

After 95 days of CO_2 bubbling, the RCA was visually examined for evidence of tufa deposits. Figure 4-10 shows that the aggregate and the filter fabric placed at the bottom were completely free of any visible tufa precipitate for the 100% RCA with a subbase gradation. The same is true for all the other chambers. However, in test chambers 3 and 5, very small quantities of a thin, non-continuous white film were observed on the walls. At most, about 1 gram of this film could be collected for further testing as follows:

Figure 4-10 100% RCA (subbase gradation) or Sample 3 after 95 days of CO_2 bubbling showing no appreciable tufa precipitate

1) The film was dried at a temperature of 60°C for three days.

2) After cooling, sub-samples were weighed and placed in Teflon CEM microwave digestion containers. Weights varied, from 0.013 grams to 0.103 grams, depending on the amount of original sample available.

3) 3.0 ml and 1.0 ml of concentrated nitric (HNO_3) and hydrochloric (HCl) acids, respectively, were added to each sample. The reaction vessels were sealed and allowed to sit for 1.5 hours.

4) 2.0 ml of concentrated hydrofluoric acid (HF) was then added to each sample and the vessels re-sealed. The samples were then heated in a CEM microwave

oven using 50 percent power for 45 minutes to 80 psi and 60 percent power for 30 minutes to 110 psi.

5) Samples were allowed to cool for 3 hours. 10 ml of 0.5-N-boric acid was added to each sample, which was then allowed to sit overnight.

6) Samples were transferred to clean plastic bottles, rinsed with 18 mega ohm water, weighed and then analyzed using a Varian Vista MPX ICP-OES.

Results of the test on these precipitates are summarized in Table 4-3. Calcium was by far the most dominant element detected indicating that the thin film may possibly be tufa. Other elements were also detected therefore, indicating that some of the film may also contain a silicate of iron, magnesium and aluminum also. Another observation of interest is that the concentrations of all the precipitate ions from Chamber 5 (finer RCA gradation) are higher than from Chamber 3. Thus, a finer gradation does lead to increased reaction product. Again, there were insufficient quantities of the film to perform an XRD.

Table 4-3 Summary of ICP-AES results on the film collected from the walls of two test chambers

Sample No.	Ca mg/gm	Mg mg/gm	Al mg/gm	Fe mg/gm	Na mg/gm	Sr mg/gm	Zn mg/gm
3	116.26	6.51	15.66	17.06	6.13	1.52	0.095
5	133.69	19.84	38.92	53.51	9.75	0.71	0.13

4.7 SUMMARY AND CONCLUSIONS

To examine the tufa precipitation potential of a Hawaiian RCA, two sets of aggregate were soaked in rain water for approximately 3 months. In one set of samples, CO_2 was continuously bubbled through while no bubbling was performed on the other set. Tests

were conducted on the rainwater over time and on the aggregate before and after CO_2 bubbling. The following summary and conclusions are offered:

(1) pH of the rainwater in RCA samples was initially very basic (~12) prior to CO_2 bubbling. Subsequently, the pH dropped to about 6.3 when carbonic acid formed after CO_2 bubbling. pH of the rainwater in RCA samples without CO_2 bubbling remained basic (between 11 and 12).

(2) ICP-AES tests on rain water with CO_2 bubbling through the Hawaiian RCA indicate that the Ca^{2+} ions have a tendency to remain in solution rather than precipitating as compared to similar experiments conducted using dolomite-based RCA by Gupta and Dollimore (2002). Since dolomite contains an abundance of Mg^{2+} ions and since the solubility of $MgCO_3$ is an order of magnitude higher than that of $CaCO_3$, the Mg^{2+} ions will preferentially remain in solution while the Ca^{2+} ions will combine with the CO_3^{2-} ions to precipitate as tufa. XRF tests indicate that the Hawaiian RCA contains very little Mg^{2+} ions. The most abundant positively charged metallic ion is Ca^{2+}, which is at least twice any other positively charged metallic ion present.

(3) XRD tests were performed on pulverized RCA before and after 3 months of CO_2 bubbling. The XRD results for the “before” and “after” samples are almost identical, suggesting that any changes in the RCA as a result of CO_2 bubbling are minimal.

(4) SEM with EDS tests were performed on thin sections of RCA before and after 3 months of CO_2 bubbling. Magnified images of the perimeter of voids in the

"before" sample is consistently smooth and regular while that of the "after" sample appears more rough and jagged. This suggests that some precipitation has occurred. However, the quantity of precipitation observed is insignificant.

(5) EDS tests on the precipitate near the void perimeter indicate the presence of Ca and O with trace amounts of Si. Since carbon is used as a conductive coating, it was also detected. The carbon quantity was significant enough to suggest that the reaction product formed in the void is tufa. However, the quantity is insignificant for it to pose any concerns for drainage.

(6) ICP-AES tests on about 1 gram of the thin, white film found in test chambers 3 and 5 indicate that it may be tufa with some silicates of iron, magnesium and aluminum also present.

(7) In conclusion, tufa may potentially form with Hawaiian RCA. However, based on the quantities observed in the experiments of RCA subjected to extreme CO_2 exposure, the evidence suggests that tufa quantities would be insignificant to cause any drainage problems.

CHAPTER 5 FORENSIC INVESTIGATION OF A DISTRESSED PAVEMENT SUPPORTED ON A BASE COURSE CONTAINING RECYCLED CONCRETE AGGREGATE

5.1 INTRODUCTION

Two billion tons of aggregate are being consumed each year in the United States and this number is continually growing (Gonzalez and Moo-Young, 2004). The impetus and pressure for pavement and geotechnical engineers to incorporate sustainability in engineering projects has led to a rise in the reuse of materials such as recycled concrete aggregate (RCA) as fill and in pavement sub-layers. Using RCA is beneficial from three perspectives as follows:

Engineering

1. Rubblization of existing concrete pavements removes cracked and aged pavement surface, improves pavement smoothness, and maintains curb height, drainage inlets and bridge clearances.
2. Crushed RCA have fractured angular surfaces, which provides greater internal friction if used as a fill compared to more rounded natural aggregate obtained from stream and river beds.
3. Crushing concrete exposes unhydrated cement. If used in pavement unbound layers, exposure to water can lead to rehydration and a subsequent strength increase.

Environmental

1. Conservation of landfill space.

2. Preservation of natural aggregate resources.
3. Conservation of energy by eliminating or reducing haul distances of RCA to the landfill and of new aggregate from the quarry.

Economical

1. Reduced transportation and material cost compared to virgin aggregate.
2. Reduced haulage also implies reduced traffic and less wear and tear on existing roads along the haul routes.

On the flip side, the absence of quality control can lead to poor performance and premature deterioration that are costly to repair but more importantly, could slow down market acceptance of this useful recycled material. This case study provides an example where early deterioration of a pavement supported on a base course containing RCA has resulted in reservations on its use in the state of Hawaii. The cause of the distress was not trivial and is meticulously investigated herein. The results hint towards contamination of RCA as the probable cause of the deterioration.

5.2 PROJECT DESCRIPTION AND OBJECTIVES

The distress of a 51-mm-thick asphalt concrete (AC) pavement supported on a 152-mm-thick base course containing 50% basalt, 25% reclaimed asphalt pavement (RAP) and 25% RCA, overlying a 2-m-thick coralline sand layer was investigated. Used as a parking lot on the island of Oahu, Hawaii, the pavement experienced over 30 eruptions greater than 25 mm high and 127 mm in diameter (Figures 5.1a and b) within one year after completion of construction and over 100 eruptions after two years. The parcel to the north is approximately 2 m higher in elevation. Therefore, drainage generally flows in a southerly direction through the site.

Figure 5.1 (a) and (b) Pavement eruptions; (c) and (d) White reaction product found in the base course

To investigate the distress, the pavement was saw cut around one of these eruptions and the base course was manually excavated. A white substance with occasional blue tinges was observed in significant quantities directly below the eruption (Figures 5.1c and d). It was postulated that this substance was related to the pavement eruptions, and was sampled for further testing and evaluation.

The objectives of this study are to: (1) chemically identify the reaction product; (2) determine the cause of this distress based on the chemistry of the reaction product; (3) perform experiments in the laboratory to replicate the reaction; (4) estimate the swell pressure that can arise as a result of this reaction; and (5) numerically simulate the heave to see if it corroborates the field observations.

5.3 BACKGROUND

There have been two other known pavements in Hawaii that suffered a similar distress. The common denominator in these three pavements is that the base courses contained RCA from a mixture of sources such as building and pavement demolition and returned ready mix concrete. While there are many advantages of using RCA in a base course as described above, there are also some known potential drawbacks. They include:

a. Alkali silica reaction (ASR);

b. Alkali carbonate reaction (ACR);

c. Sulfate attack;

d. Tufa formation;

e. Corrosion of aluminum pipes that are in close proximity;

f. High pH;

g. Lead paint contamination;

h. Asbestos contamination;

i. Decrease in permeability with time as more cementation occurs; and

j. High water absorption which may yield unusually high optimum moisture contents.

The first five drawbacks can form reaction products that have the potential to cause distress in pavements particularly the more flexible AC variety. Table 5.1 summarizes the nature of these reactions along with their expected products. In short, if the concrete source from which RCA was obtained had ASR or ACR, these problems can continue if the silicate or dolomitic rocks within the RCA are further exposed to alkalis (e.g., from brackish water) resulting in additional formation of expansive alkali-silica or alkali-carbonate products. Sulfate attack is due to exposure of RCA to high sulfate bearing soils or ground water which results in the formation of expansive ettringite (i.e., calcium sulfo-aluminate hydrate) or occasionally thaumasite crystals. Tufa forms from the precipitation of calcium ions, present in dolomitic or calcitic RCA aggregate, and dissolved CO_2 in natural waters. Song et al. (2011) showed that tufa formation is unlikely to be a problem in RCA with a Hawaiian basaltic aggregate. Finally, dissolution of RCA particles raises the pH of infiltrating water. If aluminum metal is in the vicinity (e.g., aluminum pipes), it can corrode leading to the formation of aluminum hydroxide, either in the form of gibbsite or the less stable bayerite, and hydrogen gas; both of which can produce expansion. Also not to be neglected are drawbacks *f* through *j*, which are more problematic from either a health, environmental or other performance related viewpoints rather than distress-causing but nonetheless important.

Table 5.1 Possible deterioration of RCA and their reaction products.

Distress	Reaction Equation	Reaction Products	Primary Inter-atomic Spacing of the Reaction Product (Å)	Reference
Alkali silica reaction	Reaction of silica and alkali $2NaOH + SiO_2 + 2H_2O \rightarrow Na_2H_2SiO_4 \cdot 2H_2O$ (stoichiometry inexact)	Alkali silica gel $[(Na_2O)_x(SiO_2)_y(H_2O)_z]$	Amorphous	(Glasser, 1998)
Alkali carbonate reaction	Reaction of dolomite and alkali $CaMg(CO_3)_2 + 2NaOH \rightarrow CaCO_3 + Na_2CO_3 + Mg(OH)_2$	Brucite $[Mg(OH)_2]$ Calcite $[CaCO_3]$	2.37 3.04	(Mindess et al., 2003)
Sulfate attack	Reaction of alumino-silicates and sulfate: $(CaO)_3(Al_2O_3) + 3CaSO_4 + 32H_2O \rightarrow$ $(CaO)_3(Al_2O_3)(SO_3)_3(H_2O)_{32}$ Occasionally, formation of thaumasite: $(CaO)(SiO_2)(H_2O)_8 + CaSO_4 + CaCO_3 + 7H_2O \rightarrow$ $(CaO)_3(SiO_2)(CO_2)(SO_3)(H_2O)_{15}$ (stoichiometry inexact)	Ettringite $[3CaO \cdot Al_2O_3 \cdot 3CaSO_4 \cdot 32H_2O]$ Thaumasite $[CaCO_3 \cdot CaSO_4 \cdot CaSiO_3 \cdot 15H_2O]$	9.73 9.66	(Mehta and Monteiro, 2006)
Tufa formation	Precipitation of calcium ions and dissolved CO_2 in natural waters $Ca^{2+}(aq) + CO_3^{2-}(aq) \leftrightarrow CaCO_3(\downarrow)$	Calcite $[CaCO_3]$	3.04	(Song et al., 2010)
Corrosion of aluminum	Reduction of H_2O in basic solution $Al + 3H_2O + OH^- = 3/2H_2(g) + Al(OH)_4^-$ Precipitation of $Al(OH)_3$ in form of gibbsite or bayerite crystals $Al(OH)_4^- = Al(OH)_3 + OH^-$	Gibbsite $[Al(OH)_3]$ Bayerite $[Al(OH)_3]$	4.37, 4.85 2.22, 4.35, 4.71	(Zhang et al., 2009)

5.4 EXPERIMENTAL INVESTIGATIONS

To identify the type of distress in the subject pavement, the chemistry of the white reaction product was investigated using: (1) Scanning Electron Microscopy (SEM) equipped with an X-ray Energy Dispersive Spectroscopy (EDS) detector; (2) X-ray Diffraction (XRD); and (3) Raman Spectroscopy. This is followed by laboratory simulation of the field reaction. Lastly, a swell pressure test was performed to estimate the heave pressure that can be exerted under the pavement as a result of such a reaction.

5.4.1 Identification of the Field Reaction Product

5.4.1.1 SEM with EDS

Magnified images of the white reaction product were captured using a JEOL JXA-8500F SEM by bombarding the sample with high energy electrons. These electrons interact with the sample's atoms and produce backscattered electrons (BSE), secondary electrons (SE) and characteristic X-rays. The BSE and SE are collected to produce a magnified image of the sample. The energy and wavelength of the X-rays emitted is specific to the atoms from which they emanate. As such, an EDS X-ray detector is capable of identifying the chemical composition of the sample both qualitatively (i.e., which elements are present) and quantitatively (i.e., how much of each element is present).

Figure 5.2 shows a 350× magnified BSE image of the reaction product as well as a typical EDS spectrum. The latter shows two major peaks for aluminum (Al) and oxygen (O) with traces of silica (Si), copper (Cu), chlorine (Cl), zinc (Zn), sodium (Na), and iron (Fe). Using the area under each peak, the relative concentration of that element in the sample can be determined. Table 5.2 shows the elemental composition of both the

white and blue tinge portions of the product estimated by averaging the EDS readings from four different spots on the sample. It should be pointed out that EDS is not capable of detecting elements lighter than lithium including hydrogen. The results indicate that both samples are mainly composed of aluminum (≥ 50.0%) and oxygen (≥ 15.6%) while the blue tinge portion of the product also contained some silica and copper.

The results show that the pavement distress is likely not caused by sulfate attack (no sulfur detected), alkali-silica reaction (very little alkali detected), alkali carbonate reaction (insignificant amount of calcium or no magnesium detected), nor tufa formation (insignificant amount of calcium detected).

Table 5.2 Average elemental composition of the reaction product from EDS analysis.

Element / Reaction product	Ca	Si	Al	Fe	S	Na	O	Cu	Zn	Cl
	Atomic %									
White portion of reaction product	Not detected	6.15	60.60	0.98	Not detected	1.88	22.16	3.41	2.01	2.82
Blue tinge portion of reaction product	0.86	17.07	50.07	1.85	0.26	Not detected	15.62	9.57	4.27	0.45

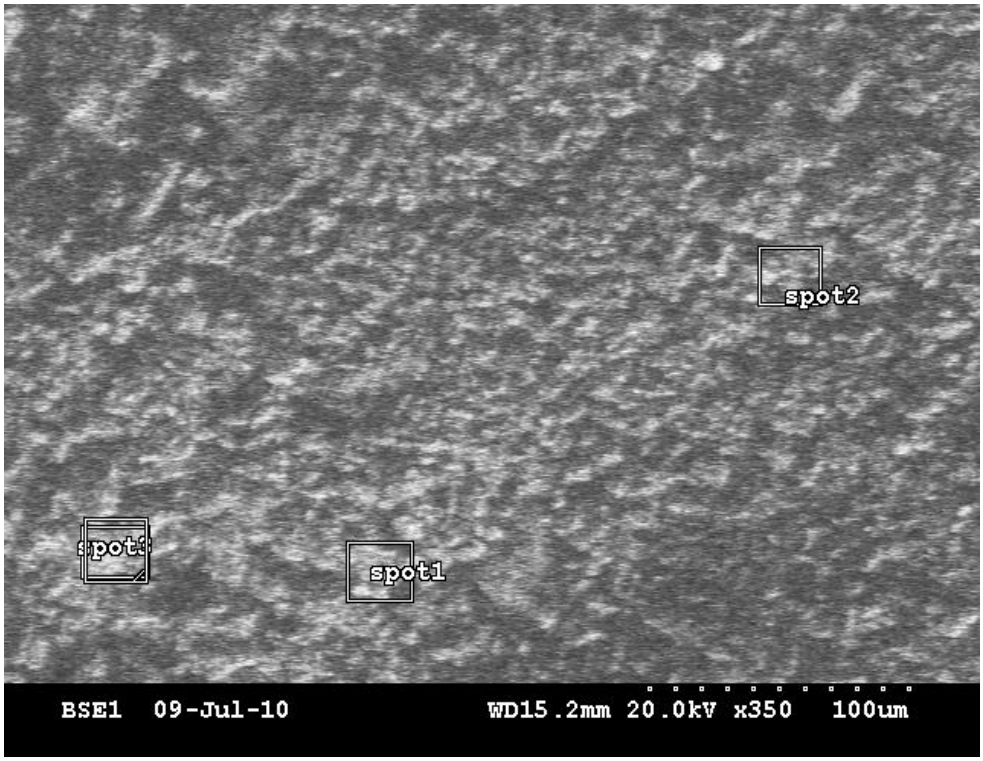

(a)

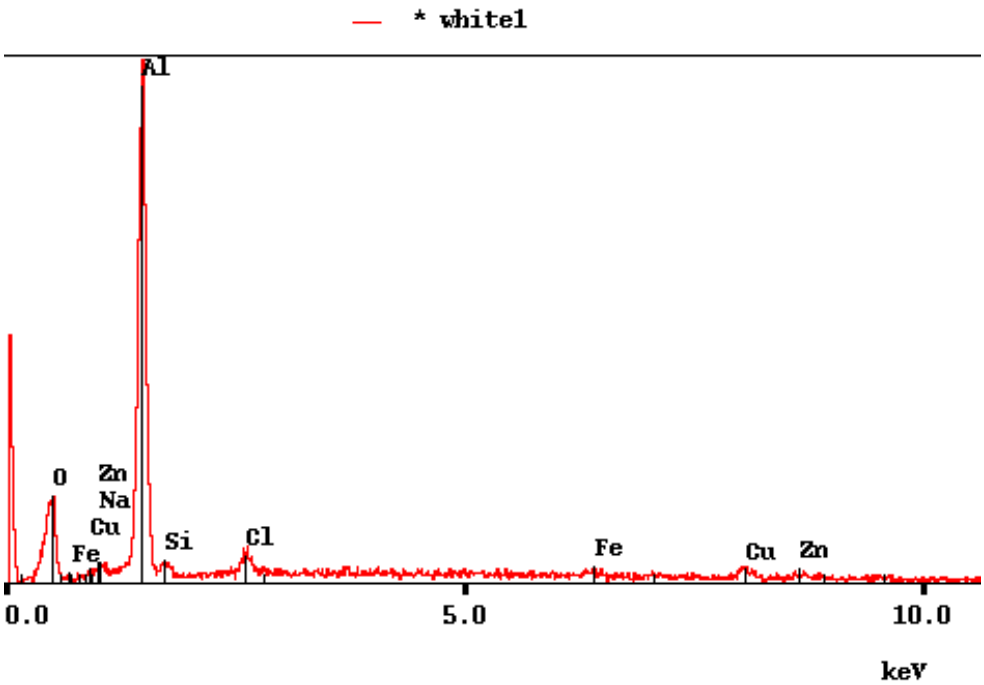

(b)

Figure 5.2 SEM with EDS analysis of the white reaction product: (a) SEM image, (b) EDS output showing the average elemental composition of spot1.

5.4.1.2 XRD

The XRD patterns of the reaction product were obtained using a PANalytical X'pert Pro MPD diffractometer. The reaction product was mounted in a sample holder, which was then placed in a goniometer. Using a 45kV, 40 mA power supply, a copper filament was bombarded by electrons to generate characteristic Cu-Kα X-rays which, after passing through a beryllium monochromator filter, were radiated towards the sample at incident angles (θ) ranging from 2.5 to 35 degrees (2θ = 5 to 70°). Constructive interferences at particular values of θ are detected as peak intensities on the XRD pattern (Figure 5.3). According to Bragg's law, the θ value corresponding to each peak is related to the inter-atomic spacing (d) of the crystals forming the sample:

$$d = \frac{n\lambda}{2Sin\theta} \tag{5.1}$$

where λ = wavelength of X-rays (1.54054Å for this test) and n is an integer. Crystalline compounds have characteristic inter-atomic spacing which can be used for their identification. For example, a peak at 2θ =18.3^o (equivalent to d = 4.85Å) can represent the mineral gibbsite [$Al(OH)_3$]. A collection of the d-spacings for a multitude of different compounds can be found in the publications of the Joint Committee on Powder Diffraction, such as standards for minerals (1974) and inorganic compounds (1991).

The XRD patterns of the reaction product (two samples of the white portion of the reaction product and one sample of the blue tinge portion of the reaction product) are shown in Figure 5.3 along with the most probable compounds corresponding to each peak. Major peaks at $2\theta = 18.3^o$ and 20.3^o (d = 4.85Å and 4.37 Å) are associated with gibbsite or $Al(OH)_3$, which is the chemical product of aluminum corrosion. This is

consistent with the EDS results that showed Al and O as the main constituents of the reaction product (again EDS does not detect H). Several less pronounced peaks associated with either gibbsite or bayerite [a meta-stable form of $Al(OH)_3$] were observed in all three XRD patterns. The peaks at $2\theta = 28.5^o$, 47.3^o and 56.1^o (d = 1.61Å, 1.05Å and 0.93Å) were also prominent in the blue tinge portion of the reaction product. These suggest the presence of silicon. Other smaller peaks, associated with iron (Fe), tenorite (CuO) and magnetite (Fe_3O_4), were also detected. The combination of tenorite and silicon is most likely responsible for giving the product its blue hue. More importantly, the XRD results corroborate the fact that the pavement distress was not caused by sulfate attack, ACR or tufa formation as the products of these reactions (see Table 5.1) were not identified in any of the XRD patterns.

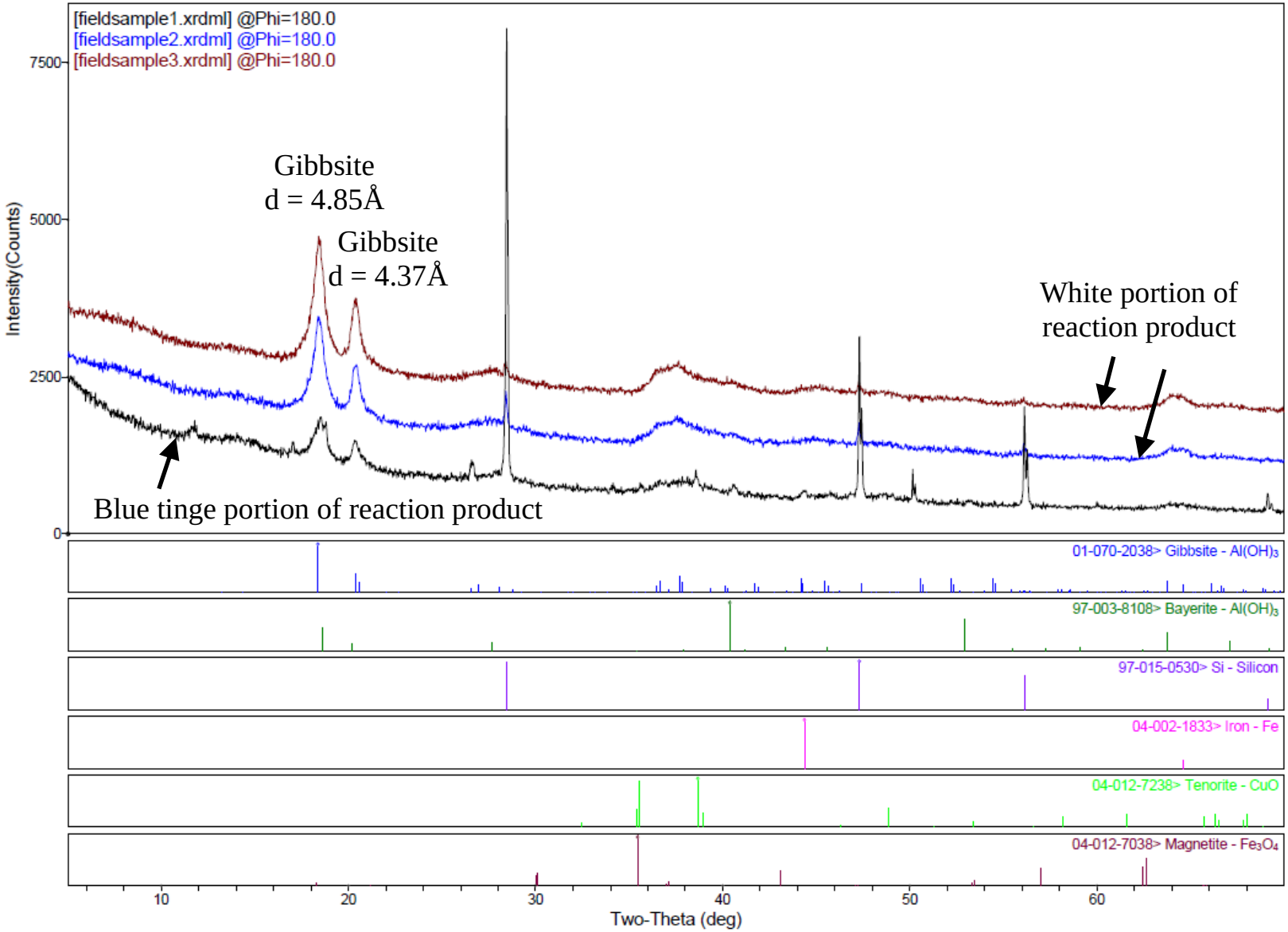

Figure 5.3 XRD test results of the reaction product excavated from the field

5.4.1.3 Raman Spectroscopy

Described by Misra et al. (2009), the equipment used to obtain the Raman spectra was an Invictus 785 nm NIR laser source along with a fiber-coupled micro-Raman RXN system manufactured by Kaiser Optical Systems, Inc. from Ann Arbor, MI. In this test, the white reaction product from the field was illuminated by a laser beam. Light from the sample was then sent through a monochromator. Based on the inelastic or Raman scattering of the monochromatic light detected, the vibrational modes of various atomic bonds within the sample is identified which can reveal the sample's chemical composition. Two Raman spectra of the field reaction product are shown in Figure 5.4 denoted as "Field." According to Ruan et al. (2001), the wavenumbers assigned to the vibrational modes for bayerite include the following: 1068 for δ(OH), 545, 569 and 899 for γ(OH) and 322, 388 and 435 for Al-O. These wavenumbers very closely matched those from the Raman spectra obtained implying that the field reaction product is bayerite. The match for gibbsite was non-existent.

The fact that the Raman spectra indicated bayerite while the XRD patterns revealed gibbsite can be explained as follows. The Raman spectra were obtained on the reaction product fresh from the field while the XRD specimen was shipped to Pennsylvania. Since bayerite is unstable, it probably spontaneously converted to gibbsite during transport due to a lack of sample preservation (e.g.; refrigeration). Nevertheless, these spectra lend credence to the XRD and EDS results, and further support the aluminum corrosion hypothesis in the distressed pavement.

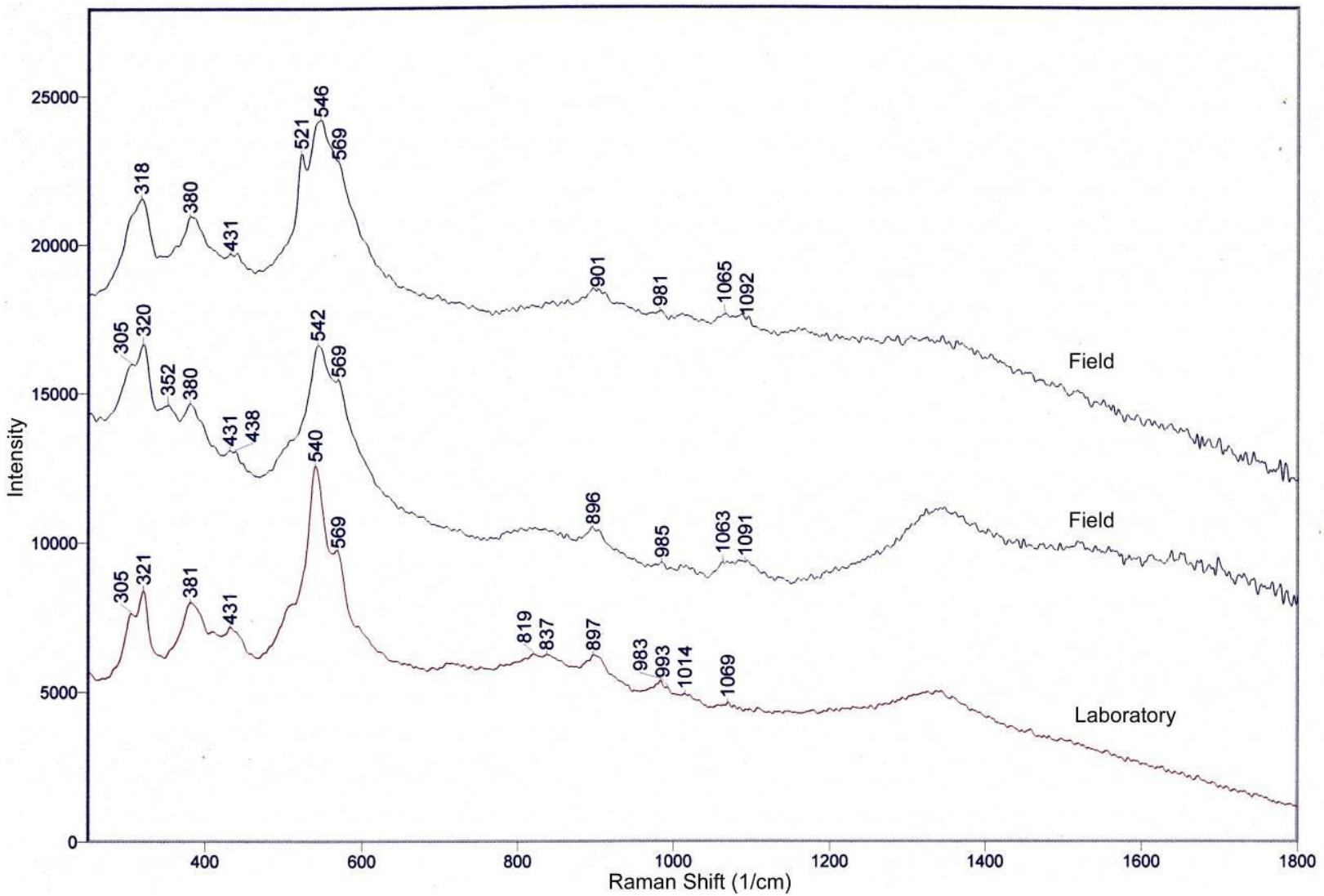

Figure 5.4 Raman spectra for the reaction product from the field and from the laboratory

5.4.2 Laboratory Simulation of Field Reaction

There is conclusive evidence that the field reaction product contained $Al(OH)_3$ as its main constituent. As shown in Table 5.1, this product can form when aluminum metal corrodes in an alkaline environment. When RCA particles were placed in 100 ml of distilled water, the pH of the water was observed to exceed 12.0 within 3 days. That the ground contours favor drainage through the site with a base course containing RCA suggests that a highly saturated alkaline environment can be created easily and naturally. Therefore, what if the source RCA partially contained building demolition waste such as aluminum metal pieces (from e.g., cladding, posts, flashing, pipes, window and door frames, etc.)? This possibility offers a plausible explanation for the pavement distress.

To test this hypothesis, this field reaction was duplicated in the laboratory by preparing the following samples:

1. 1 gram of aluminum powder or aluminum shavings in 80 grams of NaOH solution (pH = 12.0); and
2. 1 gram of aluminum powder or aluminum shavings in 28 grams of fresh cement paste (w/c = 0.4). This was then added to 72 grams of distilled water (measured pH after 24 hours = 11.8).

In all samples, extensive hydrogen gas was observed minutes after mixing. The hydrogen gas was confirmed when a lighted splint extinguished with a pop. In addition, a white reaction product resembling that in the field was observed within the first 24 hours. It was also evident that this reaction resulted in a net expansion. After three days, the reaction product was sampled and tested by Raman spectroscopy (Figure 5.4

– denoted as “Laboratory”) and X-ray diffraction (Figure 5.5). Both tests confirmed the presence of bayerite [$Al(OH)_3$] as the main reaction product. The Raman spectra for the laboratory-generated product matched very well with those from the field. One of the prominent peaks in the XRD pattern (d = 2.22Å) confirmed that the majority of $Al(OH)_3$ was in the form of bayerite. As expected, the laboratory product did not contain any silicon or other impurities.

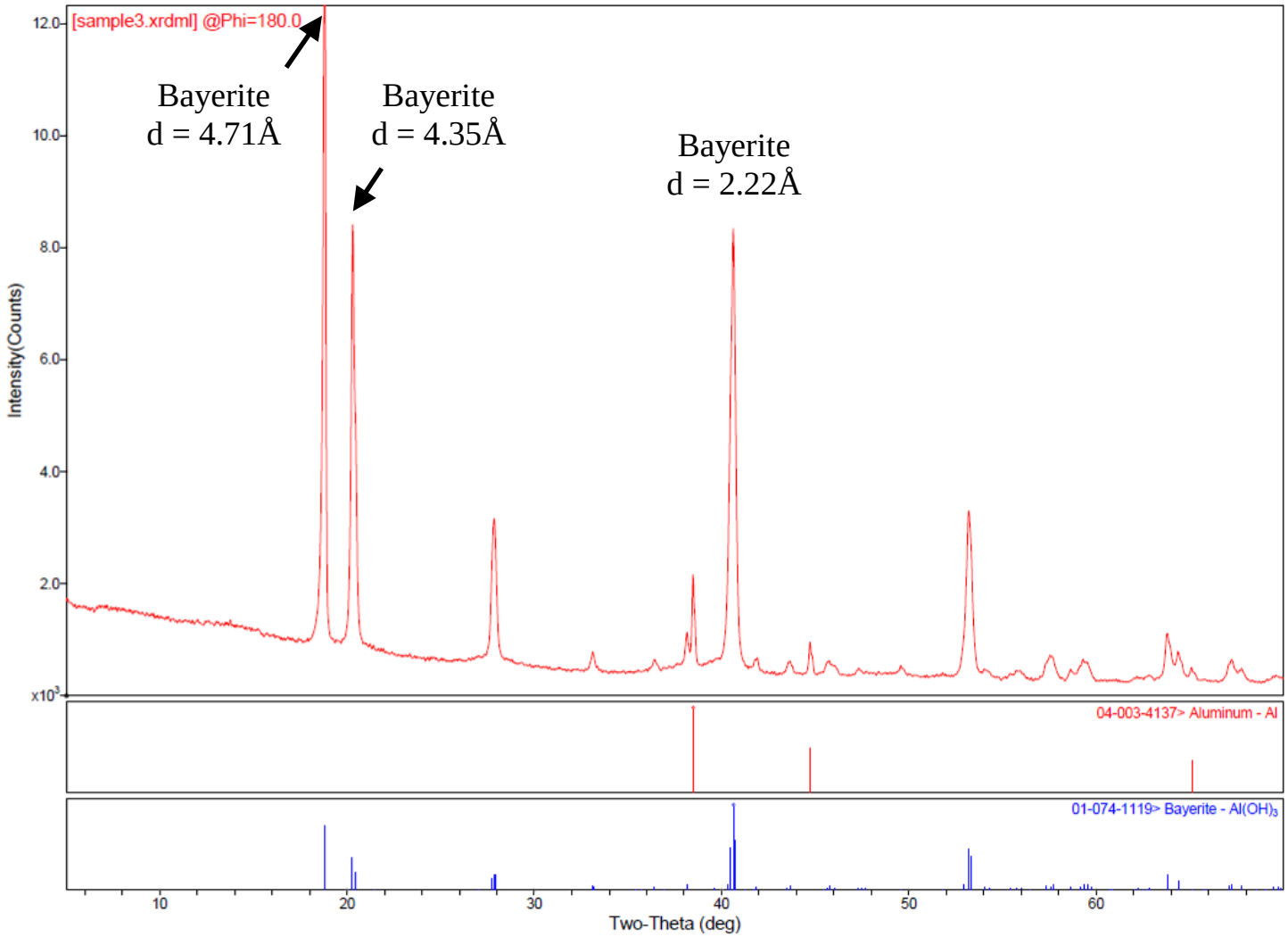

Figure 5.5 XRD test results of the reaction product synthesized in the lab.

5.4.3 Swell Pressure Test

To estimate the swell pressure exerted on the pavement as a result of this reaction, a procedure similar to ASTM D4546 Method C was followed. A 20-gram-mixture of dry aluminum powder and dry cement mixed in a 1:9 ratio by weight was set up in a Geonor h-200 swelling test apparatus (Figure 5.6a). The specimen was placed without compaction in the consolidation cell having a cross-sectional area of 20 cm^2. The consolidation cell is housed in a 10 kN loading frame with a lever arm ratio of 1:10. A vertical pressure of 200 $tons/m^2$ was applied on the specimen to simulate the effects of compaction of the base course and placement and compaction of the overlying AC. The pressure is applied by turning a hand wheel that operates a worm drive connected to a screw-thread jack, which in turn is connected to a vertical rod with a pressure gauge. After the specimen had reached equilibrium, the load was removed completely and distilled water was poured into the Lucite cylinder to completely submerge the cell and sample. While maintaining the height of the specimen constant, the swelling pressure was measured as a function of time. From the results shown in Figure 5.6c, a maximum swell pressure of 430 kPa was reached after only 15 minutes. Thereafter, the swell pressure remained constant. Prior to testing, the compliance of the apparatus was determined (Figure 5.6b) by measuring the pressure-deflection curve of two wet filter papers and porous stones without the sample. The compliance curve was necessary to correct the deflection dial gauge readings when maintaining a constant sample height.

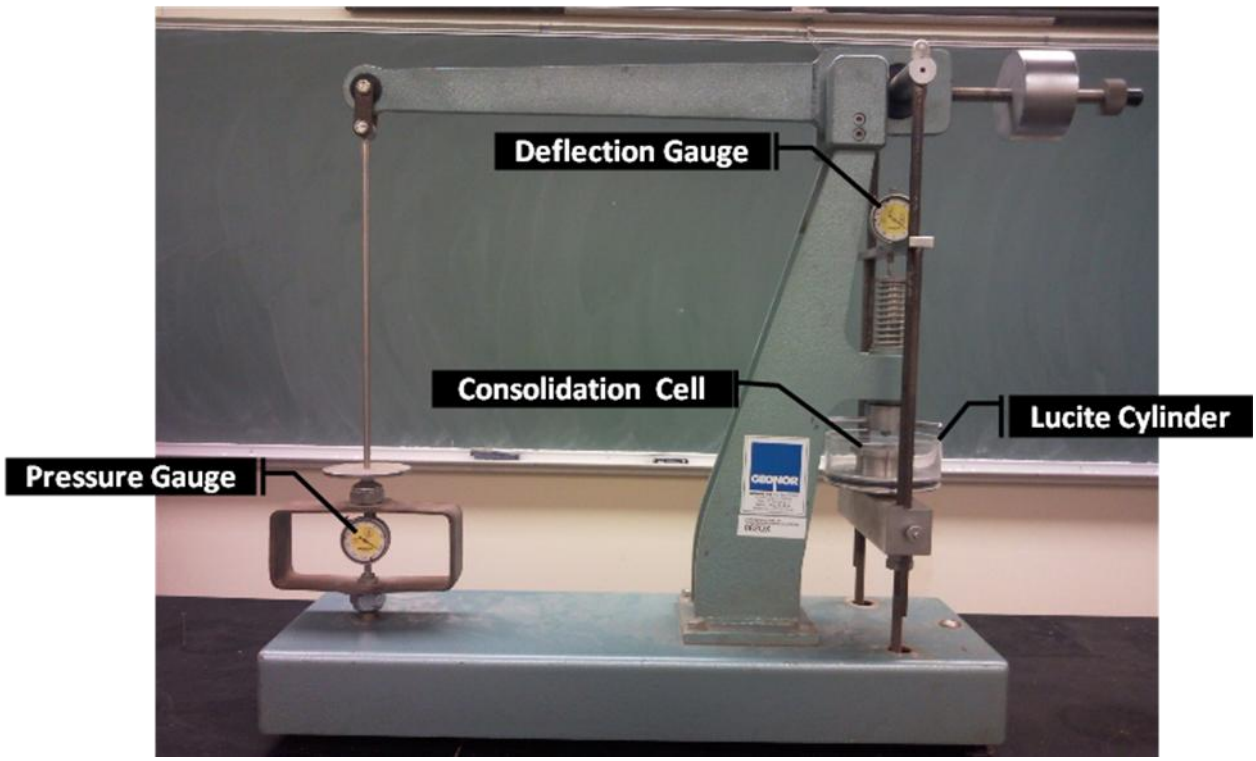
Deflection Gauge
Consolidation Cell
Lucite Cylinder
Pressure Gauge

(a)

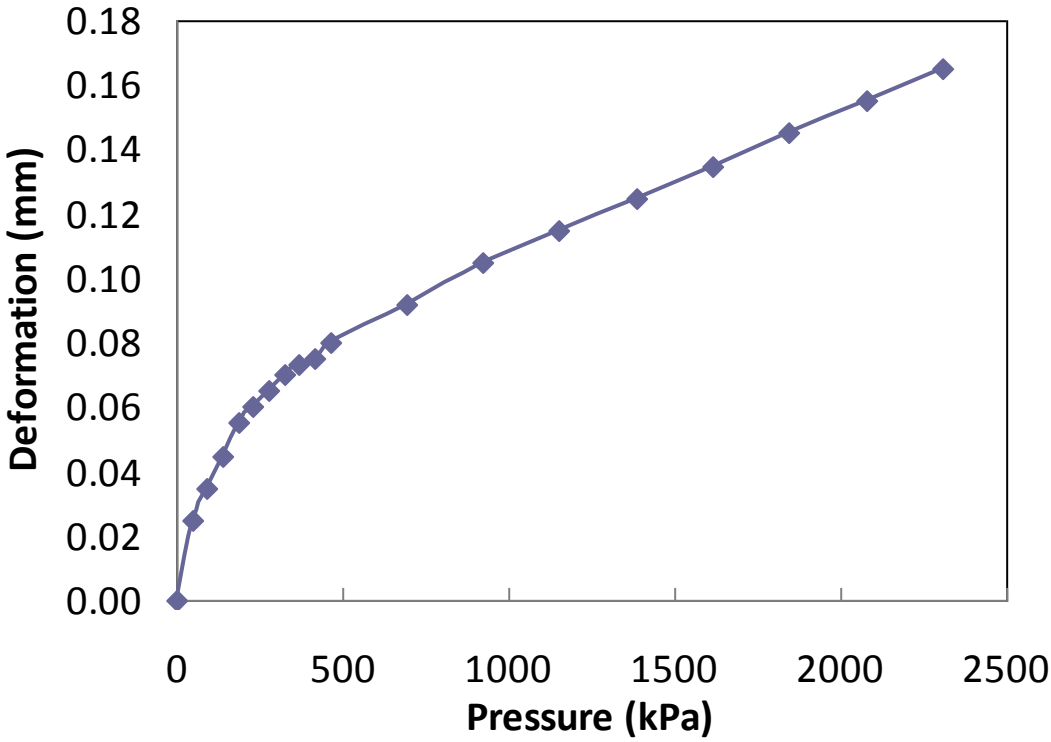
0.18
0.16
0.14
0.12
0.10
0.08
0.06
0.04
0.02
0.00
Deformation (mm)
0
500
1000
1500
2000
2500
Pressure (kPa)

(b)

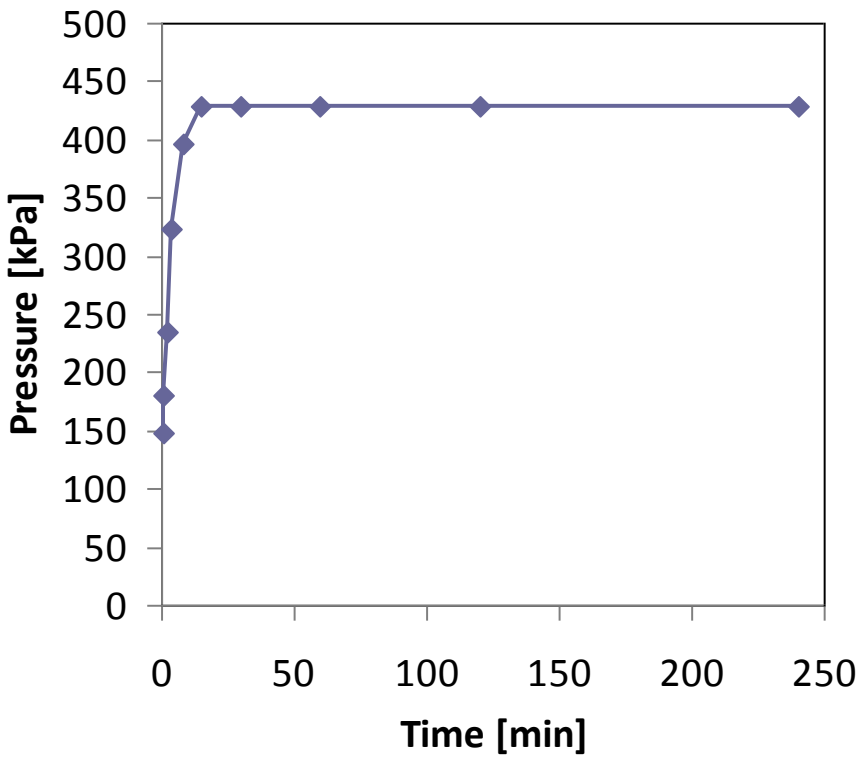

(c)

Figure 5.6 (a) Swelling test apparatus; (b) Apparatus compliance curve without sample; and (c) Swell pressure as a function of time.

The 430 kPa measured involved the swelling pressure due to a cement/aluminum mixture rather than RCA with aluminum. Tests involving finely crushed RCA and aluminum is expected to produce similar swelling pressures as the crushed RCA or cement merely provides the alkaline environment. As a result, the swelling pressure of 430 kPa was deemed representative of the field condition and is used in the numerical analysis described below.

5.5 NUMERICAL ANALYSIS

To numerically model the effects of a 430 kPa swelling pressure on a 50-mm-thick AC pavement, a 4-m-diameter, axi-symmetric model of the AC, base course and coralline sand subgrade was created in a finite element software PLAXIS (Brinkgreve, 2002) as

shown in Figure 5.7a. Horizontal and total fixities were assigned at the line of symmetry and the outer periphery of the model, respectively. Although the reaction may have been triggered by precipitation, the ground water table in general is deeper than the coralline subgrade soil and therefore, pore water pressures were not generated in the model. After generating the initial stresses, the 430 kPa heave pressure was applied over a radius equal to 50 mm from the line of symmetry. The AC was modeled as an elasto-plastic Mohr-Coulomb material with the properties summarized in Table 5.3 along with the properties of the base course and coralline sand that are of lesser significance. Since the problem is one of a pavement heave and to prevent the underlying materials from having a restraining effect on the AC in finite element modeling, a weak interface element was specified between the base course and the AC with the interface strength parameter R_{inter} = 0.01 where R_{inter} relates the interface cohesion (c_i) and friction angle (ϕ_i) to that of the base course as follows:

$$c_i = R_{inter}\, c_{base\ course} \tag{5.2}$$

$$\tan\phi_i = R_{inter} \tan\phi_{base\ course}$$

where $c_{base\ course}$ and $\phi_{base\ course}$ are the cohesion and friction angle of the base course, respectively.

Table 5.3 Summary of material properties used in the numerical analysis.

Material	Unit Weight γ (kN/m^3)	At-rest Earth Pressure Coef. K_o	Friction Angle ϕ (°)	Cohesion (kPa)	Dilatancy Angle ψ (°)	Young's Modulus E (MPa)	Poisson's Ratio ν
Asphalt concrete	23	0.357	40[1]	160[1]	10	70 to 600[2]	0.35
Base course	19	0.357	40	0	10	200	0.2
Coralline sand	19	0.357	40	0	10	70	0.2

Notes:

1. Shear strength parameters for AC are for a 5% binder content per Christensen and Bonaquist (2002).
2. E appropriate for AC with a PG64-16 binder and for the range of temperatures common in Hawaii per Archilla (2010).

The Young's modulus, E, of the AC pavement has a significant effect on the deflections. The moduli of AC can vary significantly with temperature and binder content. For an AC pavement with a 5% PG64-16 binder content (commonly used in Hawaii) and for the range of temperatures on Oahu, Hawaii, E can vary from 70 to 600 MPa (Archilla, 2010). A sensitivity analysis of E on the centerline deflection was performed. As shown in Figure 5.7b, the deflections can vary from 10 to 90 mm for this range of E, which coincides with the observed field deflections. It can also be seen from the deflected profile in Figure 5.7a that the pavement separated from the base course as a result of this uplift.

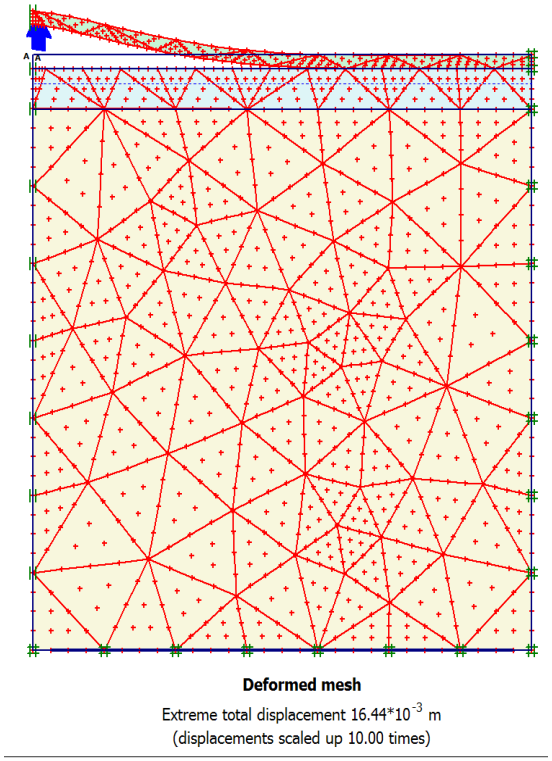

(a)

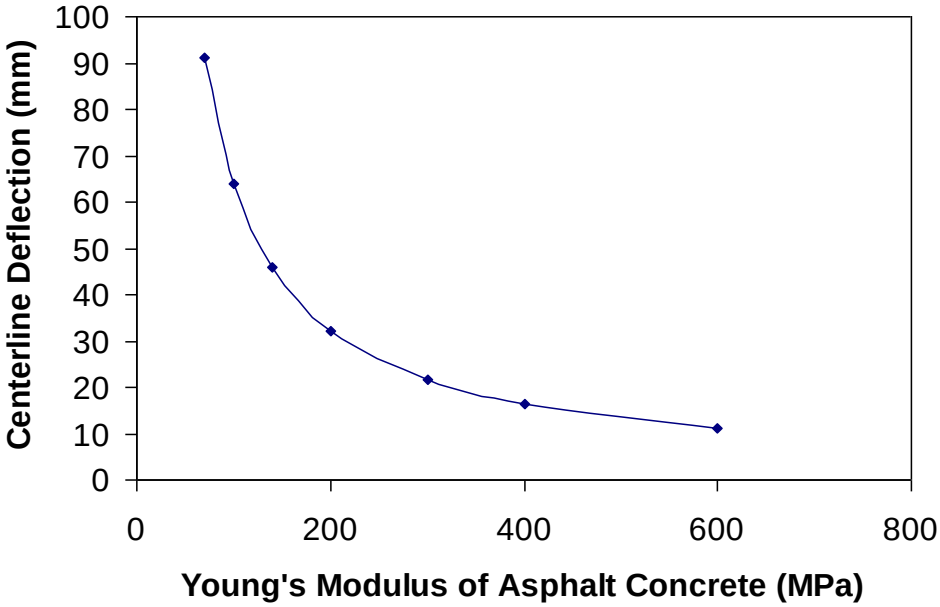

(b)

Figure 5.7 (a) Deformed mesh of the AC pavement when subjected to a swelling pressure of 430 kPa with an AC Young's modulus of 400 MPa and (b) Centerline deflection versus Young's modulus of the AC pavement.

5.6 SUMMARY AND CONCLUSIONS

A case study of a pavement containing a significant number of eruptions that were about 25 mm high and about 127 mm in diameter was forensically investigated. The distressed AC pavement was constructed on a base course containing RCA. The following observations and conclusions are offered:

- Directly below each eruption, significant amounts of a white substance were found within the base course. It was theorized that this white substance was responsible for the pavement distress and was sampled for testing.
- A combination of EDS, XRD and Raman spectroscopy identified that the primary constituent of the white substance was $Al(OH)_3$ in the form of bayerite, which is an unstable form of gibbsite. This product can form when impurities such as pieces of aluminum metal, if present in a base course, corrodes in an alkaline environment.
- An alkaline environment can exist when moisture is present in a base course containing RCA. The adjacent ground topography greatly favored drainage through this site.
- Laboratory duplication of the field reaction confirmed the formation of bayerite when aluminum metal is exposed to an alkaline environment.
- A test in a Geonor h-200 apparatus was conducted by exposing aluminum powder to an alkaline environment. It was found that a maximum swell pressure of 430 kPa was attained in just 15 minutes.
- A numerical analysis was performed by subjecting the pavement to the measured swell pressure. For a range of realistic pavement moduli, the

calculated deflections are consistent with the observed pavement deflections thus corroborating the hypothesized cause of this distress.

Considering the extensive costs and effort required to reconstruct this pavement, it is vital that sufficient quality control practices are adopted to ensure that this case history is not repeated. When using RCA as a base course, it may be prudent to follow one or more of the following:

- Allow only uncrushed concrete that can be visually inspected for use as RCA;
- Allow RCA from a supplier who can guarantee the quality. RCA from unknown sources should not be accepted unless certified by a qualified engineer/scientist that it is free of deleterious materials (such as aluminum);
- Avoid using building demolition RCA;
- Require a paper trail to document the RCA source. It is recognized that keeping such records may be challenging;
- Use a non-ferrous metal detector to determine if aluminum is present and also visually inspect the RCA prior to use.

CHAPTER 6 IMPLICATIONS OF RESEARCH RESULTS ON SPECIFICATIONS

The research results have the following implications on the specifications:

RAP

1. While the resilient modulus and shear strength of RAP is quite appreciable, its CBR is low (figures 2-12 and 2-15b) and it suffers from significant permanent deformation – more so than RCA and VA (Table 2-38). The 50% RAP:50% VA blend fared worse. Therefore, it may be prudent to limit the amount of RAP for use in unbound layers to avoid premature rutting. Saeed (2008) indicated that while 16 out of 29 DOTs polled allow the use of 100% RAP in unbound layers, 1 prohibits its use and 5 restrict it to 50% or less. In light of this and Figure 2-15b, limiting RAP to 50% may be prudent as long as the material meets all other requirements in the specifications that a VA would satisfy plus a proposed addition as described below.

2. In light of the discussion above, a minimum CBR of 80% and 60% are proposed as requirements in the specifications for base and subbase courses, respectively. This will encourage the material supplier to find a RAP blend with less than 50% RAP that will still have a high enough “performance specification” in terms of CBR. The CBR is chosen since it is a test that does not require expensive and sophisticated equipment and since it is commonly performed in industry.

3. If the field dry density and moisture content of RAP will be assessed with the nuclear gauge, the specifications require moisture offsets to be pre-determined prior to use.

4. The specifications do not allow use of other types of compaction quality assurance/quality control tests (e.g., TDR, stiffness-measuring devices) unless approved by the Engineer.

RCA

1. In terms of CBR (figures 2-12 and 2-14b), shear strength (Table 6-1), stiffness (Figure 6-1) and permanent deformation (Table 3-38), RCA is a very attractive alternative to VA. Thus from a mechanical standpoint, 100% RCA should be allowed in the unbound layers. Saeed (2008) indicated that 21 out of 29 DOTs polled allow the use of 100% RCA in unbound layers while 2 restrict it to 50% or less. No reason was provided for the restriction.

Table 6-1 Test results for “loose” and “dense” 100%RCA sheared immediately after consolidation (after Selvarajah, 2010)

Relative Compaction (%)(1)	Normal Stress (kPa)	Peak		Critical State	
		Friction Angle (degrees)	Shear Strain (%)	Friction Angle (degrees)	Shear Strain (%)
95	68.3	56.6	3.7	45.5	12.8
	101.6	55.6	2.2	42.6	12.8
	135.2	47.5	3.7	42.2	12.8
	268.8	44.2	3.3	39.8	12.8
100	68.3	62.8	1.1	43.7	12.8
	101.6	58.4	0.73	43.2	12.8
	135.2	54.4	1.5	40.2	12.8
	268.8	48.3	1.8	41.5	12.8

Notes: (1) Based on Modified Proctor

(2) Gradation of RCA is parallel to that shown in Figure 3-6 with a maximum particle size of 4.75 mm.

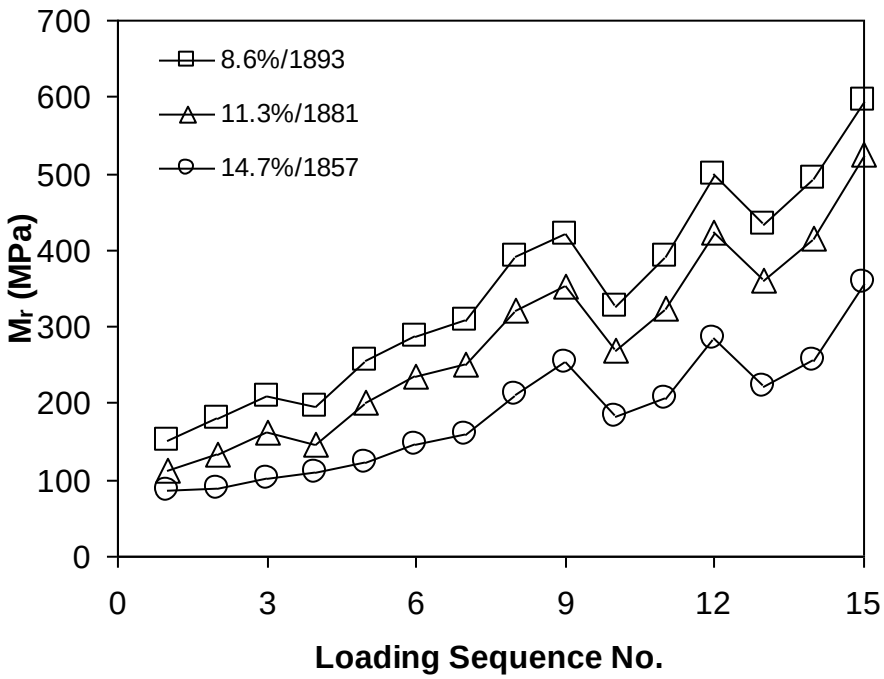

Figure 6-1 Effect of water content on M_r for RCA (Legend shows the molding water contents and dry densities in kg/m^3)

2. RCA has the potential to chemically react and cause pavement distress. Potential distresses include (a) Alkali silica reaction (ASR); (b) Alkali carbonate reaction (ACR); (c) Sulfate attack; (d) Tufa formation and (e) High pH leading to corrosion of aluminum if present. For the Hawaiian basaltic based RCA, it was shown that tufa formation is unlikely. ACR can occur only for specific aggregate types. ASR can occur if mixed with RG and this should be avoided. Therefore, sulfate attack and corrosion of aluminum are two distresses that need to be addressed in the specifications.

   (a) Although challenging to enforce, RCA with known prior distresses such as ASR, sulfate attack, etc. shall not be allowed.

(b) Use of RCA adjacent to RG shall be prohibited to avoid ASR.

(c) Sulfate attack is due to exposure of RCA to high sulfate bearing soils or ground water which results in the formation of expansive products. To prevent sulfate attack, designers should ascertain that the surrounding soil and ground water have low concentrations of sulfates. It is an issue that should be addressed at the design stage. It is proposed that the specifications prohibit the use of RCA if the ground water is brackish (i.e.; near the ocean) as the salt ions in seawater are rich in sulfates.

(d) Dissolution of RCA raises the pH of the infiltrating water. If the RCA is contaminated with aluminum metal or aluminum pipes are in the vicinity, the aluminum can corrode leading to the formation of aluminum hydroxide and hydrogen gas; both of which can produce expansion. As such, its must be prohibited near aluminum infrastructure. In addition, the specifications should prohibit any aluminum contamination. The engineer should have the right to use a non-ferrous metal detector to detect aluminum in an RCA pile. If found, the Engineer should have the right to reject that pile.

3. If the field dry density and moisture content of RCA will be assessed with the nuclear gauge, the specifications require moisture offsets to be pre-determined prior to use.

4. The presence of RCA in water profoundly increases the pH of the water. As such, RCA should not be used in drainage fill applications, including drains behind retaining walls, foundation drains, drainage blankets, and French drains.

RG

The RG obtained was crushed to a very fine gradation (Figure 2-1). This gradation renders its use as a base or sub-base course rather limited unless it is blended with VA. Blending RG containing a significant amount of fines with VA may be hazardous as the fines can cause skin irritation and appropriate safety procedures should be adopted. The need for such safety procedures has hindered its use as an aggregate on a more widespread basis. RG could have acceptable engineering characteristics for use as fill as discussed below.

1. The shear strength of pure RG is reasonably high as seen in Table 6-2. In addition, the resilient modulus of 30%RG:70%VA is not insignificant as shown in Figure 6-2.

2. The CBR of RG has been presented in Figure 2-12 and 2-16b. For RG/VA blends, there was no clear trend in the variation of CBR with %RG. Because the CBR of 25% RG:75%VA did not exceed 80%, it is recommended to limit its proportion to not more than 10% in the base course and 25% in the subbase course and fill.

3. From a chemical perspective, crushed RG is mostly silica and its use with RCA is prohibited in the specs to avoid the risk of ASR. Combinations of RAP and RCA

are allowed but not RAP and RG as the mechanical properties of these two materials are both inferior to VA and combining two inferior materials just does not make good engineering sense.

Table 6-2 Test results for “loose” and “dense” as-received 100%RG in direct shear (Ooi et al., 2008)

Relative Compaction (%)[1]	Normal Stress (psf)	Peak	
		Friction Angle (degrees)	Shear Strain (%)
85	963	42.0	10.0
	1608	42.5	15.5
	2899	42.2	13.1
	5481	40.6	12.9
95	963	60.7	6.0
	1608	58.6	5.8
	2899	53.9	7.2
	5481	50.3	11.5

Notes: (1) Based on Modified Proctor.
(2) Gradation of RG tested is the as-received gradation (Figure 2-1) scalped on the 6.35 mm sieve since the maximum particle size limit is one-tenth the diameter of the shear box (63.5 mm). Scalping was performed in accordance with CALTRANS California Test 105 (1978). Scalping did not significantly alter the as-received gradation since only 2% of the RG is between 6.35 and 9.5 mm.

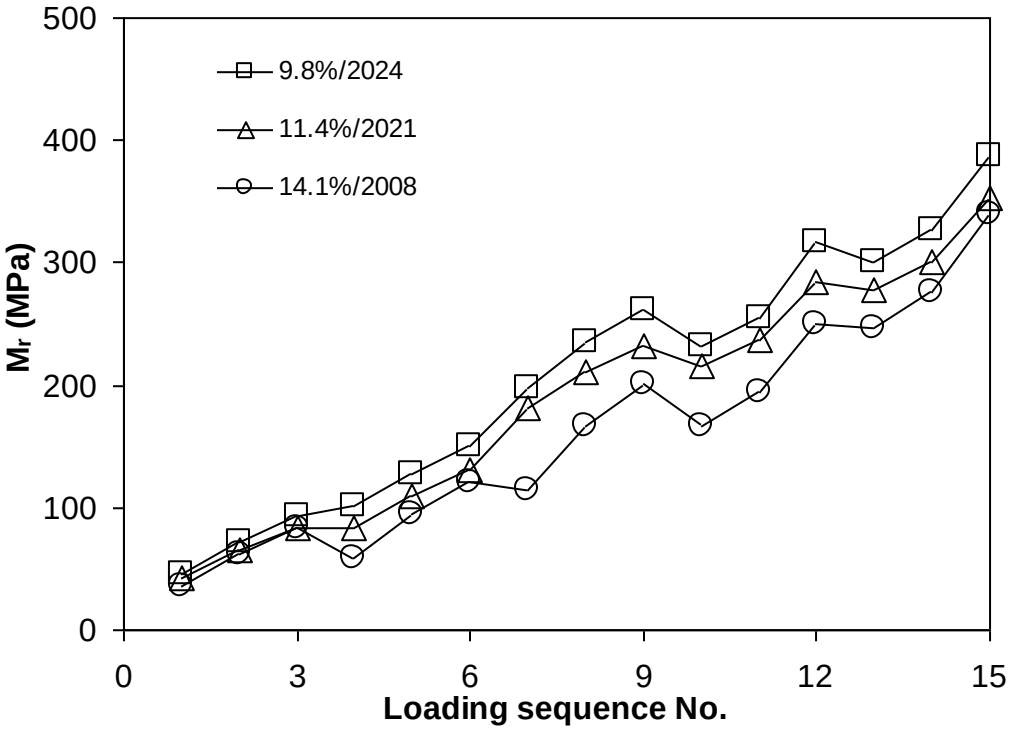

Figure 6-2 Effect of water content on M_r for 30%RG:70%VA (Legend shows the molding water contents and dry densities in kg/m^3). Gradation tested is shown in Figure 2-22.

General

In summary, the following maximum recycled material content is recommended for the various applications.

Table 6-3 Summary of maximum allowable recycled materials as a percent by dry weight of the total composite aggregate weight for various highway applications

Highway Application	**Maximum Allowable Percent by Weight (%)**		
	Cullet	**RAP**	**RCA**[1]
Untreated Permeable Base[2]	0	0	0
Untreated Base	10	50	100
Subbase	25	50	100
Structure Backfill	25	50	100
Non-Critical[3] Trench Backfill	100	100	100
Critical[4] Trench Backfill	25	50	100
Granular Material for Embankment	25	50	100
Drainage Fill Applications[5]	100	100	0

Notes

1) Use of RCA shall not be permitted within 10 feet of any metal (especially aluminum) pipe or structure and shall not be used within 3 feet of the ground water table nor below the ground water table.
2) Use of recycled material in untreated permeable base is not allowed because the untreated permeable base particles are very uniform and very large. Large particles of cullet and RCA can crush. RAP can deform readily due to the lubricating effect of asphalt and has the lowest measured CBR of the three recycled materials.
3) "Non-critical" trench backfill refers to the portion of a trench backfill that is more than 5 feet below the road surface or the entire portion of a trench backfill that is in an area not subject to traffic surcharge.
4) "Critical" trench backfill refers to the portion of a trench backfill that is 5 feet or less below the road surface and that is subject to surcharge, and the entire portion of a trench backfill that is in an embankment.
5) Drainage fill applications include, drains behind retaining walls, foundation drainage, drainage blankets and French drains.

In addition, the following have been included in the specifications:

A. Deleterious and prohibited materials are defined and procedures for limiting them are provided.

B. Recycled materials shall be tested for gradation and results submitted to the Engineer. The Engineer shall be notified to visually inspect the recycled material stockpile prior to use.

C. The Contractor shall submit a blended aggregate design prior to use or prior to changing either the source or amount originally approved. For aggregate blends,

the Contractor shall submit the means and method on how uniform mixing of the recycled and virgin aggregates is ensured. Blending at the job site is not allowed.

REFERENCES

Abdulla A.A., Mohammed, A.A. and Al-rizzo, H.M. The complex dielectric constant for Iraqi soils as a function of water content and texture. IEE Trans. Geosci. Remote Sens., 26(6), 1988, pp. 882-885.

Abu-Farsakh, M.Y., Alshibli, K., Nazzal, M., and Seyman, E. Assessment of In-Situ Test Technology For Construction Control of Base Courses and Embankments, Report No. 736-02-0995, Louisiana Department of Transportation. 2004.

Alshibli, K.A., Abu-Farsakah, M., and Seyman, E. Laboratory Evaluation of the GeoGauge and Light Falling Weight Deflectometer as Construction Control Tools. Journal of Materials in Civil Engineering. 2005. pp. 560-569.

Almássy, K. Examination of Mechanical Properties in Unbound Road Bases. Periodica Polytechnica Ser Civil Engineering, Vol. 46, No.1, 2002, pp.53-69.

Almeida, J. R. de. Development and validation of a finite element code for pavement analysis. Flexible Pavements. Edited by A. Gomes Correia, Technical University of Lisbon. Proceedings of the European Symposium Euroflex 1993, Lisbon, Portugal 20-22 September 1993.

ARA Inc. Guide for Mechanistic-Empirical Design of New and Rehabilitated Pavement Structures - Final Report. National Cooperative Highway Research Program (NCHRP) Project 1-37A, Transportation Research Board, National Research Council, 2004.

Archilla, A.R., Ooi, P.S.K. and Sandefur, K.G. Estimation of a Resilient Modulus Model for Cohesive Soils Using Joint Estimation and Mixed Effects. Journal of Geotechnical and Geoenvironmental Engineering, Vol. 133, No. 8, 2007, pp. 984-994.

Archilla, A.R. Developing Master Curve Predictive Equation Models for Local Conditions: A Case Study for Hawaii, *Journal of the Association of Asphalt Paving Technologists*, Vol. 79, 2010.

Arnold, G. Rutting of Granular Pavements. PhD Thesis, University of Nottingham, Nottingham, UK, 2004.

Aurstad, J. and I. Hoff. Crushed Asphalt and Concrete as Unbound Road Materials - Comparisons of Field Measurement and Laboratory Investigations. Bearing Capacity of Roads, Railways and Airfields. Proceedings of the 6th International Conference, Lisbon, Portugal, 2002, pp. 967-978.

Aurstad, J., J. Aksnes, J. E. Dahlhaug, G. Berntsen, and N. Uthus. Unbound Crushed Concrete in High Volume Roads - A Field and Laboratory Study. 5th International Conference on Research and Practical Applications Using Wastes and Secondary Materials in Pavement Engineering, 22-23 February, 2006.

Barksdale, R.D. Laboratory Evaluation of Rutting in Base Course Materials. Proceeding of 3rd International Conference on the Structural Design of Asphalt Pavements, London, 1972, pp. 161-174.

Bennert, T., W. J. Papp, M. Ali, and N. Gucunski. Utilization of Construction and Demolition Debris under Traffic-Type Loading in Base and Subbase Applications. In Transportation Research Record: Journal of the Transportation Research Board, No. 1714, Transportation Research Board of the National Academies, Washington, D.C., 2000, pp. 33-39.

Bennert, T. and Maher, A. The Use of Recycled Concrete Aggregate in a Dense Graded Aggregate Base Course. Project No. FHWA-NJ-2008-002, New Jersey Department of Transportation. 2008.

Biarez, J. Contribution à l'étude des propriétés mécaniques des sols et desmatériaux pulvérulents. D.Sc, Grenoble, 1961.

Blankenagel, B.J. Characterization of Recycled Concrete for Use as a Pavement Base Material. Master of Science Thesis, Brigham Young University. 2005

Blankenagel, B.J. and W.S. Guthrie. Laboratory Characterization of Recycled Concrete for Use as Pavement Base Material. In Transportation Research Record: Journal of the Transportation Research Board, No. 1852, Transportation Research Board of the National Academies, Washington, D.C. 2006, pp. 21-27.

Blyth F.G.H. and de Freitas M.H. A Geology for Engineers (seventh edition): Elsevier, NY. 1984.

Brinkgreve, R.B.J. *User's manual for PLAXIS 2D-Version 8*. A.A. Balkema Publishers, Delft, Netherlands. 2002.

Brown, S F and Dawson, A R. 1992. Two-stage approach to asphalt pavement design. Proc., 7th Int. Conf. on Asphalt Pavements. Vol.1. Nottingham. 1992. pp. 16-34.

Browning, F.R. Shear strength characteristics of crushed glass. M.S. thesis, University of Missouri-Rolla. 1970.

Bruinsma, J. E., K. R. Peterson, and M. B. Snyder. Chemical Approach to Formation of Calcite Precipitate from Recycled Concrete Aggregate Base Layers. In Transportation Research Record: Journal of the Transportation Research Board, No. 1577, Transportation Research Board of the National Academies, Washington, D.C. 1998, pp. 51-58.

California Department of Transportation (CALTRANS), "California Test 105. Calculations pertaining to gradings and specific gravities." 1978

Cambio D. and Ge, L. Effects of Parallel Gradation on Strength Properties of Ballast Materials. GSP 173 Advances in Measuring and Modeling of Soil Behavior. 2007.

Celaya, M. and Nazarian, S. Seismic Testing to Determine Quality of Hot-Mix Asphalt. *Transportation Research Record: Journal of the Transportation Research Board: Materials and Construction.* 2006. pp. 113-122.

CEN-European Committee for Standardization. EN 13286-7 Unbound and Hydraulically Bound Mixtures Test Methods - Part 7: Cyclic Load Triaxial Tests for Unbound Mixtures, 2004.

Chan, F. W. K. Permanent Deformation Resistance of Granular Layers in Pavements. PhD Thesis, Department of Civil Engineering, University of Nottingham, 1990.

Chesner Engineering. White paper and specification for reclaimed concrete aggregate for unbound soil aggregate base course. University of New Hampshire, Recycled Materials Resource Center, Project 13: Development and preparation of specifications for recycled materials in transportation applications. 2001.

Cheung, L. W. and A. R. Dawson. Effects of Particle and Mix Characteristics on Performance of Some Granular Materials. In Transportation Research Record: Journal of the Transportation Research Board, No. 1787, Transportation Research Board of the National Academies, Washington, D.C., 2002, pp. 90-98.

Christensen, W.D., and Bonaquist, R., Use of Strength Tests for Evaluating the Rut Resistance of Asphalt Concrete, *Asphalt Paving Technology*, Association of Asphalt Paving Technologists - Proceedings of the Technical Sessions, Vol. – 71, 2002, pp. 692-711.

Christopher, B. R., C. Schwartz, and R. Boudreau. Geotechnical Aspects of Pavements. U.S. Department of Transportation, Federal Highway Administration, Publication No. NHI-05-037, National Highway Institute, 2006.

Clough, G.W. and J.M. Duncan. Earth Pressure. In Foundation Engineering Handbook. 2nd edition. Edited by H. Y. Fang. Van Nostrand Reinhold, New York. 1991.

Cosentino, P.J., E.H. Kalajian, H.H. Heck III, and C. Shieh. Developing Specifications for Waste Glass and Waste-to-Energy Bottom Ash as Highway Fill Materials. Florida Institute of Technology. 1995.

Cosentino, P.J., Klajian, E.H., Shieh, C.S. (2003). Developing specifications for using recycled asphalt pavement as base, subbase, or general fill materials, Phase II. http://www.dot.state.fl.us/research-center/Completed_Proj/Summary_SMO/FDOT_BC819.pdf.

Croney, P. and Croney, D. The design and performance of road pavements. Third Edition, McGraw-Hill, New York.

CTC & Associates LLC. Laboratory Resilient Modulus Test Methods for Subgrade Materials. Based on Presentations at October 19, 2007 Workshop and Review of Related Materials for Frozen Four Pooled Fund Study - TPF-5(119), 2008. http://www.Northcentral pavement.org/ docs/ ResilientModulusReport_6-12-08.pdf.

Dames & Moore, Inc. Glass Feedstock Evaluation Project: Task 4 – Engineering Suitability Evaluation. The Clean Washington Center, Washington State Department of Trade & Economic Development, 1993.

Dawson, A. R. and F. Wellner. Plastic Behavior of Granular Materials. Final Report ARC Project 933, Department of Civil Engineering, University of Nottingham, Reference PRG 990, 1999.

Dawson, A. R. Rut Accumulation and Power Law Models for Low-Volume Pavements under Mixed Traffic. In Transportation Research Record: Journal of the Transportation Research Board, No. 2068, Transportation Research Board of the National Academies, Washington, D.C., 2008, pp. 78-86.

Dawson, A. R., M. J. Mundy, and M. Huhtala. European Research into Granular Material for Pavement Bases and Subbases. In Transportation Research Record: Journal of the Transportation Research Board, No. 1721, Transportation Research Board of the National Academies, Washington, D.C., 2000, pp. 91-99.

Dawson, A. R., P. Kolisoja, and N. Vuorimies. Understanding Low-Volume Pavement Response to Heavy Traffic Loading. ROADEXIII Northern Periphery, 2008.

Dawson, A. R., P. Kolisoja, N. Vuorimies, and T. Saarenketo. Design of Low-Volume Pavements against Rutting: Simplified Approach. In Transportation Research Record: Journal of the Transportation Research Board, No. 1989, Transportation Research Board of the National Academies, Washington, D.C., 2007, pp. 165-172.

de Vos, K. UTS 009 Unbound Materials Resilient Modulus Test Software Reference. IPC Global Limited, 2004.

Dollimore. D., J. D. Gupta, S. Lerdkanchanaporn and S. Nippani. A Thermal Analysis Study of Recycled Portland Cement Concrete (RPCC) Aggregates. Thermochimica Acta, Elsevier, Vols. 357-358, 2000, pp. 31-40.

Drever, J. I. The Geochemistry of Natural Waters (second edition): Prentice Hall, inc., Englewood Cliffs, NJ, 1988.

Drnevich, V.P., Yu, X. and Lovell, J. Beta Testing Implementation of the Purdue Time Domain Reflectometry (TDR) Method for Soil Water Content and Density Measurement. Project No. 656-1284-0156, Indiana Department of Transportation. 2003.

Duncan, J. M. and R. B. Seed. Compaction Induced Earth Pressures under K_0 Conditions. ASCE Journal of Geotechnical Engineering. Vol. 112, No. 1, 1986, pp. 1-22.

Dunlap, W.S. A Report on a Mathematical Model Describing the Deformation Characteristics of Granular Materials. Technical Report 1, Project 2-8-62-27, Texas Transportation Institute, Texas A&M University, College Station, 1963.

Egorov, K.B. Calculation of bed for foundation with inclusions and cavities. *Proc., 6th International Conference on Soil Mechanics and Foundation Engineering*, Finland, Vol. 2, 1965. pp. 41-45

Fiedler, S., Nelson, C., Berkman, E.F., and DiMillio, A. (1998) “Soil Stiffness Gauge of Soil Compaction Control” *Public Road Magazine,* Vol. 61, No. 5, April 1998, pp. 5-11

Fleming, P.R., Frost, M.W., and Lambert, J.P. (2009) “Lightweight deflectometers for quality assurance in road construction.” *Bearing Capacity of Roads, Railways, and Airfields.* pp. 809-818.

Florin, V.A. (1959) Principles of Soil Mechanics [in Russian], Vol. 1, Gosstroiizdat, Leningrad-Moscow.

Gidel G., Hornych P., Chauvin J.J., Breysse D. and Denis A. Nouvelle approche pour l’étude des déformations permanentes des graves non traitées à l’appareil triaxial à chargements répétés, Bulletin des LPC No. 233. 2001. pp 5-21.

Giese K. and Tiemann R. Determination of the complex permittivity from thin-sample time domain reflectometry: Improved analysis of the step response wave form. Adv. Mol. Relaxation Processes. 7, 1975, pp. 45-49.

Glasser, P.F. Chemistry of the Alkali-Aggregate Reaction, In: The Alkali Silica Reaction in Concrete, Ed. R.N. Swamy, Van Nostrand Reinhold, New York, 1998.

Gonzalez, G.P., and Moo-Young, H.K. Transportation Applications of Recycled Concrete Aggregate, FHWA State of the Practice National Review. 2004

Grubb, D.G., P.M. Gallagher, J. Wartman, Y. Liu, and M. Carnivale, III. Laboratory Evalution of Crushed Glass—Dredged Materials Blends. Journal of Geotechnical and Geoenvironmental Engineering, Vol. 132, No. 5, 2006, pp. 562-576.

Gudishala, R. Development of Resilient Modulus Prediction Models for Base and Subgrade Pavement Layers from In-Situ Test Results. M.S. thesis, Louisiana State University, 2004.

Gupta J. D. and W. A. Kneller. Precipitate Potential of Highway Subbase Aggregates. The University of Toledo, Ohio Department of Transportation Project No. 14479(0), 1993.

Gupta, J. D. and D. Dollimore. Magnitude Assessment of Free and Hydrated Limes Present in RPCC Aggregates. University of Toledo, Ohio Department of Transportation Project No. 14676(0), 2002.

Gupta, S., A. Ranaivoson, T. Edil, C. Benson, and A. Sawangsuriya. Pavement Design Using Unsaturated Soil Technology. Minnesota DOT Report No. MN/RC-2007-11, University of Minnesota, Minneapolis, 2007.

Guthrie, W. S., D. Cooley, and L. E. Dennis. Effects of Reclaimed Asphalt Pavement on Mechanical Properties of Base Materials. In Transportation Research Record: Journal of the Transportation Research Board, No. 2005, Transportation Research Board of the National Academies, Washington, D.C., 2007, pp. 44-52.

Haddock, J. A. E., J. T. Hand, H. Fang, and T. D. White. Determining Layer Contributions to Rutting by Surface Profile Analysis. ASCE Journal of Transportation Engineering, Vol. 131, Issue 2, 2005, pp. 131-139.

Hawaii Department of Transportation, Highways Division. Standard Specifications for Road and Bridge Construction, 2005.

Hicks, R. G. Factors Influencing the Resilient Properties of Granular Materials. Ph.D. dissertation, University of California, Berkeley, California, 1970.

Hicks, R.G., and C. L. Monismith. Factors Influencing the Resilient Properties of Granular Materials. Highway Research Record 345, Highway Research Board, National Research Council, Washington, D.C., 1971, pp. 15-31.

Hornych P., Corté J.F. and Paute J.L. Etude des déformations permanentes sous chargement répétés de trois graves non traitées, Bull liaison Labo P et Ch, 184. 1993. pp 45-55.

Hornych, P. and A. El Abd. Selection and Evaluation of Models for Prediction of Permanent Deformations of Unbound Granular Materials in Road Pavements. Document number: SAM-05-DE10. Sustainable and Advanced Materials for Road Infrastructure, Work Package 5 Performance-based specifications, 2004.

Huurman, M. Permanent deformation in concrete block pavements. PhD Thesis, Delft University of Technology, 1997.

Huurman, R. and A.A.A. Molenaar. Permanent Deformation in Flexible Pavements with Unbound Base Courses. In Transportation Research Record: Journal of the Transportation Research Board, No. 1952, Transportation Research Board of the National Academies, Washington, D.C., 2006, pp. 31-38.

Jaky, J. The coefficient of earth pressure at rest. Journal of the Hungarian Society of Architects and Engineers, Vol. 25, 1944. pp. 355–358.

Janssen, H.A. Versuche uber Getreidedruck in Silozellen. Zeitschrift des Vereines Deutscher Ingenieure. 1895.

Johnson, K. L. Plastic Flow, Residual Stresses and Shakedown in Rolling Contact. Proceedings of the 2nd International Conference on Contact Mechanics and Wear of Rail/Wheel Systems, University of Rhode Island, Waterloo Ontario, 1986.

Joint Committee on Powder Diffraction Standards. Selected Powder Diffraction Data for Minerals Data Book. First Edition. Joint Committee on Powder Diffraction Standards, Swarthmore, PA. 1974.

Joint Committee on Powder Diffraction Standards. Mineral Powder Diffraction File, Group Data Book. International Center for Diffraction Data, Swarthmore, PA, 1983.

Joint Committee on Powder Diffraction Standards. Powder Diffraction File, Alphabetical Indexes, Inorganic Phases. International Centre for Diffraction Data, Swarthmore, PA. 1991.

Khedr S. Deformation characteristics of granular base course in flexible pavements, Transportation Research Record No. 1043, 1985. pp 131-138.

Khogali, W. E. I. and El H. H. Mohamed. Mechanistic Classification of Unbound Materials. In Transportation Research Record: Journal of the Transportation Research Board, No. 2016, Transportation Research Board of the National Academies, Washington, D.C., 2007, pp. 39-48.

Kim, J.R., Kang, H.B., Kim, D., Park, D.S., and Kim, W.J. Evaluation of In Situ Modulus of Compacted Subgrades Using Portable Falling Weight Deflectometer and Plate-Bearing Load Test. Journal of Materials in Civil Engineering. 2007. pp 492-499.

Kim, W., J. F. Labuz, and S. Dai. Resilient Modulus of Base Course Containing Recycled Asphalt Pavement. In Transportation Research Record: Journal of the Transportation Research Board, No. 2005, Transportation Research Board of the National Academies, Washington, D.C., 2007, pp. 27-35.

Koerner, R.M. Designing with Geosynthetics. Fourth Edition. New Jersey: Prentice Hall. 1998.

Kolisoja, P. Resilient Deformation Characteristics of Granular Materials. Ph.D. dissertation, Tampere University of Technology, Publication No 223, Finland, 1997.

Kulhawy, F. H., and Mayne, P. W. Manual on estimation soil properties for foundation design, EPRI Report No. EL-6800, Electric Power Research Institute, Palo Alto, Calif. 1990.

Lade, P.V. Single Hardening Model for Soils: Parameter Determination and Typical Values. ASCE Geotechnical Special Publication No. 128, Soil Constitutive Models: Evaluation, Selection, and Calibration. 2005. pp. 290 – 309.

Langton, D. The Panda Lightweight Penetrometer for Soil Investigation and Monitoring Material Compaction, Ground Engineering. September1999. pp. 33-37.

Lashine, A.K.F, Brown S.F. and Pell P.S. Dynamic properties of soils, Report No. 2, Dept of Civil Engineering, University of Nottingham, 1971.

Lekarp F. and Dawson A. Modelling permanent deformation behaviour of unbound granular materials, Construction and Building Materials, Vol. 12 No. 1. 1998. pp 9-18

Lekarp, F., U. Isacsson, and A. R. Dawson. State of the Art. II: Permanent Strain Response of Unbound Aggregates, ASCE Journal of Transportation Engineering, Vol. 126, No.1, 2000, pp. 76-84.

Lenke, L.R., McKeen, R.G. and Grush, M. Evaluation of a Mechanical Stiffness Gauge for Compaction Control of Granular Media, Report No. NM99MSC-07.2, New Mexico State Highway and Transportation Department. 2001.

Lentz R.W. and Baladi G.Y. Simplified procedure to characterise permanent strain in sand subjected to cyclic loading, Proceedings Int. Symposium on Soils Under Cyclic and Transient Loading, Swansea. 1980. pp 89-95.

Li, D., and E. T. Selig. Resilient Modulus for Fine-grained Subgrade Soils. Journal of Geotechnical Engineering, ASCE, Vol.120, No. 6, 1994, pp. 939-957.

Lin, D.F., Liau, C.C., and Lin, J.D. Factors Affecting Portable Falling Weight Deflectometer Measurements. Journal of Geotechnical and Geoenvironmental Engineering. 2006. pp. 804 – 808.

Malla, R.B. and S. Joshi. Establish Subgrade Support Values for Typical Soils in New England. Report No. NETCR 57, New England Transportation Consortium, Fall River, Mass, 2006.

Marske, J. P., M. O. Garcia, A. J. Pietruszka, J. M. Rhodes and M. D. Norman. Geochemical Variations during Kilauea's Pu‘u ‘O‘o Eruption Reveal a Fine-scale Mixture of Mantle Heterogeneities within the Hawaiian Plume. Journal of Petrology, Vol. 49, 2008, pp. 1297-1318.

Mayne, P. W. and F. H. Kulhawy. Ko-OCR Relationships in Soil. ASCE Journal of the Geotechnical Engineering, Vol. 108, No. 6, 1982, pp. 851-872.

Mehta, P.K., and P.J.M. Monteiro. Concrete: Microstructure, Properties, and Materials, 3rd Ed., McGraw-Hill, New York, 2006.

Mindess, S., J.F. Young, and D. Darwin. *Concrete*, 2nd Ed., Prentice Hall, Upper Saddle River, New Jersey, 2003.

Misra, A.K., S.K. Sharma, L. Kamemoto, P.V. Zinin, Q. Yu, N. Hu and L. Melnick. Novel micro-cavity substrates for improving the Raman signal from

submicrometer size materials. *Applied Spectroscopy*, Vol. 63, No. 3, 2009, pp. 373-377.

Mohammad, L. N., A. Herath, M. Rasoulian, and Z. Zhang. Laboratory Evaluation of Untreated and Treated Pavement Base Materials: Repeated Load Permanent Deformation Test. In Transportation Research Record: Journal of the Transportation Research Board, No. 1967, Transportation Research Board of the National Academies, Washington, D.C., 2006, pp. 78-88.

Molenaar, A.A.A and A.A. Van Niekerk. Effects of Gradation, Composition, and Degree of Compaction on the Mechanical Characteristics of Recycled Unbound Materials. In Transportation Research Record: Journal of the Transportation Research Board, No. 1787, Transportation Research Board of the National Academies, Washington, D.C., 2002, pp. 73-82.

Monismith, C.L. Evolution of Long-Lasting Asphalt Pavement Design Methodology: A Perspective. Distinguished Lecture to International Symposium on Design and Construction of Long lasting Asphalt Pavements, ISAP, 2004.

Morgan, J. R. The Response of Granular Materials to Repeated Loading. Proceedings of 3rd Australian Road Board Conference, Sydney, 1966, pp. 1178-1192.

Nataatmadja, A., and Y.L. Tan. Resilient Response of Recycled Concrete Road Aggregates. Journal of Transportation Engineering, ASCE, Vol. 127, No. 5. 2001, pp. 450-453.

Nazzal, M.D. Field Evaluation of In-Situ Test Technology for Q_C/Q_A During Construction of Pavement Layers and Embankments, Master of Science Thesis, Louisiana State University. 2002.

Ni, B., T.C. Hopkins, L. Sun, and T.L. Beckham. Modeling the Resilient Modulus of Soils. Proceedings of the 6th International Conference on the Bearing Capacity of Roads, Railways, and Airfields, Vol. 2, A.A. Balkema Publishers, Rotterdam, the Netherlands, 2002, pp. 1131–1142.

Nishi M., Yoshida N., Tsujimoto T., Ohashi K. Prediction of rut depth in asphalt pavements, Proceedings 4th Int. Conf. on the Bearing Capacity of Roads and Airfields, Minneapolis, USA. 1994. pp 1007-1019

Norrish K. and B.W. Chappell. X-ray Fluorescence Spectrometry, in Physical Methods in Determinative Mineralogy, 2nd Ed., J. Zussman, ed., 201-272, Academic Press, London, 1977.

Ooi, P.S.K., A.R. Archilla, and K.G. Sandefur. Resilient Modulus for Compacted Cohesive Soils. In Transportation Research Record: Journal of the Transportation Research Board, No. 1874, Transportation Research Board of the National Academies, Washington, D.C., 2004, pp. 115-124.

Ooi, P.S.K., Li, M.M.W., Sagario, M.L.Q. and Song, Y. Shear strength characteristics of recycled glass. Transportation Research Record 2059, Journal of the Transportation Research Board. 2008. 52-62.

Ooi, P.S.K. and Pu, J. Use of Stiffness for Evaluating Compactness of Cohesive Pavement Geomaterials. Transportation Research Record 1849. 2003. pp. 11-19.

Pappin, J. W. Characteristics of a Granular Material for Pavement Analysis. PhD Thesis, Department of Civil Engineering, University of Nottingham, 1979.

Paute J.L., Jouve P., Martinez J. and Ragneau E. Modèle de calcul pour le dimensionnement des chaussées souples, Bulletin de Liaison des Laboratoires des Ponts et Chaussées, No. 156. 1988. pp 21-36.

Paute J.L., Hornych P. and Benaben J.P. Comportement mécanique des graves non traitées, Bulletin de Liaison des Laboratoires des Ponts et Chaussées, No. 190. 1994. pp 27-38.

Pennsylvania State Department of Transportation. Laboratory Evaluation of Select Engineering-Related Properties of Glass Cullet. ftp://ftp.dot.state.pa.us/public/Bureaus/design/SEMP/CG/Glass%20Cullet%20Report%20-%20Drexel%20University.pdf. Date accessed July 2007a.

Pennsylvania State Department of Transportation. Laboratory evaluation of select engineering-related properties of crushed glass blended with various soils. ftp://ftp.dot.state.pa.us/public/Bureaus/design/SEMP/CG/Crushed%20Glass%20and%20Soil%20Report.pdf. Date accessed July 2007b.

Pezo, R.F. A General Method of Reporting Resilient Modulus Tests of Soils: A Pavement Engineer's Point of View. 72nd Annual Meeting of the Transportation Research Board, Washington, D.C., 1993.

Ponizovsky, A.A. , Chudinova, S.M. and Pachepsky, Y.A. Performance of TDR calibration models as affected by soil texture. Journal Hydrol., 218(1-2), 1999, pp. 35-43.

Puppala, A. J. Correlations for Resilient Modulus Values of Subgrades and Unbound Pavement Materials. NCHRP Synthesis 382, Synthesis of Highway Practice, 2008.

Rankine, W. J. M. On the stability of loose earth. Philos. Trans. R. Soc. London 147, 1857. pp. 9–27.

Rathje, E.M., Rauch, A.F., Folliard, K.J., Trejo, D., Little, D., Viyanant, C., and Ogalla, M. Recycled Asphalt Pavement and Crushed Concrete Backfill: State-of –the-Art Review and Material Characterization," Report No. 4177-1, Texas Department of Transportation, October 2001.

Rathje, E.M., Rauch, A.F., Folliard, K.J., Trejo, D., Little, D., Viyanant, C., and Ogalla, M. "Recycled Asphalt Pavement and Crushed Concrete Backfill: Results from Initial Durability and Geotechnical Tests," Report No. 4177-2, Texas Department of Transportation, October 2002.

Recycled Materials Resource Center (2008). Guidelines for Byproducts and Secondary Use Materials in Pavement Construction. Retrieved June 28, 2009 from http://www.rmrc.unh.edu/tools/uguidelines/index.asp

Reimbert, M.L. and Reimbert, A.M. SILOS – Theory and Practice, first ed. Trans Tech Publications, Clausthal-Zellerfeld. 1976.

Ruan, H.D., R.L. Frost and J.T. Kloprogge. Comparison of Raman spectra in characterizing gibbsite, bayerite, diaspore and boehmite. *Journal of Raman Spectroscopy*, Vol. 32, 2001, pp. 745-750.

Ruban, M. Quality Control in Road Construction. India: Swets and Zeitlinger Publishers. 2002.

Runkles, B., White, N. and Ashmawy, A. Calibration and Accuracy Assessment of the TDR One-Step Method for Quality Control of Compacted Soils, Report No. BD-544-19, Florida Department of Transportation, June 2006.

Saeed, A. Performance-Related Tests of Recycled Aggregates for Use in Unbound Pavement Layers. TRB's National Cooperative Highway Research Program (NCHRP) Report 598, 2008.

Saeed, A. Performance-Related Tests of Recycled Aggregates for Use in Unbound Pavement Layers. NCHRP Report 598, Transportation Research Board, National Research Council, Washington, D.C., 2008.

Sawangsuriya, A., Edil, T.B., and Bosscher, P.J. Relationship Between Soil Stiffness Gauge Modulus and Other Test Moduli for Granular Soil. Transportation Research Record: Journal of the Transportation Research Board: Soils, Geology, and Foundations. Volume 1849. 2002. pp. 3-10.

Seed, H.B., C.K. Chan, and C.E. Lee. Resilience Characteristics of Subgrade Soils and their Relation to Fatigue Failures in Asphalt Pavements. Proc., International Conference on the Structural Design of Asphalt Pavements, University of Michigan, Ann Arbor, 1962, pp.611–636.

Seed, H.B., F.G. Mitry, C. L. Monismith, and C.K. Chan. Factors Influencing the Resilient Deformations of Untreated Aggregate Base in Two Layer Pavements Subjected to Repeated Loading. Highway Research Record, Highway Research Board, No.190, 1967, pp. 19-55.

Selig, E. T. Tensile Zone Effects on Performance of Layers Systems. Geotechnique, Vol. XXXVII, No. 3, 1987, pp. 247-354.

Selvarajah, P. Use of the parallel gradation technique to assess the shear strength of reclaimed asphalt pavement and recycled concrete aggregate in direct shear. M.S. Thesis, University of Hawaii. 2010.

Shackel, B. Repeated Loading of Soils - A Review. Australian Road Research, Vol. 5, No. 3, 1973, pp. 22-49.

Sharp, R. W. and J. R. Booker. Shakedown of Pavements under Moving Surface Loads. ASCE Journal of Transportation Engineering, Vol. 110, No. 1, 1984, pp. 1-14.

Shenton M.J. Deformation of railway ballast under repeated loading (triaxial tests), Report RP5, British Railways Research Department, 1974.

Shinn, C.J. and V. Sonntag. Using recovered glass as construction aggregate feedstock. *Transp. Res. Rec.*, 1437, 1994, pp. 8-18.

Siddiqui, S.I. and Drnevich, V.P. Use of Time Domain Reflectometry for Determination of Water Content and Density of Soil, Report No. FHWA/IN/JTRP-95/9, Joint Transportation Research Program, Indiana Department of Transportation-Purdue University, February 1995.

Snyder M. B. and J. E. Bruinsma. Review of Studies Concerning Effects of Unbound Crushed Concrete Bases on PCC Pavement Drainage. In Transportation Research Record: Journal of the Transportation Research Board, No. 1519, Transportation Research Board of the National Academies, Washington, D.C., 1996, pp. 51-58.

Soil and Environmental Engineers, Inc. and Re-Sourcing Associates, Inc. A tool kit for the use of post-consumer glass as a construction aggregate. Report No. GL-97-5 prepared for the Clean Washington Center. 1998.

Song, Y. Testing and Analysis of Recyced Materials for Highway Projects. Ph.D. Dissertation, University of Hawaii. 2009.

Song, Y., P.S.K. Ooi, E. Hellebrand and D.W. Muenow. Potential for Tufa Precipitation with Crushed Concrete Containing Coarse Basaltic and Fine Coralline Sand Aggregates. *Environmental and Engineering Geoscience.* Vol. XVII, No. 1, 2011.

Sowers, G. F., A. D. Robb, C. H. Mullis, and A. J. Glenn. The Residual Lateral Pressures Produced by Compacting Soils. Proceedings 4th International Conference on Soil Mechanics and Foundation Engineering, London, UK. Vol. 2, 1957, pp. 243-247.

Steinhert, B.C., Humphrey, D.N. and Kestler, M.A. Portable Falling Weight Deflectometer Study," NETC Project No. 00-4, New England Transportation Consortium. 2005.

Sweere, G. T. H. Unbound Granular Bases for Roads. PhD Thesis, Delft University of Technology, 1990.

Theyse, H. L. The Development of Mechanistic-Empirical Permanent Deformation Design Models for Unbound Pavement Materials from Laboratory and Accelerated Pavement Test Data. Unbound Aggregates in Road Construction: Proceedings of the 5th International Symposium on Pavements Unbound (UNBAR 5), 2000, pp. 285-293.

Topp, G.C., J.L. Davis, and A.P. Annan. Electromagnetic determination of soil water content: Measurement in coaxial transmission lines. Water Resources Research. 1980. pp. 574–582.

Troxler Electronic Laboratories, Inc. (2009) Manual of Operation and Instruction, Model 3450 RoadReader™ Plus, Surface Moisture-Density Gauge. pp. 2-1 – 2-6.

Tseng, K. and R. Lytton. Prediction of Permanent Deformation in Flexible Pavement Material. Implication of Aggregates in the Design, Construction, and Performance of Flexible Pavements, ASTM STP 1016, ASTM, 1989, pp. 154-172.

Tutumluer, E. and A. R. Dawson. TRB Workshop 2004-talk2-Laboratory Testing. Session 711: Describing Aggregate Behavior for Today's Pavements, part 2, 2004. https://netfiles.uiuc.edu/tutumlue/www/research_links/TRBWorkshop2004-Talk2-In-situ %20Performance.pdf

Tutumluer, E. and Dawson, A.R. TRB Workshop 2004-talk4-Permanent Deformation. Session 711: Describing Aggregate Behavior for Today's Pavements, Part 2, 2004. https://netfiles.uiuc.edu/tutumlue/www/research_links/TRBWorkshop2004-Talk5-In-situ%20Performance.pdf

Tutumluer, E. and Dawson, A. In Situ performance of compacted aggregate – assumptions, characterization, and experience. TRB, Washington, D.C. 2004

Uthus, L. Deformation Properties of Unbound Granular Aggregates. Ph.D. Dissertation, Norwegian University of Science and Technology, 2007.

Uzan, J. Characterization of Granular Material. In Transportation Research Record: Journal of the Transportation Research Board, No. 1022, Transportation Research Board of the National Academies, Washington, D.C., 1985, pp. 52-59.

Van Niekerk, A. A., A. A. A. Molenaar, and L. J. M. Houben. Effect of Material Quality and Compaction on the Mechanical Behavior of Base Course Materials and Pavement Performance. Unbound Aggregates in Road Construction: Proceedings of the 5th International Symposium on Pavements Unbound (UNBAR 5), Nottingham, 2000, pp. 125-138.

Varadarajan, A., Sharma, K.G., Venkatachalam, K., and Gupta, A.K. Testing and Modeling Two Rockfill Materials. Journal of Geotechnical and Geoenvironmental Engineering. 2003. pp. 206-218.

Varadarajan, A., Sharma, K.G., Abbas, S.M., and Dhawan, A.K. Constitutive Model for Rockfill Materials and Determination of Material Constants. International Journal or Geomechanics. 2006. pp. 226-237.

Verdugo, R., and De la Hoz, K. Strength and Stiffness of Coarse Granular Soils. Soil Stress-Strain Behavior: Measurement Modeling and Analysis. 2007. pp. 243 – 252.

Von Quintus, H. and B. Killingsworth. Analyses Relating to Pavement Material Characterizations and their Effects on Pavement Performance. FHWA-RD-97-085, Federal Highway Administration, McLean, VA, 1998.

Vuong, B. Evaluation of Back-Calculation and Performance Models Using a Full Scale Granular Pavement Tested with the Accelerated Loading Facility (ALF). Proceedings 4th International Conference on the Bearing Capacity of Roads and Airfields, Minneapolis, USA, 1994, pp. 183-197.

Wartman, J., D.G. Grubb, and A. S. M. Nasim. Select Engineering Characteristics of Crushed Glass. Journal of Materials in Civil Engineering, Vol. 16, No. 6, 2004, pp. 526-539

Werkmeister, S. Permanent Deformation Behavior of Unbound Granular Materials in Pavement Constructions. PhD Dissertation, Dresden University of Technology, Germany, 2003.

Werkmeister, S., A. R. Dawson, and F. Wellner. Pavement Design Model for Unbound Granular Materials. ASCE Journal of Transportation Engineering, Vol. 130, No. 5, 2004, pp. 665-674.

Witczak, M.W. and J. Uzan. The Universal Airport Pavement Design System. Report 1 of 4, Granular Material Characterization, University of Maryland, College Park, 1988.

Wolfe, W.E. and T.S. Butalia. Seasonal Instrumentation of SHRP Pavements. Final Report for Ohio DOT, Ohio State University, Columbus, 2004.

Wolff H. and Visser A.T. Incorporating elasto-plasticity in granular layer pavement design, *Proceedings Institution of Civil Engineers Transport*, Vol. 105, 1994. pp. 259-272.

Yang, S., W. Huang, C. Liao. Correlation between Resilient Modulus and Plastic Deformation for Cohesive Subgrade Soil under Repeated Loading. Transportation Research Record No. 2053, 2008, pp. 72-79.

Yau, A. and Von Quintus, H. Predicting Elastic Response Characteristics of Unbound Materials and Soils. In Transportation Research Record: Journal of the Transportation Research Board, No. 1874, Transportation Research Board of the National Academies, Washington, D.C., 2004, pp. 47–56.

Yau, A. and Von Quintus, H. Study of LTPP Laboratory Resilient Modulus Test Data and Response Characteristics. Report No. FHWA-RD-02-051, Federal Highway Administration, McLean, VA., 2002.

Yu, X. and Drnevich, V.P. Soil Water Content and Dry Density by Time Domain Reflectometry. Journal of Geotechnical and Geoenvironmental Engineering. 130(9), 2004. pp. 922 – 934.

Zhang, J., M. Klasky, and B.C. Letellier. The Aluminum Chemistry and Corrosion in Alkaline Solutions. *Journal of Nuclear Materials.* Vol. 384, 2009, pp 175-189.

APPENDIX

This section contains sections from the 2005 State of Hawaii Department of Transportation's Standard Specifications that have been modified to incorporate the use of the three recycled materials addressed in this research. Proposed modifications are annotated below. In addition, two entirely new sections are proposed for consideration for adoption. They include:

1. Section 719 RECYCLED CONCRETE AGGREGATE (RCA) AND RCA-MADE MATERIALS and
2. Section 720 RECLAIMED ASPHALT PAVEMENT (RAP) AND RAP-MADE MATERIALS

SECTION 203 - EXCAVATION AND EMBANKMENT

203.01 Description. This section describes excavating, hauling, and disposing of surplus excavated material; and placing and compacting specified materials necessary to construct project.

Roadway excavation includes excavating and compacting, or disposing of, all materials of whatever character encountered in the work.

For terminology used in this section, refer to Section 101 – Terms, Abbreviations and Definitions and ASTM D 653.

203.02 Materials.

Cullet and Cullet-Made Materials	717
Recycled Concrete Aggregate (RCA) and RCA-Made Materials	719
Reclaimed Asphalt Pavement (RAP) and RAP-Made Materials	720

Embankment material shall include mixture of excavated, selected, or borrow excavated material, or combination thereof, and ~~cullet. When cullet is not produced on the project island, or material unit price of cullet is greater than material unit price of virgin material, cullet may be excluded. Before excluding cullet, submit availability and pricing documentation.~~ one type of the following recycled materials [cullet, reclaimed asphalt pavement (RAP) or recycled concrete aggregate (RCA)]. Use of two or more types of recycled materials shall not be allowed except a three-way combination of soil, RAP and RCA is permissible. Recycled materials may be excluded when it is not produced on the project island, its material unit price is greater than the material unit price of borrow or it cannot be blended in any proportion with borrow material so as to meet the gradation requirements of Section 703.24.

Unless otherwise indicated in the contract documents, the following definitions shall apply to this section:

(A) Excavated Material: All material excavated from project site for roadway construction.

(B) Selected Material: Suitable excavated material for specific use from areas within the highway right-of-way.

(C) Borrow Excavated Material: Accepted materials from designated borrow sources outside right-of-way or excavation limits, conforming to requirements of Subsection 106.02 - Material Sources. Borrow excavated material shall conform to size and quality indicated in the contract

documents. When the contract documents do not indicate size or quality, borrow material shall be of quality suitable for intended purpose. Borrow material shall be free of roots and other organic matter, garbage, trash, junk, and other deleterious material.

203.03 Construction. Clear and grub in accordance with Section 201 - Clearing and Grubbing, before excavating. Excavate and construct embankment for road, road intersections, and road entrances to a smooth and uniform surface. Excavate so as not to disturb material outside limits of slopes or limits of grading.

(A) Excavation.

(1) General. Obliterate old roadways in accordance with Section 202 - Removal of Structures and Obstructions. Blasting will not be allowed.

When encountering possible archaeological, historical, or burial site findings, comply with requirements of Subsection 107.13(B) - Archaeological, Historical, and Burial Sites.

(2) Widening or Flattening Cut Slopes. Submit proposed locations for widening or flattening planned cut slopes to obtain material required for the following:

(a) Constructing embankment.

(b) Precluding opening unsightly borrow pits.

(c) Increasing stability of cut slopes.

Do not proceed with proposed slope widening or flattening until the Engineer accepts proposed locations. Steepening of cut slopes will not be allowed.

(3) Cut Slopes. Round tops and ends of cut slopes in accordance with the contract documents.

Finish soil cut slopes true and straight in accordance with slope lines and grades indicated in the contract documents.

Finish cut slopes that are in rock excavation, in a rough condition, with debris and loose material removed. When completed, the average plane of excavated slopes shall conform to slopes indicated in the contract documents. No points shall vary from planned slopes by more than 6 inches when measured at right angles to slope.

(4) Subexcavation. When excavation to finished grade results in subgrade or slopes of unsuitable material as defined in Subsection 101.03 - Definitions, the Engineer will require the following:

(a) Removing unsuitable material.

(b) Backfilling to finished grade with acceptable material in accordance with Subsection 203.03(C) - Embankment Construction.

Notify the Engineer two weeks prior to start of subexcavation operations. The Engineer will perform necessary cross-sectional measurements before authorizing backfill placement.

When relative compaction of original ground is less than compaction specified in Subsection 203.03(C)(3) - Compaction of Cut Areas and Embankments With Moisture and Density Tests and Subsection 203.03(C)(4) - Compaction of Embankments Without Moisture and Density Tests, compact upper 6 inches of exposed original ground in accordance with those subsections.

Unsuitable material shall become property of the Contactor and disposal of unsuitable material shall be at no increase in contract price or contract time.

(B) Excavated Material.

(1) Selected Material. Use selected material for the following:

(a) Embankment fill.

(b) Finishing top portion of roadbed.

(c) Constructing roadbed shoulders.

(d) Structure backfill.

(e) Constructing berms.

(f) Erosion control.

(g) Landscaping.

(h) Other purposes in accordance with the contract documents.

Place selected material on roadbed in accordance with Subsection 203.03(C) - Embankment Construction and selected topsoil for erosion

control in accordance with Section 209 - Temporary Water Pollution, Dust, and Erosion Control.

Keep selected material in place until it can be hauled and compacted in its final position. If allowed by the contract documents, selected material may be stockpiled at locations accepted by the Engineer, for later placement in final position.

(2) Borrow Excavated Material. Arrange to obtain borrow excavated material and pay costs involved in accordance with Subsection 106.02 - Material Sources. Submit certified test data demonstrating borrow excavated material to be incorporated in the work conforms to the contract documents. Acceptance of test data will be subject to field verification testing by the Engineer. Notify the Engineer 20 working days before opening borrow areas.

Control of borrow excavated material will be in accordance with Section 106 - Material Restrictions and Requirements.

Excavate to dimensions and elevations established for borrow pit. Remove borrow excavated material after the Engineer completes staking out and cross sectioning of borrow excavated and in-place sites for measurement and payment purposes. Establish and specify finished borrow areas approximately true to line and grade. Complete finished borrow areas so that no water will collect or stand therein.

Place selected material in fill before placing borrow excavated material.

(3) Surplus Selected Material. Unless otherwise indicated in the contract documents, and not over soft ground, use surplus selected material when and in locations accepted by the Engineer to do the following: widen embankments uniformly or flatten slopes; dispose of at Engineer's designated locations. Dispose of surplus selected material below adjacent roadbed grade. Complete embankments before disposing of surplus selected material.

When indicated in the contract documents, the quantity of surplus selected material is approximate only. Replace shortage of material caused by premature disposal of surplus selected material at no increase in contract price or contract time.

Upon completion of disposal operations, grade disposal area to provide level surface. Unused selected material shall become the Contractor's property. Supply topographic map of disposal area.

(4) Highly Sensitive Soil. When soil having high moisture content loses its stability and becomes plastic or muddy, excavate with the least manipulation or churning of soil.

(C) Embankment Construction.

(1) General. Strip live, dead, or decayed vegetation, rubbish, debris, and other foreign material from ground surface on which embankment is to be placed. When embankment is required on existing slopes steeper than five horizontal to one vertical, bench those areas as work is brought up in layers. Construct bench of sufficient width to permit operation of placing and compacting equipment. Use suitable excavated or borrow material~~, and cullet, or combination thereof~~ in accordance with Section 703.24 in embankment construction. Use of embankment material containing cullet will not be allowed on surface of embankment. Placement of rocks, broken concrete, or other solid materials will not be allowed in embankment areas where deep foundations, such as driven piles or drilled shafts, are to be placed.

When soft or swampy ground condition is encountered that cannot support weight of trucks or other hauling equipment, lower part of fill may be constructed with a working platform. Construct working platform by either placing successive loads of gravel, cobbles, and boulders in a uniformly distributed layer of thickness not greater than necessary; or by using permeable separator with granular material of adequate thickness to support construction equipment. Construct remainder of embankment in accordance with the contract documents.

For minimum depth of 2 feet from subgrade, place embankment material with maximum size of 6 inches and sand equivalent (SE) of 10 or greater, but not less than SE of soil material upon which it is placed. Except as otherwise indicated in the contract documents, embankment material below 2 feet from subgrade may consist of material with maximum size of 6 inches and SE of less than 10 but not less than SE of existing soil on which embankment is placed. Place embankment material in horizontal layers not exceeding 9 inches in loose thickness. Compact as specified before placing next layer. Manipulate material to ensure uniform density and surface smoothness, as compaction of each layer progresses. Add or remove water to obtain required density.

Embankment fill below top 2 feet from subgrade may contain material with rock fragments, hardpan, or cemented gravel larger than 6 inches but less than 3 feet in greatest dimension. Place in compacted lifts of thickness not exceeding approximate size of the rocks and not exceeding 3 feet. Process embankment material to reduce maximum size of particles so that material can be placed in specified lifts. Uniformly distribute larger rock throughout bottom of embankment and place sufficient selected material and other finer

rock around large material to fill voids and to produce a dense, compact embankment. Provide earth or fine material to fill voids when not available in excavation.

The embankment material whether blended or from a single source shall have a plasticity index not greater than 15% when tested in accordance with AASHTO T 89 and AASHTO T 90.

Finish embankment slopes, as indicated in the contract documents, to within plus or minus 3 inches of lines and grades established and such that slopes contain no unsightly or undue irregularities. Finish top of embankment surfaces in accordance with Subsection 203.03(D) - Subgrade Preparation. Replace portions that become displaced or damaged prior to acceptance at no increase in contract price or contract time.

(2) Relative Compaction Test. Relative compaction test is a procedure for determining ratio of dry unit weight (density) of in-place soil to maximum dry unit weight of same soil, as determined by the following methods:

(a) Maximum Dry Unit Weight. Test for maximum dry unit weight in accordance with AASHTO T 180, Method D. Use Hawaii Test Method HDOT TM 5 for sample preparation of sensitive soils when so designated by the Engineer. When oversized materials larger than 3/4 inch exceed 5 percent by weight of total sample, apply corrections to laboratory dry density in accordance with AASHTO T 224. When oversized materials larger than 3/4 inch exceed 30 percent, use compaction procedure specified in Subsection 203.03(C)(4) - Compaction of Embankments Without Moisture and Density Tests.

(b) Density of Soil In-Place. Test for soil in-place density in accordance with Hawaii Test Method HDOT TM 1, HDOT TM 2, and HDOT TM 3. When using the nuclear gauge to test for the in-place density of recycled concrete aggregate (RCA) or reclaimed asphalt pavement or their blends, moisture offsets shall first be determined for the same material blend that will be used on site. Without the moisture offset, the nuclear gauge shall not be acceptable for field testing of RCA, RAP or their blends. Use of other methods of quality assurance and quality control shall be prohibited unless approved by the Engineer.

(3) Compaction of Cut Areas and Embankments With Moisture and Density Tests. Prior to shaping and compacting, condition soil to moisture content within 2 percent above or below optimum moisture content determined in accordance with AASHTO T 180. Except as specified in Subsection 203.03 (C)(4) – Compaction of Embankments Without Moisture and Density Tests, moisture condition embankment material and place in

layers not to exceed 9 inches in loose thickness, and compact each layer of material as specified, before placement of next lift. Determine maximum density and relative compaction in accordance with Subsection 203.03(C)(2) – Relative Compaction Test.

In-situ soil or embankment material contained in prism within 2 feet below subgrade and within width of traveled way, auxiliary lane, and shoulder on each side shall have relative compaction of 95 percent or more. When in-situ material within 2 feet below subgrade does not conform to specified relative compaction, excavate and recompact material until specified relative compaction is achieved.

Top 6 inches of in-situ material and embankment material below top 2 feet of subgrade, and beyond traveled way, auxiliary lane, and shoulder prism, shall have relative compaction of at least 90 percent. When in-situ material cannot be compacted to 90 percent, provide working platform to allow 90 percent compaction of first lift.

(4) Compaction of Embankments Without Moisture and Density Tests. Use trial fill section to determine required degree of compaction and method to obtain that compaction, for materials with sufficient coarse material that compaction cannot be determined by Subsection 203.03(C)(2) – Relative Compaction Test. Use trial section to determine type and size of compaction equipment, lift thickness, and number of passes required to obtain compaction acceptable to the Engineer.

For rock fill placement in lifts not exceeding 2 feet in loose lift, the following compaction procedures may be used in lieu of trial section. For rock sizes not exceeding 9 inches in greatest dimension, place material in 12-inch loose lift and compact material full width using one of the following methods:

(a) Two passes of a 50-ton compression-type roller.

(b) Two passes of a vibratory roller having minimum dynamic force of 40,000 pounds impact per vibration and minimum frequency of 1,000 vibrations per minute.

(c) Eight passes of a 10-ton compression-type roller.

(d) Eight passes of a vibratory roller having minimum dynamic force of 30,000 pounds impact per vibration and minimum frequency of 1,000 vibrations per minute.

Operate compression-type rollers at speeds less than 4 miles per hour and vibratory rollers at speeds less than 1.5 miles per hour. For rock sizes not exceeding 14 inches in greatest dimension, place material in 18-inch loose lift

and compact material full width with increase in number of roller passes in Subsections (a) and (b) herein by two, and increase number of roller passes in Subsections (c) and (d) herein by four. For rock sizes not exceeding 18 inches in greatest dimension, place material in 24-inch loose lift and compact material full width with increase in number of roller passes in Subsections (a) and (b) herein by four, and increase number of roller passes in Subsections (c) and (d) herein by eight. Use trial fill section as specified in this subsection for embankment with rock sizes 19 to 36 inches in maximum dimension.

(D) Subgrade Preparation. Prepare subgrade to required density, cross section, and grade.

(1) General. Prepare subgrade after completing and backfilling drainage facilities and structures and compacting earthwork.

Remove rocks or lumps and fill voids with suitable materials. Material used to fill voids shall conform to specified material to be placed on subgrade.

(2) Density Requirement. Compact finish subgrade to relative compaction of 95 percent for depth of 6 inches immediately before placing subsequent material thereon.

(3) Surface Tolerances of Subgrade. Finish subgrade upon which pavement structure is to be placed shall not vary more than 0.04-foot above or below theoretical grade.

203.04 Measurement. The Engineer will measure:

(A) Roadway excavation per cubic yard. The Engineer will compute quantities of roadway excavation by average end area method and centerline distances. Curvature correction will not be applied to quantities within roadway prism, as indicated in the contract documents. In computing excavation quantities from outside the roadway prism, where roadway centerline is used as a base, curvature correction will be applied when centerline radius is 1,000 feet or less.

When roadway excavation quantities by average end area method cannot be computed due to the nature of a particular operation or changed conditions, the Engineer will determine and use computation method that will produce an accurate quantity estimate.

(B) Borrow excavated material per cubic yard. The Engineer will compute quantities of borrow material incorporated into the work on a volume basis, using average end area method in place at work site.

(C) Selected material for planting soil and selected material for decorative boulder will be paid on a lump sum basis. Measurement for payment will not apply.

203.05 Payment. The Engineer will pay for the accepted pay items listed below at the contract price per pay unit, as shown in the proposal schedule. Payment will be full compensation for the work prescribed in this section and the contract documents.

The Engineer will pay for each of the following pay items when included in the proposal schedule:

Pay Item	**Pay Unit**
Roadway Excavation	Cubic Yard

The Engineer will pay for:

(A) 15 percent of the contract bid price upon completion of obliterating old roadways and hauling.

(B) 30 percent of the contract bid price upon completion of preparing subgrade.

(C) 40 percent of the contract bid price upon completion of placing selected material in final position, rounding of slopes, and using water for compaction.

(D) 15 percent of the contract bid price upon completion of disposing of surplus excavation material.

Borrow Excavated Material	Cubic Yard

The Engineer will pay for:

(A) 10 percent of the contract bid price upon completion of staking out and cross sectioning existing condition at borrow excavated and in-place sites and establishing borrow area.

(B) 5 percent of the contract bid price upon completion of providing, replacing, and maintaining temporary and permanent fencing, and confining livestock.

(C) 15 percent of the contract bid price upon completion of all necessary storing and processing of borrow material.

(D) 15 percent of the contract bid price upon completion of watering and hauling material to work site.

(E) 20 percent of the contract bid price upon completion of placing, grading, and compacting material in accordance with contract requirements at work site.

(F) 15 percent of the contract bid price upon completion of restoring and regrading borrow area.

(G) 10 percent of the contract bid price upon completion of staking out and cross sectioning final condition at borrow excavated and in-place sites.

(H) 10 percent of the contract bid price upon completion of removing and disposing of excess and unsuitable material from work site.

Selected Material for Planting Soil	Lump Sum
Selected Material for Decorative Boulder	Lump Sum

The Engineer will pay for accepted quantities of subexcavation, as roadway excavation at the contract unit price per cubic yard, when ordered by the Engineer, for work prescribed in Subsection 203.03(A)(4) – Subexcavation. Payment will be full compensation for the work prescribed therein and in the contract documents.

The Engineer will pay for accepted quantities of unlined gutter excavation as roadway excavation at the contract unit price per cubic yard, when gutter is located as follows: within median area of a divided highway; and between roadbed shoulder and adjacent cut slope. Payment will be full compensation for removing and disposing of excavated material; backfilling and compacting; and for the work prescribed in the contract documents.

The Engineer will not pay for stockpiling selected material, placing selected material in final position, or placing selected material in windrows along tops of roadway slopes for erosion control work, separately and will consider the cost as included in the unit prices for the various excavation contract pay items. The cost is for work prescribed in this section and the contract documents.

The Engineer will not pay for selected material from ditch, channel, or structure excavation, when used instead of borrow excavation.

The Engineer will not pay for overhaul separately and will consider the cost as included in the unit prices for the various excavation contract pay items. The cost is for work prescribed in this section and the contract documents.

The Engineer will not pay for embankment separately and will consider the cost as included in the unit price for roadway excavation. The cost is for work prescribed in this section and the contract documents.

END OF SECTION 203

SECTION 204 - EXCAVATION AND BACKFILL FOR MISCELLANEOUS FACILITIES

204.01 Description. This section describes the following:

(A) Excavating and backfilling to depths and lines established for foundations of roadway and sign lighting standards, and traffic signal standards.

(B) Excavating and backfilling trenches for utilities pipes (including water, sewer, telephone, oil, and gas lines) and conduits (including roadway and sign lighting, traffic signal, and other communications systems).

(C) Excavating and backfilling for water and sewer manholes and appurtenances.

(D) Disposing of surplus material from excavations.

Excavating and backfilling for water and sewer pipes, manholes, and appurtenances are described further in Section 624 – Water System and Section 625 – Sewer System.

204.02 Materials.

Structure Backfill Material	703.20
Trench Backfill Material	703.21
Geotextiles for Underdrain Applications	716.03
Cullet and Cullet-Made Materials	717
Recycled Concrete Aggregate (RCA) and RCA-Made Materials	719
Reclaimed Asphalt Pavement (RAP) and RAP-Made Materials	720

Structure and trench backfill material shall ~~include mixture of aggregate and cullet. When cullet is not produced on the project island, or material unit price of cullet is greater than material unit price of structure backfill or greater than material unit price of trench backfill, cullet may be excluded for that backfill application. Before excluding cullet, submit availability and pricing documentation.~~ consist of either 100% virgin aggregate, or of a mixture of virgin aggregate and one type of the following recycled materials [cullet, reclaimed asphalt pavement (RAP) or recycled concrete aggregate (RCA)]. Use of two or more types of recycled materials shall not be allowed except a three-way combination of virgin aggregate, RAP and RCA is permissible. Recycled materials may be excluded when it is not produced on the project island, its

material unit price is greater than the material unit price of virgin aggregate or it cannot be blended in any proportion with virgin aggregate so as to meet the gradation requirements of Sections 703.20 and 703.21.

Trench gravel backfill material shall conform to AASHTO M 43, size number 67. When tested in accordance with AASHTO T 96, the LA abrasion shall not exceed 40 percent at 500 revolutions.

Controlled Low Strength Material (CLSM) in accordance with Section 314 – Controlled Low Strength Material (CLSM) for Utilities and Structures may be used in place of trench and structure backfill material, subject to the Engineer's acceptance. Where CLSM is allowed, provide drainage system to accommodate underground water seepage. CLSM will not be allowed as trench backfill when installing aluminum and aluminum-coated pipe conduits.

Provide plastic marking tape that is acid and alkali-resistant polyethylene film, 6 inches wide with minimum thickness of 0.004 inch. Provide tape with minimum strength of 1750 psi lengthwise and 1500 psi crosswise. Manufacture tape with integral wires, foil backing, or other means to enable detection by a metal detector when tape is buried up to 3-feet deep. Manufacture tape specifically for marking and locating underground utilities. Provide metallic core of tape encased in a protective jacket or provided with other means to protect it from corrosion. Tape shall conform to the following colors and shall bear a continuous printed inscription describing the specific utility: Red: Electric; Yellow: Gas, Oil, Dangerous Materials; Orange: Telephone, Telegraph, Television, Police, and Fire Communications; Blue: Water System; Green: Sewer Systems.

204.03 Construction.

(A) Structure and Trench Excavation.

(1) General. Notify the Engineer 10 working days before excavating for structures and trenches.

The Contractor shall be responsible for the stability of temporary open cuts during construction of structures or trenches and shall take appropriate measures to meet OSHA requirements.

Excavate in such a manner as to prevent damage to pavements, sidewalks, structures, landscaping, and other improvements. Excavate immediately before installation of conduit and other appurtenances. Stockpile excavated material in a location that shall not cause damage, obstruct vehicular and pedestrian traffic, or interfere with surface drainage.

In excavation operations, do not disturb ground below elevations indicated in the contract documents. If ground below elevations indicated in the contract documents is disturbed, excavate disturbed ground until undisturbed ground is reached. Backfill this area with Class D concrete until required foundation elevation is reached.

Keep foundation excavation dry by draining, bailing, pumping, or driving sheathings.

When material from excavation does not meet quality requirements specified for backfill in accordance with Subsection 204.02 – Materials, furnish conforming material, as required.

Deposit remaining structure or trench excavation material that is not used as backfill, in roadway embankments in accordance with Subsection 203.03(B)(1) – Selected Material. Dispose of surplus selected material in accordance with Subsection 203.03(B)(3) – Surplus Selected Material.

(2) Foundation Treatment. When footing concrete or masonry is to rest upon rock, fully uncover rock and remove rock surface to a depth sufficient to expose sound rock. Roughly level rock surface or cut to steps; and roughen rock surface.

Grout seams in rock under pressure. The Engineer will pay cost in accordance with Subsection 104.02 - Changes.

While excavating for non-pile foundations where footing concrete or masonry is to rest on an excavated surface other than rock, do not disturb excavation bottom. Remove foundation material to final grade immediately prior to placing concrete or masonry.

Complete driven pile foundation excavation to footing bottom before driving piles therein. Remove excess materials remaining in the excavation, after pile driving, to footing bottom elevation.

In pile foundations, excavating a sufficient distance below footing bottom will be allowed, as indicated in the contract documents, at no increase in contract price or contract time. When ground surface has risen above plan grade after pile driving, remove surplus material at no increase in contract price or contract time. When ground surface is below plan grade after pile driving, backfill and compact to plan grade with acceptable material, at no increase in contract price or contract time.

(3) Inspection. When the Engineer needs to determine character of foundation material, excavate test pits, drill test borings, and perform foundation bearing tests in accordance with Section 211 - Exploratory Work at Structure Footings.

When structure excavation to foundation grade is completed, request that the Engineer inspect and accept foundation elevation and character before placing concrete or masonry and reinforcing steel in the footing.

(B) Structure and Trench Backfill. Do not deposit fill material against back of foundations and manholes until test samples indicate that concrete has developed strength required in Subsection 503.03(E) – Loading.

Cure test samples under conditions similar to those affecting the structure. Continue backfilling so that excessive unbalanced loads are not introduced against the structure.

Place backfill material in uniform horizontal layers not exceeding 8 inches in loose thickness, before compaction. Moisten and compact each layer of backfill until relative compaction of not less than 95 percent is achieved in accordance with Subsection 203.03(C)(2) – Relative Compaction Test. The Engineer may reduce 95 percent compaction requirement in situations where such compaction is not feasible.

~~When the Engineer cannot use field density test, compact each layer of backfill with vibratory or other accepted equipment on granular backfill material.~~

Compaction of backfill material by ponding or jetting will not be allowed.

Where bottom of utility pipe is located within 12 inches or below normal ground water level, use trench gravel backfill material to at least 12 inches above pipe or to bottom of pavement structure. Gravel material shall be completely encapsulated by geotextile conforming to Subsection 716.03 - Geotextiles for Underdrain Applications.

When required, place sufficient fill at structures, utility pipes, and conduits ahead of other grading operations to permit public traffic to cross.

Compact backfill material in the following areas to a relative compaction of not less than 90 percent:

(1) Footings not beneath surfacing.

(2) Other locations where the contract documents indicate 90 percent relative compaction for structure or trench backfill.

Place plastic marking warning tapes for appropriate type of utility directly above pipe, within a depth of 3 feet from finish grade, unless otherwise indicated in the contract documents.

204.04 Measurement.

(A) Trench excavation will be paid on a lump sum basis. Measurement for payment will not apply.

(B) Trench backfill will be paid on a lump sum basis. Measurement for payment will not apply.

204.05 Payment. The Engineer will pay for the accepted pay items listed below at the contract price per pay unit, as shown in the proposal schedule. Payment will be full compensation for the work prescribed in this section and the contract documents.

The Engineer will pay for each of the following pay items when included in the proposal schedule:

Pay Item	**Pay Unit**
Trench Excavation for_____	Lump Sum
Trench Backfill for_____	Lump Sum

The Engineer will pay for removal of material from depths greater than 3 feet below depths indicated in the contract documents in accordance with Subsection 104.02 - Changes.

The Engineer will not pay for trench excavation for roadway and sign lighting and traffic signal system conduits separately and will consider the cost for those items as included in the contract prices for the various contract pay items. The cost is for work prescribed in this section and the contract documents.

The Engineer will not pay for structure excavation and structure backfill for miscellaneous facilities separately and will consider the cost for those items as included in the contract prices for the various contract pay items. The cost is for the work prescribed in this section and the contract documents.

The Engineer will not pay for excavation and backfill for water and sewer manholes and appurtenances separately and will consider the cost for those items as included in the contract prices for the various contract pay items. The cost is for the work prescribed in this section and the contract documents.

END OF SECTION 204

SECTION 205 - EXCAVATION AND BACKFILL FOR BRIDGE AND RETAINING STRUCTURES

205.01 Description. This section describes the following:

(A) Excavating and backfilling to depths and lines established for bridge, overhead-mounted expressway sign, and retaining (reinforced concrete or cement rubble masonry) structure foundations.

(B) Other excavating and backfilling specifically designated in the contract documents as structure excavations and backfills.

(C) Disposing of surplus material from structure excavations.

(D) Bailing, draining, sheathing, and constructing cofferdams, if necessary, and subsequently removing sheathing and cofferdams.

205.02 Materials.

Filter Material	703.18
Structure Backfill Material	703.20
Cullet and Cullet-Made Materials	717
Recycled Concrete Aggregate (RCA) and RCA-Made Materials	719
Reclaimed Asphalt Pavement (RAP) and RAP-Made Materials	720

Structure backfill material shall ~~include mixture of aggregate and cullet. When cullet is not produced on the project island, or material unit price of cullet is greater than material unit price of structure backfill, cullet may be excluded. Before excluding cullet, submit availability and pricing documentation.~~ consist of either 100% virgin aggregate, or of a mixture of virgin aggregate and one type of the following recycled materials [cullet, reclaimed asphalt pavement (RAP) or recycled concrete aggregate (RCA)]. Use of two or more types of recycled materials shall not be allowed except a three-way combination of virgin aggregate, RAP and RCA is permissible. Recycled materials may be excluded when it is not produced on the project island, its material unit price is greater than the material unit price of virgin aggregate or it cannot be blended in any proportion with virgin aggregate so as to meet the gradation requirements of Section 703.20.

Controlled Low Strength Material (CLSM) in accordance with Section 314 – Controlled Low Strength Material (CLSM) for Utilities and Structures may be used in place of structure backfill material, subject to the Engineer's acceptance.

Where CLSM is allowed, provide drainage system to accommodate underground water seepage.

205.03 Construction.

(A) Structure Excavation.

(1) General. Notify the Engineer 10 working days before excavating for structures.

The Contractor shall be responsible for the stability of temporary open cuts during construction of structures or trenches and shall take appropriate measures to meet OSHA requirements.

In structure excavation operations, do not disturb ground below elevations indicated in the contract documents. If ground below elevations indicated in the contract documents is disturbed, excavate disturbed ground until undisturbed ground is reached. Backfill this area with Class D concrete until required foundation elevation is reached.

Keep foundation excavation dry by draining, bailing, pumping, driving sheathings; or by constructing cofferdams and cribs.

When material from excavation does not meet quality requirements specified for backfill in accordance with Subsection 205.02 - Materials, furnish conforming material, as required.

Deposit remaining structure excavation material that is not used as structural backfill, in roadway embankments in accordance with Subsection 203.03(B)(1) – Selected Material. Dispose of surplus selected material in accordance with Subsection 203.03(B)(3) – Surplus Selected Material.

(2) Cofferdams. Construct cofferdams for foundation construction to depths well below bottom of footings to ensure stability and to adequate heights to seal off all water. Brace well and make as watertight as necessary for proper performance of work that must be conducted inside cofferdam. Provide interior cofferdam dimensions so as to give sufficient clearance for driving piles, constructing forms, and when not placing seal, permitting pumping from outside the forms.

When clearance indicated in the contract documents between outside line of footings and piles, or interior walls or

surfaces are insufficient to permit pile driving or form building, the Contractor may enlarge cofferdams to provide sufficient clearance. The Engineer will consider enlargement exceeding one foot outside footing dimensions indicated in the contract documents as being for the sole purpose of expediting work of the Contractor and of no value to the State. The Engineer will not include for payment, excavation and backfill that exceed described limits.

Correct or enlarge cofferdams that are tilted or moved out of position during the process of sinking. Conduct such work at no increase in contract price or contract time.

In tidal waters or in streams at a time of probable flood, vent cofferdam walls at low water elevation to ensure equal hydrostatic head both inside and outside of cofferdam during pouring and setting of seals.

Shoring in cofferdams that will induce stress, shock, or vibration in the permanent structure will not be allowed.

When permitted, cross struts or bracing may extend through foundation concrete. Such struts or bracing below low water will be allowed to remain in place. Remove struts or bracing above low water. Fill volume with concrete of the same mix as that specified for surrounding concrete.

If requested by the Engineer, submit drawings and design calculations, signed by Hawaii Licensed Structural Engineer, showing proposed method of cofferdam construction and other details left open to the Contractor's choice or not fully indicated in the contract documents for substructure work.

After completion of structure, remove cofferdams, including sheathing and bracing, to a depth of 1 foot below streambed. Remove cofferdams in a manner that will not disturb or damage finished concrete or masonry.

(3) Foundation Treatment. When footing concrete or masonry is to rest upon rock, fully uncover rock and remove rock surface to a depth sufficient to expose sound rock. Roughly level rock surface or cut to steps; and roughen rock surface.

Grout seams in rock under pressure. The Engineer will pay cost in accordance with Subsection 104.02 - Changes.

While excavating for non-pile foundations where footing concrete or masonry is to rest on an excavated surface other than rock, do not disturb excavation bottom. Remove foundation material to final grade immediately prior to placing concrete or masonry.

Complete driven pile foundation excavation to footing bottom before driving piles therein. Remove excess materials remaining in the excavation, after pile driving, to footing bottom elevation.

In pile foundations, excavating a sufficient distance below footing bottom will be allowed, as indicated in the contract documents, at no increase in contract price or contract time. When ground surface has risen above plan grade after pile driving, remove surplus material at no increase in contract price or contract time. When ground surface is below plan grade after pile driving, backfill and compact to plan grade with acceptable material, at no increase in contract price or contract time.

(4) Inspection. When the Engineer needs to determine character of foundation material, excavate test pits, drill test borings, and perform foundation bearing tests in accordance with Section 211 - Exploratory Work at Structure Footing.

When structure excavation to foundation grade is completed, request that the Engineer inspect and accept foundation elevation and character before placing concrete or masonry and reinforcing steel in the footing.

(B) Structure Backfill. Place structure backfill material A behind bridge abutments, wingwalls, and retaining walls. Do not deposit fill material against back of concrete abutments, piers, concrete retaining walls, and foundations until test samples indicate that concrete has developed strength required in Subsection 503.03(E) - Loading.

Cure test samples under conditions similar to those affecting the structure. Continue backfilling so that excessive unbalanced loads are not introduced against the structure.

When spreading and compacting backfill, do not operate heavy equipment closer to abutment or retaining walls, than a distance equal to the height of backfill above top of footing. Compact area remaining, in layers not more than 4 inches in compacted thickness, with power-driven hand tampers suitable for material being compacted.

Place backfill material in uniform horizontal layers not exceeding 8 inches in loose thickness, before compaction. Moisten and compact each

layer of backfill until relative compaction of not less than 95 percent is achieved in accordance with Subsection 203.03(C)(2) – Relative Compaction Test. The Engineer may reduce 95 percent compaction requirement in situations where such compaction is not feasible.

~~When the Engineer cannot use field density test, compact each layer of backfill with vibratory or other accepted equipment on granular backfill material.~~

Compaction of backfill material by ponding or jetting will not be allowed.

When required, place sufficient fill at bridges ahead of other grading operations to permit public traffic to cross.

Compact structure backfill in the following areas to a relative compaction of not less than 90 percent:

(1) Footings for slope protection, slope paving, and aprons.

(2) Retaining walls, except portions under surfacing, and crib walls.

(3) Footings not beneath surfacing.

(4) Other locations where the contract documents indicate 90 percent relative compaction for structure backfill.

(C) Filter Material. Place backfill filter material at bridge abutments and retaining walls in accordance with the contract documents.

Make subgrade as impervious as possible to direct drainage toward weep holes. Impervious material is defined as materials passing the No. 200 sieve and compacted to minimum 90 percent of maximum density, when tested in accordance with AASHTO T 180, Method D.

205.04 Measurement.

(A) Structure Excavation. Structure excavation will be paid on a lump sum basis. Measurement for payment will not apply.

(B) Structure Backfill. Structure backfill for bridge abutments, wingwalls, and retaining walls will be paid on a lump sum basis. Measurement for payment will not apply.

(C) Filter Material. Filter material will be paid on a lump sum basis. Measurement for payment will not apply.

205.05 Payment. The Engineer will pay for the accepted pay items listed below at the contract price per pay unit, as shown in the proposal schedule. Payment will be full compensation for the work prescribed in this section and the contract documents.

The Engineer will pay for each of the following pay items when included in the proposal schedule:

Pay Item	**Pay Unit**
Structure Excavation for _____	Lump Sum
Structure Backfill for _____	Lump Sum
Filter Material	Lump Sum

The Engineer will pay for removal of material from depths greater than 3 feet below depths indicated in the contract documents in accordance with Subsection 104.02 - Changes.

END OF SECTION 205

SECTION 304 - AGGREGATE BASE COURSE

304.01 Description. This section describes furnishing and placing aggregate base on a prepared surface.

304.02 Materials.

Aggregate for Untreated Base	703.06
Water	712.01
Cullet and Cullet-Aggregate Mixtures as Construction Materials	717.01
Cullet Materials for Roadways	717.02
RCA and RCA-Aggregate Mixtures as Construction Materials	719.01
RCA for Roadways	719.02
RAP and RAP-Aggregate Mixtures as Construction Materials	720.01
RAP for Roadways	720.02

Aggregate base course shall consist of either 100% virgin aggregate, or of a mixture of virgin aggregate and one type of the following recycled materials [cullet, reclaimed asphalt pavement (RAP) or recycled concrete aggregate (RCA)]. Use of two or more types of recycled materials shall not be allowed in a base course except a three-way combination of virgin aggregate, RAP and RCA is permissible. Recycled materials may be excluded when it is not produced on the project island, its material unit price is greater than the material unit price of virgin aggregate or it cannot be blended in any proportion with virgin aggregate so as to meet the gradation requirements of Section 703.06.

304.03 Construction.

(A) Hauling and Placing. Haul, deposit, and spread aggregate base on a prepared surface in a manner that minimizes rutting, uneven compaction, and segregation. Should segregation occur, remove segregated material and replace with material conforming to the contract documents, at no increase in contract price or contract time.

Where compacted thickness is greater than 6 inches, spread and compact mixture in two or more lifts approximately equal in thickness. Maximum compacted thickness of one lift shall be 6 inches.

(B) Shaping and Compacting. Prior to shaping, add water uniformly to aggregate base, as necessary, to obtain moisture content within 2 percent of the optimum moisture content for compaction.

Immediately after spreading aggregate base, shape and compact each lift across full width using power roller. Roll in direction parallel to centerline of road. For areas inaccessible to roller, compact using tampers or compactors.

Compact each lift to produce uniform surface texture and to attain at least 95 percent of maximum density in accordance with Subsection 203.03(C)(2) - Relative Compaction Test.

Limit surface deviations of finished areas to not more than ½ inch above or below theoretical grade. Correct surface deviations more than ½ inch above or below theoretical grade by scarifying, adding or removing material, blading, and compacting. Reshape high or low spots with self-propelled, pneumatic-tired motor grader. Use graders with wheelbase not less than 15 feet long and blade not less than 10 feet long.

304.04 Measurement. Aggregate base will be paid on a lump sum basis. Measurement for payment will not apply.

304.05 Payment. The Engineer will pay for the accepted aggregate base on a contract lump sum basis. Payment will be full compensation for the work prescribed in this section and the contract documents.

The Engineer will pay for the following pay item when included in the proposal schedule:

Pay Item	**Pay Unit**
Aggregate Base	Lump Sum

END OF SECTION 304

SECTION 305 - AGGREGATE SUBBASE COURSE

305.01 Description. This section describes furnishing and placing aggregate subbase on a prepared surface.

305.02 Materials.

Aggregate for Subbase	703.06
Water	712.01
Cullet and Cullet-Aggregate Mixtures as Construction Materials	717.01
Cullet Materials for Roadways	717.02
RCA and RCA-Aggregate Mixtures as Construction Materials	719.01
RCA for Roadways	719.02
RAP and RAP-Aggregate Mixtures as Construction Materials	720.01
RAP for Roadways	720.02

Aggregate subbase course shall consist of either 100% virgin aggregate, or of a mixture of virgin aggregate and one type of the following recycled materials [cullet, reclaimed asphalt pavement (RAP) or recycled concrete aggregate (RCA)]. Use of two or more types of recycled materials shall not be allowed in a subbase course except a three-way combination of virgin aggregate, RAP and RCA is permissible. Recycled materials may be excluded when it is not produced on the project island, its material unit price is greater than the material unit price of virgin aggregate or it cannot be blended in any proportion with virgin aggregate so as to meet the gradation requirements of Section 703.17.

305.03 Construction.

(A) Hauling and Placing. Haul, deposit, and spread aggregate subbase on a prepared surface in a manner that minimizes rutting, uneven compaction, and segregation. Should segregation occur, remove segregated material and replace with material conforming to the contract documents, at no increase in contract price or contract time.

Where compacted thickness is greater than 6 inches, spread and compact mixture in two or more lifts approximately equal in thickness. Maximum compacted thickness of one lift shall be 6 inches.

(B) Shaping and Compacting. Prior to shaping, add water uniformly to aggregate subbase, as necessary, to obtain moisture content within 2 percent of the optimum moisture content for compaction.

Immediately after spreading aggregate subbase, shape and compact each lift across full width using power roller. Roll in direction parallel to centerline of road. For areas inaccessible to roller, compact using tampers or compactors.

Compact each lift to produce uniform surface texture and to attain at least 95 percent of maximum density in accordance with Subsection 203.03(C)(2) - Relative Compaction Test.

Limit surface deviations of finished areas to not more than ½ inch above or below theoretical grade. Correct surface deviations more than ½ inch above or below theoretical grade by scarifying, adding or removing material, blading, and compacting. Reshape high or low spots with self-propelled, pneumatic-tired motor grader. Use graders with wheelbase not less than 15 feet long and blade not less than 10 feet long.

304.06 Measurement. Aggregate subbase will be paid on a lump sum basis. Measurement for payment will not apply.

304.07 Payment. The Engineer will pay for the accepted aggregate subbase on a contract lump sum basis. Payment will be full compensation for the work prescribed in this section and the contract documents.

The Engineer will pay for the following pay item when included in the proposal schedule:

Pay Item	**Pay Unit**
Aggregate Subbase	Lump Sum

END OF SECTION 305

SECTION 306 – UNTREATED PERMEABLE BASE COURSE

306.01 Description. This section describes furnishing and placing untreated permeable base on a prepared surface.

306.02 Materials.

Coarse Aggregate	703.04(A)
Filler	703.04(B)
Water	712.01

Use of recycled asphalt pavement (RAP), recycled glass cullet and recycled concrete aggregate (RCA) shall not be allowed in the untreated permeable base.

306.03 Construction.

(A) Equipment. Use static steel power rollers weighing not less than 10 tons, with compression on rear wheels of not less than 323 ponds per inch of tire width.

Use long-bristle brooms.

(B) Untreated Permeable Base Course Edge Preparation. Before placing untreated permeable base, construct adjacent embankment areas to finished surface elevation. Construct embankment in accordance with Subsection 203.03(C) - Embankment Construction. Provide form or choker to retain untreated permeable base material by cutting embankment material as nearly vertical as possible. Position toe of cut at exterior bottom limit of untreated permeable base material. Dispose of cut embankment material in accordance with Subsection 201.03(F) - Removal and Disposal of Material.

(C) Hauling and Placing. Haul, deposit, and spread untreated permeable base on a prepared surface in a manner that minimizes rutting, uneven compaction, and segregation. Should segregation occur, remove segregated materials and replace with material conforming to the contract documents, at no increase in contract price or contract time.

Before depositing coarse aggregate, place permeable separator on subgrade or subbase in accordance with Section 313 – Permeable Separator.

When required compacted thickness is 9 inches or less, place coarse aggregate in one lift. When required compacted thickness is more than 9 inches, construct in two or more lifts of approximately equal thickness.

Construction equipment will not be allowed to make sudden stops, starts, or turns on coarse aggregate. Spread coarse aggregate using loader or grader. Place coarse aggregate on permeable separator with at least 12 inches of material between equipment tires or tracks and permeable separator. When required thickness is less than 12 inches, limit size and weight of construction vehicles so that rutting in coarse aggregate is not greater than 3 inches deep. Only placement, spreading, and smooth drum, non-vibratory compaction equipment will be allowed on the first lift above permeable separator.

(D) Shaping and Compacting. Immediately after spreading coarse aggregate, shape and compact each lift across full width using power roller. Roll in direction parallel to centerline of road. For areas inaccessible to roller, compact using tampers or compactors.

For each lift, roll area to be compacted, without interruption, a minimum of 8 complete coverage passes.

When thoroughly compacted, untreated permeable base course shall conform to shape and dimension indicated in the contract documents. Limit surface deviations of finished areas to not more than ½ inch above or below theoretical grade.

After rolling final lift, spread filler in a thin layer, not exceeding 30 pounds of filler per square yard of coarse aggregate surface area. Filler shall be sufficiently dry to choke surface voids without caking or bridging. Sprinkle surface with water and roll with two complete coverage passes. Scatter excess filler by light brooming.

Apply primer on filler surface in accordance with Section 420 – Primer for Untreated Permeable Base Course within 4 hours after roller compaction.

Use sufficient filler and water to keep edges of untreated permeable base course consolidated and compacted.

(E) Protection of Untreated Permeable Base Course. Keep traffic off untreated permeable base course, except for construction equipment directly connected with primer operation.

Prevent foreign-material contamination that would reduce free draining properties of untreated permeable base course. If contaminant or filler, or both settle below surface voids, remove and reconstruct full depth of untreated permeable base course at no increase in contract price or contract time.

304.08 Measurement. Untreated permeable base course will be paid on a lump sum basis. Measurement for payment will not apply.

304.09 Payment. The Engineer will pay for the accepted untreated permeable base course on a contract lump sum basis. Payment will be full compensation for the work prescribed in this section and the contract documents.

The Engineer will pay for the following pay item when included in the proposal schedule:

Pay Item	**Pay Unit**
Untreated Permeable Base Course	Lump Sum

The Engineer will not pay for permeable separator, filler, and primer for untreated permeable base course separately and will consider the cost for those items as included in the contract price for the untreated permeable base course contract pay item. The cost is for the work prescribed in this section, Section 313 – Permeable Separator, Section 420 – Primer for Untreated Permeable Base Course, and the contract documents.

END OF SECTION 306

SECTION 624 - WATER SYSTEM

624.01 Description. This section describes constructing water systems and appurtenances.

The terms "County Water Works System" or "Board of Water Supply (BWS)" will be interchangeable and mean organization of respective County.

Use appropriate County Water Works System requirements for items of work or materials required, but not specifically covered by contract documents.

624.02 Materials.

Aggregate for Untreated Base	703.06
Structure Backfill Material	703.20
Trench Backfill Material	703.21
Concrete Brick	704.02
Asphalt	705.06(C)
Concrete Cylinder Pipe	706.18
Ductile Iron Pipe, Fittings and Special Castings for Water System	707.01(B)
Copper Service Pipe and Appurtenances	707.11
Reinforcing Steel	709.01
Frames, Grates, Covers and Ladder Rungs	712.07
Pipe Collar for Valve Box	712.22
Precast Concrete Meter and Valve Boxes and Covers	712.23
Valves and Appurtenances	712.24
Fire Hydrants and Appurtenances	712.26
Cullet Materials for Utility Structures	717.03
RCA for Utility Structures	719.03
RAP for Utility Structures	720.03

Use Class B concrete conforming to Section 601 – Structural Concrete for reaction beams, reaction test blocks, and jackets.

Inspect and test pipes, fittings, special castings, gate valves and butterfly valves. Furnish two copies of manufacturer's certificate of test for pipes, fittings, special castings and valves in accordance with Subsection 106.04 - Material Sample.

624.03 Construction.

(A) General. Arrange work so no interruption in water service or damage to existing water system and appurtenances occurs. Repair damages made to existing water system and appurtenances at no increase in contract price or contract time.

Locations of existing water system and appurtenances shown in contract documents are approximate. If the Engineer requires changes in alignment, grade or location due to unforeseen conflict with proposed highway project, the Engineer may be responsible for such alterations and cost.

Maintain access for Fire Department to existing fire hydrants within project site. Install relocated fire hydrants before removing existing fire hydrants.

Notify County Water Works System in writing at least one week before commencement of work on water system.

Arrange with County Water Works System to cut off unused water mains and service laterals, meter boxes, and other appurtenances before commencement of clearing, grubbing, and grading operations. Excavate for cut off work.

If corporation stop tapping into new main is larger than that allowed by County Water Works System, install double hub fitting with boss tapped for appropriate size corporation stop.

Invert grades of water mains and service laterals shall provide the following minimum cover requirements from top of pipe to finish grades:

(1) Pavement areas: Minimum three feet, sleeve or concrete jacket for six-inch or larger water mains.

(2) Under ditches: Minimum two feet, one foot, if paved.

(3) All other areas: Minimum three-foot cover.

(4) Highway utility encroachment committee may reduce the three-foot minimum clearance specified above to two feet if ground conditions are ascertained to be rocky material, provided utility lines do not encroach into the pavement structure.

(5) Minimum cover of utility service lines under sidewalk areas and areas adjacent to the right-of-way (outside of shoulder and pavement areas) shall be one-foot six inches.

Comply with requirements for the Occupational Safety and Health Administration 29 CFR Parts 1910.146, Permit-Required Confined Spaces for General Industry and Hawaii Occupational Safety and Health (HIOSH) Confined Space Standard #12-104-1.

(B) Trench Excavation.

(1) General. Pile excavated material next to trench, or haul and store to site acceptable to the Engineer. Maintain access to existing driveways, fire hydrants, meters, vehicular traffic and pedestrian walkways.

In fill areas, compact fill to subbase or to elevation 4 feet above top of pipe barrel, whichever is less, before excavating trench.

Expose existing mains by hand to verify their locations and depths.

Excavate trenches in accordance with Section 204 – Excavation and Backfill for Miscellaneous Facilities, and as modified below.

For removal of existing water system and appurtenances, provide trenches of sufficient size and depth to permit their removal without damage. Carefully remove materials to be salvaged. Replace materials damaged by the Contractor at no increase in contract price or contract time.

Do not open trench more than 750 feet ahead of installed and tested pipe. Do not construct trench with jumps or spaces unless acceptable to the Engineer. Maintain excavation during installation of water systems and placing of backfill.

Construct trench widths for various size pipes not encased in concrete in accordance with Table 624.03-1 – Trench Widths for Water System.

TABLE 624.03-1 – TRENCH WIDTHS FOR WATER SYSTEM	
Diameter of Pipe Inches	**Width of Trench Inches**
42	66
36	54
30	48
24	42
20	36
16	30
12	24
8	24
6	24
4	24
Below 4	12

Increases in widths to those specified in Table 624.03-1 – Trench Widths for Water System may be made at no increase in contract price or contract time.

For water mains encased in concrete, provide trench width of concrete jacket plus 20 inches. If no forms are specified for jacket, provide a trench width equal to width of concrete jacket. Use depth of trench as bottom of concrete jacket.

Excavate trenches to a depth of six inches below invert grade shown in contract documents, except as noted above for concrete encased mains. The Engineer reserves the right to eliminate six inches of excavation below invert grade and the right to raise or lower invert grade, or to change alignment.

Correct trenches over-excavated below specified grade with trench backfill material, compacted, at no increase in contract price or contract time.

(2) Bell Holes. Enlarge bell holes at pipe joints to provide room for completing joints.

(3) Reaction Blocks. Excavate to place reaction and test blocks.

(4) Removal of Mud and Other Unsuitable Material from Trench Bottom. If soft, spongy, or other unsuitable material is encountered at specified depths, remove material under pipe to maximum depth

of 30 inches below invert grade of pipe. Backfill space to 6 inches below invert grade of pipe with untreated base. Use untreated base with maximum aggregate size of 1-1/2 inches. Compact untreated base until relative compaction is not less than 95 percent.

(5) Sheathing. Properly sheath and brace excavation to provide secure excavation. Remove sheathing and bracing before completing backfill. When sheathing is necessary, widen trench beyond those widths specified in Subsection 624.03(B)(1) - General.

(6) Dewatering. Keep trenches free from water while installing and testing pipe and backfilling trench. Comply with NPDES requirements and other applicable regulations. Obtain NPDES construction dewatering permit for discharge of uncontaminated ground water.

(7) Service Laterals and Service Connections and Meter Boxes. Excavate and backfill in accordance with Section 204 – Excavation and Backfill for Miscellaneous Facilities.

(8) Use of Explosives. The use of explosives is not permitted, in accordance with Subsection 104.10 – Use of Explosives.

(9) Connections or Adjustments of Water Mains. If connections to, or adjustments of existing water mains are required, perform necessary excavation, placing of untreated base, and backfilling.

Before trenching for new main, expose existing main by hand to detect actual location and grade for connection. Excavate trench for exposing existing main to length, width, and depth ordered by the Engineer.

Provide materials, excavate, backfill and do work required to connect new or relocated meters to house services.

(C) Trench Backfill.

(1) General. Do not use adobe, clay or material of similar nature for backfill. When removal of unsuitable excavated materials creates shortage of backfill material, furnish suitable material. Material from roadway or other excavation may be used.

(2) Preparation of Trench Bottom. After excavating trench to proper depth below invert grade of pipe, backfill trench bottom to required invert grade of trench with trench backfill material.

(3) Backfilling. Upon completion of testing of mains and appurtenances, conform to following:

(a) For mains 12 inches and smaller, copper pipes, service laterals, services connections and appurtenances, backfill trench with Trench Backfill A material to 6 inches above top of pipe, except as specified in subparagraph (c) below.

(b) For mains 16 inches and larger, place Trench Backfill A material to 12 inches above top of pipe. Use maximum lift of six inches.

(c) For pipe inverts below the 4-foot elevation, County datum or in areas where the ground is continuously wet, use gravel material conforming to AASHTO M 43, Size Number 67, encapsulated in permeable separator, to minimum 12 inches above top of pipe or to 12 inches above water level, whichever is higher. Use maximum lift of six inches.

(d) Backfill remainder of trench with trench backfill material, conforming to Subsection 703.21 – Trench Backfill Material.

(e) Place Trench Backfill A and B materials, and Structural Backfill B material in layers not exceeding six inches in loose thickness. Compact each layer to not less than 95 percent relative compaction conforming to Subsection 203.03(C)(2) Relative Compaction Test.

Upon completion of disinfection work, remove risers. Backfill these areas with trench backfill material to not less than 95 percent relative compaction.

(D) Laying Pipe. Inspect and test pipes and appurtenances before installation. Mark circumference of spigot ends of pipe showing depth of bell before installation.

Lay each pipe so barrel of pipe has bearing along its laying length with bell end properly set to grade and alignment. Center spigot end of pipe and embed firmly against bell end of pipe previously laid with uniform clearance around bell. Hold pipe firmly in place by proper blocking on each side of pipe. Do not lay pipe on blocks.

For cathodic protected pipe, handle pipe and appurtenances with slings cushioned along areas in contact with pipe and appurtenances to protect pipe coating.

Do not use springing or buckling of pipe lengths as means of fitting them into place between installed pipe or special castings. Clean and scrape pipes and appurtenances of foreign matter and protuberances. Keep pipes and appurtenances clean until assembly of joint is completed.

If water, mud, or other foreign matter enter joints before assembly of joint, and after installation of pipes or appurtenances, open joints affected and clean joints before replacing and resetting pipes or appurtenances.

Keep trench and pipe free of water. If water enters pipe, clean inner portion of pipe before continuing with pipe installation.

Cold cutting with cold chisel and hammer will be allowed for 12-inch and smaller cast iron pipes. Trim cut edges to be even and free from projections.

Pipes 16 inch and larger shall be machine cut.

If installation of sleeves is necessary in pipelines, contact space between ends of adjoining pipes by welding in place not less than four filler pieces of same material as pipe. Use filler pieces 4 inches wide, of suitable length, and equally spaced around circumference of pipe.

When pipe laying is stopped, close openings tightly with cast iron removable plugs held securely in place.

Do not use pipes and appurtenances for water mains for other purposes before installation.

(E) Gate Valves. Inspect valves to ensure their proper working order before installation. If valves under pressure tests show leakage, stop leaks. Use proper, standardized tools for operating valves. Install proper size corporation stops on sides of valves as specified. When backfilling valves, remove and replace corporation stops with brass plugs. Support valves with blocks as specified. After completing manhole, or before constructing valve boxes, clean valve of rust and foreign matter. Paint valve with one coat of corrosion preventive paint acceptable to the Engineer.

(F) Joints for Ductile Iron Pipe and Appurtenances.

(1) Mechanical Joints. Clean bell and spigot end of pipe and rubber gasket before assembly. Place gland, followed by gasket, over spigot end of pipe that is inserted into bell. Face small side of

gasket and lip side of gland towards bell. Push gasket into position so that gasket seats evenly in bell as gland is moved against face of gasket.

Dip threaded ends of bolts in fuel oil for lubrication before assembly.

Insert bolts with threaded ends on gland side. Screw nuts by hand and make nuts hand-tight in pairs (180 degrees apart). Tighten bolts alternately (180 degrees apart) to desired tension with ratchet wrench acceptable to the Engineer, beginning at bottom, then top and so on. Conform normal range of bolt torques for standard cast iron bolts in joint to Table 624.03-2 – Bolt Torques.

TABLE 624.03-2 – BOLT TORQUES	
Bolt Size, Inches	**Range of Torque, Foot - Pounds**
5/8	40 - 60
3/4	60 - 90
1	70 - 100
1-1/4	90 - 120

Provide uniform distance around pipe between face of bell and face of gland. After completion of joint, paint bolts with one coat of asphalt paint.

(2) Slip Joint. Wipe gasket seat in socket of pipe and gasket with cloth. Place gasket in socket with large, round end entering first. Spring gasket into gasket seat so that groove fits over bead in seat.

Apply thin film of non-toxic lubricant, as supplied by manufacturer, to inner diameter of gasket to facilitate insertion of pipe. Apply thin film of lubricant to outer portion of plain end of pipe for about 1 inch back from end.

Construct joint by exerting sufficient force on entering pipe to move its plain end past gasket until pipe makes contact with base of socket.

When cutting pipes in field, taper outer portion of cut end approximately 1/8 inch at angle of 30 degrees to centerline of pipe with coarse file or portable grinder.

(3) Flanged Ends Joint. Provide flange with face true and free of projection. Clean face of flange of rust and foreign matter. Use full face gaskets. Cut gaskets carefully to fit flanges and bolt holes.

Bring up flanges to true alignment and fit flanges with uniform tension on bolts. Tighten bolts specified for mechanical joints. Paint bolt threads with graphite before tightening.

(G) Pipes, Service Laterals and Service Connections, Including Appurtenances.

(1) General. Service Lateral is that portion of installation from water main up to and including stopcock end of lateral. Service Connection is that portion of installation from stopcock end of service lateral up to and including stop cock at meter box.

Appurtenances used with Pipes, Service Laterals and Service Connections means fittings, corporation stops, valves, bushings, and stop cocks that will be installed in service lateral and service connections.

(2) Installation. Install service laterals and service connections at specified locations and of sizes and types specified.

Conform to following procedure for solder joints:

(a) Cut pipe or tube to desired length with tube cutter or fine hacksaw (32-tooth blade). Remove burrs with file or scraper.

(b) Clean outer portion of tube end that fits into solder cup of fitting with sandcloth or sandpaper. Remove dark spots.

(c) Before soldering, ensure pipe end section is circular in shape and not deformed. Use shaping/sizing tools on non-circular sections to provide proper connection.

(d) Clean solder cup of fittings carefully with wire brush, sandcloth, or sandpaper. Remove dark spots.

(e) Use no-lead flux acceptable to the Engineer. Brush light, even coating of flux onto outside of tube and half way into inside of fitting. Do not use acid or zinc chloride.

(f) Insert tube into fittings as far as tube will go. Turn tube back and forth few times to distribute flux evenly. Do not wipe joints before inserting into place.

(g) Heat fitting uniformly with torch until solder melts on contact with heated fitting. Remove flame from joint to be soldered. Using only solders acceptable to the Engineer,

feed solder to joint at one or two points. Do not feed solder around full circumference of tube. When ring of solder appears around tube at fitting, stop solder feeding and wipe excess off with cloth.

(h) For connections to tubes of 1-1/4 inch diameter and larger, move fitting on tube or tap with tool handle or mallet as solder is fed to break surface tension and ensure even distribution of solder.

(i) Conform to County Water System Standards for corrosion control requirements for copper services.

(3) Pipe Sleeves Through Retaining Walls. When constructing cement rubble masonry walls or concrete retaining walls with later installation of service connections through retaining walls, insert 2-inch minimum diameter pipe sleeves at locations indicated in contract documents.

(H) Fire Hydrants. Install fire hydrant and appurtenant pipe fittings and valves as indicated in contract documents. Install fire hydrants with 4-1/2 inch steamer nozzle faced no more than 15 degrees to left or right of line running from center of hydrant and perpendicular to street curb. Install fire hydrants with barrels vertical. After checking hydrant for alignment and grade, wedge barrel tightly against side of trench. Wedges may be removed after concrete anchor block placed at bottom elbow has set.

Place concrete thrust block around bottom elbow to at least 12 inches above invert of elbow. Do not disturb concrete thrust block for minimum of three days, or as ordered by the Engineer.

Use standard tools to operate fire hydrants.

If there is no standard curbing, protect fire hydrants with installation of curb guards.

Before final inspection, clean fire hydrants of oil, grease, dirt or other foreign matter. Paint fire hydrant in accordance with Subsection 712.26 – Fire Hydrants and Appurtenances.

(I) Concrete Reaction and Test Blocks, Concrete Jacket, and Reaction Beams. If pipeline appurtenances are subject to unbalanced thrust, brace them properly with plain or reinforced concrete reaction blocks.

For testing purposes, provide reinforced concrete blocks in accordance with County Water Works System Standards.

Cure concrete reaction and test blocks, concrete jackets, and reaction beams for seven days before applying pressure in pipes.

Due to various types of vertical bends and surrounding ground conditions, design of reaction blocks will vary. Costs for reaction block redesign due to unauthorized excavation shall be at no increase in contract price or contract time.

Install reinforced concrete jackets around ductile iron pipe as specified in contract documents.

(J) Testing. Pipes and appurtenances are subject to pressure tests in presence of the Engineer.

Whenever any section can be isolated as unit, perform separate test on each section of pipeline with its appurtenances. If valves are available at each end of section, perform test between valves. If valves are not available, install necessary plugs or caps, properly braced to withstand required test pressure. When section of pipeline is ready for testing, tap test holes into pipe and connect test holes to test pump with suitable piping. Between tap and pump, install stop cock. Between stop cock and tap, install pressure gage furnished by County Water Works System.

Fill section of pipeline to be tested completely with water. Ensure that there are no air pockets. Open stopcock and raise hydrostatic pressure to required pressure in accordance with Table 624.03-3 – Test Pressure.

TABLE 624.03-3 – TEST PRESSURE	
Class of Pipe	**Test Pressure**
150	150 psi
250	250 psi
above 250	50 psi above static pressure of installed system

Shut stopcock and observe pressure gage for 30 minutes. For acceptance, pressure shall not drop more than 10 pounds per square inch, during this period.

The Engineer may require tests to cover sections or combination of sections, and may require additional tests.

Provide equipment and material necessary for tests. After stopping visible leaks and completing tests, install brass plugs in holes made for testing purposes.

(K) Connections to or Adjusting of Existing Mains. Notify the Engineer in writing before proceeding with connections to, or adjusting of existing mains. Deliver this notice three working days before commencing with this work.

Furnish materials required for work, and complete necessary excavation.

Provide concrete reaction blocks and manholes, and complete backfill and other incidental items of work.

Do not operate valves or hydrants unless authorized by the Engineer. County Water Works System will operate valves 16 inches and larger.

Provide material, excavate, backfill and connect new or relocated meters to house services.

(L) Disinfection. Flush and disinfect water mains, service laterals, and appurtenances before acceptance. Notify the Engineer and County Water Works System 72 hours before time for disinfection. Provide connections for disinfection. Properly dispose water used in disinfecting and flushing in accordance with applicable Department of Health and NPDES requirements.

Provide temporary cleanouts at locations indicated in contract documents to ease disinfecting of water mains. After disinfecting mains and receiving certification for disinfecting, remove temporary cleanouts. Provide brass plugs to replace corporation stops.

(M) Meter Boxes and Cast Iron Frames and Covers.

(1) General. Construct meter boxes and cast iron frames and covers.

(2) Installation. Construct meter boxes of:

(a) Bricks set in full mortar beds in accordance with standard brick construction.

(b) Precast concrete with necessary reinforcing steel.

Install meter boxes at locations indicated in contract documents. Install cast iron frames and covers of proper size and dimension in full mortar beds at each meter box. Paint cast iron frames and covers with one coat of high grade asphaltum paint.

(N) Air Relief Valves and Appurtenances. Construct air relief valves and appurtenances. Appurtenances include pipes, fittings, corporation stops, unions and vertical check valves. Clean air relief valves of rust and foreign matter. Paint air relief valves with one coat of corrosion preventive paint acceptable to the Engineer.

(O) Water Supply for Construction. County Water Works System will measure quantity of water used for construction. County Water Works System will provide and disconnect meter. Arrange with County Water Works System and pay costs for such installations and disconnections. County Water Works System will furnish invoices for cost of installation and disconnection of meters. Pay for cost of replacements or repairs resulting from damage to meter, hydrant and other property used.

Provide water supply equipment and materials necessary to provide adequate water supply for proper construction of water mains. Equipment and materials may include temporary pipes and fittings, pumping, and storage facilities.

(P) Maintaining Existing Water System. Maintain existing water system in service during construction period, and until new water system is placed in service and existing services are transferred to new system.

Immediately notify the Engineer and County Water Works System of damages to existing system. County Water Works System will do necessary repairs. County Water Works System will bill the Contractor for costs incurred in this work.

After installing new system or portions of new system, remove existing meters and reconnect existing meters to new system. New system includes its appurtenances, service laterals, service connections, and boxes. For work ordered by State, and to be done by County Water Works System personnel, County Water Works System will send invoices directly to State. County Water Works System will not charge or pay cost of this work to the Contractor.

(Q) Removing, Reinstalling or Returning Existing Pipe. Clean existing pipe that is to be removed and reinstalled in new locations before installing.

Existing pipe includes its appurtenances, fire hydrants, gate valves, and manhole frames and covers. Paint manhole frames and covers with one coat of high-grade asphaltum paint.

Clean and return existing pipe removed and not reinstalled to County Water Works Storage Yard as ordered by the Engineer.

Assume responsibility for removing, reinstalling, or returning these existing pipes. Pay for damages to materials during these operations.

(R) Abandoning Existing Pipe. If ordered, expose portions of abandoned pipe. If top of pipe is less than 24 inches below finished grade, remove and dispose existing pipe off right-of-way. If abandoning pipe in place, plug ends of abandoned pipe with Class C concrete. Backfill in accordance with Section 204 – Excavation and Backfill for Miscellaneous Facilities.

(S) Corrosion Protection. Apply corrosion protection to pipes, valves and fittings as specified in County Water System Standards. Use specified materials and methods of application.

(T) Valve Markers. Install valve markers for establishing location of gate valves and air relief valves.

Fill markers with concrete and set markers plumb in Class B concrete footing. Paint pipe yellow. Paint top 4 inches of markers for air relief valves red.

624.04 Measurement. Water system will be paid on a lump sum basis. Measurement for payment will not apply.

624.05 Payment. The Engineer will pay for accepted water system on a contract lump sum basis. Payment will be full compensation for work prescribed in this section and contract documents.

The Engineer will pay the following pay item when included in proposal schedule:

Pay Item	**Pay Unit**
Water Systems	Lump Sum

The Engineer will pay for:

(A) Excavation and backfill under Section 204 – Excavation and Backfill for Miscellaneous Facilities.

(B) Concrete in reaction blocks, test blocks, jackets, and reaction beams under Section 503 – Concrete Structures.

(C) Reinforcing steel under Section 602 – Reinforcing Steel.

END OF SECTION 624

SECTION 625 - SEWER SYSTEM

625.01 Description. This section describes constructing sewer systems and appurtenances.

Terms "Sewage" or "Wastewater" and "Division of Sewers" or "Division of Wastewater Management" (DWM) will be interchangeable depending on respective County.

625.02 Materials.

Bed Course Materials for Crushed Rock Cradle	703.16
Structure Backfill Material	703.20
Trench Backfill Material	703.21
Joint Mortar for Pipe	705.02
Jointing Compound for Sewer Pipe	705.11
RCP for Sewer System	706.02(B)
Vitrified Clay Pipe (VCP) and Fittings for Sewer System	706.08
PVC for Sewer System	706.09
Cast Iron Pipe and Fittings for Sewer System	707.01(A)
Ductile Iron Pipe, Fittings and Special Castings for Water System	707.01(B)
Reinforcing Steel	709.01
Cullet Materials for Utility Structures	717.03
RCA for Utility Structures	719.03
RAP for Utility Structures	720.03

Conform concrete for sewer structures to Section 601 – Structural Concrete. Use Class C concrete for non-reinforced concrete blocks, cradles, and jackets. Use Class B concrete for reinforced concrete blocks, cradles, and jackets.

Modify concrete in contact with sewage or sewage gases as follows:

(1) Incorporate water reducing admixture conforming to Subsection 711.03(B) – Admixture Acceptance.

(2) Use Type II portland cement or modified Type I portland cement with maximum limit of 8 percent on tricalcium aluminate.

Use 2-inch square redwood, or 1-1/2 inch diameter PVC pipe, of required length for markers for house connection reducers.

625.03 Construction

(A) Open Trench Excavation for Sewer Pipes. Excavate trenches in accordance with Section 204 – Excavation and Backfill for Miscellaneous Facilities and below:

(1) Trench Widths. Construct trench widths in accordance with Table 625.03-1 – Trench Widths for Sewer Pipes.

TABLE 625.03-1 - TRENCH WIDTHS FOR SEWER PIPES	
Pipe Size - Inches	**Trench Width – Inches**
6	24
8	24
10	24
12	30
15	38
18	41
21	45
24	50
27	53
30	57
36	69
42	76
48	84
54	91

Increases in widths over those specified in Table 625.03-1 - Trench Widths for Sewer Pipes may be made at no increase in contract price or contract time.

If trench width is greater than that specified in Table 625.03-1 – Trench Widths for Sewer Pipes, and such condition results in greater load of overburden than Department designed pipe for, provide at no increase in contract price or contract time:

(a) Higher strength replacement pipe.

(b) Higher class of bedding.

Pile excavated material next to trench, or haul and store to site acceptable to the Engineer. Obstructing movement of vehicular traffic and pedestrian walkways will not be allowed. Maintain access to existing driveways, fire hydrants, and meters.

For pipe installation in new embankment, construct embankment:

(a) To required height.

(b) For a distance on each side of pipe location not less than five times diameter of pipe.

Excavate trench with sides as nearly vertical as permitted by soil conditions. Shore trench in accordance with OSHA requirements.

Excavating more than 300 feet ahead of installed pipe will not be allowed. Trench left unfilled more than 300 feet behind installed pipe will not be allowed.

(2) Trench Depths. Excavate trench to depth in accordance with contract documents. Follow OSHA requirements.

If trench excavation is deeper than specified in the contract documents, bring trench to specified grade, at no increase in contract price or contract time:

(a) With bed course material.

(b) Class C concrete placed with cradle.

If mud or other unsuitable material is encountered at specified grade, excavate below specified grade to depth and width ordered by the Engineer, and backfill with bed course material.

If contract documents specify concrete to bed pipe, consider top of concrete as top of bedding. Bedding material includes one of following:

(a) Concrete.

(b) Beach sand conforming to Subsection 703.01 – Fine Aggregate for Concrete.

(c) No. 8 or No. 67 aggregate conforming to gradation requirements of ASTM C 33.

(d) Native free-draining granular material having a minimum sand equivalent of 30 or having a coefficient of permeability greater than 0.001 centimeter per second.

(e) Other materials acceptable to the Engineer.

(3) Sheathing and Bracing.

(a) General. Provide and maintain sheathing and bracing required to support excavation. Follow OSHA requirements.

(b) PVC Pipe. If timber sheeting is used below top of PVC pipe, drive timber sheeting approximately 2 feet below bottom of pipe. Leave timber sheeting in place about 1-1/2 feet above top of pipe.

(c) Movable Trench Sheeting, Trench Boxes or Shields. If bottom of sheeting, box, or shield extends below top of pipe, use movable trench supports only:

1. On shelf above pipe with pipe installed in narrow, vertical-wall subditch.

2. If located at least 2-1/2 pipe diameters away from flexible pipe.

unless means to reconsolidate bedding or side support material disturbed by shoring removal is acceptable to Engineer.

(4) Dewatering of Trenches. Keep drainage or seepage water below level of subgrade:

(a) When installing pipe, cradles or jackets.

(b) During periods of construction work inspection.

(c) During leakage tests.

Consider subgrade as bottom of concrete blocks or jacket. Keep trenches free of water while installing and testing pipe and backfilling trench. Comply with NPDES requirements and other applicable regulations. Obtain NPDES construction dewatering permit for discharge of uncontaminated ground water.

(B) Installation of Sewer Pipe.

(1) General. Lay pipe starting from lowest point with spigots facing direction of flow. Fit and match pipe together to provide sewer true to line and grade with smooth and uniform invert.

Do not use blocks and wedges to adjust pipe to proper line and grade, except as required for jackets and cradles. Uniformly support pipe for its entire length.

Close exposed ends of sewers with accepted temporary covers at end of each work day. If water, mud or other foreign matter enters joints after pipe installation, open, clean, and replace affected joints.

Check pipes that become submerged in water during the night each morning. Re-lay pipes that have floated from their proper positions at no increase in contract price or contract time. Before final inspection, visually inspect lines, and remove mud and other foreign matter within sewer line.

Comply with requirements of Hawaii Occupational Safety and Health (HIOSH) Confined Space Standard §12-67.2-2.

For sewer manhole, see Subsection 626.03(B)(2) - Sewer Manholes.

(2) Vitrified Clay Pipe. Install vitrified clay pipe with compression joints. Wipe or brush the pipe with lubricant or adhesive recommended by pipe manufacturer on contact surfaces of joints. Push spigot into bell until joint snaps into position.

Do not use poured or formed joints using cement, sulfur compounds, bituminous materials, or other materials forming rigid joint.

Use jointing compound recommended by pipe manufacturer for joining 6-inch by 4-inch extra heavy cast iron or ductile iron reducer to 6-inch vitrified clay sewer pipe and 4-inch house sewer.

(3) Cast Iron and Ductile Iron Pipe and Appurtenances. Construct in accordance with Subsections 624.03(D) – Laying Pipe and 624.03(F) – Joints for Ductile Iron Pipe and Appurtenances.

(4) Reinforced Concrete Pipe. Clean inside surface of concrete bell and concrete spigot end, including groove, before making joint. Lubricate rubber gasket and annular groove in spigot. Stretch and place gasket uniformly in annular groove in spigot. Lubricate inside bell surface 2 inches from end of pipe. Use soft vegetable soap compound lubricant recommended by manufacturer.

Before assembling joint, place metal or wooden spacers against shoulder of bell and provide proper space between abutting ends of pipe.

Telescope and seat spigot into bell. Do not mortar joints, inside or outside.

Insert thin metal feeler gage between bell and spigot. Check position of rubber gasket around complete circumference of pipe. If gasket is not in proper position;

(a) Withdraw pipe.

(b) Check gasket for cuts and damages.

(c) Re-lay pipe.

(d) Recheck gasket position.

Provide joint openings:

(a) Within tolerance recommended by manufacturer.

(b) Consistent with design of pipe.

(c) To not exceed 1/2 inch.

If joint opening exceeds any of above requirements, withdraw pipe, correct defect, and re-lay pipe.

(5) PVC Pipe. Wipe clean and lubricate compression joints with lubricant provided by manufacturer before inserting spigot end of pipe into bell end.

Handle, load, unload, and store PVC pipe with care. Store pipe and fittings under cover. Transport pipe and fittings in vehicle with bed long enough to allow length of pipe to lie flat.

Place four inches of bedding material below pipe, plus additional bedding material above the bottom of pipe equal to 0.4 times outside diameter of pipe. If laying pipe in rock excavation, remove six inches of rock below pipe and place six inches of bedding below pipe.

Cover pipe with minimum of 3 inches of accepted backfill material within 24 hours after placing pipe in trench.

Bedding from bottom of pipe to 12 inches above pipe may be compacted by jetting, provided applied water does not soften or damage foundation material. Use 1-1/2 inch nozzle curved to circumference of installed pipe with sufficient length to reach invert of pipe. Conduct compaction along entire length of pipe on alternate sides with each side compacted four times. Provide additional material and compaction if settlement is greater than 1/6 diameter of pipe. Maintain required grades. Compact backfill from 12 inches above pipe to finish surface in accordance with Section 204 – Excavation and Backfill for Miscellaneous Facilities.

Provide special watertight manhole couplings for manhole connections. Cast couplings directly into cast-in-place manholes, or grout couplings into precast concrete manholes with non-shrink or expansion-type grout.

(6) Leakage Tests.

(a) General. Test sewers and sewer manholes for leakage in presence of the Engineer. Provide equipment and material necessary for tests including water and labor. Perform leakage test with results acceptable to the Engineer before placing backfill, concrete cradles, concrete jackets, or permanent resurfacing.

(b) Force Mains. Test force mains in accordance with Subsection 624.03(J) – Testing.

(c) Gravity Lines. Do not perform exfiltration leakage test if difference in elevation between inverts of adjacent manholes exceeds 10 feet.

If ground water is above top of pipe, perform leakage (infiltration) tests as follows:

(1) After laying pipe and completing connections to manholes, backfill pipe trench to prevent floating of pipe.

(2) Close end of sewer at upper structure to prevent entrance of water. Stop pumping of ground water for at least three days. Test the test portion for infiltration.

(3) Use maximum quantity of infiltration of 200 gallons per day per inch of inside diameter per mile of pipe.

(4) Reduce infiltration over limit specified above to within permissible limit before sewer is acceptable the Engineer. Repair visible leaks, despite limits of leakage tests.

If ground water is below top of pipe laid, perform leakage (exfiltration) tests as follows:

(1) Test each portion of sewer between successive manholes by closing the inlet of the lower manhole and and closing the inlet of upper manhole with stoppers. Fill pipe and upper manhole with water:

(a) At least 4 feet above invert of upper manhole.

(b) Or, not less than 1 foot above high end of highest house connection on test portion.

(2) If construction of manhole is delayed, use barrel on bank to provide necessary pressure required for testing.

(3) Keep water present in trench below level of subgrade of sewer during test, and during patching or repairing required by test.

(4) Use maximum quantity of exfiltration 200 gallons per day per inch of inside diameter per mile of pipe.

(5) Reduce exfiltration over limit specified above to within permissible limit before acceptance by the

Engineer. Repair visible leaks, despite limits of leakage tests.

(d) Low Pressure Air Test

(1) Clean pipe to be tested.

(2) Plug pipe outlets with test plugs. Securely brace each plug.

(3) Add air until internal pressure of line reaches approximately 4 pounds per square inch. After reaching this pressure, allow pressure to stabilize. Pressure will normally drop as air temperature stabilizes, usually taking two to five minutes depending on pipe size. Reduce pressure to 3-1/2 pounds per square inch before starting test.

(4) Start test when pressure:

(a) Has stabilized.

(b). Is at or above starting test pressure of 3-1/2 pounds per square inch.

If pressure does not drop more than 1 pound per square inch during test time, line has passed test.

(5) Ground water above pipe will reduce air loss. If section of line under test shows significant infiltration, perform infiltration test.

(6) Air test may be dangerous if line is prepared improperly. Install and brace plugs to prevent blowouts.

Provide pressurizing equipment with regulator set at 10 pounds per square inch to avoid over-pressurizing and damaging acceptable line. Do not allow workers in manholes during testing.

TABLE 625.03-2 - MINIMUM AIR TEST TIME FOR VARIOUS PIPE SIZES			
Nominal Pipe Size, Inches	**T (Time) minutes /100 feet**	**Nominal Pipe Size, Inches**	**T (Time) minutes /100 feet**
3	0.2	21	3.0
4	0.3	24	3.5
6	0.7	27	4.2
8	1.2	30	4.8
10	1.5	33	5.4
12	1.8	36	6.0
15	2.1	39	6.6
18	2.4	42	7.3

(7) Mandrel Test for Deflection of PVC Pipe. Perform mandrel test 30 days after completing trench backfill. In roadway areas, 30- day period begins after installation and compaction of bedding, backfill and subbase to within 2 feet of finished pavement grade.

Pull rigid nine-sled mandrel through pipe by hand between adjacent manholes to measure for obstructions such as deflections, joint offsets, and lateral pipe intrusions. Use mandrel conforming to ASTM D 3033 and ASTM D 3034. Furnish material, equipment, and labor required for test, and perform test in presence of the Engineer.

If mandrel fails to pass, pipe is considered overdeflected. If pipe is not damaged, uncover and reinstall pipe. Remove damaged pipe from work site. Do not reround or use other methods or processes to reduce or remedy overdeflections.

(8) Connections to Existing Sewers.

(a) General. Arrange with County Division of Sewers for making connections to existing sewers.

(b) Breaking into Existing Manholes. Connect to existing manholes and channelize inverts in presence of County Division of Sewers inspector. In making connection, place tight fitting false form on inside portion of manhole. Remove materials falling inside

existing sewer pipe. Pay for damages to existing manhole and sewer pipe resulting from this work. After completing connection, work on required channelizing within existing manhole.

(c) Sewer Enclosed Within New Manhole. If building new manhole over existing sewer main, cut existing sewer line in presence of County Division of Sewers inspector. Clear new manhole of mud, debris, and standing water before cutting existing sewer line.

(d) Saddle Wye. If required to install new lateral from existing sewer main, provide saddle wye tap-in in presence of County Division of Sewers inspector.

(C) Trench Backfill. Do not place backfill until testing of pipe and appurtenances is acceptable to the Engineer. After installing and testing pipe, immediately backfill trench and around manhole. Backfill in accordance with Section 204 – Excavation and Backfill for Miscellaneous Facilities.

If using sheathing, fill and tamp cavities formed below invert grade before proceeding with backfill of trench.

Place and tamp trench backfill material placed below horizontal plane 12 inches above top of pipe by hand shoveling so that backfill material is in contact with entire periphery of pipe. Use Trench Backfill A material conforming to Subsection 703.21 – Trench Backfill Materials.

Backfill remainder of trench with Structural Backfill B or Trench Backfill B material conforming to Subsection 703.20 – Structure Backfill Material or 703.21 - Trench Backfill Materials.

For sewer pipes that are cradled, bring initial backfill up to top of pipe, moisten, and tamp.

In lawns, gardens, and other cultivated areas, backfill upper 12 inches with planting soil or loam and tamp. Plant grass, reset plants and shrubs, and irrigate area for seven days.

(D) Concrete Blocks. Provide concrete blocks next to each bell on both pipes and fittings.

(E) Concrete Cradle. Provide concrete cradles under entire length of pipe as specified in contract documents. Before placing concrete, rest pipes firmly on concrete blocks. Keyway or curing is not required. Provide reinforcement as specified in contract documents.

(F) Crushed Rock Cradle. Provide crushed rock cradle under entire length of pipe as specified in contract documents. Provide bed course material in layers not exceeding 8 inches in loose thickness and compact.

(G) Concrete Jackets. Provide concrete jackets as specified in contract documents. Use small concrete blocks to support pipes, and provide reinforcement as specified in the contract documents. Cure reinforced concrete jackets for five days. Plain concrete jackets do not require curing.

(H) House Sewer Connection. Arrange connections to cause least inconvenience for sewer user.

(I) Removing or Abandoning Existing Sewer System. If requested by the Engineer, expose portions of existing sewer pipe to be removed or abandoned. Excavate in accordance with Subsection 625.03(A) – Open Trench Excavation for Sewer Pipes.

If top of pipe is less than 24 inches below finished grade, and the Engineer orders pipe removed, proceed with pipe removal work. The Engineer will order exact position of cutting for pipe removal work. Plug open ends of abandoned pipes with Class B concrete. Plug ends of existing pipes to remain in use with vitrified clay cap.

Backfill open trench with accepted select material and tamp in uniform horizontal layers not exceeding 8 inches in loose thickness. Use backfill tampers to provide relative compaction of not less than 95 percent.

Clean and deliver salvaged materials as ordered by the Engineer.

625.04 Measurement. Sewer systems will be paid on a lump sum basis. Measurement for payment will not apply.

625.05 Payment. The Engineer will pay for accepted sewer systems on a contract lump sum basis. Payment will be full compensation the work prescribed in this section and contract documents.

The Engineer will pay for following pay item when included in proposal schedule:

Pay Item	Pay Unit

Sewer Systems Lump Sum

The Engineer will pay for excavation and backfill for sewer pipes under Section 204 – Excavation and Backfill for Miscellaneous Facilities.

The Engineer will not pay separately for concrete blocks, cutting and plugging of abandoned sewers, concrete plugs for ends of abandoned sewers, and vitrified clay caps at ends of existing sewers that will remain in use. Consider cost for these items as included in sewer system contract pay items.

END OF SECTION 625

SECTION 703 - AGGREGATES

703.04 Aggregate for Untreated Permeable Base. Use of recycled materials shall not be permitted in the untreated permeable base. Aggregate for untreated permeable base shall conform to the following:

(A) Coarse Aggregate. Coarse aggregate shall consist of crushed and screened basalt that is free of soft or disintegrated pieces, clay, ~~dirt~~, organics, and other deleterious substances.

Coarse aggregate shall conform to Table 703.04-1 – Aggregate Test Requirements.

TABLE 703.04 – 1 – AGGREGATE TEST REQUIREMENTS		
Test	**Test Method**	**Requirement**
Los Angeles Abrasion	ASTM C 535 (Coarse Aggregate) AASHTO T 96 (Filler)	40 Percent Maximum
Grading	AASHTO T 27	Refer to Table 703.04-2

(B) Filler. Filler material shall conform to Subsection 703.04(A) – Coarse Aggregate, except grading shall conform to Table 703.04-2 – Grading Requirements.

TABLE 703.04-2 - GRADING REQUIREMENTS		
Screen Size	**Coarse Aggregate Modified Size 4 (Percent Passing By Weight)**	**Filler Size 8 (Percent Passing By Weight)**
2 inch	100	-
1-1/2 inch	75-100	-
1 inch	15-55	-
¾ inch	0-15	-
½ inch	-	100
3/8 inch	0-5	85-100
No. 4	-	10-30
No. 8	-	0-10
No.16	-	0-5

703.06 Aggregate for Untreated Base. Aggregate for untreated base shall consist of ~~crushed stone~~ one of the following:

1. 100% virgin aggregate
2. a mixture of virgin aggregate and cullet

3. a mixture of virgin aggregate and RAP
4. a mixture of virgin aggregate and RCA, or
5. a mixture of virgin aggregate, RAP and RCA.

The untreated base shall be free of organics, vegetable matter and other deleterious substances. A maximum of 10% cullet, 50% RAP or 100% RCA by dry weight of the mixture is permitted in the untreated base course. Use of more than one type of recycled material shall not be allowed in a base course except a three-way combination of virgin aggregate, RAP and RCA is permissible. The requirements for cullet, RCA and RAP shall conform to 717.02 – Cullet Materials for Roadways, 719.02 – RCA for Roadways, and 720.02 – RAP for Roadways, respectively. ~~(Neither reclaimed asphalt pavement (RAP) nor reclaimed concrete pavement will be allowed for untreated base.)~~

Crushing of virgin aggregate shall be regulated so that at least 80 percent, by weight, of material retained on the No. 4 sieve is crushed and has at least one mechanically fractured face.

Aggregate for untreated base, in combination with binder material, if used, shall conform to Table 703.06-1 – Untreated Base Test Requirements and Table 703.06-2 – Untreated Base Grading Requirements. The tabulated requirements apply to the virgin aggregate when used alone and to the combined virgin aggregate and recycled material when used as a blend.

TABLE 703.06-1 – UNTREATED BASE TEST REQUIREMENTS		
Test	**Test Method**	**Requirement**
Los Angeles Abrasion	AASHTO T 96	40 Percent Maximum
Sand Equivalent	AASHTO T 176	35 Percent Minimum
Plasticity Index	AASHTO T 90	6 Percent Maximum
Grading	AASHTO T 27	Refer to Table 703.06-2
California Bearing Ratio	AASHTO T 193	80 percent minimum[1]

Note: 1) The CBR shall be at least 80 percent as measured on a sample compacted at optimum moisture content and after 4 days of soaking. The sample shall be subjected to a surcharge equal to 10 lbs during soaking and penetration. The optimum moisture content and maximum dry unit weight shall be determined in accordance with AASHTO T 180 Method D, prepared using 5 layers at 56 blows.

TABLE 703.06-2 – UNTREATED BASE GRADING REQUIREMENTS			
Sieve Size	**Percent Passing by Weight**		
	2-1/2 inch Maximum Nominal	**1-1/2 inch Maximum Nominal**	**3/4 inch Maximum Nominal**
3 inch	100	-	-
2-1/2 inch	90 - 100	-	-
2 inch	-	100	-
1-1/2 inch	65 - 90	90 - 100	-
1 inch	-	-	100
¾ inch	45 - 70	50 - 90	90 - 100
No.4	25 - 45	25 - 50	35 - 55
No. 200	3 - 9	3 - 9	3 - 9

Unless otherwise indicated in the contract documents, 1-1/2 inch maximum nominal size aggregate shall be furnished.

Material used as foundation for corrugated metal pipe culvert shall be tested in accordance with Hawaii Test Method HDOT TM 4 and shall have field resistivity and pH value that provide minimum 50-year service life for gage being installed. Material used as backfill against aluminum pipe shall have field resistivity of more than 500 ohm-centimeter and pH value between 5.5 and 9.0, using same test procedure. The use of RCA shall not be permitted within 10 feet of any aluminum or metal pipe or structure.

703.17 Aggregate for Subbase. Aggregate for subbase shall consist of one of the following:

1. 100% virgin aggregate (such as gravel, stone, basalt, or coral, or combination thereof)
2. a mixture of virgin aggregate and cullet
3. a mixture of virgin aggregate and RAP
4. a mixture of virgin aggregate and RCA, or
5. a mixture of virgin aggregate, RAP and RCA.

The aggregate for subbase shall be free of organics, ~~overburden~~, vegetable matter, and other deleterious substances. A maximum of 25% cullet, 50% RAP or 100% RCA by dry weight of mixture is permitted in the subbase. ~~RCA shall not be used in the top 6 inches of the subbase when the subbase lies below a permeable base layer.~~

Use of more than one type of recycled material shall not be allowed in a subbase except a three-way combination of virgin aggregate, RAP and RCA is permissible. The requirements for cullet, RCA and RAP shall conform to 717.02 – Cullet Materials for Roadways, 719.02 – RCA for Roadways, and 720.02 – RAP

for Roadways, respectively. ~~(Neither reclaimed asphalt pavement (RAP) nor reclaimed concrete pavement will be allowed for untreated base.)~~

The tabulated requirements apply to the virgin aggregate when used alone and to the combined virgin aggregate and recycled material when used as a blend. When tested in accordance with AASHTO T 27, subbase shall conform to Table 703.17-1 – Subbase Grading Requirements.

TABLE 703.17-1 – SUBBASE GRADING REQUIREMENTS		
Sieve Size	**Percent Passing by Weight**	
	Subbase Material Placed in Top 6 Inches	**Subbase Material Placed Below Top 6 Inches**
6 inch	-	100
2-1/2 inch	100	-
No. 4	20 - 60	20 - 60
No. 200	0 - 15	0 - 15

When tested in accordance with AASHTO T 176, SE value shall not be less than 25. A minimum SE of 20 shall be provided when material passing No. 4 sieve is entirely crushed coral limestone.

When tested in accordance with AASHTO T 89 and AASHTO T 90, subbase shall conform to Table 703.17-2 – Subbase Plasticity Index.

TABLE 703.17-2 – SUBBASE PLASTICITY INDEX	
Percent Passing No. 200 Sieve	**Plasticity Index**
0 - 9	15 Percent Maximum
10 - 15	10 Percent Maximum

When tested in accordance with AASHTO T 193, the CBR shall be at least 60 percent as measured on a sample compacted at optimum moisture content and after 4 days of soaking. The sample shall be subjected to a surcharge equal to 10 lbs during soaking and penetration. The optimum moisture content and maximum dry unit weight shall be determined in accordance with AASHTO T 180 Method D, prepared using 5 layers at 56 blows.

The use of RCA shall not be permitted within 10 feet of any aluminum or metal pipe or structure.

703.20 Structure Backfill Material. Structure backfill material shall consist of one of the following:

1. 100% virgin aggregate
2. a mixture of virgin aggregate and cullet
3. a mixture of virgin aggregate and RAP
4. a mixture of virgin aggregate and RCA, or

5. a mixture of virgin aggregate, RAP and RCA.

Structure backfill shall be free of organics, vegetable matter and other deleterious substance. A maximum of 25% cullet, 50% RAP or 100% RCA by dry weight is permitted in the structure backfill. Use of more than one type of recycled material shall not be allowed in the structure backfill except a three-way combination of virgin aggregate, RAP and RCA is permissible. The requirements for cullet, RCA and RAP shall conform to 717.02 – Cullet Materials for Roadways, 719.02 – RCA for Roadways, and 720.02 – RAP for Roadways, respectively.

The tabulated requirements apply to the virgin aggregate when used alone and to the combined virgin aggregate and recycled material when used as a blend. Structure backfill shall conform to the grading requirements in Table 703.20-1 - Structure backfill grading requirements and other requirements of this subsection

TABLE 703.20-1 – STRUCTURE BACKFILL GRADING REQUIREMENTS		
Sieve Size	**Percent Passing by Weight**	
	Structure Backfill Material A	**Structure Backfill Material B**
3 inch	100	100
No. 4	20 – 75	20 – 100
No. 200	0 – 15	-

SE shall be tested in accordance with AASHTO T 176. Structural backfill material A shall have minimum SE of 20. Structural backfill material B shall have SE equal to or greater than SE of surrounding soil in area to be backfilled.

The use of RCA shall not be permitted within 10 feet of any aluminum or metal pipe or structure.

703.21 Trench Backfill Material. Trench backfill material shall consist of one of the following:

1. 100% virgin aggregate
2. a mixture of virgin aggregate and cullet
3. a mixture of virgin aggregate and RAP
4. a mixture of virgin aggregate and RCA, or
5. a mixture of virgin aggregate, RAP and RCA.

Two types of trench backfills are defined: (1) “non-critical” trench backfill refers to the portion of a trench backfill that is more than 5 feet below the road surface or the entire portion of a trench backfill that is in an unpaved area; and

(2) “critical” trench backfill refers to the portion of a trench backfill that is 5 feet or less below the road surface and that is subject to surcharge, and the entire portion of a trench backfill that is in an embankment. For non-critical trench backfill, a maximum of 100% cullet, 100% RAP or 100% RCA by dry weight is permitted for use. For critical trench backfill, a maximum of 25% cullet, 50% RAP or 100% RCA by dry weight is permitted for use.

Use of more than one type of recycled material shall not be allowed in the trench backfill except a three-way combination of virgin aggregate, RAP and RCA is permissible. The requirements for cullet, RCA and RAP shall conform to 717.02 – Cullet Materials for Roadways, 719.02 – RCA for Roadways, and 720.02 – RAP for Roadways, respectively. Coarse aggregate material shall be used for trenches where invert of pipe is in swampy areas or under water. Coarse aggregate material shall conform to ASTM C 33, size number 67, and shall be completely encapsulated with geotextile conforming to Subsection 716.03 – Geotextiles for Underdrain Applications. Trench backfill material shall be free of trash, roots, organic matter, and other deleterious materials.

The tabulated requirements apply to the virgin aggregate when used alone and to the combined virgin aggregate and recycled material when used as a blend. The requirements for trench backfill shall conform to Table 703.21-1 – Trench Backfill Grading Requirements and the other requirements of this subsection.

TABLE 703.21-1 – TRENCH BACKFILL GRADING REQUIREMENTS

Sieve Size	**Percent Passing by Weight**	
	Trench Backfill Material A (Critical)	**Trench Backfill Material B (Non-critical)**
3 inch	-	100
1 inch	100	-
No. 4	75 – 100	20 – 100
No. 200	0-15	-

Trench backfill material placed against corrugated metal pipe culvert shall be tested in accordance with Hawaii Test Method HDOT TM 4 and shall have field resistivity and pH values that provide a minimum 50-year service life for the gage being installed. Trench backfill material placed against aluminum pipe shall have a field resistivity of more than 500 ohm-centimeter and a pH value between 5.5 and 9.0, using the same test procedure. The use of RCA shall not be permitted within 10 feet of any aluminum or metal pipe or structure.

(A) Trench Backfill Material A. Trench backfill material shall be sandy material classified as SW, ~~SP,~~ SM, or SW-SM~~, or SP-SM~~ in accordance with ASTM D 2487. SE value of trench backfill A, determined in accordance with AASTHO T 176, shall not be less than 20 and not less

than SE value of surrounding soil in trench to be backfilled. ~~Reclaimed asphalt pavement (RAP) shall not be used for trench backfill material A.~~

(B) Trench Backfill Material B. SE value of trench backfill B, determined in accordance with AASHTO T 176, shall be not less than SE value of surrounding soil in trench to be backfilled.

703.23 Aggregate for Dressing of Shoulders. Aggregate for dressing of shoulders shall conform to Subsection 703.17 – Aggregates for Subbase, except that 100 percent of material shall pass 1-1/2 inch sieve.

703.24 Granular Material for Embankment. Granular material for embankment shall consist of one of the following:

1. 100% virgin aggregate (such as gravel, stone, lava rock, coral, or cinders, or combination thereof)
2. a mixture of virgin aggregate and cullet
3. a mixture of virgin aggregate and RAP
4. a mixture of virgin aggregate and RCA, or
5. a mixture of virgin aggregate, RAP and RCA.

A maximum of 25% cullet, 50% RAP or 100% RCA by dry weight is permitted in the embankment fill. Use of more than one type of recycled material shall not be allowed in the granular material for embankment except a three-way combination of virgin aggregate, RAP and RCA is permissible. Granular material for embankment shall be free of organics, ~~overburden~~, vegetable matter, and other deleterious substances. Pit run material is acceptable. The requirements for cullet, RCA and RAP shall conform to 717.02 – Cullet Materials for Roadways, 719.02 – RCA for Roadways, and 720.02 – RAP for Roadways, respectively.

The tabulated requirements apply to the virgin aggregate when used alone and to the combined virgin aggregate and recycled material when used as a blend. When tested in accordance with AASHTO T 27, grading shall conform to Table 703.24-1 – Embankment Material Grading Requirements.

TABLE 703.24-1 – EMBANKMENT MATERIAL GRADING REQUIREMENTS	
Sieve Size	**Percent Passing by Weight**
6 Inch	100
3 Inch	75 – 100
No. 4	20 – 75
No. 200	0 - 15

END OF SECTION 703

SECTION 717 - CULLET AND CULLET-MADE MATERIALS

717.01 Cullet and Cullet-Aggregate Mixtures as Construction Materials. Construction-grade cullet (recycled crushed glass) shall have a uniform grading from fine to coarse, with 100 percent of material passing the 3/8–inch sieve and not more than 5 percent by weight passing the No. 200 sieve. Cullet shall be blended with ~~natural~~ virgin aggregate~~s~~ in accordance with Subsections 717.02 - Cullet Materials for Roadway, 717.03 - Cullet Materials for Utility Structures, or 717.04 - Cullet Materials for Drainage Systems.

Cullet content is defined as the percentage of cullet, by dry weight of the total composite aggregate weight, ~~of construction–grade cullet used in roadway, utility, and drainage applications,~~ with or without addition of ~~natural~~ virgin aggregate~~s~~. Finished product shall meet the specified grading requirements ~~shall be met~~.

Cullet shall be processed so as to limit the quantity of shard-like particles in the portion retained on the No. 4 sieve to less than one percent by mass as measured by ASTM D4791.

Debris is defined as deleterious material that includes container tops, plastics, papers, labels, food residue, foil, wood and other non-ceramic constituents of cullet. Debris shall be limited to maximum levels as specified in tables 717.02-1 – Cullet in Roadway Applications, 717.03-1 – Cullet in Utility Applications, and 717.04-1 – Cullet in Drainage Applications. In addition, the mass of paper shall not exceed 0.05 percent of the mass of the glass cullet. ~~Hazardous material will not be allowed in cullet.~~

The percent debris shall be determined on a mass basis as follows. A representative sample of glass cullet is placed in an oven heated to 110°C (±5°C) and dried to constant mass and then visually segregated into: (1) glass cullet, (2) paper, and (3) debris as defined above other than paper. The percentage of each component shall be determined by dividing the mass of the component by the mass of cullet and rounded to the nearest 0.01 percent.

The cullet shall be tested as follows:

(1) Collect a minimum of one ~~six~~ representative sample per X cubic yards of cullet and measure the percent debris and the percent paper, where X = 1500 cubic yards of the final cullet-blended product times the percent cullet in the blend. Submit the results for all ~~six~~ determinations.
(2) Request the Engineer to visually inspect the cullet stockpile. Based on visual inspection, the results of the gradation analyses (see below) the percent debris and the percent paper, the Engineer will determine the

suitability of the cullet. The Engineer has the right to conduct independent testing to verify the submitted test results.

The final cullet-blended product shall be tested as follows: Conduct and submit a minimum of one ~~six~~ gradation analysis per 1500 cubic yards of the final cullet blended product~~cullet material~~.

The Contractor shall submit a blended aggregate design prior to use or prior to changing either the source or amount of cullet originally approved. For aggregate blends, the Contractor shall submit the means and method on how uniform mixing of the recycled and virgin aggregates is ensured. Blending at the job site shall not be permissible.

Under no circumstances shall cullet be used adjacent to or placed in contact with any recycled concrete aggregate (RCA).

Compaction requirements shall be met for each application.

717.02 Cullet Materials for Roadways. Cullet and cullet-aggregate mixtures for base course (untreated or hot mix glassphalt base course mix), subbase, and embankments shall conform to Table 717.02-1 – Cullet in Roadway Applications. When used as a base course, it should also conform to AASHTO Standard Specification M318-02: Glass Cullet Use for Soil-Aggregate Base Course, except that the percent of glass cullet in the blend with unrecycled aggregate shall be limited to 10% instead of the 20% as stated in AASHTO M318-02.

TABLE 717.02-1 - CULLET IN ROADWAY APPLICATIONS		
Roadway Applications	**Maximum Cullet Content (Percent By Weight of mixture)**	**Maximum Debris Level (Percent By Weight of Cullet)**
Base Course	10	0.20
Subbase	~~10 to~~ 25	0.20
Embankments	~~10 to~~ 25	~~0.30~~0.20

All crushing of the cullet necessary to meet the gradation and debris material requirements shall be performed prior to blending.

717.03 Cullet Material for Utility Structures. Cullet for trench bedding and backfill in cut areas more than 5 feet below road surface and in unpaved ~~cut~~ areas ~~not subject to surcharge~~ shall conform to Table 717.03-1 – Cullet for Use as Non-Critical Trench Backfill. Trench bedding and backfill in the following areas shall conform to embankment requirements in Table 717.02-1 – Cullet in Roadway Applications: cut areas 5 feet or less below road surface; cut areas subject to surcharge; and embankment areas for full depth.

TABLE 717.03-1 - CULLET FOR USE AS NON-CRITICAL TRENCH BACKFILL		
Utility Trench Bedding And Backfill Applications	**Maximum Cullet Content (Percent By Weight)**	**Maximum Debris Level (Percent By Weight of Cullet)**
Drainage Pipes	100	0.20
Sewer Pipes	100	~~0.30~~0.20
Electrical Conduits	100	~~0.30~~0.20
Fiber Optic Lines	100	~~0.30~~0.20

All crushing of the cullet necessary to meet the gradation and debris material requirements shall be performed prior to placement.

717.04 Cullet Materials for Drainage Systems. Except in surcharged cut areas and in embankment areas, cullet for drainage fill applications, including drains behind retaining walls, foundation drains, drainage blankets, and French drains shall conform to Table 717.04-1 – Cullet in Drainage Applications. In surcharged cut areas and in embankment areas, cullet for drainage fill applications described in this subsection shall conform to subbase requirements in Table 717.02-1 – Cullet in Roadway Applications.

TABLE 717.04-1 - CULLET IN DRAINAGE APPLICATIONS		
Drainage Fill Applications	**Maximum Cullet Content (Percent By Weight)**	**Maximum Debris Level (Percent By Weight of Cullet)**
Retaining Walls	100	0.20
Foundation Drainage	100	0.20
Drainage Blankets	100	0.20
French Drains	100	0.20

END OF SECTION 717

SECTION 719 – RECYCLED CONCRETE AGGREGATE (RCA) AND RCA-MADE MATERIALS

719.01 RCA and RCA-Aggregate Mixtures as Construction Materials. RCA shall consist of material derived from the crushing of Portland cement concrete having a grading from fine to coarse, and with 100 percent of material passing the 1.5–inch sieve. RCA shall be blended with virgin aggregate in accordance with Subsections 719.02 - RCA for Roadway, or 719.03 - RCA for Utility Structures.

RCA content is defined as the percentage of RCA, by dry weight of the total composite aggregate weight, with or without addition of virgin aggregate. Finished product shall meet the specified grading requirements.

Deleterious material in RCA includes brick, ceramics and bituminous concrete materials. Deleterious materials shall be limited to the maximum levels as specified in tables 719.02-1 - RCA in Roadway Applications, or 719.03-1 - RCA for Use as Non-Critical Trench Backfill. In addition, the mass of "prohibited" materials such as wood, metal **(excluding aluminum which is not allowed at all in RCA. The Engineer has the right to use a non-ferrous metal detector to detect the presence of aluminum and if present, has the right to reject that pile of RCA.)**, plaster and gypsum board shall not exceed 0.1 percent of the mass of the RCA, assuming that the RCA is obtained by crushing concrete on its own. If the RCA is obtained by crushing concrete simultaneously with other materials (e.g., virgin rock), the mass of "prohibited" materials shall not exceed 0.03 percent of the mass of the final blended product.

When reclaimed asphalt pavement (RAP) is to be blended RCA, the RAP shall be free of any temporary striping that contains aluminum to prevent the aluminum from corroding. Aluminum will corrode in an alkali-rich environment, which can exist in the presence of RCA and moisture.

The percent deleterious and prohibited materials shall be determined on a mass basis as follows. A representative sample is dried to constant mass and then visually segregated into: (1) aggregate, (2) deleterious materials as defined above, and (3) "prohibited" material as defined above. The percentage of each component shall be determined by dividing the mass of the component by the mass of the RCA if the RCA is obtained by crushing concrete on its own, or by the mass of the final RCA-blended product if concrete is crushed with other materials (e.g., virgin rock), and rounded to the nearest 0.01 percent.

Concrete structures that were adjacent to any aluminum that corroded in its presence, that have suffered from sulfate attack, alkali silica reaction, or any other known distresses shall not be crushed and used as RCA.

RCA shall not be used where exposure to high (as determined by the engineer) sulfate content in the soil, ground water or other external sources is likely. RCA shall be prohibited when the ground water is determined to be highly brackish (near the ocean) by the Engineer to minimize the possibility of sulfate attack.

Hazardous materials including asbestos and lead-based paint shall not be allowed in the RCA. Provide documentation regarding each off-site source of RCA with sufficient documentation that the off-site source locations and the RCA are not deemed as hazardous and are **NOT** subject to regulation under federal or state solid and hazardous waste laws, regulations and policies including but not limited to RCRA Subtitles C[1] and D[2], and:

1. Hawaii Revised Statutes (HRS) 342J and Hawaii Administrative Rules (HAR) Title 11, Chapters 261 through 280 for lead-based paint waste regulations, and
2. Hawaii Revised Statutes (HRS) 342P and Hawaii Administrative Rules (HAR) Title 11, Chapters 501 through 504 for asbestos waste regulations.

The documentation provided shall conform to generally accepted engineering standards for site assessments and environmental evaluations conducted by a qualified environmental scientist. Specific environmental requirements for RCA shall include testing that shows that the following criteria are met:

1. The RCA shall be free of lead-based paint. The U.S. Department of Housing and Urban Development defines lead-based paint as any paint, varnish, shellac or other coating that contains lead equal to or greater than 1.0 mg/cm^2 as measured by x-ray fluorescence (XRF) or laboratory analysis, or 0.5% by weight (5000 μg/g, 5000 ppm or 5000 mg/kg) as measured by laboratory analysis in accordance with their Guidelines for the Evaluation and Control of Lead-Based Paint Hazards in Housing. Note that this definition for lead-based paint applies to undemolished concrete. In this light, the following criterion shall be met:

   The testing shall be performed only on the paint, and not on the concrete before demolition. In this case, the total concentration of lead in the paint shall not exceed 1.0 mg/cm^2 as measured by x-ray fluorescence (XRF), or 0.5% by weight (5000 μg/g, 5000 ppm or 5000 mg/kg) as measured by laboratory analysis. The laboratory test used to determine lead-based paint is “total concentration of lead.”

   In addition, the RCA shall meet the definition of inert fill as defined in Hawaii Revised Statutes (HRS), Chapter 342H, Solid Waste Pollution.

2. The RCA shall be free of asbestos.

The Engineer has the right to conduct independent testing to verify the submitted test results.

The RCA and/or blend shall be wetted prior to use to prevent fugitive dust from becoming airborne.

~~The Contractor shall notify the Engineer the original source of the aggregate including the facility name and address from where the concrete was demolished to obtain the RCA.~~ The Contractor shall not use RCA from unknown sources unless certified by a qualified engineer/scientist that it is free of aluminum, lead-based paint and asbestos. Off-site sources of RCA must have written acceptance by the Engineer prior to blending and/or placement.

The RCA shall be further tested as follows:

(1) If the RCA is obtained by crushing concrete on its own, collect a minimum of one representative sample per X cubic yards of RCA and measure the percent deleterious material and the percent prohibited material, where X = 1500 cubic yards of the final RCA-blended product times the percent RCA in the blend. If the RCA is obtained by crushing concrete simultaneously with other materials (e.g., virgin rock), collect a minimum of one representative sample per 1500 cubic yards of the final RCA-blended product and measure the percent deleterious material and the percent prohibited material. Submit the results for all determinations.
(2) Request the Engineer to visually inspect the RCA stockpile during and after crushing. Based on visual inspection, the results of the gradation analyses (see below), the percent deleterious material and the percent prohibited material, the Engineer will determine the suitability of the RCA. The Engineer has the right to conduct independent testing to verify the submitted test results.
(3) Conduct and submit a minimum of one gradation analysis per 1500 cubic yards of the final RCA or its blended product.

The Contractor shall submit a blended aggregate design prior to use or prior to changing either the source or amount of RCA originally approved. For aggregate blends, the Contractor shall submit the means and method on how uniform mixing of the recycled and virgin aggregates is ensured. Blending at the job site shall not be permissible.

Furnish shipping documents and a Contractor certification that the material delivered on-site, is in fact, that which has been documented by prior submittal.

Compaction requirements shall be met for each application. The Contractor is warned that use of rubber tired rollers may be problematic should any fugitive steel fragments be present in the RCA during compaction.

RCA and RCA-aggregate mixtures shall not be used within 10 feet of any metal pipes or metal structures and shall not be used within 3 feet of the ground water table nor below the ground water table.

719.02 RCA for Roadways. RCA and RCA-aggregate mixtures for untreated base course, subbase, and embankments shall conform to Table 719.02-1 – RCA in Roadway Applications. When used as a base course, it should also conform to AASHTO Standard Specification for Reclaimed Concrete Aggregate for Unbound Soil-Aggregate Base Course, AASHTO Designation: M 319-02.

TABLE 719.02-1 - RCA IN ROADWAY APPLICATIONS

Roadway Applications	RCA Content (Percent By Weight of mixture)	Maximum Deleterious Material (Percent By Weight of RCA)	Maximum Deleterious Material (Percent By Weight of Mixture)
Base Course	100	5.00	1.25
Subbase	100	5.00	1.25
Embankments	100	5.00	1.25

719.03 **RCA for Utility Structures.** RCA for trench bedding and backfill in cut areas more than 5 feet below road surface and in unpaved areas shall conform to Table 719.03-1 – RCA for Use as Non-Critical Trench Backfill. Trench bedding and backfill in the following areas shall conform to the requirements in Table 719.02-1 – RCA in Roadway Applications: cut areas 5 feet or less below road surface; cut areas subject to surcharge; and embankment areas for full depth.

TABLE 719.03-1 - RCA FOR USE AS NON-CRITICAL TRENCH BACKFILL

Utility Trench Bedding And Backfill Applications	RCA Content (Percent By Weight)	Maximum Deleterious Material (Percent By Weight of RCA)	Maximum Deleterious Material (Percent By Weight of Mixture)
Drainage Pipes	100	5.00	1.25
Sewer Pipes	100	5.00	1.25
Electrical Conduits	100	5.00	1.25
Fiber Optic Lines	100	5.00	1.25

719.04 RCA for Drainage Systems. RCA and RCA mixtures shall be prohibited for use in drainage fill applications, including drains behind retaining walls, foundation drains, drainage blankets, and French drains.

END OF SECTION 719

SECTION 720 – RECLAIMED ASPHALT PAVEMENT (RAP) AND RAP-MADE MATERIALS

720.01 RAP and RAP-Aggregate Mixtures as Construction Materials. RAP shall consist of milled or crushed asphalt pavement having a gradation from fine to coarse with 100 percent of material passing the 3/4–inch sieve. When used on its own or when mixed with virgin aggregate, the material shall conform to the gradation requirements as specified in the respective sections in accordance with its intended use. RAP shall be blended with virgin aggregate in accordance with Subsections 720.02 - RAP for Roadway, or 720.03 - RAP for Utility Structures.

RAP content is defined as the percentage of RAP, by dry weight of the total composite aggregate weight, with or without addition of virgin aggregate. Finished product shall meet the specified grading requirements.

Deleterious material in RAP includes debris and lumps of cohesive soil in sufficient quantity as to be detrimental to the proper bonding, finishing or strength of the RAP mixture. Deleterious materials shall be limited to the maximum levels as specified in Tables 720.02-1 – RAP in Roadway Applications and 720.03-1 – RAP in Utility Applications.

The percent deleterious material shall be determined on a mass basis as follows. A representative sample of RAP is air-dried to constant mass and then visually segregated into: (1) RAP and (2) deleterious materials as defined above. The percentage of each component shall be determined by dividing the mass of the component by the mass of RAP and rounded to the nearest 0.1 percent.

When RAP is to be blended with crushed recycled concrete aggregate (RCA), the RAP shall be free of any temporary striping that contains aluminum to prevent the aluminum from corroding. Aluminum will corrode in an alkali-rich environment, which can exist in the presence of RCA and moisture.

When RAP is stockpiled from a previous State of Hawaii Department of Transportation project and the composition of the existing pavement is known, the Engineer may approve the material on the basis of composition. When the composition of the RAP is not known, the RAP shall be tested as follows:

(1) Collect a minimum of one representative sample per X cubic yards of RAP and measure the percent deleterious material, where X = 1500 cubic yards of the final RAP-blended product times the percent RAP in the blend. Submit the results for all determinations.
(2) Request the Engineer to visually inspect the RAP stockpile. Based on visual inspection, the results of the gradation analyses (see below) and percent deleterious material, the Engineer will determine the suitability of the RAP. The Engineer has the right to conduct independent testing to verify the submitted test results.

The final RAP-blended product shall be tested as follows: conduct and submit a minimum of one gradation analysis per 1500 cubic yards of the final RAP blended product. Prior to blending, the RAP shall be air-dried to surface dry condition. Oven drying shall not be performed on RAP.

The Contractor shall submit a blended aggregate design prior to use or prior to changing either the source or amount of RAP originally approved. For aggregate blends, the Contractor shall submit the means and method on how uniform mixing of the recycled and virgin aggregates is ensured. Blending at the job site shall not be permissible.

Compaction requirements shall be met for each application.

720.02 RAP for Roadways. RAP and RAP-aggregate mixtures for untreated base course, subbase, and embankments shall conform to Table 720.02-1 – RAP in Roadway Applications.

TABLE 720.02-1 - RAP IN ROADWAY APPLICATIONS		
Roadway Applications	**RAP Content (Percent By Weight of mixture)**	**Maximum Deleterious Material (Percent By Weight of RAP)**
Base Course	50	3.0
Subbase	50	5.0
Embankments	50	5.0

All crushing of the RAP necessary to meet the gradation and deleterious material requirements shall be performed prior to blending.

720.03 RAP for Utility Structures. RAP for trench bedding and backfill in cut areas more than 5 feet below road surface and in unpaved areas shall conform to Table 720.03-1 – RAP for Use as Non-Critical Trench Backfill. Trench bedding and backfill in the following areas shall conform to the requirements in Table 720.02-1 – RAP in Roadway Applications: cut areas 5 feet or less below road surface; cut areas subject to surcharge; and embankment areas for full depth.

TABLE 720.03-1 - RAP FOR USE AS NON-CRITICAL TRENCH BACKFILL		
Utility Trench Bedding And Backfill Applications	**RAP Content (Percent By Weight)**	**Maximum Deleterious Material (Percent By Weight of RAP)**
Drainage Pipes	100	5.0
Sewer Pipes	100	5.0
Electrical Conduits	100	5.0
Fiber Optic Lines	100	5.0

All crushing of the RAP necessary to meet the gradation and deleterious material requirements shall be performed prior to placement.

718.04 RAP for Drainage Systems. RAP and RAP mixtures shall be prohibited for use in drainage fill applications, including drains behind retaining walls, foundation drains, drainage blankets, and French drains.

END OF SECTION 720